THE RELIABILITY OF CAPACITY-DESIGNED COMPONENTS IN SEISMIC RESISTANT SYSTEMS

A DISSERTATION
SUBMITTED TO THE DEPARTMENT OF
CIVIL AND ENVIRIONMENTAL ENGINEERING
AND THE COMMITTEE ON GRADUATE STUDIES
OF STANFORD UNIVERSITY
IN PARTIAL FULFILMENT OF THE REQUIREMENTS
FOR THE DEGREE OF
DOCTOR OF PHILOSOPHY

Victor Knútur Victorsson
August 2011

Abstract

Capacity design principles are employed in structural design codes to help ensure ductile response and energy dissipation in seismic resisting systems. In the event of an earthquake, so called "deformation-controlled" components are expected to yield and sustain large inelastic deformations such that they can absorb the earthquake´s energy and soften the response of the structure. To ensure that this desired behavior is achieved, the required design strength of other components (capacity-designed components) within the structure is to exceed the strength capacity of the deformation-controlled components. While the basic concept of capacity design is straightforward, its implementation requires consideration of many factors related to the variability in component strengths, overall inelastic system response, seismic hazard and tolerable probability of system collapse. Capacity design provisions have tended to be established in an ad-hoc manner which has led to concerns as to whether the current seismic provisions are over-conservative, leading to uneconomical designs, or un-conservative, potentially creating unsafe designs. While there is no agreement on the answer, there is agreement as to the need for a more rational basis to establish capacity design provisions.

Motivated by this need for a more rational basis to establish capacity design provisions, the objectives of this research are to contribute to the understanding of the reliability of capacity-designed components in seismic resistant systems and to develop a reliability-based methodology for establishing the required design strengths of capacity-designed components in seismic resistant systems. More specifically, the objectives of this research are to identify the main factors that influence the reliability of capacity-designed components, to assess how their reliability affects the system reliability, to determine what the appropriate component reliability is and to integrate this information into a methodology to establish the required design strengths of capacity-designed components. Topics that are explored in this research are: (1) quantifying the expected demand on capacity-designed components, (2) assessing the influence of the structural response modification factor, R-factor, and member overstrength on the reliability of

capacity-designed components, (3) assessing the impact of the seismic hazard curve on the reliability of capacity-designed components and (4) assess the consequences of capacity-designed components' failure on the overall system reliability.

To achieve the aforementioned objectives and to demonstrate the use and applicability of the developed methodology, dynamic analyses of 1-story, 6-story and 16-story Special Concentrically Braced Frames are conducted and the reliability of the brace connections and columns investigated. The results demonstrate that the initiation of connection failures is associated with the initiation of brace yielding. As structural building systems are typically designed for only a fraction of the estimated elastic forces that would develop under extreme earthquake ground motions, failure of brace connections can occur at low ground motion intensities with high frequences of exceedance. Therefore, in low-redundancy systems, failure of brace connections can have unproportionally adverse effect on the system collapse probability. As a consequence, if consistent risk is desired, higher required design strength of brace connections is required when the ground motion intensity of brace yielding initiation is low than when the ground motion intensity is high. Based on the analysis results, the ground motion intensity, or spectral acceleration at which braces yield, $Sa_{y,exp}$, can be related to the R-factor and member overstrength. Dynamic analyses where brace connection failures are included in the simulations show that failure of brace connection does not necessarily equal collapse and that the probability of collapse given connection failure depends on the ground motion intensity. At spectral accelerations close to the MCE demand, the probability of collapse due to connection failure was 25%-30% for the cases studied.

The demand on columns in braced frames is a complex matter as it is very system, height and configuration dependent The braced frame analysis results demonstrate that unless there are only a couple of braces exerting demand on columns, capacity design principles overestimate the expected demand on them and the difference increases as the number of stories increases. This is caused by the low likelihood of simultaneous yielding of all braces, different member overstrength between stories and further complicated in the case of braced frames with the differences in brace tension and compression strength capacities.

The proposed reliability framework considers the main factors believed to influence the reliability of capacity-designed components and the end result is a framework for establishing required component design strength that provides risk consistency between different seismic resistant systems and seismic areas. The factors considered are the system R-factors and member overstrengths, site seismic hazard curves, assumed influence of failure of capacity-designed components on system collapse behavior, and the tolerable increased probability of frame collapse due to the failure of capacity-designed components.

Acknowledgements

A number of individuals have contributed significantly to my research and life at Stanford University. First and foremost, I would like to thank my three advisors, my main advisor, Professor Greg Deierlein, and co-advisors, Professor Jack Baker and Professor Helmut Krawinkler. I am fortunate to have had the opportunity to work with these three brilliant and dedicated scholars. Their enthusiasm and commitment to structural engineering is inspiring and under their influence I have grown as an engineer and researcher.

I would also like to thank Professor Benjamin Fell at California State University – Sacramento. His assistance and guidance with structural modeling at the early stages of my graduate student career was invaluable.

Thanks to all the students, staff and faculty associated with the John A. Blume Earthquake Engineering Center. The Blume Center is an amazing place, both socially and academically, and a pleasure to work in. I am thankful for the opportunity to work closely with a few former and current Blume Center students, most notably, Dimitrios Lignos, Ting Lin and Abhineet Gupta. I am very grateful of their contributions, and enjoyed working with each of them. I would like to thank administrative associates Racquel Hagen and Kim Vonner for their support to the Blume Center and its students. I would also like to show my gratitude to the staff of the Hume Writing Center at Stanford University. Their Dissertation Bootcamp helped me tremendously in improving my work habits and in writing this thesis.

Finally, I would like to thank my parents, Victor and Kristin, brothers and dear friends who have supported me throughout. Without you, the completion of this thesis would not have been possible.

Contents

List of Tables

List of Figures

xxvi

Chapter 1

Introduction

1.1 Motivation

Largely for economic and practical reasons, structural building systems are typically designed for only a fraction of the estimated elastic forces that would develop under extreme earthquake ground motions. The reduced forces are justified by design provisions that ensure ductile response and hysteretic energy dissipation. In the event of an earthquake, so called "deformation-controlled" components are expected to yield and sustain large inelastic deformations, such that they can dissipate energy, dampen the induced vibrations, and protect other critical structural components from excessive force or deformation demands. Structural systems employ capacity design principles to ensure that this desired behavior is achieved by designing so-called "force-controlled" structural components with sufficient strength to resist the forces induced by the yielding deformation-controlled components. Force-controlled components are sometimes referred to as "capacity-designed components" since their design strengths are based on the strength capacities of deformation-controlled components.

An example application of capacity design principles is the seismic design of braced frames. During large ground motions, the braces in the frames are expected to yield in tension and buckle in compression, thereby absorbing energy as well as limiting the maximum forces that can be developed in the brace connections, columns, beams and foundations. In turn, the brace connections, columns, beams and foundations are typically designed to resist the forces associated with the tensile yield strength and compressive buckling strength of the braces.

To help ensure that the desired behavior is achieved, structural design codes include provisions to control the margin between the expected capacities of the force-controlled

components and the expected demands from the deformation-controlled components. In reliability terms, the goal is to achieve a small probability of the induced force demands exceeding the capacities of force-controlled components. This is done by reducing the design strengths, through the use of resistance factors, ϕ, and by increasing required strength, through the use of load factors, γ, or an overstrength factor, e.g. the ASCE 7-10 (2010) Ω_0 factor. While the basic concept of seismic capacity-based design is straightforward, theoretically rigorous development of appropriate strength adjustment factors requires consideration of many issues related to the variability in component strengths, overall inelastic system response, seismic hazard, tolerable probability of demand exceeding capacity and tolerable probability of system collapse. Capacity design provisions in current design codes and standards have generally been established in an ad-hoc manner that has resulted in inconsistencies in the capacity design factors for different seismic force resisting systems. This has led to concerns as to whether the capacity-design requirements in current provisions, e.g. the ASCE 7-10 *Minimum Design Loads for Buildings and Other Structures* (2010), AISC *Seismic Provisions* (2010a) and ACI 318 *Building Code Requirements for Structural Concrete and Commentary* (2010), are over-conservative, leading to uneconomical designs, or un-conservative, potentially creating unsafe designs. While there is no agreement on the solution, there is agreement on the need for a more rational basis to establish capacity design factors.

1.2 Objectives

The primary objectives of this research are (1) to improve understanding of the reliability of capacity-designed components in seismic resisting structural systems, (2) to develop a reliability-based methodology for establishing the required design strengths of capacity-designed components in seismic resistant systems and (3) to apply the proposed methodology to brace connections and columns in Special Concentrically Braced Frames (SCBF′s). Ultimately, the intent is to provide a methodology for establishing capacity-design requirements that provide more consistent seismic collapse safety among different

2

types of structural seismic systems and materials that are applied in regions of differing seismic hazard.

Specific topics that are explored in this research are:

1. *Expected Demand on Capacity-Designed Components:* Studies are conducted to identify factors that influence force demands on capacity-designed components in seismic resistant systems and to quantify the expected demands. Included are cases where the capacity-designed components are subjected to force demands from one or more deformation-controlled components.

2. *System Design Factors and Member Overstrength:* Assess the influence of system design parameters, such as the structural response modification factor (the R-factor) and other design criteria or practices, on the reliability of capacity-designed components. This includes evaluation of how structural component and system overstrength, such as due to the use of resistance factors (ϕ), nominal material values, discrete member sizing, drift limits, architectural constraints, etc., impact component force demands and overall system collapse safety.

3. *Seismic Hazard Curve:* Assess the impact of the seismic hazard curve on the reliability of capacity-designed components and the significance of variations between the seismic hazards for different geographic locations. This includes consideration of how the new risk-targeted seismic hazard maps (e.g., ASCE 7 2010) affect the frequency of yielding and the reliability of capacity-designed components.

4. *Component and System Reliability:* Assess the consequences of capacity-designed components' failure on the overall system reliability and how that information can be used to choose appropriate target reliability of capacity-designed components.

1.3 Scope of Study

The focus of this research is to develop a reliability-based methodology for establishing the required design strengths of capacity-designed components in seismic resistant systems. The proposed methodology is intended to be consistent with current design approaches, wherein the required design strengths of capacity-designed components are established by adjusting the margins between the force demands induced by deformation-controlled members on the force-controlled members. To develop the methodology, advantage is taken of the AISC *Load and Resistance Factor Design* (LRFD) component reliability methodology (Ravindra and Galambos 1978, Ravindra et al. 1978, Galambos et al. 1982), the SAC/FEMA *Demand and Capacity Factor Design* (SAC-DCFD) reliability methodology, and the system collapse safety reliability methodology of FEMA P695 (FEMA, 2009). The research examines force demands both from cyclic tests of deformation-controlled components and nonlinear dynamic analyses of seismic force-resisting systems.

While the proposed methodology is developed for component design, the underlying reliability basis considers the overall system collapse safety that is consistent with current building code requirements. In this regard, the target reliability used in the methodology is indexed to the system collapse safety assumed in the development of the new ASCE 7 (ASCE 2010) risk-targeted seismic design value maps (Luco et al., 2007). Nonlinear dynamic analyses are conducted of 1-story, 6-story and 16-story seismically designed ductile braced frame systems to examine the influence of component (brace connection) failure on the overall system collapse safety. These analyses incorporate the nonlinear strength and stiffness degradation of braces, beams and columns, including the effects of brace buckling and fracture along with brace connection failure. Uncertainties considered in the nonlinear analyses and resulting methodology include variability in both ground motions (seismic hazard intensities, ground motion frequency content and duration) and structural materials and model parameters (material yield strengths, fabrication tolerances, and degradation parameters).

The proposed reliability-based methodology is applicable to any seismic resistant systems following capacity design principles and results in risk consistent capacity-

designed components. However, in this study the capacity-design of two components of special concentrically braced steel frames (SCBF's) are investigated in detail: SCBF brace connections and SCBF columns. These components are chosen to demonstrate the methodology and to support its applicability and limitations when (a) capacity-designed components are subjected to the demand from a single deformation-controlled component, as in the case of brace connections in SCBF's and (b) capacity-designed components are subjected to the demand from multiple deformation-controlled components, as in the case of columns in multi-story SCBF's. In addition to SCBF brace connections and columns, the reliability methodology is used to examine the component design requirements of bolted end plate moment connections that are prequalified for use in steel Special Moment Frames.

1.4   Organization and Outline

The report is divided into seven main chapters and five appendices.

Chapter 2 gives a detailed background on capacity design principles and capacity design provisions in structural design codes. Previously developed methods to assess structural component and system reliability are summarized, insofar as they relate to the proposed development.

Chapter 3 summarizes the development and key features of the proposed reliability methodology for capacity-design components. Included are the key mathematical equations major underlying assumptions of the method. It is seen that system design factors, such as the system response modification factor (i.e., the R-factor used in US seismic codes), structural overstrength and the seismic ground motion hazard curve have a significant effect on the reliability of capacity-designed components. In addition to being necessary factors to calculate the reliability of capacity-designed components, these findings can allow for potentially reducing the required strength of capacity-designed components of systems that rely less on inelastic deformation to achieve their minimum collapse safety performance or are designed in geographic regions were the design

spectral accelerations have relatively low frequencies of occurrence. The resulting methodology establishes the required design strengths of capacity-designed components that provides for more consistent risk between different seismic force resisting systems. Further details of the mathematical formulation for the reliability methodology are summarized in Appendix C.

Chapter 4 summarizes studies to examine the reliability of brace connections in single-story SCBF's. Incremental nonlinear dynamic analyses are conducted to investigate brace connection force demands, connection failure reliability and overall system collapse reliability. Two frame designs are considered, with different brace sizes and overstrength. The case-study frames are analyzed in two phases. First, median models of the frames are created and analyzed through incremental dynamic analysis to develop the frames´ collapse fragility curves, assuming that the connections do not fail. The calculated maximum force demands on the connections are then used to evaluate the probability of connection failure, considering uncertainties in both the imposed force demands and the connection strengths. A modified collapse fragility curve is then developed, based on the assumed influence of connection failure on frame collapse. In the second phase of the study, one of the two frames is re-analyzed with brace fracture and complete modeling uncertainty included. Uncertainties in the model parameters are included using a Monte Carlo simulation method. This second set of analyses provides data to assess both the influence of modeling uncertainty on the frame collapse fragility as well as influence of connection failure on the frame collapse behavior. The single story analyses presented in Chapter C are further supported by detailed analysis studies in Appendices A and B.

Chapter 5 investigates the demand and reliability of brace connections and the axial column force demand on in multi-story SCBF's. The multi-story SCBF analyses illustrate how the methodology applies to systems where higher mode and inelastic redistribution effects need to be considered. Models of 6- and 16-story SCBF´s, designed as part of the evaluation of FEMA P695 methodology (NIST GCR 10-917-8, 2010), are analyzed to assess the frames´ collapse fragility curves and the demands on the capacity-designed components. Additionally, to investigate overstrength effects, an alternative design of a

6-story SCBF is investigated, where brace sizes are held constant up the height of the structure. These studies examine the applicability and limitations of the methodology for multi-story systems with redundancy and higher mode effects.

Chapter 6 summarizes the proposed methodology and demonstrates its use and applicability through an SCBF design example. Capacity design factors are recommended for selected failure modes in brace connections. Appendix D provides a corresponding example for special moment frame connections; and Appendix E summarizes the statistical data on material properties and other design parameters used in the examples of Chapter 6 and Appendix D.

Chapter 7 summarizes the important findings and contributions of this study and discusses future research topics that have emerged from this work.

Chapter 2

Background on Capacity-Based Design and Structural Reliability

2.1 Introduction

This chapter summarizes background on capacity design principles and capacity-design provisions in structural design codes and reliability methods that are utilized in establishing the required design strength of capacity-designed components. The chapter begins with discussing the overall reasons behind and the goals of capacity design principles in structural design codes and how US structural design codes go about achieving those goals. To address those topics, the capacity-design provisions in ASCE 7-10 *Minimum Design Loads for Buildings and Other Structures* (2010), AISC *Seismic Provisions* (2010a) and ACI 318 *Building Code Requirements for Structural Concrete and Commentary* (2010) are presented.

The chapter then reviews three reliability methods that provide background for developing a reliability-based methodology for establishing the required design strength of capacity-designed components. These are the *Load and Resistance Factor Design* (LRFD) component methodology, developed for static, strength-based problems under various load types, the SAC *Demand and Capacity Factor Design* (SAC-DCFD) reliability methodology, developed for seismic design and assessment of structures and the FEMA P695 *System Reliability Methodology* (FEMA, 2009), developed to evaluate seismic design provisions through inelastic static and dynamic analyses of structural systems under earthquake ground motions.

Lastly, the chapter discusses challenges of relating component reliability to system reliability and possible ways to address those challenges.

2.2 Capacity-Based Design

Most modern building codes employ capacity design principles to help ensure ductile response and energy dissipation capacity in seismic resisting systems. The design provisions are geared toward restricting significant inelastic deformations to those structural components that are designed with sufficient inelastic deformation capacity. Those are generally referred to as deformation-controlled components. Other structural components, referred to as force-controlled components, are designed with sufficient strength to remain essentially elastic. Examples of applications of capacity design principles in building codes are the design provisions for brace connections, columns and beams in steel Special Concentrically Braced Frames in the 2010 AISC *Seismic Provisions*. (AISC, 2010a) The design provisions aim to confine significant inelastic deformation in the braces while the brace connections, columns and beams remain essentially elastic. To help ensure this behavior, the required design strengths of brace connections, columns and beams are to exceed the expected strength of the braces.

Capacity design provisions for force-controlled components can be further differentiated between those that can be defined solely based on the strength of adjacent members, as the brace and brace connection example above, to those that require information of overall system behavior, such as columns in steel braced frames. The required axial strength for columns in seismic resistant steel frames is based on the load from all yielding members exerting demand on them, including the effects of material overstrength and strain hardening.

Another example of capacity design provisions that require information of overall system behavior are the design provisions for columns in reinforced concrete Special Moment Frames in the 2008 ACI 318 *Building Code Requirements for Structural Concrete and Commentary* (ACI 318, 2008). To confine inelastic deformations to beams (weak beam – strong column), the minimum required nominal flexural strength of columns is to exceed the factored nominal flexural strength of beams joining into the column where the column flexural strengths depend on the axial loads.

Requirements for capacity design are not as clear cut as is often perceived. Establishment of margins between demand and capacity to ensure the desired behavior requires consideration of uncertainties in both local component strengths and overall indeterminate system response. Moreover, the extent to which capacity design is or should be enforced to create ideal mechanisms is a matter of debate and involves a trade-off between structural robustness and economy. There are also cases where it can prove almost physically impossible to create the ideal mechanism.

Eccentrically Braced Frames (EBFs) are seismic force-resistant frames commonly used in seismic areas. The deformation-controlled components in EBFs are the so-called shear-links. A shear-link is the beam section between two beam-brace intersections or beam-brace intersection and a beam-column joint. The design provisions in the 2010 AISC *Seismic Provisions* for EBFs aim to confine inelastic deformations to the shear links while the braces the beam outside the link area remain essentially elastic. However, since the shear link and the beam outside the link area are part of the same member, the design provisions recognize the difficulty of excluding yielding the beam outside the link area and allow for limited yielding. The design provisions in ACI 318-08 for shear walls in reinforced Special Structural Walls follow a similar pattern. The desired failure mode in SSW is flexural yielding at the base of the shear wall, as opposed to shear failure, due to the ductile response flexural yielding provides. However, the design provisions acknowledge that the desired flexural failure mode can be difficult to achieve, especially in shear walls with a small height-to-length ratio, and rather than rigorously enforcing it in those cases, the shear strength is further increased to help ensure a ductile response through inelastic shear deformations.

To enforce strict capacity design principles, large margins between the strength of force- and deformation-controlled components are required. However, in striving for a balance between safety and economy, design provisions in the United States generally do not enforce as stringent capacity design requirements, as the two examples of EBF shear link and the SSW shear strength above demonstrated. Rather, the design provisions in the United States apply capacity design principles and margins to varying degrees, such that the likelihood of undesirable modes of behavior are minimized but not necessarily

eliminated entirely. This approach is justified by tests, analyses, and observations of actual building performance, which suggest that sufficient building safety can be attained without the development of complete plastic mechanisms that would otherwise require very large capacity design margins. The design provisions for the minimum required nominal flexural strength of columns in steel and reinforced concrete Special Moment Frames are a good example of this. Much research (Paulay, 1986; Nakashima and Sawaizumi, 2000; Medina and Krawinkler, 2005; Choi and Park, 2009) has demonstrated that if inelastic deformation is to be confined to beams only, a significant increase in the margin between demand and capacity is required but as sufficient building safety is achieved with current margins, limited column yielding is accepted. Similarly, the Pacific Earthquake Engineering Center´s (PEER) Tall Building Initiative (TBI; 2010) has taken a step to differentiate between failure modes by separating the component design of force-controlled components, called force-controlled actions therein, into two categories, "force-controlled critical actions", whose failure mode poses severe system consequences, and "force-controlled non-critical actions", whose failure does not result in structural instability and requiring different margins based on the category.

2.2.1 ASCE 7-10 Capacity Design Provisions

ASCE 7-10 specifies the minimum design loads for seismic force resistant systems. To ensure economical design as well as ductile response and energy dissipation during seismic events, the elastic seismic forces (V_{DBE}) are reduced through the use of the seismic response modification factor, R. The seismic force resistant system is then designed using the reduced forces, the seismic design forces (V), with the implication that inelastic deformations in components will occur under large ground motions. Selected components within the seismic force resistant systems are then designed based on the reduced forces (V) and therefore designed to deform inelastically. These are components that have been proven capable of significant inelastic deformation capacity and are referred to as deformation-controlled components. Other components, i.e. the force-controlled components, are designed to remain elastic. To help ensure this desired behavior, the seismic design forces are multiplied by an overstrength factor, i.e. the Ω_0

factor (Figure 2-1). Ω_0 approximates the characteristic overstrength in seismic force-resistant systems above the design strength ($V_{u,exp}$) and by multiplying the seismic design force by Ω_0, the maximum forces that the force-controlled components are likely to experience are approximated. (ASCE, 2010) Note that the term Ω_0 applies to the overstrength factor for a class of structures, whereas Ω is the overstrength factor for a specific structure, as might be measured using a static pushover analysis. Figure 2-1 shows an inelastic force deformation curve where the aforementioned variables, V_{DBE}, V, $V_{u,exp}$, R and Ω are presented illustratively. Ω_0 is therefore meant capture the expected capacity of deformation-controlled components and so the increased loads on force-controlled members above the seismic design loads. The overstrength reflected by Ω_0 arises due to the difference between member design strengths and expected strengths (i.e., ϕR_n versus R_{exp}) conservative biases in nominal strength equations, member overstrength due to drift limits and discrete member sizing, as well as the system's redundancy and inelastic force re-distribution. ASCE 7-10 limits the seismic design loads on force-controlled components to not exceed the forces that can be delivered to them by yielding of deformation-controlled components in the structure, using expected material properties and excluding resistance factors, ϕ. (pp. 86)

2.2.2 AISC Capacity Design Provisions

The design requirements in the 2010 AISC *Seismic Provisions* generally follow the format of the AISC *Specification* (2010c) where the design strengths (resistance factor multiplied by the nominal resistance) of members or components should equal or exceed the required strengths. For force-controlled components proportioned following capacity design principles, the required strengths are generally based on capacities of deformation-controlled components, which are adjusted to account for material overstrength, strain hardening, and other factors that increase strengths beyond their nominal values. Table 2-1 summarizes capacity design requirements from the AISC *Seismic Provisions* (2010a) and the AISC *Prequalified Connection Requirements* (2010b). The following is a summary of factors considered in the required design strength calculations:

a) Expected versus Nominal Steel Yield Strength: The R_y accounts for the increase between the expected yield strength versus the minimum specified yield strength, F_y, categorized according to ASTM steel material designations, steel grade, and application (e.g., plate versus rolled shapes). The factors specified in the AISC *Seismic Provisions* represent measured strengths from a representative sample of mill certificates.

b) Expected versus Nominal Steel Tensile Strength: The R_t factor accounts for the difference between the expected ultimate strength versus the minimum specified ultimate strength, F_u, with the same categories as the R_y factors. The statistical basis for the R_t factors are ratios of F_u/F_y evaluated by Liu (2003).

c) Strain Hardening: Factors specified for strain hardening are not as well established on a statistical basis, since they depend on both the material properties and the level of strain demands in the deformation-controlled components. Moreover, the strain hardening factors tend to be combined with other effects. Factors range from no allowance for strain hardening (e.g., for axial strength of brace connections, the required design strength is equal to the yield capacity) to values up to 1.25. The factors are typically specified as a simple coefficient (e.g., 1.1 or 1.2), however, the AISC *Prequalified Connection Requirements* include the factor, C_{pr}, that is based on a stress demand equal to the average between F_y and F_u.

d) Other Adjustment Factors: Other adjustment factors are sometimes specified to account for a range of issues, which may or may not have a clear statistical basis. For example, the β factor to adjust for compression strengths of buckling restrained braces (BRBs) is based on BRB test data. On the other hand, factors for strength of columns are primarily on judgment as to the expectations regarding the inelastic deformation mechanisms, recognizing that forces in the steel columns and components may be limited by other factors such as foundation strengths. In the case of welded column splices, yet other factors based on

judgment are introduced to account for fracture critical issues that are not explicitly considered in design.

With regard to capacities, in most cases the AISC *Seismic Provisions* (2010a) enforce use of the standard nominal strength criteria and resistance ϕ–factors from the AISC *Specification (2010c)*. For example, the SCBF provisions require that the components of the brace connection will be proportioned such that the design strength for each of the possible modes of failure will be evaluated according to the AISC *Specification*. However, the AISC *Seismic Provisions* and the AISC *Prequalified Connection Requirements* do not always adhere to the standard design strength provisions of AISC *Specification*. For example, the AISC *Prequalified Connection Requirements* introduce alternative resistance ϕ-factors and nominal strength equations to check certain limit states in prequalified connections. The AISC *Seismic Provisions* also apply some modifications to the standard design strength equations, such as in EBFs, where the design strengths of beams outside the link region are increased by the R_y factor in recognition of the fact that the link and the beam are built of the same material. Similar modification is applied in net section failure of braces in SCBF, where the design strength of the net section is increased by the R_t factor in recognition of the fact that the demand is from the same member, i.e. the expected yield strength of the brace. Expected (as opposed to nominal) material strengths are used for some other design strength checks, where the material overstrengths in the required design strengths and design strengths are correlated.

2.2.3 ACI Capacity Design Provisions

The design requirements in the 2008 ACI 318 *Building Code Requirements for Structural Concrete and Commentary* generally follow a similar format as the AISC *Specification* (2010c) where the design strengths (capacities) of members or components should equal or exceed the required strengths (force demands). For force-controlled components proportioned following capacity design principles, the required design strengths are based on capacities of deformation-controlled components, excluding

resistance ϕ–factors, which are in many cases adjusted to account for strain hardening of the reinforcing steel that increases strengths beyond their nominal values. Table 2-2 summarizes the main capacity design requirements from the ACI 318 (2008).

For the design strength, in most cases the ACI 318 *Building Code Requirements* (2008) enforce use of the standard nominal strength criteria and resistance ϕ–factors. However, some adjustments are made for shear strength in seismic design. For example in SMF and SSW design, the shear strength is increased by using a resistance factor (ϕ) of 0.60, instead of the standard $\phi = 0.75$, if the nominal shear strength of the members is less than the shear due to the flexural strength of the member. For diaphragms, ϕ for shear cannot exceed the ϕ for shear used for the vertical components of the seismic force-resisting system; effectively requiring ϕ to be 0.60 if that is the ϕ-value used for the shear wall design. For joints and diagonally reinforced coupling beams, the shear strength is decreased by using a ϕ of 0.85. Also, the minimum flexural strength of columns, determined with $\phi = 1.00$, shall exceed the factored (factor is 6/5) sum of the nominal strengths of beams framing into the joint.

2.3 Structural Reliability

The following subsections include a brief overview of the following two approaches that incorporate reliability aspects for design and will be used as the basis for the capacity design methodology:

Load and Resistance Factor Design (LRFD) Methodology: The basic method employed to check component strength limit states by applying factors to load and resistance effects at the component (member or connection level).

SAC Demand and Capacity Factor Design (SAC-DCFD) Methodology: A method developed to check component or system limit states in seismic design with recognition of the dynamic and nonlinear displacement basis of the problem.

FEMA P695 Reliability Methodology: A method developed to evaluate seismic design provisions through inelastic static and dynamic analyses of structural collapse behavior under earthquake ground motions.

2.3.1   Load and Resistance Factor Design

The *Load and Resistance Factor Design* (LRFD) methodology is a component methodology that was developed in the 1970's for static, strength-based limits under various load types (Ravindra and Galambos 1978, Ravindra et al. 1978, Galambos et al. 1982). It begins with probabilistic descriptions of the key design elements (material strengths, member dimensions, applied loads, etc.), and it ends with numerical factors (load and resistance factors) that are applied to mean or nominal values of the load (demand) and resistance (capacity). The methodology implies that if the factored capacity exceeds the factored demand then a specified reliability has been equaled or exceeded, i.e., the failure probability is less than the specified tolerable values.

The LRFD design criterion is based on satisfying the following condition:

$$\phi R_n \geq \gamma Q_n \qquad (2\text{-}1)$$

where Q_n and R_n are the respective nominal values of the load, Q, and resistance, R, γ is the load factor and ϕ is the resistance factor. The design factors, γ and ϕ, account for the uncertainties inherent in determination of the nominal resistance and nominal load effects due to national variation in the loads, material properties, the accuracy of nominal strength equations, etc. If the probability distributions of Q and R are known, then the probability that load exceeds resistance (P_f) can be controlled through the choice of γ and ϕ according to the following:

$$P_f = P(R < Q) = \int_0^\infty F_R(x) f_Q(x) dx \qquad (2\text{-}2)$$

where F_R is the cumulative probability distribution function for R and f_Q the probability density function for Q. As implemented in the US design specifications, the LRFD reliability scheme does not explicitly calculate probabilities of failure. Instead it estimates the so called reliability index, β, through the first order second moment (FOSM) method.

If the probability distributions of Q and R are normal and if Q and R are statistically independent, the expression for the reliability index is:

$$\beta = \frac{R_m - Q_m}{\sqrt{\sigma_R^2 + \sigma_Q^2}} \qquad (2\text{-}3)$$

where Q_m and R_m are the mean values of load and resistance, respectively, and σ_Q and σ_R their standard deviations. The randomness in Q arises due to randomness in load intensities, uncertainties in the transformation of loads into load effects, and uncertainties in structural analysis. The randomness in R arises due to variations in mechanical properties of materials, variations in dimensions and of uncertainties in the theory underlying the design definition of nominal member strength. (Ravindra and Galambos 1978) Q_m and R_m are therefore the products of the following parameters:

$$Q_m = Q_n (\prod \mu_{x_{Qi}}) \qquad (2\text{-}4)$$

$$R_m = R_n (\prod \mu_{x_{Ri}}) \qquad (2\text{-}5)$$

where the μ's are the mean values of the statistical parameters which represent the randomness of Q and R, relative to their nominal values, Q_n and R_n

If Q and R both have lognormal distributions, the reliability index is:

$$\beta = \frac{\ln\left(\dfrac{\hat{R}_m}{\hat{Q}_m}\right)}{\sqrt{\sigma_{\ln R}^2 + \sigma_{\ln Q}^2}} \qquad (2\text{-}6)$$

where $\hat{Q}_m$ and $\hat{R}_m$ are the median values of Q and R, and $\sigma_{\ln Q}$ and $\sigma_{\ln R}$ their lognormal standard deviations. LRFD uses small variance approximations which allow for mean values to be used interchangeably with median values and coefficients of variation, V, to be used interchangeably with lognormal standard deviations. The small variance approximation is accurate when $V < 0.3$. Assuming low variances, the reliability index for lognormal distributions can then be expressed as:

$$\beta = \frac{\ln\left(\dfrac{R_m}{Q_m}\right)}{\sqrt{V_R^2 + V_Q^2}} \qquad (2\text{-}7)$$

The reliability index, β, is a relative measure of reliability. As demonstrated in Figure 2-2, if the limit state function is $Z = R - Q$ where $z < 0$ represents failure and R and Q are normally distributed variables, then β is the number of standard deviations (σ_z) that the mean of Z (μ_z) is from zero (i.e.,the limit state failure criterion). If R and Q are statistically independent and all possible uncertainties are included in the analysis, then β, as calculated using Equation 2-3 for normally distributed variables and 2-6 for lognormally distributed variables, can be related to the probability of failure. Table 2-3 and Figure 2-3 show the relationship between the probability of failure and the reliability index, β, calculated with the following equation, where Φ^{-1} is the inverse cumulative standard normal distribution function:

$$\beta = \Phi^{-1}\left(P_f\right) \qquad (2\text{-}8)$$

When only a subset of uncertainties are considered or when the probability distributions of R and Q are non-normal, Table 2-3 can still be used to approximate the probability of failure. However, as the results are not exact in such cases, the approximate probabilities are more appropriate for relative comparisons as opposed to absolute measurement of the failure risks.

Once the statistical parameters have been established, typically through a combination of experimental data and judgment, the reliability index (or the probability of failure) of each limit state can be calculated for a specified combination of ϕ and γ (or alternatively,

the ratio of ϕ/γ). Thus, ϕ and/or γ can then be varied to achieve the desired reliability index. Alternatively, if a certain reliability index, β, has been decided upon, the target safety level is achieved if:

$$R_m \geq \exp\left[\beta\sqrt{V_R^2 + V_Q^2}\right]Q_m \qquad (2\text{-}9)$$

The factor $\exp\left[\beta\sqrt{V_R^2 + V_Q^2}\right]$ can be considered as a "total" load and resistance factor. In the AISC LRFD this total factor was approximated by the product of two factors, $\exp[\alpha\beta V_R]$ and $\exp[\alpha\beta V_Q]$, in which α is a coefficient equal to about 0.7 called a "splitting factor". With this approximation, one can write the safety check as:

$$\exp[-\alpha\beta V_R]R_m \geq \exp[\alpha\beta V_Q]Q_m \qquad (2\text{-}10)$$

Adaptation of LRFD to Demand and Capacity Terminology: The LRFD reliability method described above can be adapted to calculate the conditional reliability of capacity-designed components in structural systems where the reliability is conditioned upon forces induced by seismic deformation demands on the structure. For consistentcy with capacity-based design terminology, the terms R and Q are replaced with capacity, C, and demand, D, respectively. The term C represents the capacity of the force-controlled member, e.g. a connection in a braced frame, and D represents the force demands induced by yielding of one or more deformation-controlled members, e.g. the brace force in a braced frame. Similarly, ϕ and γ will be referred to as capacity and demand factors.

Lognormal probability distributions are often chosen to describe the behavior of structural components, e.g. structural steel behavior (Galambos et al., 1982). Following lognormal probability distribution assumptions, the expression for the reliability index of capacity-designed components, conditioned upon a specific system deformation demand, is as follows (see Appendix C for a more detailed derivation of Equation 2-11 to 2-14):

$$\beta = \frac{\ln\left(\dfrac{\hat{C}_m}{\hat{D}_m}\right)}{\sqrt{V_C^2 + V_D^2 - 2\rho V_C V_D}} \qquad (2\text{-}11)$$

$$\left(\frac{\hat{C}_m}{\hat{D}_m}\right) = \left(\frac{D_n}{\hat{D}_m}\right)\left(\frac{\hat{C}_m}{C_n}\right)\frac{\gamma}{\phi} \qquad\qquad (2\text{-}12)$$

$$V_C = \sqrt{\sum V_{x_{Ci}}^2} \qquad\qquad (2\text{-}13)$$

$$V_D = \sqrt{\sum V_{x_{Di}}^2} \qquad\qquad (2\text{-}14)$$

where $\hat{D}_m$ and $\hat{C}_m$, and D_n and C_n are the median and nominal values of the demand and capacity probability distributions, respectively, V_D and V_C their lognormal standard deviations, and ρ is the correlation coefficient between demand and capacity. Equations 2-13 and 2-14 assume that the random variables representing demand are uncorrelated and likewise for the random variables representing capacity. In most cases, the correlation coefficient between demand and capacity is zero, since the demand and capacity effects are independent. However, in some cases ρ is non-zero, where there is some correlation between the random factors affecting demand and capacity. Examples where the demand and capacity are correlated include rupture of net section in a yielding brace connection of an SCBF and the plastic hinge capacity of a beam outside of a yielded link in an EBF. These are both cases where the demand and capacity are controlled by the same member and therefore variations in material strength and member dimensions are correlated between demand and capacity. Similarly, in reinforced concrete walls, there is a correlation between the wall shear capacity and the induced shear forces that are limited, to some extent, by the flexural strength of the wall. Strong-column weak beam requirements of concrete frames are another example where the force demands imposed by the beams have some correlation to the capacity of the column. However, since the strength of the concrete members depends on certain components that are common to the demand and capacity (e.g., concrete and workmanship) and others that are independent (different reinforcing bars in beams/columns and wall shear/flexure), these examples show that there is not always a clear cut distinction with regards to degree of correlation between demand and capacity. In the absence of other information, it is proposed to assume ρ equal to 0 for components that are clearly independent and ρ equal to 0.5 for components where some correlation is likely to exist.

For the reliability calculations of capacity-designed components, small variance approximations are not taken advantage of when lognormal probability distributions apply, as the LRFD methodolgoy does, and the median and lognormal standard deviation, often called the dispersion, of statistical parameters used instead (V_D and V_C). However, since variance is all likelihood sufficiently small, if mean and coefficient of variation are used instead of median and lognormal standard deviation, the results should be approximately the same.

Assuming the demand and capacity probability distributions are normal (as opposed to lognormal), the expression for the reliability index of capacity-designed components, conditioned upon a specific deformation demand, is:

$$\beta = \frac{C_m - D_m}{\sqrt{\sigma_C^2 + \sigma_D^2 - 2\rho\sigma_C\sigma_D}} \tag{2-15}$$

$$\left(\frac{C_m}{D_m}\right) = \left(\frac{D_n}{D_m}\right)\left(\frac{C_m}{C_n}\right)\frac{\gamma}{\phi} \tag{2-16}$$

$$\sigma_C = \sqrt{\sum \sigma_{x_{Ci}}^2} \tag{2-17}$$

$$\sigma_D = \sqrt{\sum \sigma_{x_{Di}}^2} \tag{2-18}$$

where D_m and C_m are the mean values of load and resistance, respectively, and σ_D and σ_C are their standard deviations.

2.3.2 SAC Demand and Capacity Factor Design

The SAC *Demand and Capacity Factor Design* (SAC-DCFD) methodology is a reliability methodology that was developed as a part of the SAC Federal Emergency Management Agency (SAC/FEMA) program (Cornell et al 2002, Yun et al, 2002). It provides probabilistic framework for seismic design and assessment of structures, recognizing the dynamic and nonlinear displacement basis of the problem, such that a

22

specified performance objective is achieved. The performance objective is expressed as the probability of exceeding a specified performance level. Similar to LRFD, the SAC-DCFD methodology begins with a probabilistic model of demand and capacity and ends with numerical factors (called demand and capacity factors) that are applied to mean or nominal values of the demand and capacity. The framework ensures that if the factored capacity exceeds the factored demand then the specified performance objective is achieved.

The SAC-DCFD design criterion is based on satisfying the following condition:

$$\left\{ \exp\left[-\frac{1}{2}\frac{k}{b}\beta_C^2 \right] \right\}\hat{C}_m \geq \left\{ \exp\left[-\frac{1}{2}\frac{k}{b}\beta_{D|S_a}^2 \right] \right\}\hat{D}_m^{\ P_0} \qquad (2\text{-}19)$$

which can be expressed in terms of factored demand and capacity as:

$$\phi\hat{C}_m \geq \gamma\hat{D}_m^{\ P_0} \qquad (2\text{-}20)$$

where $\hat{D}_m^{\ P_0}$ is the median drift demand under a given ground motion intensity, which in turn is defined as the spectral acceleration with annual probability of P_0 of being exceeded, $\hat{C}_m$ is the median drift capacity, k and b are local "slopes" of the seismic hazard curve (Sa versus mean annual frequency of recurrence) and of the median deformation demand curve (peak drifts versus Sa), respectively. The $\beta's$ are the standard deviations of the natural logs of demand, D, and capacity, C, which are numerically equal to the coefficients of variation, COV's, for smaller values, e.g. V<0.3. The SAC/FEMA use of β follows the tradition of the nuclear industry where the early roots of some of these developments lie. However, in order to avoid confusion with the reliability index from the LRFD scheme and to be consistent with LRFD, the standard deviations of the natural logs of D and C are called $V's$ here (assuming small variance) and the SAC-DCFD equation becomes:

$$\left\{ \exp\left[-\frac{1}{2}\frac{k}{b}V_C^2 \right] \right\}\hat{C}_m \geq \left\{ \exp\left[-\frac{1}{2}\frac{k}{b}V_{D|S_a}^2 \right] \right\}\hat{D}_m^{\ P_0} \qquad (2\text{-}21)$$

The similarities between the SAC-DCFD equation (2-21) and the LRFD one described earlier (3.12) are clear when compared together:

$$\exp\left[-\alpha\beta V_R\right]R_m \geq \exp\left[\alpha\beta V_Q\right]Q_m \qquad (2\text{-}22)$$

Structural analysis (e.g. Incremental Dynamic Analysis) is needed to determine the median drift demand for a given spectral acceleration on a given frame. By following the procedure, a frame is subjected to a ground motion with spectral acceleration, *Sa*, with annual probability P_0 of being exceeded. The outcome is the median drift demand $\hat{D}_m^{P_0}$ under that ground motion intensity. Using the median drift demand calculated, the capacity required to ensure probability as low as P_0 of the demand exceeding the capacity can be estimated as well. Figure 2-4 illustrates the main points of the SAC-DCFD reliability framework. On the right hand side, the spectral acceleration is plotted versus the maximum inter-story drift ratio and on the left hand side versus it is plotted versus the spectral acceleration hazard. Dynamic analyses are performed at different spectral accelerations for several ground motion records. The maximum inter-story drift ratio is recorded for each dynamic analysis, resulting in a distribution, with a median, $\hat{D}_m^{P_0}$, and dispersion, $V_{D|Sa}$, of the maximum inter-story drift demand at specified ground motion intensity. Equation 2-21 can then be used to either calculate the required capacity such that the probability of demand exceeding capacity is tolerable or given capacity, to calculate if the probability is tolerable. Although the demand $\hat{D}_m^{P_0}$ is established by using records of just one *Sa* level, the whole range of *Sa* levels was considered in the development of SAC-DCFD framework, where *Sa* levels were weighted by their relative likelihood of being felt at the site.

2.3.3 FEMA P695 Quantification of Building Seismic Performance Factors

The FEMA P695 *Quantification of Building Seismic Performance Factors* (FEMA, 2009) was developed to evaluate seismic design provisions through inelastic static and dynamic analyses of structural systems under earthquake ground motions. The intention

of the FEMA P695 reliability methodology is to provide a rational basis for establishing global seismic performance factors (SPF's), including the response modification coefficient (R factor), the system overstrength factor (Ω_0) and the deflection amplification factor (C_d), of seismic force resisting systems proposed for inclusion in modern building codes. The underlying basis of the method is to assess structural collapse performance by nonlinear analysis of so-called "archetype designs" and to ensure a consistent risk across all structural system types and materials. The details of the methodology can be found in FEMA P695 *Quantification of Building Seismic Response Parameters* (FEMA, 2009).

The FEMA P695 framework assesses the reliability of structural systems by subjecting median models of structural archetypes, which are considered to closely represent the system considered, to multiple ground motion records of increasing intensity, i.e. the Incremental Dynamic Analysis (IDA), until structural collapse is detected. (Vamvatsikos and Cornell, 2002). Structural collapse occurs when IDA response plot reaches a plateau. Figure 2-5 illustrates the IDA process for a single ground motion. The circles on the figure are the maximum story drift ratios (DR) recorded during dynamic analyses plotted versus the ground motion spectral acceleration. Generally, the DR increases as the spectral acceleration increases until the frame collapses. The DR and spectral acceleration at which collapse is imminent in the simulation are referred to as DR_{SC} and $S_{T(SC)}$ where the subscript SC stands for a simulated collapse mode. Due to both modeling limitations and practicality, some deterioration mechanisms leading to collapse may not be included in the structural models. However, provisions are included in the FEMA P695 methodology to assess the effects of deterioration mechanisms that are not explicitly simulated but could cause collapse. These collapse modes are referred to as non-simulated collapse modes. Examples include fracture in connections or hinge regions of steel moment frame components, axial failure of steel columns or shear and axial failure in reinforced concrete columns. The non-simulated collapse modes are estimated after the incremental dynamic analysis has been performed and for each time history analysis, if the capacity of the non-simulated collapse mode is exceeded, prior to the collapse of the structure according to the time history analysis, the collapse point is

adjusted. Figure 2-5 shows the DR and spectral acceleration of a non-simulated collapse mode, DR_{NSC} and $S_{T(NSC)}$.

Given the inherent variability in earthquake ground motions and possible variability in the nonlinear response of a structural system to different ground motions (see Figure 2-6), the results from the IDA are formulated in a probabilistic framework to evaluate whether the collapse safety is tolerable. Based on the maximum considered earthquake (MCE) ground motions, the so-called collapse margin ratio, CMR, is calculated. The CMR is the median collapse level spectral acceleration, S_{CT}, at the period of the system, T, divided by the MCE spectral acceleration, S_{MT}, at the period of the system, T. To account for the unique spectral shape of extreme ground motions and their effect on behavior, the CMR is then adjusted (based on the seismic hazard intensity and the nonlinear deformation characteristics of the building) to calculate an adjusted CMR, or ACMR. Based on the ACMR, the system is either deemed acceptable or unacceptable.

A second evaluation on whether the collapse safety is tolerable is to calculate the probability of collapse under the MCE ground motions. The IDA response histories are used to create a collapse fragility curve through a cumulative distribution function, CDF (see Figure 2-7). The collapse fragility curve relates the ground motion intensity to the probability of collapse. The collapse fragility curve is assumed to be lognormal with a median equal to the ACMR and a specified dispersion. The specified dispersion, whose value depends on how well the dynamic analyses are believed to capture the major sources of uncertainty that contribute to variability in collapse capacity, varies from 0.275 to 0.950. From the collapse fragility curve, the probability of collapse under the MCE ground motions is calculated, where the tolerable value is 10%.

The uncertainties considered in the FEMA P695 methodology are the following: a) Record-to-Record Uncertainty, due variability in frame response to different ground motion records b) Modeling Uncertainty, which includes uncertainties involved in the idealization of the structural behavior and the characterization of the modeling parameters for analysis c) Design Requirements-Related Uncertainty, which is based on the completeness and appropriateness of the design requirements and the extent which the

archetype systems represents the actual structural design of the systems d) Test Data-Related Uncertainty, which is based on the robustness and comprehensiveness of the test data used to support the development of nonlinear archetype analysis models. Some of these uncertainties are modeled explicitly and some are incorporated through judgment with the use of the specified collapse fragility dispersion It should be pointed out that failure of capacity-designed components is not explicitly accounted for in the FEMA P695 dynamic analysis procedure and collapse fragility development. However, it could be argued that the fraction of the collapse fragility curve dispersion due to Modeling Uncertainty and Design Requirements-Related Uncertainty account for the risk of failure of capacity-designed components.

In a related effort, as part of Project 07, the MCE seismic design maps have been revised to provide more consistent collapse risk safety throughout various regions of the United States. (Luco et al., 2007) The basis of this effort is to achieve a uniform target collapse risk of 1% in 50 years and is therefore a move from the previous uniform-hazard ground motions to uniform-risk ground motions. Recognizing that collapse capacity of structures is uncertain, the use of uniform-hazard ground motions for design results in structures with non-uniform collapse probability due to site-to-site variability in the shape of ground motion hazard curves. To calculate collapse probabilities, lognormal collapse fragility curves with dispersion of 0.8 (partially based on FEMA P695 analyses results and recommendations) are integrated with site ground motion hazard curves. With a fixed dispersion, only a single value of the lognormal collapse capacity curve is required to fully describe it, and based on FEMA P695 recommendations of 10% probability of collapse at the MCE intensity, that is the value chosen. The MCE intensity is then increased or decreased for a given site, depending on if the calculated collapse probability exceeds the 1% target or not. These combined efforts are significant since, for the first time, they codify a target collapse safety risk that can provide the basis for establishing seismic design guidelines. The calculated collapse probability depends on the specified dispersion of the collapse fragility curve. Whether the dispersion of 0.8, and therefore the target 1% collapse probability, is assumed to include the possibility of failure of capacity-designed components is unclear.

2.3.4 Component vs. System Reliability

The target reliability of a component should be related to the impact of its failure on the system's performance, as the ultimate goal is to limit the annual probability of system collapse to a tolerable level. However, achieving this ultimate goal is far from an easy task considering all the variables and uncertainties involved in the process. Calibrating the probability of failure of each component within a system, such that the annual probability of system collapse is tolerable, can therefore prove to be infeasible. One is thus often forced to focus on component structural reliability with the assumption that by satisfying reliability requirements at the component level, the system reliability is tolerable. However, with the component failure consequences unknown, it can be challenging to decide upon the required component reliability.

Figure 2-8 is a schematic diagram of the full scope of a reliability analysis of a seismic resistant system. The figure is separated into 6 different levels based on the details and complexities of the reliability analysis, ranging from a component to a full structure reliability analysis. At the top of the figure is the actual structure of interest. The end goal is to ensure its reliability, i.e. to limit its annual probability of collapse to a tolerable level. However, it is essentially impossible to analyze the reliability of the actual structure so the best alternative is to create a detailed analytical model of the complete idealized structure, a model that is believed to capture the structure's behavior accurately (Level 5). This includes modeling the whole seismic force-resistant system (SFR system) and the lateral resistance of the gravity system, including all possible failure modes, to capture the true capacity of the structure and the benefits of its redundancy. Further, due to variability in components' strengths and ductilities, including the variability of all random variables (modeling uncertainty) is necessary when calculating the structure's reliability. Similarly, the correlation between the random variables needs to be included as it counteracts the positive benefits of redundancy. Currently, seismic design codes do not take advantage of the lateral resistance of the gravity system and in return, no special detailing of the gravity system is required with regards to seismic forces. Therefore, taking advantage of the possible reduction in collapse probability due to the inclusion of the gravity system in the analysis might not be

warranted. The Level 4 analysis in Figure 2-8 is in all respects the same as the Level 5 analysis except the lateral resistance of the gravity system is neglected but redundancy within the SFR system is included. Level 3 further simplifies the analysis by only modeling a part of the SFR system, illustrated in Figure 2-8 by modeling only one of the two bays comprising the SFR system. The Level 3 analysis is therefore one where the benefits of redundancy are limited.

The reliability analyses described in Level 3, 4 and 5 are very detailed, and time and computer intensive, largely due to the direct inclusion of modeling uncertainty. Including modeling uncertainty requires multiple realizations of each structure with different random variable input values. Currently, this renders them fairly impractical, especially if the goal is to analyze the reliability of a whole suite of structures subjected to different ground motion records at multiple intensities. To go around that obstacle, all the aforementioned analyses levels can be performed with median models to capture the median response of the structure. That causes Level 3 and Level 4 to merge into effectively the same analysis, as redundancy and correlation within the SSF system is now neglected, and both become similar to Level 5 analysis, except there the gravity system is included. This is essentially the approach that FEMA P695 takes to assess the collapse risk of seismic resistant systems. The analytical models are median models where expected values of all model parameters are used. To account for the fact that modeling uncertainty is not directly included in the analysis, the dispersion of the resulting collapse fragility curve is specified directly, rather than being based only analysis results, and its value depends largely on the ground motion variability and the overall confidence in the analytical model.

Level 2 is a simplified SFR system where only a system subassembly is modeled. By modeling only a system subassembly, the number of random variables is significantly reduced. Reducing the number of random variables allows for possibility of performing a full uncertainty analysis, which can assist in evaluating whether some of the assumptions made in the previous levels are justified, e.g. the specified dispersion in collapse fragility. Level 1 is the simplest but most commonly used reliability analysis. It is a component

reliability analysis with no system behavior considerations. Level 1 analysis is the basis of the LRFD component reliability methodology.

The reliability methodologies discussed here, LRFD and FEMA P695, each address the objectives they set out to meet but provide limited information on the relationship between component and system reliability. LRFD is a component limit state methodology where objective is to limit the probability of exceeding a specific limit state. It does not explicitly account for system reliability considerations except that it requires lower probability (higher β) of exceeding connection limit states than member yielding limit states based on the believe that exceeding connection limit states has more severe consequences on the system reliability than exceeding member yielding limit states. (Galambos, 1990). The higher reliability index for connections reflects a long tradition of designing connections stronger than the members connected by them and in the development of LRFD the target probability of connection failure was set arbitrarily at 2.5 orders of magnitude lower than member failure, which is represented in the recommended reliability indices of 4.5 and 3.0 for connections and members, respectively. (Ravindra and Galambos 1978, Ellingwood et al. 1980) Acknowledging that the LRFD limit state design does not explicitly account for system reliability, Galambos (1990) suggested a further distinction between different limit states based on the presumed consequences of exceeding them on the system reliability by introducing a new resistance/capacity factor, a "system factor" (ϕ_s) that could be multiplied with the already established ϕ-factors. The suggested ϕ_s–factors ranged from 0.7 if exceeding the limit state results in complete damage to 1.1 if exceeding if it results in only slight damage.

On the other hand, the FEMA P695 methodology evaluates the reliability of systems and it generally lacks the resolution to assess the impact of the reliability of individual components on the system reliability. Redundancy within the structural system and uncertainty around components' strength, stiffness and ductility is not included in the methodology. Also, the non-simulated collapses modes, which are based on exceeding deterministic values in the analysis (drift, rotations etc.), generally assume system collapse if those values are exceeded. Capacity-designed components are assumed not to fail in the methodology.

The SAC-DCFD methodology can be applied either at the component level or at the system level, and can therefore be applied at any of the six levels listed in Figure 2-8. It was developed specifically to check component or system limit states in seismic design with recognition of the dynamic and nonlinear displacement basis of the problem. It results in an annual probability of the chosen limit state being exceeded while only checking it at one ground motion intensity. At the system level, similar to the FEMA P695 methodology, it lacks the resolution to assess the impact of the reliability of individual components on the system reliability.

Still, there are ways to assess the relationship between component reliability and system reliability that can at least assist with understanding the impact of certain design criteria. Sensitivity analysis can provide very insightful information on the response of structures when model input parameters are varied. Often the approach is taken to fix all variables at median values and then vary variables individually above and below the median. Although a deterministic analysis, it provides information on which random variables have the most impact on the structural response and has been used in many studies, e.g. in Porter et al (2002) to examine which sources of uncertainty most strongly affect the repair cost of a high-rise non-ductile reinforced-concrete moment-frame building in a future earthquake. For many capacity-designed components, e.g. brace connections, sensitivity analysis can provide limited information if not properly performed. Increasing connection strength is likely not to change the structural response and unless the connection strength is decreased enough, such that it fractures in the structural analysis, decreasing the strength might not change the structural response either.

If the distributions of all, or at least most major, variables and the correlations between them are known, realizations of each modeling random variable can be generated using Monte-Carlo simulation methods (Melchers, 1999; Rubinstein, 1981) This process is then repeated multiple times and for each set of simulated random variables, the system reliability is assessed through methods such as incremental dynamic analysis. The end result is a probability of collapse (or any other performance measure being analyzed) distribution associated with the distribution of the input random variables. Vamvatsikos and Fragiadakis (2009) and Dolsek (2009) both used Monte Carlo methods

combined with an efficient Latin Hypercube sampling method, a variance reduction technique, to propagate model parameter uncertainty to the actual system seismic performance on a nine-story steel moment resisting frame and a four-story reinforced concrete frame, respectively. Although straightforward to implement and perhaps the most comprehensive method to assess system reliability, Monte Carlo methods are computationally intensive as the number of required simulations to achieve a stable solution can be very large, especially when assessing small probabilities of failure, and the time to complete each analysis is non-negligible. In addition, as all random variables are lumped together, the Monte Carlo simulation methods give limited insight on the influence of individual random variables, rather the impact of the uncertainties of random variables as a whole on the system behavior. To assess the influence of individual variables, the above procedure needs to be performed again with different distributions for the input random variables, i.e. sensitivity analysis, which could be taken to represent a change in the design provisions, thus further increasing analysis the time.

Response surface (Melchers, 1999; Pinto et al., 2004) is another method that can be employed to assess system reliability with modeling uncertainties included. It can be thought of as a hybrid technique between sensitivity analyses and full Monte Carlo simulations, or any other technique that requires a closed form limit state function. By systematically varying the input parameters such that most of the sample space is covered and then assessing the system response of interest for each case, a limit state function or a response surface is created by fitting a functional form between the input parameters and the system response. With the relationship between the input parameters and the system response known, a full Monte Carlo simulation can be performed using that estimated functional form with minimal computational effort. Liel (2008) used Monte Carlo simulations coupled with a response surface method to evaluate the collapse uncertainty of reinforced concrete buildings, showing that modeling uncertainties will in most cases both increase the dispersion of the system response as well as decrease the predicted median collapse point compared to median model results. Generally, the response surface method has worked well in structural reliability assessments, but its accuracy depends largely on the characteristics of the limit state function, with highly nonlinear functions providing less reliable results. (Melchers, 1999; Rajashekhar and Ellingwood, 1993)

2.4 Summary

Capacity design provisions are included in most modern seismic design codes. The goal of employing capacity design principles is to ensure ductile response and energy dissipation capacity in seismic resisting systems. The method to achieve this goal is to confine significant inelastic deformations to selected structural components while others are designed with sufficient strength to remain essentially elastic. While the concept is clear, its implementation is more challenging. In an attempt to achieve the goals of capacity design, US structural design codes adjust the design demand and the design capacity by applying various factors to the relevant limit state equations. ASCE-7-10 includes an overstrength factor, the Ω_0-factor, which is meant capture the expected capacity of deformation-controlled components and therefore the increased loads on force-controlled members above the seismic design loads. The AISC *Seismic Provisions* have made progress in addressing some of the issues of capacity-based design by introducing the R_y-factor to provide a consistent basis to evaluate "expected yield strength" of deformation-controlled components. Other factors, such as factors to account for strain hardening, the C_{pr}-factor in the AISC *Prequalified Connection Requirements* and the β-factor used to adjust for compression strengths of BRB´s have also been introduced to assist in confining significant inelastic deformations to selected components. Similarly, to assist in achieving the goals of capacity design ACI 318-08 includes a factor of 1.25 to account for strain hardening in reinforcing steel in shear strength design. However, these factors, which are intended to create a margin between demand and capacity to ensure the desired behavior, have largely been established in an ad-hoc manner, resulting in inconsistencies in the assumed deformation demands of components and therefore inconsistencies in the reliability of capacity-designed components.

Many methodologies have been established to assess structural reliability. Here, three of them were presented. The *Load and Resistance Factor Design* (LRFD) methodology is a component methodology that was developed in the 1970's for static, strength-based problems under various load types. It ensures a tolerable component reliability index for a specified set of load and resistance factors. The SAC *Demand and Capacity Factor Design* (SAC-DCFD) methodology is a reliability methodology that was

developed as a part of the SAC Federal Emergency Management Agency (SAC/FEMA) program (Cornell et al 2002, Yun et al, 2002). SAC-DCFD was developed specifically for seismic design and it ensures a tolerable annual probability of demand exceeding capacity. Demand and capacity can be defined at the component level or at the system level. The FEMA P695 *Quantification of Building Seismic Performance Factors* is a system reliability methodology, developed to evaluate seismic design provisions through inelastic static and dynamic analyses of structural systems under earthquake ground motions with the objective of ensuring consistent risk across all structural system types and materials. In the FEMA P695 methodology, the tolerable probability of collapse for a structural system is 10% at the MCE ground motion intensity. In the development of new MCE seismic design maps as part of Project 07, the collapse fragility curves developed by FEMA P695 were integrated site seismic curves and the collapse fragility curves adjusted until a target collapse probability of 1% in 50 years was attained. These two efforts, FEMA P695 and Project 07, are the first to explicitly state target system reliability for seismic design.

To relate the reliability of a component to the system reliability, the consequences of component failures need to be known, a task far from easy considering all the variables and uncertainties involved in the process. Many methods are available to assess the relationship between component and structural reliability, each with its pros and cons. Sensitivity analysis is simple and a straightforward to implement and provides important information on which variables have the largest impact on the structural response. However, it is both deterministic in nature and may give limited insight into the response sensitivity of capacity-designed components whose values may not change the response unless a certain threshold is exceeded. Monte Carlo simulation method is easy to implement and perhaps the most comprehensive method to assess structural response. Still, for most structural reliability assessments where nonlinear analysis is required, it may prove to be too computationally intensive and provide limited insight into the impact of individual variables. The response surface method combines the two methods mentioned above, and has been shown to work well in structural reliability. Its accuracy however, is very dependent on the shape of the limit state function, with highly nonlinear functions providing less accurate results.

Table 2-1: Summary of Capacity Design Requirements in the AISC (2010) Seismic Provisions

Component or System	AISC Section	Description of Capacity Demand Requirements[*]
Material Properties	A3	R_y and R_t factors for determining expected yield and ultimate strengths of steel materials (Table A3.1)
Columns	D1.4	Required axial strength provisions, based on (a) amplified seismic load, (b) load from yielding members including the effects of material overstrength and strain hardening, (c) limiting resistance of foundation
Column Splices	D2.5	Required strength of welded splices in seismic resisting system based on (a) 200% of calculated loading effect, or (b) at least 50% of the strength of the expected yield strength of column flanges ($R_yF_yb_ft_f$).
Column Bases	D2.6	Required strength of bases shall be lesser of a) M_{pc}/H (shear) and $1.1R_yF_yZ_x$ (moment), or (b) the shear/moment calculated using the amplified seismic load.
SMF Connections	E3.6	Required shear strength of beam column connections shall be based on load combinations with amplified seismic load, $E = 2[1.1R_yM_p/L_h]$. Other design aspects covered by pre-qualified connection provisions or demonstrated by tests.
SMF Columns	E3.4	Minimum required column flexural strengths determined without ϕ factors and compare with beam flexural strengths calculated based on $1.1R_y\,F_yZ_x$
SMF Column Splices	E3.6	Minimum required flexural strength equal to $R_y\,F_yZ_x$ and shear equal to $\Sigma M_{pc}/H$.
SMF Prequalified Connections	AISC (2010b)	Connection welds, bolts and other components generally designed to resist maximum probable moment, $C_{pr}R_yF_yZ$, where C_{pr} is a factor for strain hardening (determined as average of F_y and F_u and limited to 1.2). Resistance factors used in conjunction with the maximum probable moment are $\phi_d = 1.0$ for ductile limit states and $\phi_n = 0.9$ for non-ductile limit states.
SCBF Brace	F2.5	For braces with net section issues, the minimum required tensile strength at the net section is $R_y\,F_yA_g$ or the maximum force that can be delivered by the system.
SCBF Brace Connection	F2.6	Minimum required (a) axial strength of $R_y\,F_yA_g$, less than amplified load effect, (b) flexural strength $1.1R_yM_p$, (c) compressive strength $1.14F_{cre}A_g$
SCBF Chevron Beam	F2.4	Min. required flexural strength based on unbalanced vertical force from $R_yF_yA_g$ in tension brace and 0.3 times $1.14F_{cre}A_g$ in compression brace, plus gravity loads.
SCBF Columns	F2.3	Required strength based on larger of a) load from all braces at their expected strength b) tension braces at their expected strength and compression braces at their expected post-buckling strength but never to exceed load from amplified seismic load in which all compression braces have been removed.
EBF Link-Column Connection	F3.6	Required strength of link-to-column connection is the nominal shear strength of the link V_n at the maximum rotation angle. Testing is required to demonstrate deformation capacity of connection for some cases.
EBF Braces	F3.4	Minimum required strength equal to axial force associated with 1.25 or 1.4 (I-shaped/box shaped) times expected shear strength of link, R_yV_n.
EBF Beams	F3.4	Minimum required strength equal to moment and axial force associated with 1.25 or 1.4 (I-shaped/box shaped) times expected shear strength of link, $R_y\,V_n$. The available beam strength may also be increased by R_y.
EBF Beam-Column Connections	F3.6	For EBF's with moment connections, the required strength of beam-column connections is the same as for OMF, $1.1R_yM_p$.
BRBF Beams and Adjoining Members.	F4.2	Required strength of adjacent members (e.g., Chevron beams) and their connections shall be based on adjusted brace strengths, $\beta\omega R_yP_{ysc}$ in compression and ωR_yP_{ysc} in tension.
BRBF Brace Connections	F4.6	Required strength of brace connections shall be 1.1 times the adjusted brace strengths in tension and compression

[*]For explanation of symbols, see Notations section

Table 2-2: Summary of Capacity Design Requirements in the ACI 318-08 (2008)

Component or System	ACI Section	Description of Capacity Demand Requirements[*]
Material Properties	21	A factor of 1.25 is applied to reinforcing steel stress, f_y, for shear strength design forces to account for strain hardening.
Reinforcement	21.1.5	a) The actual yield strength based on mill tests does not exceed f_y by more than 18,000 psi; and b)The ratio of the actual yield strength is not less than 1.25
IMF Shear Strength Requirements	21.3.3	Minimum required shear strength of beams and columns determined with ϕ factors shall exceed: a) The shear due to nominal moment strength developing at each restrained end b) The maximum shear from design where the earthquake demand is twice that prescribed in building codes
SMF Columns	21.6.2	Minimum required nominal column flexural strengths determined without ϕ factors and compare with factored nominal beam flexural strengths: $\Sigma M_{nc} \geq (6/5)M_{nb}$
SMF Shear Strength Requirements	21.6.5	The design shear force, V_e, shall be determined from consideration of the maximum probable moment strengths, M_{pr}, at each and of the member. M_{pr} is determined using $\phi = 1.0$ and a reinforcing steel stress equal to at least $1.25f_y$
SMF Joints	21.7.2	Joint shear force generated by the flexural reinforcement is calculated for a stress of $1.25f_y$ in the reinforcement.
Precast SMF Ductile Connections	21.8.2	Minimum required nominal shear strength, V_n, without ϕ factors to exceed $2V_e$ of flexural members where V_e is calculated in 21.6.5 using $1.25f_y$ for reinforcement stress.
Precast SMF Strong Connections	21.8.3	Minimum required design strength of connections, S_n, with ϕ factors to exceed the probable strength at intended yield locations, S_e, calculated using $1.25f_y$ for reinforcement stress and $\phi = 1.0$. For column-to-column connections: $\phi S_n \geq 1.4S_e$, $\phi M_n \geq 0.4M_{pr}$ and $\phi V_n \geq V_e$

*For explanation of symbols, see Notations section

Table 2-3: Relationship between probability of failure and the reliability index, β

Probability of Failure	Reliability Index, β
0.50	0.00
0.25	0.67
0.15	.99
0.10	1.28
0.0	1.64
0 01	2.33
10^{-3}	3.09
10^{-4}	3.72
10^{-5}	4.26
10^{-6}	4.75

$$V = V_{DBE}/R$$
$$\Delta_{In} = C_d\Delta$$
$$\Omega = V_{u,exp}/V$$
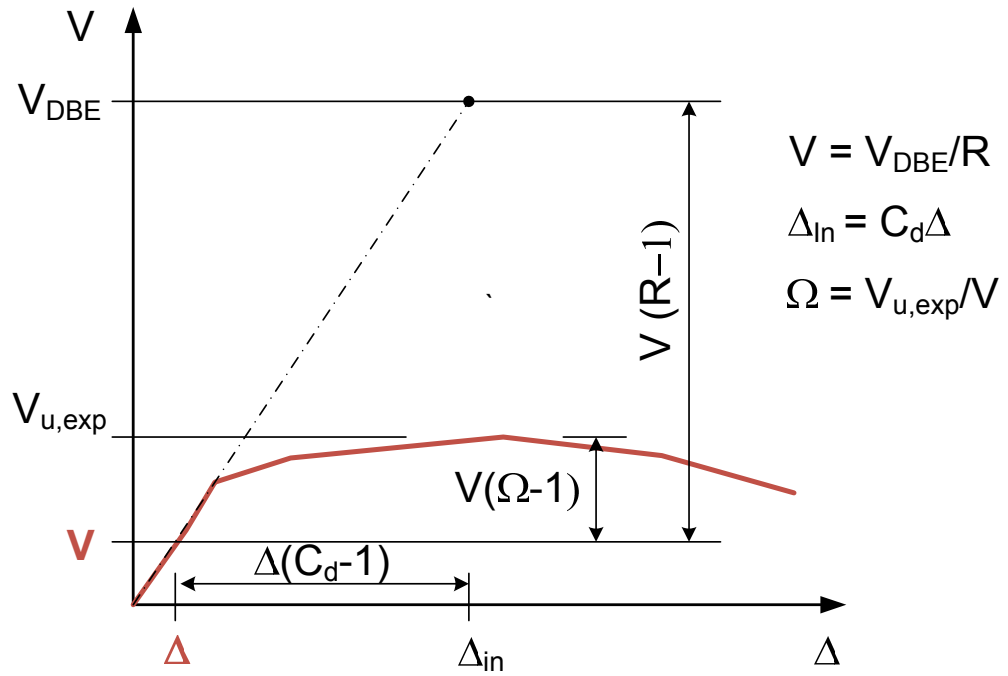
Figure 2-1: Idealized inelastic base shear versus story drift curve
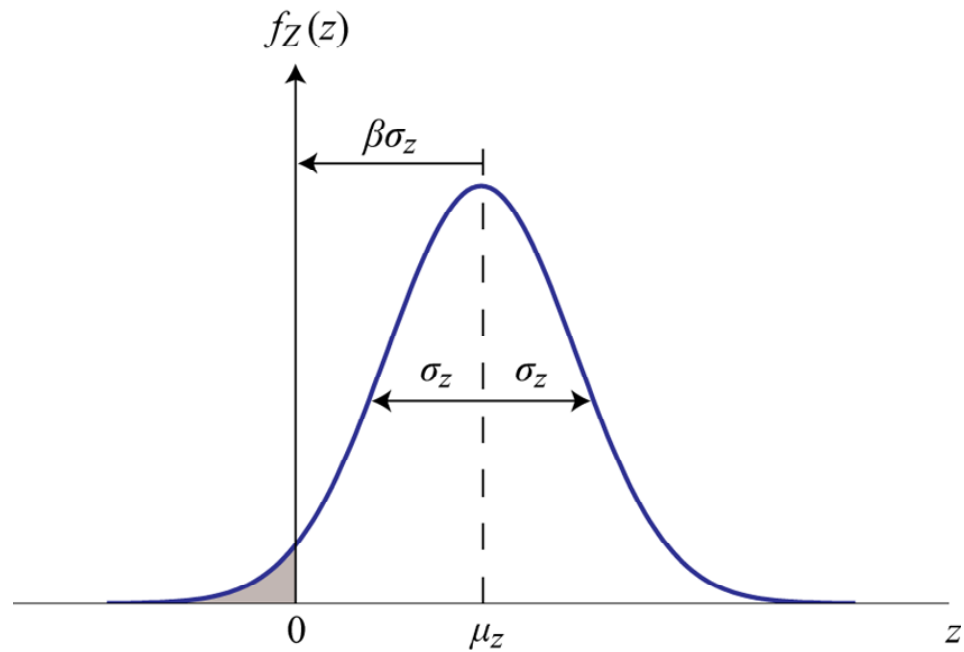
Figure 2-2: Illustration of the reliability index, β, and its relationship with the failure criterionrepresented by z<0
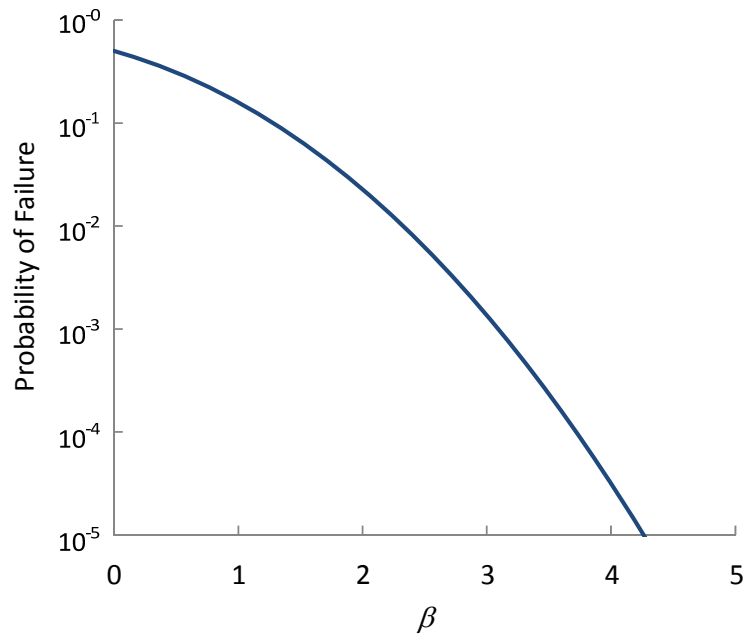
Figure 2-3: Relationship between probability of failure and the reliability index, β
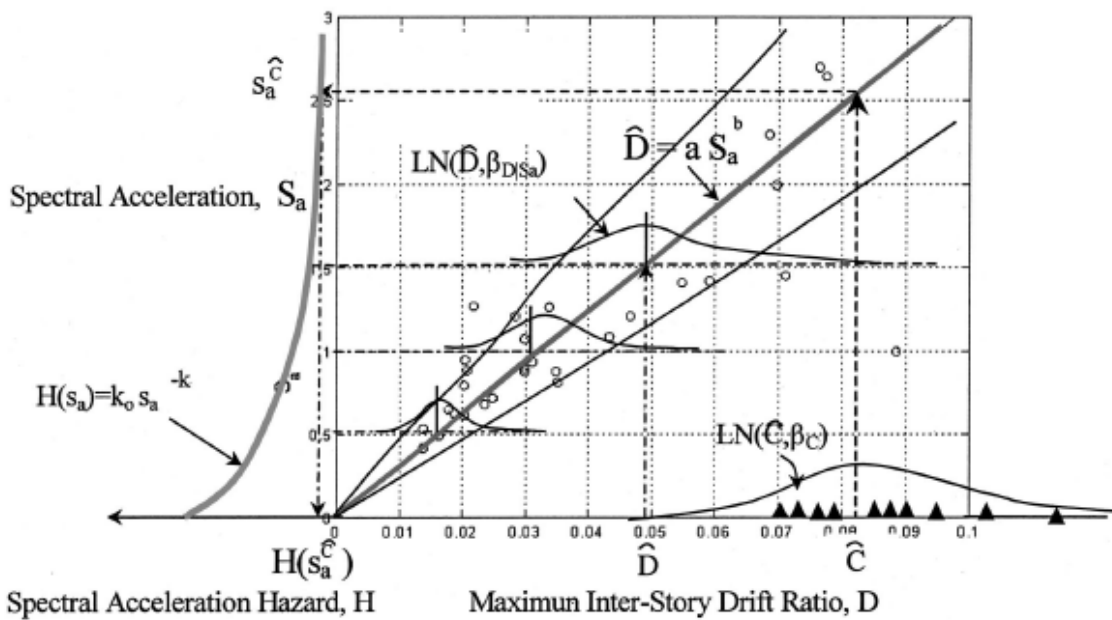
Figure 2-4: Illustration of the SAC-DCFD reliability framework (Image from Cornell et al., 2002)
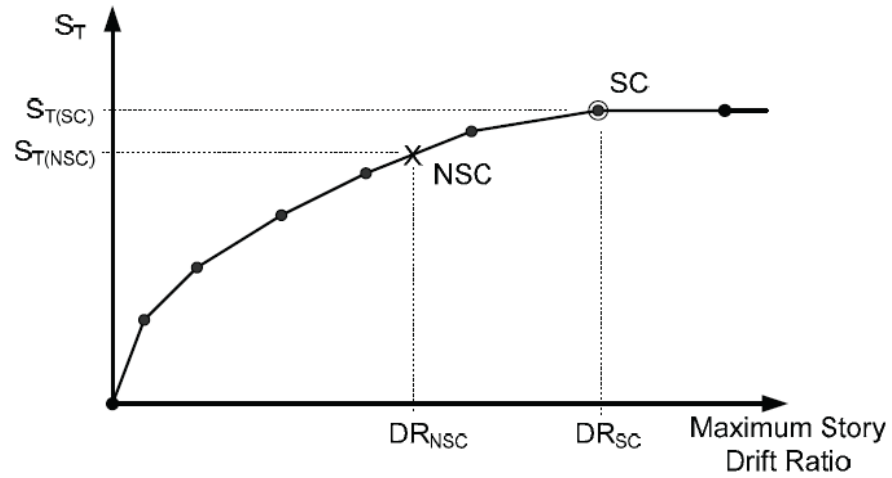
Figure 2-5: Collapse of a system with simulated and non-simulated collapse modes using IDA (Image from FEMA, 2009).
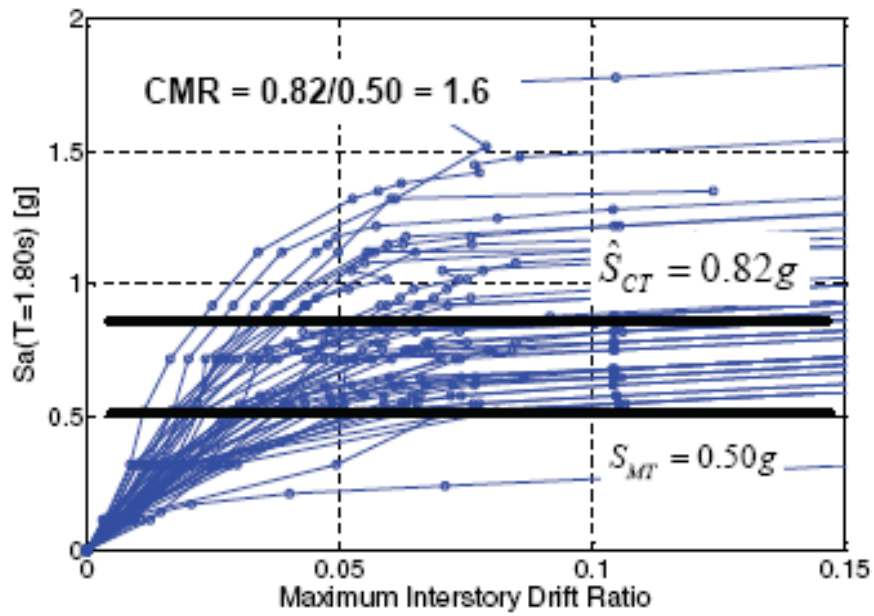
Figure 2-6: IDA response plot and collapse margin ratio (Image from FEMA, 2009).
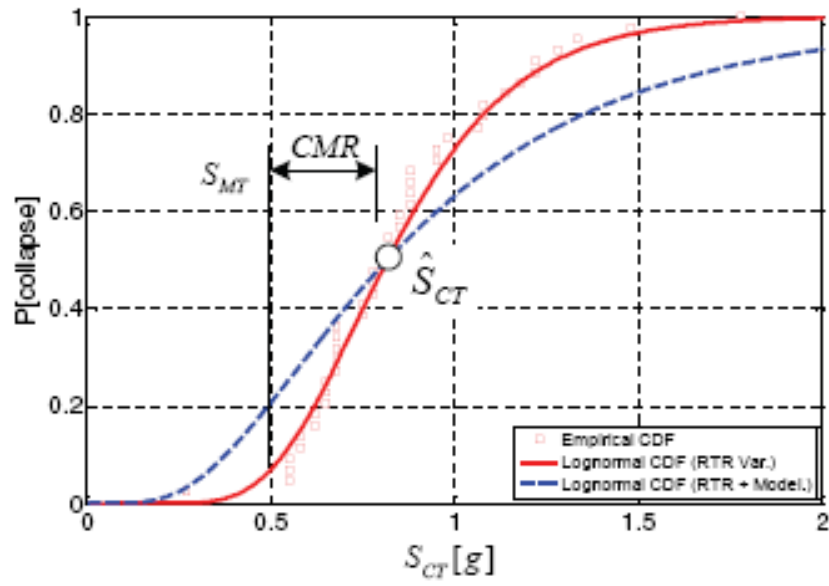
Figure 2-7: Collapse fragility curves (Image from FEMA, 2009).

Actual Structure

5) Complete Idealized Building System (SFR + Gravity)
- Full Uncertainty or Simplified β's
- Member Overstrength
- Redundancy and Correlation
- Gravity System Effects Included
- Capacity Designed Elements Included/Excluded

4) SFR System with Redundancy
- Full Uncertainty or Simplified β's
- Member Overstrength
- Redundancy and Correlation
- No Gravity System
- Capacity Designed Elements Included/Excluded

FEMA P695 Archetype
- Median Models
- Simplified β's
- Capacity Designed Elements Excluded
- FR Connections Included in Braced Frames

3) Archetype SFR System with Limited Redundancy
- Full Uncertainty or Simplified β's
- Member Overstrength
- No Gravity System
- Capacity Designed Elements Included/Excluded

2) Simplified SFR System
- System Subassembly
- Full Uncertainty of Selected Components
- Member Overstrength

Current LRFD
- Component Reliability

1) Components
- No System Considerations
- Variability in Demand and Capacity

Figure 2-8: Structural Reliability: A schematic diagram of different levels of complexity in structural reliability models. While the goal is to evaluate the actual structure's reliability, most reliability analyses are performed at the component level, a system subassembly level or at best with simplified models of the actual structure where multiple variables and uncertainties are excluded from the analysis. SFR System = Seismic Force Resisting System

41

Chapter 3

A Reliability-Based Methodology for Establishing the Required Design Strength of Capacity-Designed Components

3.1 Introduction

In this chapter a reliability-based methodology is presented for establishing the required design strength of capacity-designed components. The goal is to provide a framework that developers of design standards can use when establishing the required design strengths of capacity-designed components that result in consistent reliability between different systems. The chapter begins with a detailed description of the development of the methodology, from the examination of deformation-controlled components´ behavior to the determination of how capacity-designed component´s failure affects the system reliability. Special attention is given to the impact of the system response modification factor, i.e. the R-factor, and system overstrength on the reliability of capacity-designed components.

Although a component reliability methodology, the capacity design reliability methodology considers both system design parameters that affect component reliability as well as the relationship between component and system reliability. The methodology incorporates relevant aspects of the LRFD component reliability methodology, the FEMA P695 system reliability methodology and risk consistent MCE maps of Project 07. Guidelines for implementation of the methodology are provided.

3.2 Development of the Methodology

The reliability-based methodology for establishing the required design strength of capacity-designed components utilizes the well-established LRFD component reliability methodology with appropriate adjustments to address issues specific to capacity-based design. The design strength of capacity-designed components is set by adjusting the load and resistance factors, γ and ϕ, until desired reliability is achieved. To be consistent with capacity-based design terminology, load and resistance is referred to as demand and capacity, and similarly, the load and resistance factors as demand and capacity factors and collectively as capacity design factors. Demand and capacity factors are then applied to nominal values of demand and capacity to ensure the failure probability is less than that specified as tolerable. When demand and capacity probability distributions are lognormally distributed, the basic equation to calculate the ratio between capacity design factors is:

$$\frac{\gamma}{\phi} = \frac{\hat{D}_m}{D_n} \frac{C_n}{\hat{C}_m} \exp\left(\beta_{R,Ha} \sqrt{V_C^2 + V_D^2 - 2\rho V_C V_D}\right) \qquad (3\text{-}1)$$

where $\hat{D}_m$ and $\hat{C}_m$, and D_n and C_n are the median and nominal values of the demand and capacity probability distributions, respectively, V_D and V_C their lognormal standard deviations, and ρ the correlation between demand and capacity. The capacity design reliability index, $\beta_{R,Ha}$, provides a measure of probability of demand exceeding capacity of capacity-designed components. Equation 3-1 is a re-arrangement of the LRFD Equations 2-11 and 2-12 from before, except that the definition and meaning of certain terms are different.

The key differences between the calculation of capacity design factors as compared to the conventional LRFD formulation is in the way the capacity design reliability index, $\beta_{R,Ha}$, and the demand parameters are selected. The demand in capacity-based design is based on the strength capacity of the deformation-controlled components, as opposed to more conventional loading effects due to dead, live and wind loads. The induced forces from the deformation-controlled components can also vary depending on the deformation

44

demands in the structure. The reliability index in the LRFD methodology was originally calibrated to pre-LRFD design equations and then used as a comparative value for different failure modes. The reliability index, $\beta_{R,Ha}$, in Equation 3-1 serves a similar purpose but takes the system effects (i.e. the system´s response modification coefficient, or R-factor and member overstrength) and the system's site ground motion hazard curve into consideration. The subscript of the reliability index refers to the influence of the R-factor and the site ground motion hazard curve (*Ha*) on the required index. The goal is to attain a consistent level of risk due to failure of capacity-designed components in various structural systems. Equation 3-1 assumes lognormal probability distributions. If the probability distributions are not lognormally distributed, Equation 3-1 would need to be reformulated.

The demand in capacity-based design is unique relative to other design concepts in the sense that the demand on force-controlled components originates mainly from other components within the system, i.e. from the deformation-controlled components as they undergo inelastic deformation during seismic events. The design of the deformation-controlled components therefore needs to be included in the methodology. Figure 3-1 shows brace responses when braces are subjected to different cyclic loading protocols: a far-field and a near-field tension protocol. A common characteristic of both tests is that the braces yield in tension at relatively low deformations. This results in brace connections experiencing demands close to their maximum tensile demands at relatively low deformations: deformations, which are likely to occur under low to moderate earthquake intensities. Beyond this, one can see that the loading protocol can affect the maximum tension forces reached in the braces. Figure 3-2 demonstrates how brace forces develop under random earthquake loading. It shows incremental dynamic analysis results for a single story SCBF where both the maximum drift (Figure 3-2c) and the maximum brace force (Figure 3-2b) are recorded. For a given probability distribution of the brace connection capacity and using the brace demand distribution from the analyses, the probability of connection failure can be calculated, e.g. using Equation 2-2 from Chapter 2. It is evident that the probability of connection failure is negligible before brace yielding and then saturates as the braces reach their maximum demands (Figure 3-2d). The probability of connection failure can be controlled through the γ/ϕ-ratio, which

defines the connection capacity relative to the demand. Referring to Fig. 3-2d, the spectral acceleration when yielding initiates is the only other parameter needed to describe the relationship between the probability of connection failure to spectral acceleration demand. This behavior is likely to apply equally to other deformation-controlled components. Predicting the ground motion intensity causing initiation of deformation-controlled member yielding, $Sa_{y,exp}$, is therefore pivotal in the development of the methodology. A more detailed discussion of the single story SCBF incremental dynamic analysis results can be found in Chapter 4.

When designing deformation-controlled components, the required design strength is based on the seismic design forces of the overall frame. Following the *ASCE 7* design standard, the seismic design forces are based on the spectral acceleration for the maximum considered earthquake (MCE) at the fundamental period of the structure, Sa_{T1}. This spectral intensity is then (a) multiplied by two-thirds to get the design basis earthquake (DBE) intensity and (b) divided by the frame's response modification coefficient, or R-factor, to get the design spectral acceleration, Sa_{design}. Thus, the seismic design forces are associated with earthquake intensities significantly lower than the maximum considered earthquake. Still, due to the use of capacity (resistance) factors (ϕ), member over-design and the use of nominal material values and nominal strength equations, yielding is not expected to initiate at Sa_{design}, but rather at some spectral acceleration larger than Sa_{design}. However, unlike Sa_{design}, $Sa_{y,exp}$ is not unique for the whole structure as it is based on components' overall over-design, which varies from one component to the next and between stories. The component with the lowest $Sa_{y,exp}$ is therefore most likely to yield first, i.e. it is the weakest link, and could therefore possibly shield other components from yielding. In addition, when the demand on capacity-designed components originates from multiple deformation-controlled components, $Sa_{y,exp}$ is not as clearly defined since overstrength of the different deformation-controlled components varies.

To illustrate these points, an example of a 3-story SCBF is used. Figure 3-3 shows an elevation view of the frame. The braces are the deformation-controlled components, while the brace connections, beams, columns and foundation are capacity-designed

components. The demand on a given brace connection on the 2nd story originates from the brace it is connecting to the frame. If the tension and compression capacity of the braces in that story are identical, $Sa_{y,exp}$ for the demand on that connection can be calculated based on the brace overdesign multiplied by Sa_{design}. The fact that braces in concentrically braced frames work in pairs and have different tension and compression capacities, complicates the calculations, but this is discussed later. The same calculations can be done for the 1st and 3rd story, and unless optimally designed, the calculated $Sa_{y,exp}$ for those will differ from each other and from the 2nd story. Similarly, $Sa_{y,exp}$ for the demand on a beam in a given story is the same as it is for the brace connections in that story. The difference is that the demand on a beam originates from both braces in a given story. As this example demonstrates, $Sa_{y,exp}$ can vary from story to story. Therefore, for the demand on the 1st story columns, which is based on the braces above yielding and buckling, there is no clear $Sa_{y,exp}$. $Sa_{y,exp}$ becomes more indistinct as the number stories and braces above increases since the likelihood of simultaneous yielding or buckling of the braces decreases as the number of them increases. As will be demonstrated with columns in multi-story braced frames in Chapter 5, capacity design principles do often not explain the demand on columns well since the full capacity is rarely reached.

Figure 3-4 shows an idealized static nonlinear pushover curve of a story in a 1-bay braced frame, either a single story frame as in Figure 3-2 or a story within a multi-story frame. Of interest is to estimate the story shear, which can be related back to spectral acceleration that causes yielding of the tensile brace. The design story or base shear is V. Due to over-design for any number of reasons, the factored nominal story or base shear strength, ϕV_n, exceeds V. Excluding capacity factors, (ϕ) and using expected material values and strength equations, as opposed to nominal ones, the expected story or base shear yield strength, $V_{y,exp}$, will exceed ϕV_n and due to strain hardening, the expected story or base shear ultimate strength, $V_{u,exp}$ exceeds $V_{y,exp}$. In Figure 3-4, $V_{y,exp}$ corresponds to the second kink in the idealized static nonlinear pushover curve, corresponding to the point where the tension brace yields after the compression brace has buckled. The compression strength of a brace is always less than its tension strength. Therefore buckling occurs prior to tensile yielding for a pair of two opposing braces. The

ratio between $V_{y,exp}$ and V is referred to as the story or base shear yield over-strength, $\Omega_{y,exp}$, and the ratio between the elastic design demand, V_{DBE}, and $V_{y,exp}$ as R_μ. (See Equation 3-2 and 3-3) R_μ is here defined as the yield response modification factor as it relates the elastic demand to the expected yield strength. Following Equation 3-3, $Sa_{y,exp}$ can be related to the maximum considered earthquake's spectral acceleration, Sa_{MCE}, through Equation 3-4. As will be demonstrated in Chapter 4, $Sa_{y,exp}$ of the single story SCBF from Figure 3-2 is 0.40g calculated using Equation 3-4. By inspection of Figure 3-2b, this is a good estimate of the spectral accelerations at which brace yielding initiates.

$$\Omega_{y,exp} = \frac{V_{y,exp}}{V} \tag{3-2}$$

where

$$R_\mu = \frac{V_{DBE}}{V_{y,exp}} \tag{3-3}$$

$$Sa_{y,exp} = \frac{\frac{2}{3} Sa_{MCE}}{R_\mu} \tag{3-4}$$

Knowing $Sa_{y,exp}$, the site ground motion hazard curve can be used to predict the probability that the force-controlled components will experience large forces and cause the deformation-controlled components to yield. Figure 3-5 shows this schematically where on the right hand side there are idealized static nonlinear response curves versus story drift for two systems with different $Sa_{y,exp}$ and on the left hand side are representative seismic hazard curves for the Eastern and Western US. Based on $Sa_{y,exp}$ of the two systems, the seismic hazard curves can be used to calculate the probability that $Sa_{y,exp}$ is exceeded, i.e. that deformation-controlled components yield. Figure 3-5 shows that the system with higher $Sa_{y,exp}$ has a lower probability of experiencing forces large enough to yield its deformation-controlled components compared to the system with lower $Sa_{y,exp}$. Table 3-1 has calculated values for the probability in 50 years that the spectral acceleration of the design basis earthquake, Sa_{DBE}, divided by R_μ (i.e. $Sa_{y,exp}$) is exceeded for a San Francisco site (Lat = 38.0, Long = -121.7) and a New Madrid site (Lat

= 35.2, Long = -89.9) when T_1 = 0.2s. The seismic design values (Sa_{T1}) and the probability of exceedance are from the 2008 USGS hazard maps for each site. (Peterson et al., 2008)

Table 3-1 shows that for a frame with R_μ = 6 (Frame 1) in San Francisco, there is a 90.9% probability in 50 years that the frame will experience a large enough earthquake ground motion for its members to yield, while for a frame with R_μ = 2 (Frame 2) in San Francisco, that probability is down to 28.7%. Because of the low-R-factor, Frame 2 has only 1/3 the probability of the force-controlled member yielding compared to Frame 1. This suggests that the connection capacity factors could be less stringent for Frame 2 compared to Frame 1. These results are reasonable when thinking about the impact the R-factor has on frame behavior. Frames with large R-factors depend more on inelastic force redistribution and inelastic behavior then frames with smaller R-factors during seismic events and therefore the reliability of the force-controlled components becomes more critical.

Table 3-1 also demonstrates the difference between two different sites. A frame with R_μ = 4 in San Francisco is approximately 4 times more likely to experience yielding of its members compared to the same frame located in the New Madrid area. This difference arises from how the seismic design forces are determined, i.e. by dividing the spectral acceleration of the MCE ground motion by a fixed constant. For sites with "steep" hazard curves, such as for San Francisco where the probability of exceeding a specified spectral acceleration decreases rapidly as the spectral acceleration increases, the likelihood of seeing the design forces is considerably larger than for sites with more gradually inclined hazard curves. The new risk-targeted seismic design maps (Luco et al., 2007) have mitigated this difference somewhat as the slope of the hazard curves is accounted for when calculating MCE spectral accelerations. This has generally resulted in lower MCE spectral acceleration values for the Central and Eastern US than before (from 10% to 30% reduction) while the Western US values have been less affected (reduced by up to 10% or increased by up to 15% (Luco et al., 2007)), all depending on the slope of the seismic hazard curve and the assumed shape of the collapse fragility curve used in the

collapse probability calculations. The first two lines in Table 3-1 demonstrate how the values have changed for those two sites with the new risk-targeted seismic design maps.

The effects of the R-factor, member overstrength and the seismic hazard curve on the probability of component yielding indicate that these factors need to be considered in the reliability framework. Knowing the spectral acceleration at which yielding is expected to occur, $Sa_{y,exp}$ from Equation 3-3, the force-controlled component demand can be expressed as a function of Sa and R_μ. Using the total probability theorem (Benjamin and Cornell, 1970), the site ground motion hazard curve (which provides frequencies of exceedance of each Sa) can be combined with the probability of demand exceeding capacity for a given Sa, to compute the mean annual frequency of demand on a force-controlled components exceeding its capacity, $MAF(D>C)$. In discrete form, the $MAF(D>C)$ becomes:

$$MAF(D > C) = \sum_{all\ x_i} P(D > C | Sa = x_i) * MAF(Sa = x_i) \qquad (3\text{-}5)$$

where $MAF(Sa=x_i)$ is the mean annual frequency of observing a spectral acceleration in some narrow range around x_i, defined by the following equation (which approximates the derivative of the site ground motion hazard curve at a given ground motion intensity times the narrow range around x_i, i.e. dx).

$$MAF(Sa = x_i) = \frac{(MAF(Sa > x_{i+1}) - MAF(Sa > x_{i-1}))}{2} \qquad (3\text{-}6)$$

In continuous integral form, Equation 3-5 is:

$$MAF(D > C) = \int P(D > C | Sa = x) |dMAF(x)| \qquad (3\text{-}7)$$

where the notation $|dMAF(x)|$ means the absolute value of the derivative of the site's ground motion hazard curve times dx.

The summation in Equation 3-5 can be avoided by simplifying the probability of demand exceeding capacity function to a step function, as demonstrated in Figure 3-6,

where the probability is zero when $Sa < Sa_{y,exp}$ and then a constant when $Sa > Sa_{y,exp}$. This approximation allows for simply multiplying that constant with the mean annual frequency of $Sa_{y,exp}$ being exceeded, $MAF(Sa > Sa_{y,exp})$, to calculate the mean annual frequency of demand exceeding capacity. $MAF(Sa > Sa_{y,exp})$ can be read directly from the ground motion seismic hazard curve.

$$MAF(D > C) \cong P(D > C | Sa > Sa_{y,\exp}) * MAF\left(Sa > Sa_{y,\exp}\right) \qquad (3\text{-}8)$$

where

$$P\!\left(D > C | Sa\right) = \begin{cases} 0 & if \quad Sa \leq Sa_{y,\exp} \\ A & if \quad Sa > Sa_{y,\exp} \end{cases} \qquad (3\text{-}9)$$

Re-arranging Equation 3-8, the probability of demand exceeding capacity post-yielding can be calculated, given the mean annual frequency of demand exceeding capacity and the mean annual frequency $Sa > Sa_{y,exp}$, as shown in Equation 3-10.

$$P(D > C | Sa > Sa_{y,\exp}) \cong \frac{MAF(D > C)}{MAF(Sa > Sa_{y,\exp})} = \Phi\!\left(\beta_{R,Ha}\right) \qquad (3\text{-}10)$$

The reliability index, $\beta_{R,Ha}$, for Equation 3-1 can thus be calculated by using the inverse standard normal cumulative distribution function, according to the following:

$$\beta_{R,Ha} = \Phi^{-1}\!\left(\frac{MAF(D > C)}{MAF\left(Sa > Sa_{y,\exp}\right)}\right) \qquad (3\text{-}11)$$

Now that a method to calculate $\beta_{R,Ha}$ has been developed, the last two steps to complete the reliability framework are to decide upon an appropriate mean annual frequency of demand exceeding capacity, $MAF(D > C)$, and to decide what deformation demand to use to represent the post-yielding demand.

The tolerable mean annual frequency of demand exceeding capacity is subjective and depends on the consequences of the demand exceeding capacity, which in turn depend on factors such as redundancy in the structural system and the correlation between the

51

components within the system. As a practical matter, it is proposed to make certain assumptions to come up with a baseline number, which can be changed later if desired. Here the assumption is made that the probability of failure of capacity-designed components at a given spectral acceleration multiplied by the probability that component failure causes frame collapse can be added to the probability of frame collapse from incremental dynamic analysis at a given spectral acceleration (see Equation 3-12). Further, it is assumed that the probability that component failure causes frame collapse is independent of the ground motion intensity, Sa. However, as will be demonstrated in the examples in Chapter 4 and Chapter 5, this probability depends on the ground motion intensity and for the specific cases analyzed it is low at the lower ground motion intensities. These assumptions are made for several reasons. First, the failure of capacity-designed components can be neglected during the initial structural analysis and instead considered at the component level by checking member forces, greatly simplifying the structural analysis. Second, by adjusting the probability that that a capacity-designed component's failure causes collapse, the methodology allows for differentiating between components whose failure is believed to cause collapse directly (often due to low redundancy within the system) from others whose failure is not believed to have severe adverse effects. Lastly, they give a rational basis for establishing component reliability and will promote discussion and steer decision making toward the question of: "What is the tolerable probability of collapse of a structure in 50 years due to failure of capacity-designed components?" Project 07 has set the current standards of tolerable collapse probability to 1% in 50 years (Luco et al. 2007). However, current system reliability methodologies (FEMA P695) exclude the possibility of failure of capacity-designed components, at least explicitly, in the collapse probability calculations, often on the premise that capacity design principles will ensure that they do not fail. Therefore the question becomes, if failure of capacity-designed components was included in the analysis, what would be the total tolerable probability of collapse? And if the system has a lower probability of collapse then the tolerable threshold, can the design requirements on capacity-designed components be relaxed?

The system reliability is calculated by the following equation:

$$P\big(Coll\big|Sa\big) = P\big(Coll_{Sys}\big|Sa\big) + P\big(Coll_{D>C}\big|D>C\big) \times P\big(D>C\big|\overline{Coll}_{Sys},Sa\big) \qquad (3\text{-}12)$$

where $P(Coll\,|\,Sa)$ is the total probability of collapse given Sa and $P(Coll_{Sys}\,|\,Sa)$ is the probability of frame collapse at a given spectral acceleration, as calculated from incremental dynamic analysis procedures but excluding consideration of failures of capacity-designed components. $P(Coll_{D>C}\,|\,D>C)$ is the probability of frame collapse due to demand exceeding the capacity of capacity-designed components and $P(D>C\,|\,\overline{Coll}_{Sys},Sa)$ is the probability of demand exceeding the capacity of a capacity-designed component. At low spectral accelerations, the probability of a system level frame collapse excluding failure of capacity-designed components, $P(Coll_{Sys}\,|\,Sa)$, is close to zero, but as pointed out before, the capacity-designed components may fail at these low spectral accelerations and thus can contribute to the overall probability of frame collapse. And because of the much greater frequency of occurrence of ground motions with low Sa levels, failures of capacity-designed components at low ground motion intensities contribute significantly to the annual frequency of system failure. Figure 3-7 demonstrates this point illustratively. Figure 3-7a shows both a frame collapse fragility curve at a given spectral acceleration excluding considerations of capacity-designed components' failures as well as a frame collapse fragility curve when it is assumed that the probability of component failure (Figure 3-7b) causes frame collapse. When the two collapse fragility curve are integrated with the site ground motion hazard curve in Figure 3-7c (Los Angeles, Lat 33.99, Long = -118.16, T_1 = 0.2s), the calculated probabilities of frame collapse vary significantly, or from 1.0% to 4.0% in 50 years despite the only a 5.0% probability of component failure at the MCE ground motion intensity.

With $P(Coll_{Sys}\,|\,Sa)$ close to zero at the low Sa levels, conditioning the probability of demand exceeding capacity on the non-collapse of the system in the second term of Equation 3-12 can justly omitted as the probability of non-collapse is close to 100% in the region of interest. Equation 3-12 can then be re-written as:

$$P(Coll|Sa) = P(Coll_{Sys}|Sa) + P(Coll_{D>C}|D > C) \times P(D > C|Sa) \qquad (3\text{-}13)$$

To calculate the mean annual frequency of collapse, Equation 3-13 is integrated with a site ground motion hazard curve. This integration can be performed numerically as:

$$MAF(Coll) = \sum_{all \ x} \left(P(Coll_{Sys}|Sa) + P(Coll_{D>C}|D > C) \times P(D > C|Sa) \right) \times MAF(Sa = x_i) \quad (3\text{-}14)$$

Following the assumption from Equations 3-8 and 3-9 that $P(D>C|Sa>Sa_{y,exp})$ is a constant, Equation, 3-14 can be re-written as:

$$MAF(Coll) = \sum_{all \ x} P(Coll_{Sys}|Sa) \times MAF(Sa = x_i) + P(Coll_{D>C}|D > C) \times MAF(D > C) \quad (3\text{-}15)$$

The mean annual frequency of collapse can be converted into a probability of collapse in 50 years (making the typical assumptions that Sa occurrences are Poissonian) with Equation 3-16:

$$P(Collapse)_{50 \, years} = 1 - e^{-50\lambda} = 1 - e^{-50 MAF(Coll)} \qquad (3\text{-}16)$$

As these calculations are mainly dealing with small probabilities of collapse, the added contribution of collapse due to demand exceeding the capacity of force-controlled components can be calculated as follows:

$$\Delta P(Coll_{D>C})_{50 \, years} = 1 - e^{-50\lambda} = 1 - e^{-50 P(Coll_{D>C}|D>C) \times MAF(D>C)} \qquad (3\text{-}17)$$

With Project 07 having set the tolerable probability of collapse to 1.0% in 50 years, it seems appropriate to specify the tolerable added probability of collapse due to failure of capacity-designed components relative to 1% in 50 years. Table 3-2 provides target $\beta_{R,Ha}$ -values calculated with Equation 3-11, for different R_μ in two different locations with probability of demand exceeding capacity of force-controlled components from 0.05% in 50 years to 1.00% in 50 years. Assuming that failure of capacity-designed components always leads to collapse, i.e. $P(D>C)$ in 50 years = $\Delta P(Coll_{D>C})$ in 50 years, Table 3-2

can also be viewed as the target $\beta_{R,Ha}$-values such that the tolerable added probability of collapse in 50 years is 0.05% to 1.00%.

Table 3-2 has target $\beta_{R,Ha}$-values to be used in Equation 3-1, which will result in consistent reliability of capacity-designed components based on R_μ and site ground motion hazard curve. Table 3-2 shows that systems with high R_μ will require a higher $\beta_{R,Ha}$ in order for the capacity-designed components in those systems to be as reliable as those in systems with low R_μ. Table 3-2 also shows that systems located at in the Western US will require higher $\beta_{R,Ha}$'s than systems located in the Central or Eastern US, a result of the probability of the deformation-controlled components' yielding being higher in the Western US. For a more detailed discussion on the site hazard curve effects on the target β-values, see Section 3.2.1. In addition to a system with lower R_μ having lower target $\beta_{R,Ha}$-values then a system with higher R_μ for a fixed probability of component failure in 50 years, the system with the lower R_μ will generally also have lower probability of collapse as the system is stronger and it will require larger ground motions to cause collapse. Therefore, if both systems are to be treated equally, i.e. with equal probability of collapse, the systems with the lower R_μ should also be allowed to have higher probability of component failure, allowing them even lower $\beta_{R,Ha}$-values and thus lower γ/ϕ-ratios.

The final step in the reliability framework is to decide upon what force level to use to represent the post-yielding demand. The suggested demand, based on test results from braces in SCBF, bolted end-plate moment connections and RBS sections in SMRF, is the maximum demand the force-controlled components will experience up to the MCE ground motion demand under cyclic loading protocols. This will generally be the maximum forces that the deformation-controlled components develop and will therefore include strain hardening effects. When developing a database on the required statistical parameters for this reliability framework, collecting only the maximum values from test data simplifies the task significantly as those results are generally readily available. Moreover there is less ambiguity about the maximum values then say the demand at yielding and it avoids the need to develop a demand versus deformation database. If near-

field pulse-like demand is considered to be more appropriate, monotonic test results can be substituted for the cyclic test results or an approximate conversion from cyclic to monotonic values can be used.

3.2.1 Location Effects on Calculated $\beta_{R,Ha}$

The proposed methodology for establishing the required design strength of capacity design components for seismic resistant systems depends on the site ground motion hazard curve. The calculated capacity design reliability index, $\beta_{R,Ha}$ or γ/ϕ - ratio varies therefore from one the location to the next. For general applicability of the methodology and its implementation in structural design codes the variation in γ/ϕ values may be too cumbersome to implement. To investigate how sensitive the reliability index, $\beta_{R,Ha}$, or the γ/ϕ - ratio are to the site ground motion hazard curve, and if there is a hazard curve parameter, .e.g. the local "slope" of the hazard curve, that might be used to quickly estimate them, ground motion hazard curves for 9 sites, each with 6 periods, are chosen. The chosen sites are listed in Table 3-3 along with the local "slopes" of the hazard curve, k, in the region of interest. The local "slopes" are calculated according to Equation 3-18 where the slope is calculated between the design basis earthquake spectral acceleration, Sa_{DBE} and $Sa_{DBE}/4$ and the corresponding hazard levels.

$$k = \frac{\ln(Ha_1) - \ln(Ha_2)}{\ln(Sa_2) - \ln(Sa_1)} \qquad (3\text{-}18)$$

For each of the ground motion hazard curves, the $\beta_{R,Ha}$ is calculated using Equation 3-19 for different $MAF(D>C)$ and for R_μ = 2, 4 and 6. The $MAF(D>C)$ is calculated based on $\Delta P(Coll_{D>C})_{50\,years}$ of 0.10%, 0.20% and 0.50% and $P(Coll_{D>C}|D>C)$ = 1.0 using Equation 3-21

$$\beta_{R,Ha} = \Phi^{-1}\left(\frac{MAF(D>C)}{MAF(Sa > Sa_{y,\exp})}\right) \qquad (3\text{-}19)$$

$$Sa_{y,\exp} = \frac{\frac{2}{3} Sa_{MCE}}{R_\mu} \tag{3-20}$$

$$MAF(D > C) = \frac{-\ln\left(1 - \Delta P(Coll_{D>C})_{50\,years}\right)}{50 P\left(Coll_{D>C} \middle| D > C\right)} \tag{3-21}$$

Tables 3-4 to 3-6 along with Figures 3-7 to 3-9 show representative results of the recommended $\beta_{R,Ha}$ based on the different parameters analyzed.

For a given R_μ and $P(D>C)$ in 50 years, the local "slope" of the hazard curve predicts the recommended $\beta_{R,Ha}$ well. Based on these results, if the local "slope", k, of a ground motion hazard curve is computed, where the slope is calculated between Sa_{DBE} and $Sa_{DBE}/4$ using Equation 3-18, the $\beta_{R,Ha}$ can easily be obtained without looking further into the ground motion hazard curve. These results demonstrate that for regions with similar shaped ground motion hazards, the calculated $\beta_{R,Ha}$ will be similar. Lastly it is of interest to see if R_μ and $\Delta P(Coll_{D>C})_{50\,years}$ can be included in a function to calculate $\beta_{R,Ha}$. A linear regression analysis was used to find the best functional form to calculate $\beta_{R,Ha}$ and it is presented in Equation 3-22. How well the suggested function calculates the $\beta_{R,Ha}$ is presented in Figure 3-11 where the predicted $\beta_{R,Ha}$ is the value calculated using Equation 3-22 and the true $\beta_{R,Ha}$ is calculated using Equation 3-19.

$$\beta_{R,Ha} = 0.75\ln(k) + 0.13 R_\mu - 1.36 \Delta P(Coll_{D>C})_{50\,years} + 2.07 \tag{3-22}$$

$$R^2 = 0.94$$

Since Equation 3-22 includes no system dependent variables and the coefficient of determination, R^2, is close to 1.0, it can be useful to determine general values of the reliability index for any component within any systems following capacity design principles.

3.2.2 Effect of Risk-Targeted MCE Target on Calculated $\beta_{R,Ha}$

Seismic design forces are based on the spectral acceleration for the maximum considered earthquake (MCE) at the fundamental period of the structure, Sa_{T1}. This spectral intensity is then (a) multiplied by two-thirds to the design basis earthquake (DBE) intensity and (b) divided by the frame's response modification coefficient, or R-factor. Depending on the slope of the seismic hazard curve, this approach can result in greatly varying return periods (frequencies of exceedence) for design level spectral accelerations of buildings located at different geographic locations. For sites with steep hazard curves, the likelihood of seeing the design forces is considerably larger than for sites with a more gradually inclined hazard curves. This can be seen in Table 3-7 and illustratively in Figure 3-12 where ground motion hazard curves for the San Francisco and the New Madrid sites used previously are plotted. Table 3-7 demonstrates that a frame with $R_\mu = 4$ in San Francisco is approximately 4 times more likely in 50 years to experience the design forces compared to a similar frame located in the New Madrid area, or 72.0% compared to 18.1%.

With the new ASCE Standard 7-10, the MCE ground motion values provided have moved from a consistent hazard value of 2.0% probability of being exceeded in 50 years, as in ASCE Standard 7-05, to ground motion values that will result in consistent risk of 1.0% probability of structural collapse in 50 years. To come up with new risk-targeted seismic design maps, a generic frame collapse fragility curve was integrated with the site ground motion hazard curves. The generic collapse fragility curve is based on a lognormal distribution with a variable median and a fixed logarithmic standard deviation of β equal to0.8. The median of the fragility curve was then adjusted such that the result of the integration equaled a mean annual frequency of frame collapse of 0.02%, or 1.00% in 50 years. The spectral acceleration at the 10th percentile of the frame collapse fragility curve was then defined as the MCE spectral acceleration. The development of the new seismic design maps is described in Luco et al. (2007).

The result of these new risk-targeted seismic design maps is generally a decrease in the MCE ground motion values in the Central and Eastern US and a slight increase in the MCE values in the Western US, all depending on the shape of the hazard curves.

Similarly, the design spectral accelerations also increased or decreased accordingly. Figure 3-12 shows the shift in the design spectral acceleration for the two sites used here when $R_\mu = 4$. As a consequence of this shift from a hazard-targeted seismic design maps to risk-targeted design maps, where consideration is given to the shape of the hazard curves, the difference in the likelihood of seeing the design spectral accelerations has been reduced, although for large R-factors the difference is still considerable. Table 3-7 shows spectral accelerations and corresponding hazard levels calculated using the new design maps for the San Francisco and the New Madrid site and compares them to values calculated using the old seismic design maps. Table 3-8 summarizes the $\beta_{R,Ha}$ values based on the 2005 and 2010 seismic design maps and shows how the calculated $\beta_{R,Ha}$ values would differ for the two seismic design maps, although the difference is minimal.

3.2.3 Difference in Calculated Required Design Strengths between Different Systems in Different Locations

The goal of the methodology is not to necessarily advocate different required design strengths for different systems (R_μ) or systems in different seismic areas, but to provide a methodology that results in consistent reliability of capacity-designed components when applied. However, due to the varying probabilities of experiencing specific deformation demands, the outcome is that systems in seismic areas where the seismic hazard curve is relatively flat and systems that rely less on inelastic deformation to achieve their performance goals can justifiably be allowed relaxation in the required design strengths of capacity-designed components if consistent probability of component failure is the ultimate goal.

But will the difference between calculated required design strengths be significant, i.e. is it worth having different γ/ϕ-ratios for different sites and different frames? To investigate that question, the methodology's basic equation (Equation 3-1) is used to calculate the required γ/ϕ-ratios for a range of R_μ's, *MAF(D>C)*, total demand and capacity dispersion, $V_{tot,}$ and two different ground motion seismic hazard curves, one

from San Francisco and the other one from New Madrid. For this analysis, Equation 3-1 is re-written as:

$$\frac{\gamma}{\phi} = \frac{\hat{D}_m}{D_n} \frac{C_n}{\hat{C}_m} \exp\left(\beta_{R,Ha} \sqrt{V_C^2 + V_D^2 - 2\rho V_C V_D}\right) = B \times \exp(\beta_{R,Ha} \times V_{tot}) \qquad (3\text{-}23)$$

where for this analysis, B is a constant set to 1.0, $\beta_{R,Ha}$ is calculated according to Equation 3-11 and $Sa_{y,exp}$ according to Equation 3-3. The results are presented in Figures 3-13 to 3-17.

Figure 3-13 and 3-14 show that the γ/ϕ-ratio is more sensitive to R_μ in San Francisco than in New Madrid. Therefore, the possible reduction in required design strengths due to R_μ is more pronounced in areas where the seismic hazard curve is fairly steep, such as San Francisco, than in areas where it is flatter, such as New Madrid. For both locations analyzed, the sensitivity increases when R_μ is less than 2. Figure 3-15 shows that the difference between calculated required design strengths between the two locations analyzed depends very much on the total dispersion, V_{tot}. For component strengths, the total dispersion can be expected to be around 0.2 to 0.3 and for R_μ between 2 and 4, the difference between the required design strengths for the two locations can be 10% to 25%. The difference in required design strengths between the two locations reduces as R_μ decreases. This is a result of the difference in the frequency between the seismic design forces reducing as R_μ decreases.

3.3   The Methodology and Guidelines for Future Use

The proposed methodology to establish the required design strength of capacity-designed components, which will be referred to as the Capacity Design Factor methodology as the required design strength is set by adjusting the capacity design factors, γ and ϕ, is to use Equation 3-1 to establish capacity design factors for components in seismic resistant systems whose strength probability distribution is lognormal.

$$\frac{\gamma}{\phi} = \frac{\hat{D}_m}{D_n} \frac{C_n}{\hat{C}_m} \exp\left(\beta_{R,Ha} \sqrt{V_C^2 + V_D^2 - 2\rho V_C V_D}\right) \qquad (3\text{-}1)$$

The methodology is based on the LRFD component reliability methodology but adapted for capacity-based design concepts. Comparison between the LRFD methodology and the Capacity Design Factor methodology is presented in Table 3-9. $\hat{D}_m$ and $\hat{C}_m$, and D_n and C_n are the median and nominal values of the demand and capacity probability distributions, respectively, V_D and V_C their lognormal standard deviations, and ρ the correlation between demand and capacity. The demand probability distribution is based on maximum strength demands up to deformation demands corresponding to the MCE ground motion intensity. The capacity design reliability index, $\beta_{R,Ha}$, provides a measure of probability of demand exceeding capacity of capacity-designed components, for a specified pair of γ and ϕ. The reliability index, $\beta_{R,Ha}$, is based on the seismic resisting system's R-factor and member overstrength, the site ground motion hazard curve, of the influence of capacity-designed component failures on the system collapse safety, and the tolerable added probability of frame collapse due capacity-designed components failure. Table 3-10 has recommended target $\beta_{R,Ha}$ for varying R_μ between 1 and 6 for two US sites, one in the Western US and one in the Central and Eastern US, and for probabilities of demand exceeding capacity ranging from 0.05% to 1.00% in 50 years. Table 3-10 shows that for R_μ of 4 and probability of demand exceeding capacity of 0.20% in 50 years, $\beta = 3.00$ in the Western US and $\beta = 2.3$ in the Central and Eastern US. When components′ strength probability distributions are not lognormal, the basic equation needs to be reformulated.

R_μ is based on the code R-factor and the member overstrength in yielding capacity due to the use of capacity design factors, nominal material values and strength equations, discrete member sizing etc. As described previously, R_μ provides a convenient way to keep track of the $S_{ay,exp}$, which is important for assessing the likelihood of the capacity-designed members experiencing design forces. For optimally designed systems, the ratio of R/R_μ can conservatively be estimated as 1.5 by only considering overdesign due to the use of capacity factors, ϕ, nominal material values instead of expected material values

when sizing members and modest overdesign due to other constraints. However, the R/R_μ-ratio can become considerably higher than 1.5 when all factors and constraints are accounted for. If that is the case, R_μ can be calculated for individual design cases as it will provide an opportunity to relax the capacity design factors. A procedure to calculate R_μ is demonstrated in Table 3-12 and an example of R_μ calculations for a 6-story SCBF are included in Chapter 5.

To calibrate the capacity design factors using the proposed Capacity Design Factor methodology, Table 3-13 provides step by step through the parameters that need to be considered such that the chosen capacity design factors result in consistent reliability between different seismic resisting systems located in different seismic areas. As mentioned previously, the assumption is made that the probability of failure of capacity-designed components, multiplied by the probability that component failure causes frame collapse, can be added to the probability of frame collapse from incremental dynamic analysis. Following this reasoning, the components that contribute little to the probability of frame collapse are allowed higher probabilities of failure. Table 3-11 shows recommended probabilities of demand exceeding capacity based on both the tolerable added probability of frame collapse due to failure of capacity-designed components as well as the consequences of component failure. Redundancy and correlation within the structural systems will control the severity of component failure consequences and these effects are likely to be very case specific. The examples in Chapter 4 and Chapter 5 will investigate the probability of frame collapse due to connection failures for single-story and multi-story SCBFs.

3.4   Conclusions

In this chapter, a reliability-based methodology is developed to establish the required design strengths of capacity-designed components in seismic resistant systems. The methodology provides a framework for design standard developers to use when establishing the required design strengths of capacity-designed components such that the reliability is consistent between different components, systems and seismic regions. The

methodology considers the main factors believed to influence the reliability of capacity-designed components and incorporates them into the suggested capacity design reliability index, $\beta_{R,Ha}$. The factors considered are the system R-factors and member overstrengths, site seismic hazard curves, assumed influence of failure of capacity-designed components on system collapse behavior, and the tolerable increased probability of frame collapse due to the failure of capacity-designed components. Applying the methodology is straightforward provided that the necessary statistical data is available.

As a consequence of seeking risk consistent capacity-designed components, applying the methodology results in different required design strengths for different systems and for systems in different seismic areas, based on R_μ and $P(Sa>Sa_{y,exp})$. The difference in required design strengths due to R_μ is larger in areas where the seismic hazard curve is fairly steep, such as the Western US, than in areas where it is flatter, such as the Central and Eastern US. For both cases, the sensitivity of required design strength to R_μ becomes more pronounced for very low R_μ, i.e. for R_μ less than 2. The difference between calculated required design strengths of components within systems with the same R_μ, but in different locations, depends very much on the component strength dispersions. For component strengths, the total dispersion (both demand and capacity), V_{tot}, can be expected to be around 0.2 – 0.3 and for R_μ between 2 and 4, the required design strengths for the Central and Eastern US are about 10%-25% less than for the Western US. The difference reduces as R_μ decreases as the difference in the frequency between the seismic design forces reduces. The new risk-targeted seismic design maps reduced this difference slightly by considering the shape of the seismic ground motion hazard curves in the calculations of the MCE spectral accelerations. All the results presented here were based on the new ASCE 7 (2010) risk-targeted seismic design maps.

For practical purposes, the methodology makes two key assumptions. The first key assumption is the simplification of the probability of component failure versus spectral acceleration curve. To allow for a closed form solution of the reliability index, $\beta_{R,Ha}$, it is assumed that the curve can be simplified as being zero at spectral accelerations below the expected yield spectral acceleration, $Sa_{y,exp}$, and a fixed constant above $Sa_{y,exp}$. As will be

demonstrated in subsequent chapters, when capacity design principles describe well the expected demand on capacity-designed components (e.g. braces and brace connections) as opposed to when capacity design principles merely represent the theoretical maximum demand components can experience (e.g. columns in multi-story frames), this assumption provides reasonable results. Alternatively, the probability of component failure curve can integrated with the site ground motion hazard curve.

Second key assumption arises when relating the probability of component failure to frame collapse. The tolerable probability of collapse due to failure of capacity-designed components is suggested to be proportional to the tolerable collapse probability of 1.0% in 50 years used as the basis for the new risk-targeted seismic design maps. The methodology assumes that the probability of failure of capacity-designed components multiplied by the probability that the failure causes frame collapse can be added to the probability of frame collapse from analysis excluding component failure. The methodology assumes that the probability of capacity-designed components causing frame collapse is independent of the ground motion intensity. However, a subsequent chapter will demonstrate that it is not necessarily the case and that the probability decreases as the ground motion intensity decreases, thus greatly reducing the adverse consequence of capacity-designed components' failure on the frame collapse probability at low ground motion intensities. Regardless, this assumption allows for a rational basis for deciding upon the required reliability of capacity-designed components by relating their reliability to the system reliability by allowing for differentiating between components whose failure consequences are considered minor and those whose failure consequences are considered severe.

Table 3-1: Probability in 50 years that frames ($T_1 = 0.2s$) located in San Francisco or New Madrid, will experience yielding of members based on 2008 USGS hazard maps and R_μ

Spectral Acceleration	San Francisco (Lat = 38.0, Long = -121.7)		New Madrid (Lat = 35.2, Long = -89.9)	
	$Sa_{T1} = x$	$P(Sa>x)$ in 50 years	$Sa_{T1} = x$	$P(Sa>x)$ in 50 years
$Sa_{MCE,2005}$	1.38g	2.0%	1.29g	2.0%
$Sa_{MCE,2010}$	1.44g	1.8%	1.04g	2.9%
$Sa_{DBE}=2/3Sa_{MCE,2010}$	0.96g	6.1%	0.69g	5.2%
$Sa_{DBE}/(R_\mu=2)$	0.48g	28.7%	0.35g	10.5%
$Sa_{DBE}/(R_\mu=3)$	0.32g	54.4%	0.23g	14.6%
$Sa_{DBE}/(R_\mu=4)$	0.24g	72.0%	0.17g	18.1%
$Sa_{DBE}/(R_\mu=5)$	0.19g	84.8%	0.14g	21.5%
$Sa_{DBE}/(R_\mu=6)$	0.16g	90.9%	0.12g	24.8%

Table 3-2: Target $\beta_{R,Ha}$ -values to use when establishing capacity design factors. The target $\beta_{R,Ha}$ -values depend on R_μ, the location and the tolerable probability of demand exceeding capacity.

System R_μ	San Francisco Lat = 38.0, Long = -121.7)					New Madrid (Lat = 35.2, Long = -89.9)				
	$P(D>C)$ in 50 years					$P(D>C)$ in 50 years				
	0.05%	0.10%	0.20%	0.50%	1.00%	0.05%	0.10%	0.20%	0.50%	1.00%
1	2.4	2.1	1.9	1.4	1.0	2.3	2.1	1.8	1.3	0.9
2	3.0	2.8	2.5	2.2	1.9	2.6	2.4	2.1	1.7	1.3
3	3.2	3.0	2.8	2.5	2.2	2.4	2.5	2.2	1.9	1.6
4	3.4	3.2	3.0	2.7	2.4	2.8	2.6	2.3	2.0	1.6
5	3.5	3.3	3.1	2.8	2.5	2.9	2.6	2.4	2.0	1.7
6	3.5	3.3	3.1	2.9	2.6	2.9	2.7	2.5	2.1	1.8

Table 3-3: Calculated local slopes, _k_, of the chosen hazard curves calculated between Sa_{DBE} and $Sa_{DBE}/4$.

Site	Period					
	0.1s	0.2s	0.3s	0.5s	1.0s	2.0s
Los Angeles (Lat=34.0, Long=-118.2)	2.13	2.22	2.23	2.28	2.30	2.32
San Francisco (Lat=38.0, Long=-121.7)	2.13	2.17	2.23	2.27	2.26	2.31
Eureka (Lat=41.3, Long=-124.3)	1.40	1.37	1.32	1.23	1.29	1.43
Sacramento (Lat=38.7, Long=-121.6)	2.36	2.44	2.50	2.50	2.42	2.34
Memphis (Lat=35.2, Long=-89.9)	0.96	0.96	0.94	0.90	0.89	0.85
Seattle (Lat=47.6, Long=-122.3)	1.90	1.91	1.90	1.86	1.81	1.78
Portland (Lat=45.5, Long=-122.7)	1.60	1.62	1.61	1.54	1.50	1.49
Las Vegas (Lat=36.2, Long=-115.1)	1.69	1.84	1.92	1.99	1.94	1.88
Stanford (Lat=37.4, Long=-122.2)	1.80	1.78	1.71	1.59	1.51	1.53
New York (Lat=40.7, Long= -74.0)	1.08	1.17	1.23	1.31	1.35	1.39
Boston (Lat=42.4, Long= -71.1)	1.24	1.34	1.40	1.42	1.37	1.36
Charleston (Lat=32.8, Long= -79.9)	0.85	0.86	0.83	0.80	0.79	0.79

Table 3-4: Calculated $\beta_{R,Ha}$ according to Equations 3-19 and 3-20 for each ground motion hazard curve when $R_\mu = 2$ and *P(D>C)* in 50 years is 0.10%

Site	Period					
	0.1s	0.2s	0.3s	0.5s	1.0s	2.0s
Los Angeles	2.75	2.75	2.76	2.76	2.78	2.80
San Francisco	2.74	2.75	2.76	2.77	2.78	2.80
Eureka	2.60	2.58	2.57	2.53	2.51	2.54
Sacramento	2.72	2.75	2.77	2.80	2.81	2.79
Memphis	2.37	2.36	2.35	2.33	2.29	2.21
Seattle	2.68	2.67	2.67	2.66	2.65	2.64
Portland	2.58	2.59	2.58	2.57	2.56	2.51
Las Vegas	2.54	2.58	2.59	2.61	2.61	2.52
Stanford	2.70	2.68	2.68	2.64	2.61	2.61
New York	2.29	2.33	2.34	2.36	2.39	2.39
Boston	2.34	2.39	2.41	2.43	2.44	2.41
Charleston	2.30	2.28	2.27	2.24	2.22	2.19

Table 3-5: Calculated $\beta_{R,Ha}$ according to Equation s 3-19 and 3-20 for each ground motion hazard curve when R$_\mu$ = 4 and *P(D>C)* in 50 years is 0.20%

Site	Period					
	0.1s	0.2s	0.3s	0.5s	1.0s	2.0s
Los Angeles	2.93	2.96	2.97	2.97	2.98	3.00
San Francisco	2.93	2.95	2.97	2.98	2.98	2.99
Eureka	2.65	2.64	2.62	2.57	2.57	2.63
Sacramento	2.98	3.01	3.03	3.04	3.02	3.00
Memphis	2.33	2.32	2.30	2.27	2.24	2.15
Seattle	2.83	2.83	2.83	2.81	2.79	2.77
Portland	2.67	2.68	2.68	2.65	2.63	2.60
Las Vegas	2.70	2.77	2.80	2.82	2.79	2.70
Stanford	2.83	2.82	2.79	2.74	2.69	2.70
New York	2.29	2.35	2.39	2.42	2.46	2.50
Boston	2.39	2.46	2.49	2.51	2.51	2.50
Charleston	2.23	2.22	2.19	2.16	2.13	2.11

Table 3-6: Calculated $\beta_{R,Ha}$ according to Equation s 3-19 and 3-20 for each ground motion hazard curve when $R_\mu = 6$ and *P(D>C)* in 50 years is 0.50%

Site	Period					
	0.1s	0.2s	0.3s	0.5s	1.0s	2.0s
Los Angeles	2.85	2.87	2.88	2.89	2.89	2.91
San Francisco	2.84	2.86	2.88	2.88	2.87	2.88
Eureka	2.52	2.51	2.49	2.45	2.44	2.52
Sacramento	2.93	2.96	2.97	2.96	2.93	2.89
Memphis	2.10	2.10	2.08	2.04	2.00	1.89
Seattle	2.72	2.72	2.71	2.69	2.66	2.64
Portland	2.52	2.54	2.54	2.50	2.47	2.44
Las Vegas	2.62	2.70	2.72	2.73	2.67	2.59
Stanford	2.72	2.72	2.69	2.63	2.56	2.57
New York	2.08	2.16	2.20	2.26	2.29	2.26
Boston	2.20	2.28	2.33	2.36	2.35	2.27
Charleston	1.97	1.96	1.93	1.89	1.87	1.85

Table 3-7: Spectral accelerations and the probability of exceedance for a San Francisco and New Madrid site calculated based on both on the old hazard-targeted seismic design maps and the new risk-targeted seismic design maps. T = 0.2s.

Spectral Acceleration	San Francisco Lat = 38.0, Long = -121.7)				New Madrid (Lat = 35.2, Long = -89.9)			
	Sa_{T1} = x		P(Sa>x) in 50 years		Sa_{T1} = x		P(Sa>x) in 50 years	
	2005	2010	2005	2010	2005	2010	2005	2010
$Sa_{MCE,2005}$	1.38g	1.44g	2.0%	1.8%	1.29g	1.04g	2.0%	2.9%
$Sa_{DBE}=2/3Sa_{MCE,2010}$	0.92g	0.96g	6.8%	6.1%	0.86g	0.69g	3.9%	5.2%
$Sa_{DBE}/(R_\mu=2)$	0.46g	0.48g	31.1%	28.7%	0.43g	0.35g	8.7%	10.5%
$Sa_{DBE}/(R_\mu=3)$	0.31g	0.32g	56.4%	54.4%	0.29g	0.23g	12.4%	14.6%
$Sa_{DBE}/(R_\mu=4)$	0.23g	0.24g	74.5%	72.0%	0.22g	0.17g	15.4%	18.1%
$Sa_{DBE}/(R_\mu=5)$	0.18g	0.19g	86.1%	84.8%	0.17g	0.14g	18.3%	21.5%
$Sa_{DBE}/(R_\mu=6)$	0.15g	0.16g	92.2%	90.9%	0.14g	0.12g	21.0%	24.8%

Table 3-8: $\beta_{R,Ha}$ based on Equation 3-8, calculated using both the old hazard-targeted seismic design maps and the new risk-targeted seismic design maps. T = 0.2s.

R_μ	San Francisco Lat = 38.0, Long = -121.7)				New Madrid (Lat = 35.2, Long = -89.9)			
	P(D>C)							
	2005		2010		2005		2010	
	0.10%	1.00%	0.10%	1.00%	0.10%	1.00%	0.10%	1.00%
1	2.2	1.1	2.1	1.0	2.0	0.7	2.1	0.9
2	2.8	1.9	2.8	1.9	2.3	1.2	2.4	1.3
3	3.0	2.3	3.0	2.2	2.4	1.4	2.5	1.6
4	3.2	2.4	3.2	2.4	2.5	1.6	2.6	1.6
5	3.3	2.6	3.3	2.5	2.6	1.6	2.6	1.7
6	3.4	2.7	3.3	2.6	2.6	1.7	2.7	1.8

Table 3-9: Comparison between LRFD and proposed methodology for establishing capacity design factors

Variables	Load and Resistance Factor Design	Capacity Design Factors
D_m/D_n	Central values of the load effect statistical parameters including: 1) Dead load 2) Live load 3) Wind load 4) Other loads	Central values of the following demand statistical parameters: 1) Ratio of component strengths at deformation demands equal to MCE ground motion demands to strengths predicted by nominal equations. Demands determined from a) Cyclic tests and/or b) Nonlinear dynamic analysis 2) Material strengths 3) Geometrical properties (fabrication) 4) Record-to-Record
C_m/C_n	Central values of the following resistance statistical parameters 1) Ratio of expected resistance strengths to strengths predicted by nominal equations 2) Material strengths 3) Geometrical properties (fabrication)	Same as LRFD
V_D	Variability of load effect statistical parameters	Variability of the demand statistical parameters
V_C	Variability of resistance statistical parameters	Same as LRFD
ρ	Correlation between statistical parameters $\rho = 0.0$ as it is generally not included in LRFD	Correlation between statistical parameters $\rho = 0.5$ when demand and capacity originate from the same member, $\rho = 0$ otherwise
β	β was chosen based on average values in structural design prior to LRFD. Suggested values: $\beta = 2.5 - 3.0$ for members $\beta = 4.0 - 4.5$ for connections	$\beta_{R,Ha}$ will depend on: 1) The frame's R-factor 2) The member overstrength 3) The site's seismic ground motion hazard curve 4) Tolerable $P(D>C)$ in 50 years • $\Delta P(CollD>C)$ in 50 years • $P(CollD>C \mid D>C)$

Table 3-10: Minimum $\beta_{R,Ha}$ for Western US and Central and Eastern US

System R_μ	San Francisco Lat = 38.0, Long = -121.7)					New Madrid (Lat = 35.2, Long = -89.9)				
	P(D>C) in 50 years					*P(D>C)* in 50 years				
	0.05%	0.10%	0.20%	0.50%	1.00%	0.05%	0.10%	0.20%	0.50%	1.00%
1	2.4	2.1	1.9	1.4	1.0	2.3	2.1	1.8	1.3	0.9
2	3.0	2.8	2.5	2.2	1.9	2.6	2.4	2.1	1.7	1.3
3	3.2	3.0	2.8	2.5	2.2	2.4	2.5	2.2	1.9	1.6
4	3.4	3.2	3.0	2.7	2.4	2.8	2.6	2.3	2.0	1.6
5	3.5	3.3	3.1	2.8	2.5	2.9	2.6	2.4	2.0	1.7
6	3.5	3.3	3.1	2.9	2.6	2.9	2.7	2.5	2.1	1.8

Table 3-11: Recommended *P(D>C)* in 50 years for components.

Consequences of Failure			Tolerable *ΔP(Coll)* in 50 years		
Description		$P(Coll_{D>C}|D>C)$	0.05%	0.10%	0.20%
Severe	*Failure of component causes frame collapse. Structural redundancy is very low and/or correlation between components high*	100%	0.05%	0.10%	0.20%
Considerable	*Failure is likely to cause frame collapse. Structural redundancy is low and/or correlation between components fairly high*	50%	0.10%	0.20%	0.40%
Moderate	*Failure is unlikely to cause frame collapse. Structural redundancy is high and/or correlation between components fairly low*	20%	0.25%	0.50%	1.00%
Small	*Failure rarely causes frame collapse. Structural redundancy is very high and/or correlation between components low*	10%	0.50%	1.00%	2.00%

Table 3-12: A procedure to calculate R_μ

Step	Description
1	Design a frame according to code specification
2	Calculate the expected yield shear force of every story, $V_{y,exp}$, using expected material properties. Where member strengths is different depending on if it's in tension or compression, as is the case for braces in SCBF, use the average between the two.
3	Perform a Response Spectrum Analysis using the design spectrum and record the story shear forces, V_{RSA}
4	Calculate the minimum $V_{y,exp}/V_{RSA}$ ratio
5	$Sa_{y,exp} = Sa_{T1} * \min(V_{y,exp}/V_{RSA})$
6	$R_\mu = 2/3 \; Sa_{MCE} / Sa_{y,exp}$

Table 3-13: Steps to calibrate the capacity design factors following the proposed methodology when component strength probability distributions are lognormal

Step 1	Capacity Statistical Properties	
	How	**Comment**
X_1: **Component Model Variable**	Median and dispersion of variable are obtained through comparison of capacity strengths from test data to predicted strengths using nominal strength equations	Measured material and geometrical properties are used in predicting strengths through the nominal strength equations
X_2: **Material Strength Variable**	Median and dispersion of variable are obtained through comparison of material strengths from test data to nominal material strengths	Depending on the failure modes, R_y and R_t are either included or excluded in the design equations
X_3: **Fabrication Variable**	Median and dispersion of variable are obtained through comparison of measured geometrical properties to nominal ones	Recommended values: $X_{m,3} = 1.00$, $V_{X3} = 0.05$
C_m/C_n	$X_{m,1} * X_{m,2} * X_{m,3}$	Multiplication of median values of the statistical parameters
V_C^2	$V_{X1}^2 + V_{X2}^2 + V_{X3}^2$	When sufficient test data is not available, the recommended $V_c = 0.15$ for ductile failure modes and $V_c = 0.25$ for brittle failure modes
Step 2	Demand Statistical Properties	
	How	**Comment**
X_4: **Load Model Parameter Variable**	Median and dispersion of variable are obtained through comparison of strengths from test data where members are subjected to cyclic loading to predicted strengths using nominal strength equations	Members will generally have reached their maximum capacity before the MCE ground motion demand so this variables becomes the ratio between the maximum values from test data to predicted strengths
X_5: **Material Strength Variable**	Median and dispersion of variable are obtained through comparison of material strengths from test data to nominal material strengths	With the introduction of R_y and R_t in the nominal strength, C_n, the average value of this factor is between 0.95 and 1.05
X_6: **Fabrication Variable**	Median and dispersion of variable are obtained through comparison of measured geometrical properties to nominal ones	Recommended values: $X_{m,6} = 1.00$, $V_{X3} = 0.05$
X_7: **Record-to-Record Variable**	Median and dispersion of variables are obtained through comparison of strengths from dynamic analysis at given intensities to expected strengths	Recommended values: $X_{m,7} = 1.00$, $V_{X3} = 0.05$
D_m/D_n	$X_{m,4} * X_{m,5} * X_{m,6} * X_{m,7}$	Multiplication of the median values of the statistical parameters
V_D^2	$V_{X4}^2 + V_{X5}^2 + V_{X6}^2 + V_{X7}^2$	When sufficient test data is not available, the recommended $V_D = 0.20$
Step 3	Correlation Coefficient, ρ	
	How	**Comment**
ρ	Correlation between statistical parameters is analyzed through published test data when demand and capacity originate from the same member	Correlation will generally be between the material and fabrication variable. ρ_{14} and ρ_{25} can be individually estimated or a suggested value of $\rho_{DC} = 0.5$ can be used

Step 4	Yield Response Modification Factor, R_μ	
	How	**Comment**
R_μ	Use Table 3-12	For optimally design, the ratio of R/R_μ = 1.5 – 2.0 should be used. If due to various reasons, members are considerably overdesigned, a designer can calculate R_μ for his design, see Table 3-7
Step 5	Hazard Curve Effects	
	How	**Comment**
Hazard Curve	The hazard curve effects are broken into 3 categories. Is the frame located in the Western US, Nort-Western US or Central and Eastern US?	A more site specific analysis can be performed and the *MAF(Sa>Sa$_{y,exp}$)* calculated directly.
Step 6	Tolerable *P(D>C)* in 50 years	
	How	**Comment**
P(D>C) in 50 years	It is up to code developers to determine the tolerable probability but recommended values are in Table 3-11 with 0.10% in 50 years being the default value	Higher probability can be justified if consequences of component failure is considered small, mainly due to system being highly redundant an components uncorrelated
Step 7	$\beta_{R,Ha}$	
	How	**Comment**
$\beta_{R,Ha}$	Use R_μ, *P(D>C)* and frame location to choose $\beta_{R,Ha}$ from Table 3-10	If a more detailed analysis is performed, Equation 3-8 can be used to calculate the minimum $\beta_{R,Ha}$
Step 8	Calculate γ/ϕ - ratio	
	How	**Comment**
γ/ϕ	Use Equation 3-1	Equation 3-1 calculates the γ/ϕ - ratio. In many cases, ϕ is already fixed at the capacity side so the variable to change is γ

a)   b)
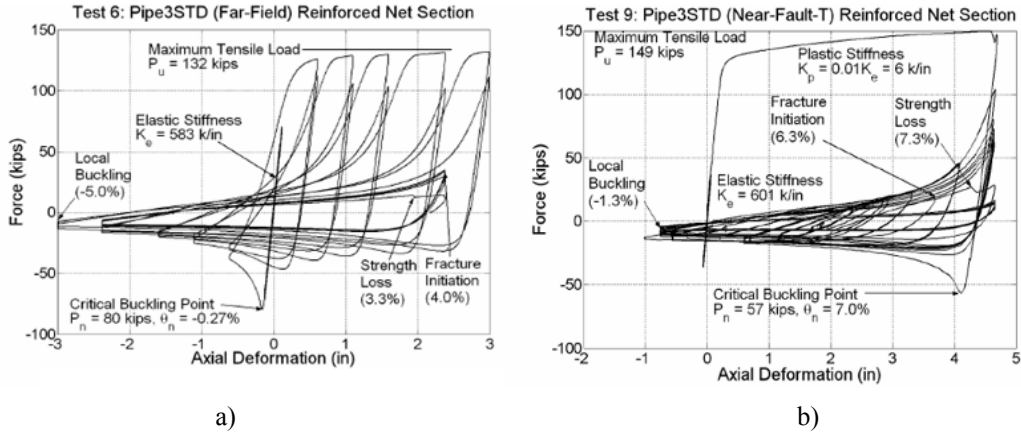
Figure 3-1: Brace response during a) Far-field loading b) Near-fault tension loading (Images from Fell et al., 2006)
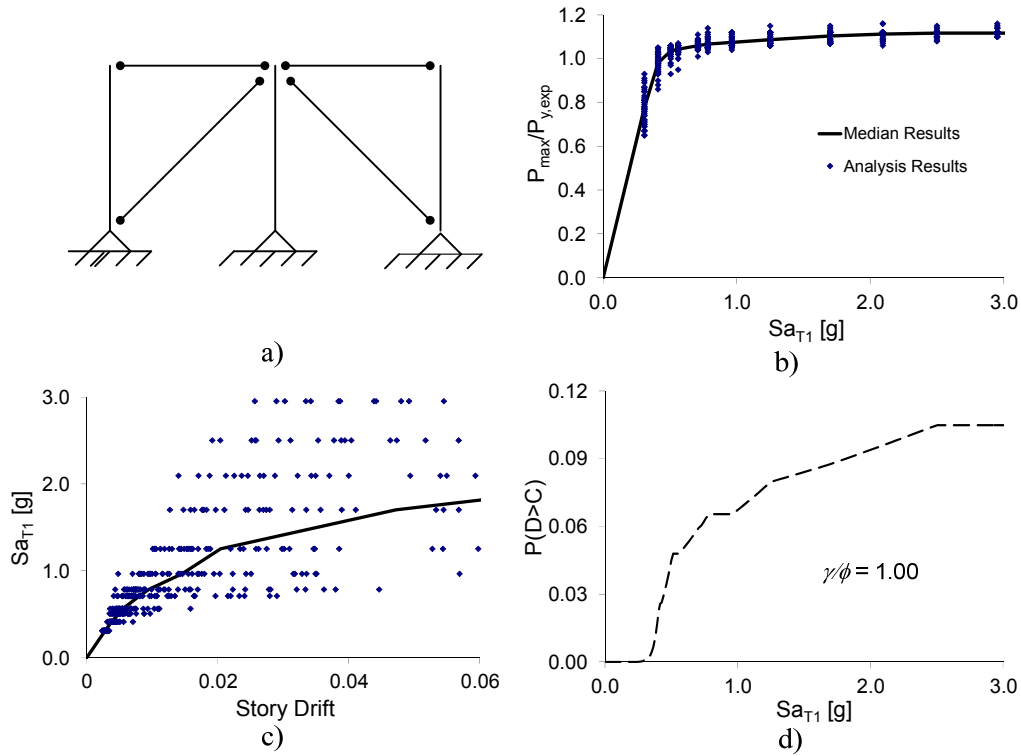
Figure 3-2: Results from IDA study on a single story SCBF showing the spectral acceleration at which brace tension yielding occurs and its relationship with the probability of connection failure. a) Elevation of frame analyzed. b) Maximum brace forces, P_{max}, recorded in each analysis normalized by expected yield strength, $P_{y,exp}$. c) Maximum story drift ratio recorded in each analysis. d) Probability of connection failure vs. spectral acceleration for a given connection capacity and dispersion
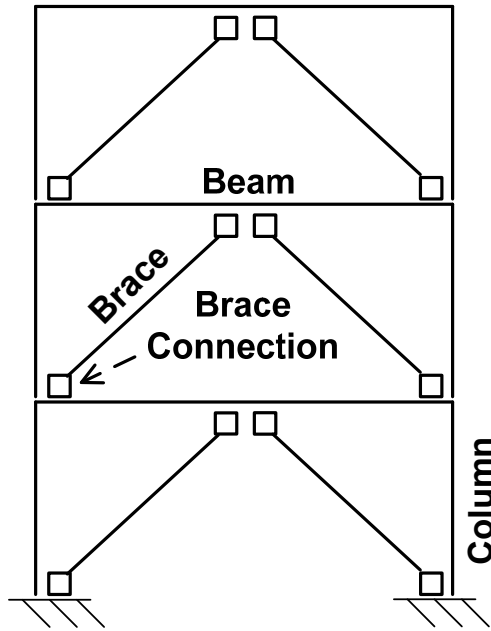
Figure 3-3: 3-Story Special Concentrically Braced Frame.

$$R = V_{DBE}/V$$

$$R_\mu = V_{DBE}/V_{y,exp}$$

$$\Omega_{y,exp} = V_{y,exp}/V$$
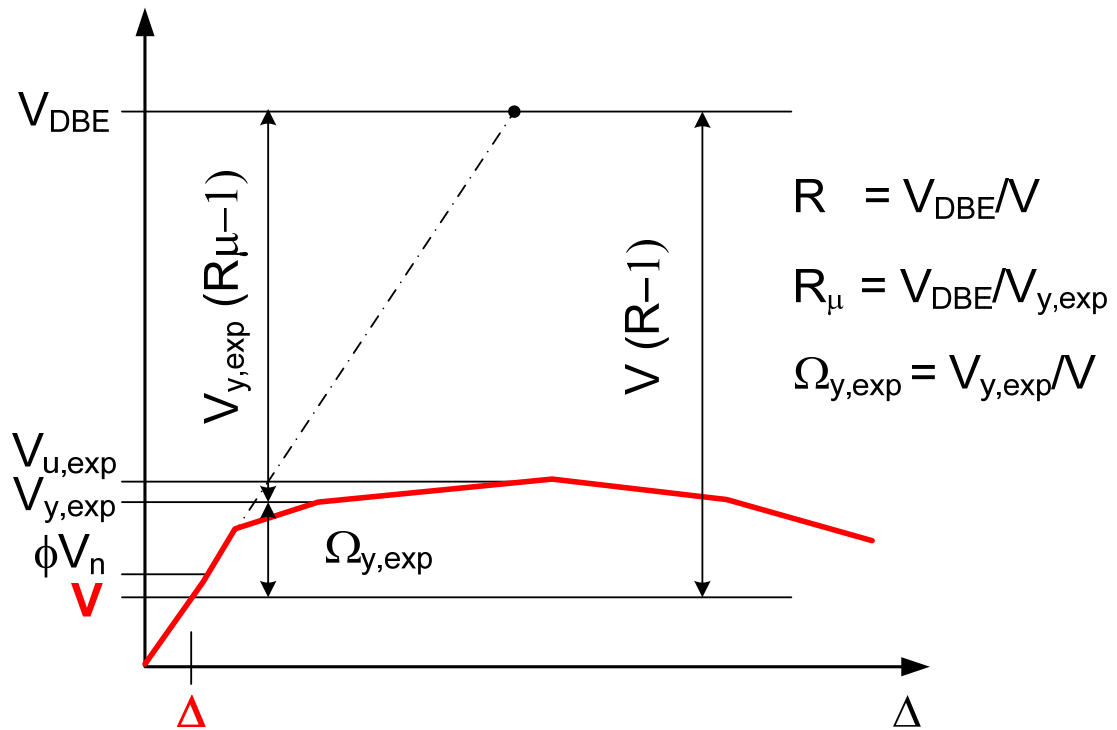
Figure 3-4: Idealized static nonlinear response (pushover curve) of a 1-bay braced frame comparing the design story or base shear, *V*, to the factored nominal story or base shear strength, ϕV_n, the

expected story or base shear yield strength $V_{y,exp}$ and the expected story or base shear ultimate strength, $V_{u,exp}$
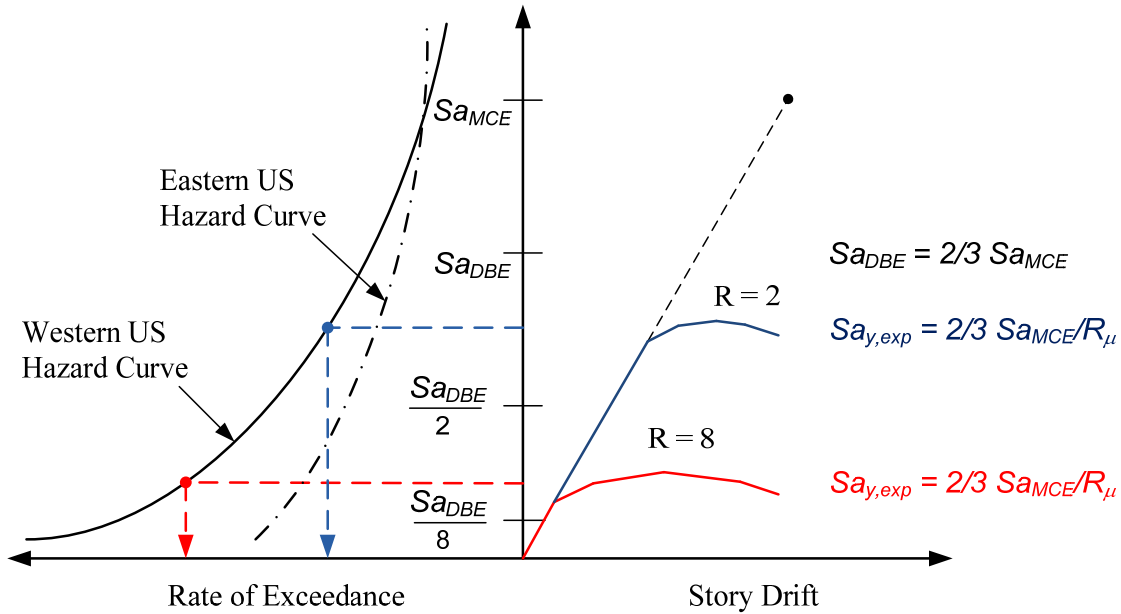
Figure 3-5: Relationship of the site ground motion hazard curve (left) to the static nonlinear response curves (right) to illustrate the rate of exceedance of the spectral acceleration corresponding to yield in the structure. Characteristic hazard curves are shown for the Eastern and Western United States, and response curves are shown for structures designed with two R-values (2 and 8).
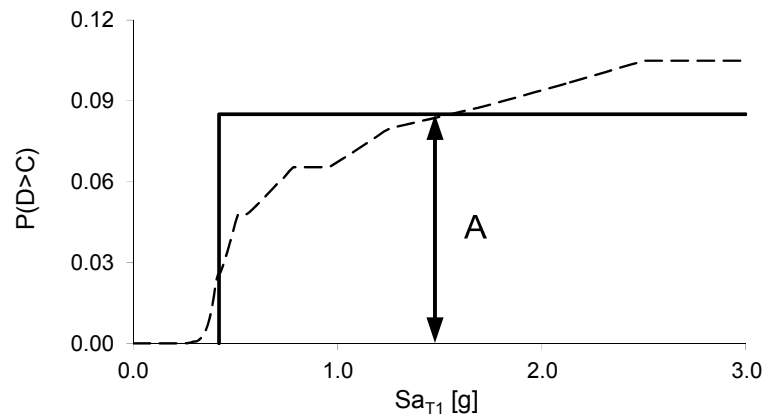
Figure 3-6: Probability of imposed demand on a component exceeding its capacity ($\gamma/\phi = 1.00$) as a function of ground motion intensity. The curvilinear $P(D>C|Sa)$ function is approximated by the step function with probability A.

78

a)

0.50

0.40

0.30

0.20

0.10

0.00

Probability of Collapse

If P(Coll$_{D>C}$|D>C) = 1.0:
Close to constant ΔP(Collapse)
past yielding of deformation-
controlled components

ΔP(Collapse) at MCE
due to failure of capacity-
designed components

Frame collapse fragility w/o
component failures
(Median = 3.67, Beta = 0.6)

Frame collapse fragility with
component failures

Sa$_{T1}$ [g]

0.0   1.0   2.0   3.0   4.0

a)

b)

0.06

0.04

0.02

0.00

Probability of Component Failure

Sa$_{T1}$ [g]

0.0   1.0   2.0   3.0   4.0

b)

c)

10^{-1}

10^{-2}

10^{-3}

10^{-4}

10^{-5}

10^{-6}

Mean Annual Rate of Exceedance

P(Collapse) in 50 years w/o
component failures = 1.00%

P(Collapse) in 50 years with
component failures = 4.00%

Site Hazard Curve

Sa$_{T1}$ [g]

0.0   1.0   2.0   3.0   4.0

c)

Figure 3-7: Possible consequences of component failure on the system collapse fragility curve and the probability of collapse in 50 years. a) The probability of frame collapse including and excluding component failure b)The probability of component failure c) Los Angeles ground motion hazard curve (Lat 33.99, Long -118.16).
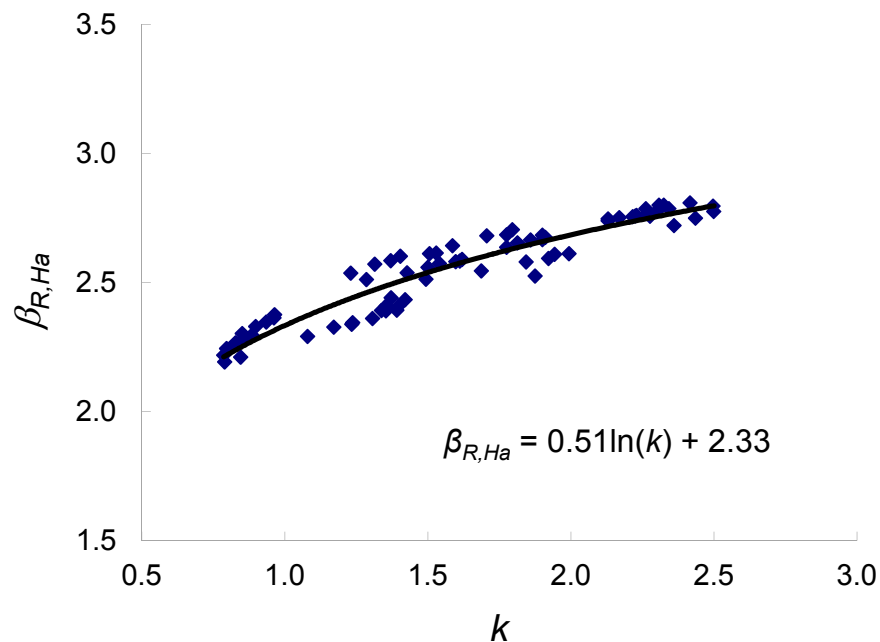
Figure 3-8: The calculated $\beta_{R,Ha}$ from Table 3-4 as a function of the local "slope" k when $R_\mu = 2$ and $P(D>C)$ in 50 years is 0.10%.

$$\beta_{R,Ha} = 0.51\ln(k) + 2.33$$
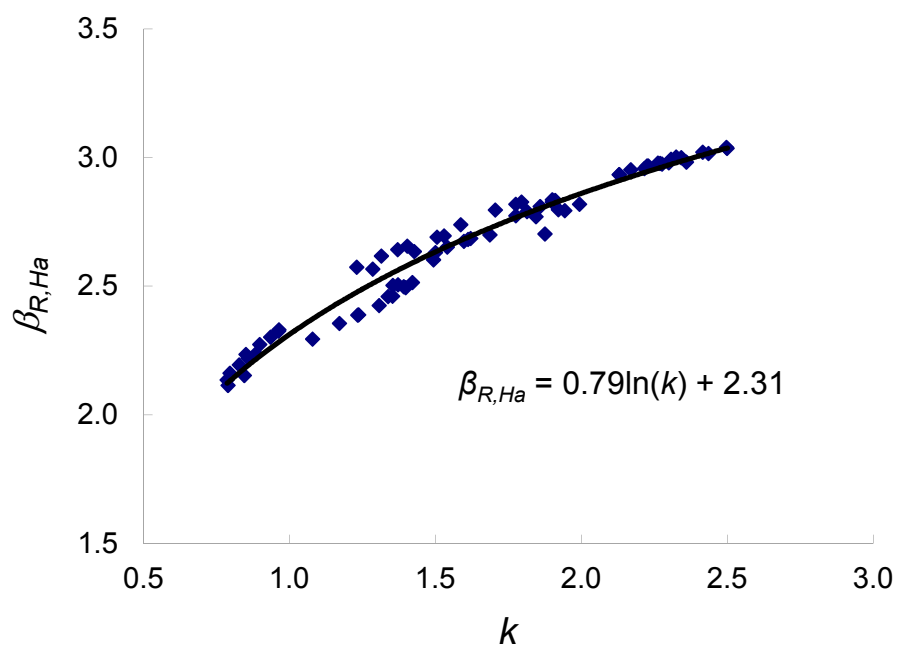
Figure 3-9: The calculated $\beta_{R,Ha}$ from Table 3-5 as a function of the local "slope" k when $R_\mu = 4$ and $P(D>C)$ in 50 years is 0.20%.

$$\beta_{R,Ha} = 0.79\ln(k) + 2.31$$
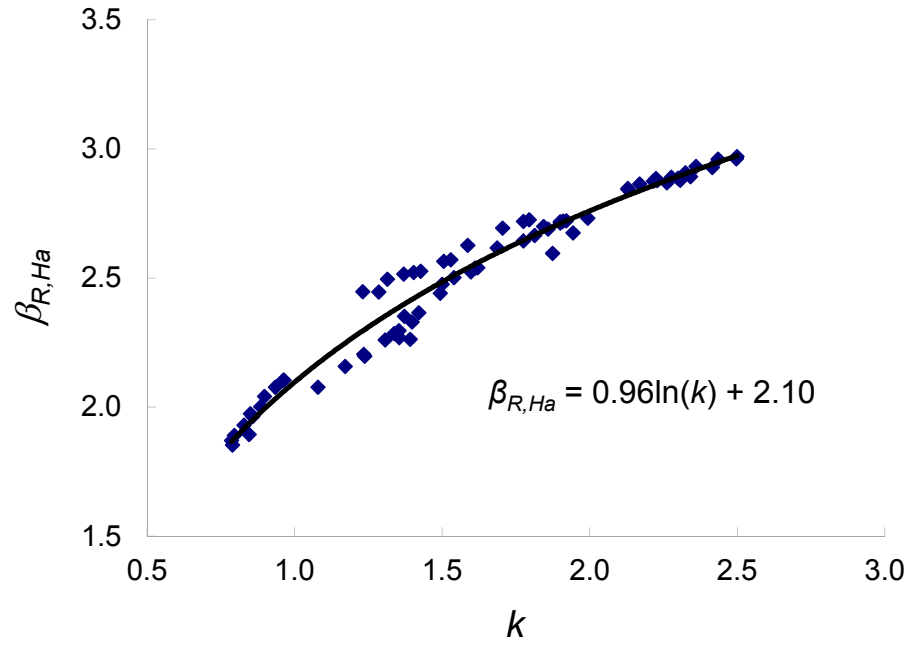
Figure 3-10: The calculated $\beta_{R,Ha}$ from Table 3-6 as a function of the local "slope" k when $R_\mu = 6$ and $P(D>C)$ in 50 years is 0.50%
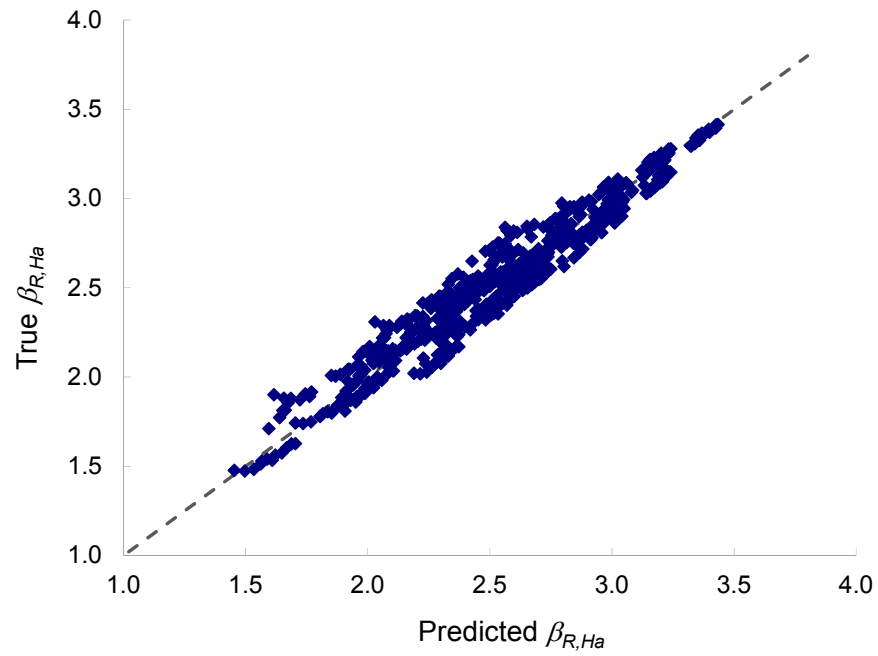
Figure 3-11: True $\beta_{R,Ha}$ vs. the predicted $\beta_{R,Ha}$ (Equation 3-19 and 3-22).
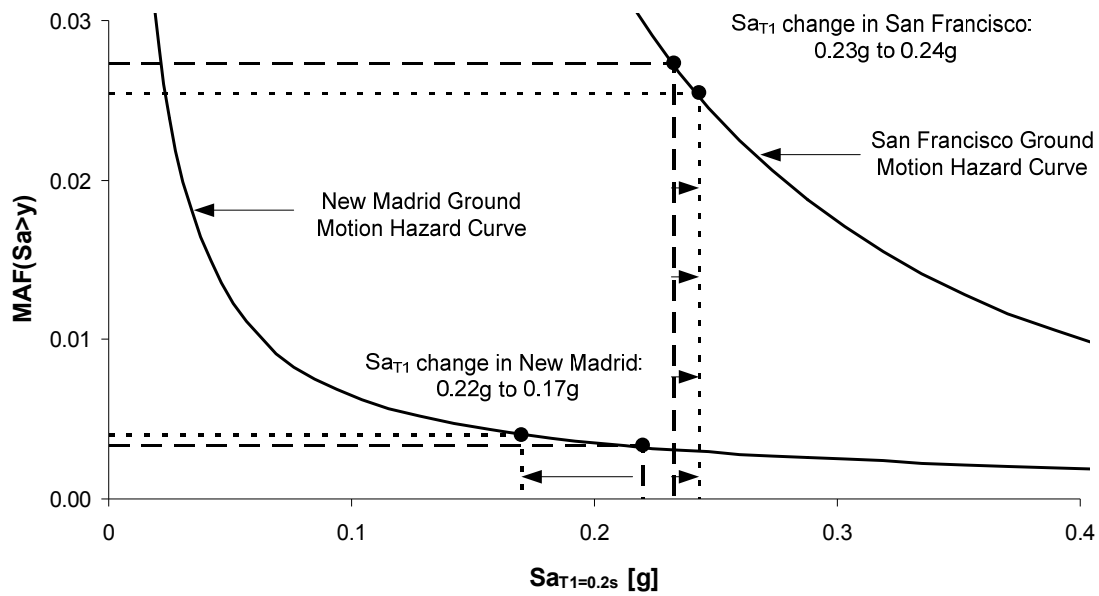
Figure 3-12: New and old design spectral accelerations for a R_μ system of 4 located in San Francisco and New Madrid. The MAF of exceeding the design spectral acceleration has increased with the new hazard curves for New-Madrid but decreased for San Francisco.
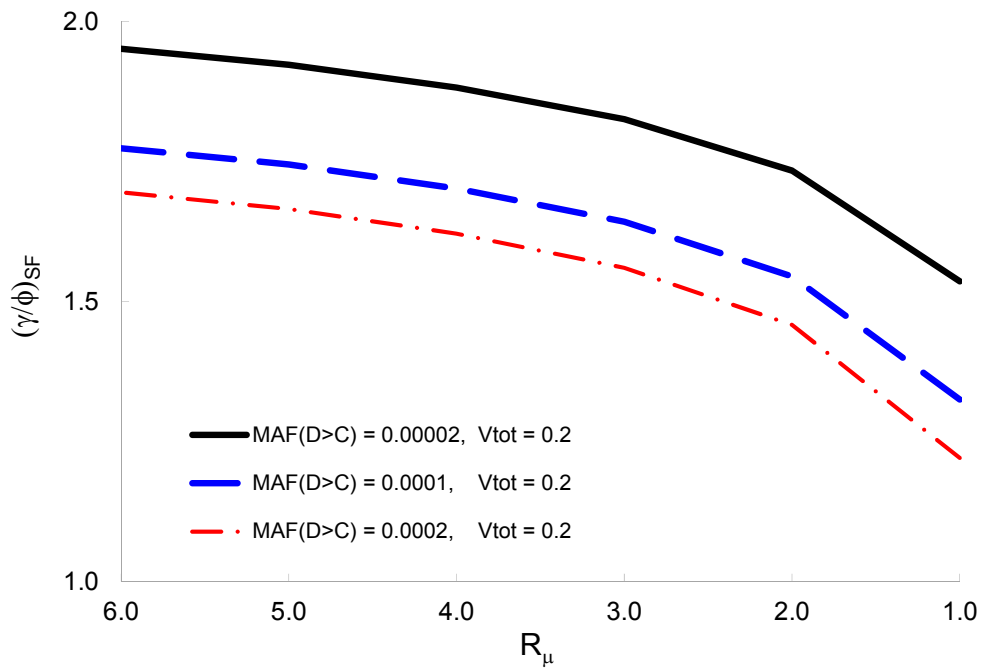
Figure 3-13: γ/ϕ-ratio sensitivity to R_μ and *MAF(D>C)* for frames located in San Francisco. C_m/C_n and $D_m/D_n = 1.0$

82
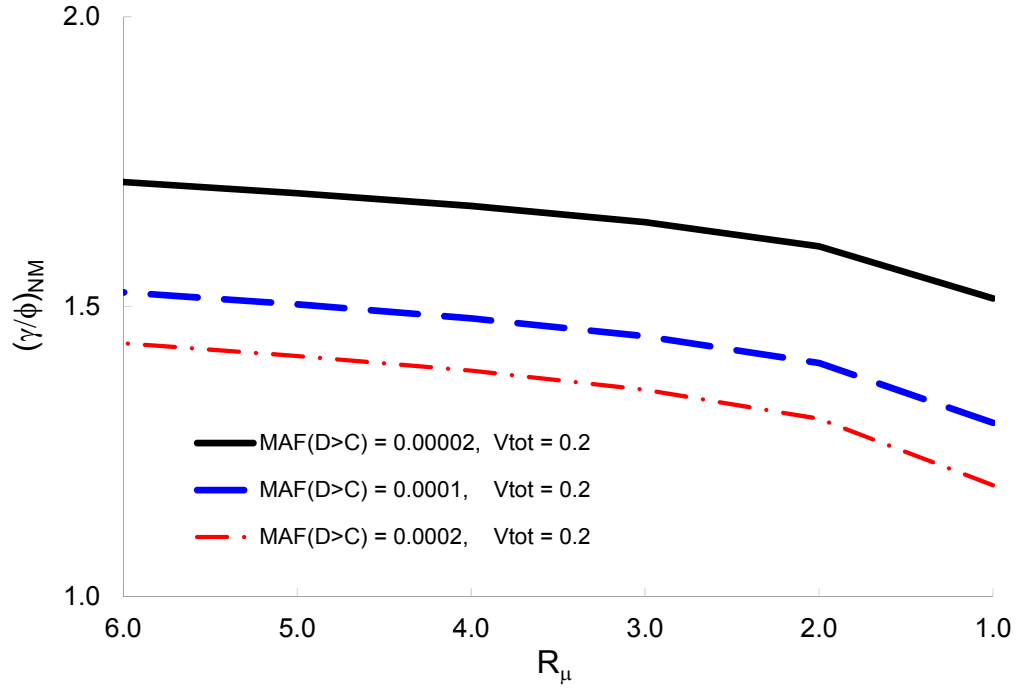
Figure 3-14: γ/ϕ-ratio sensitivity to R_μ and *MAF(D>C)* for frames located in New Madrid. C_m/C_n and $D_m/D_n = 1.0$.
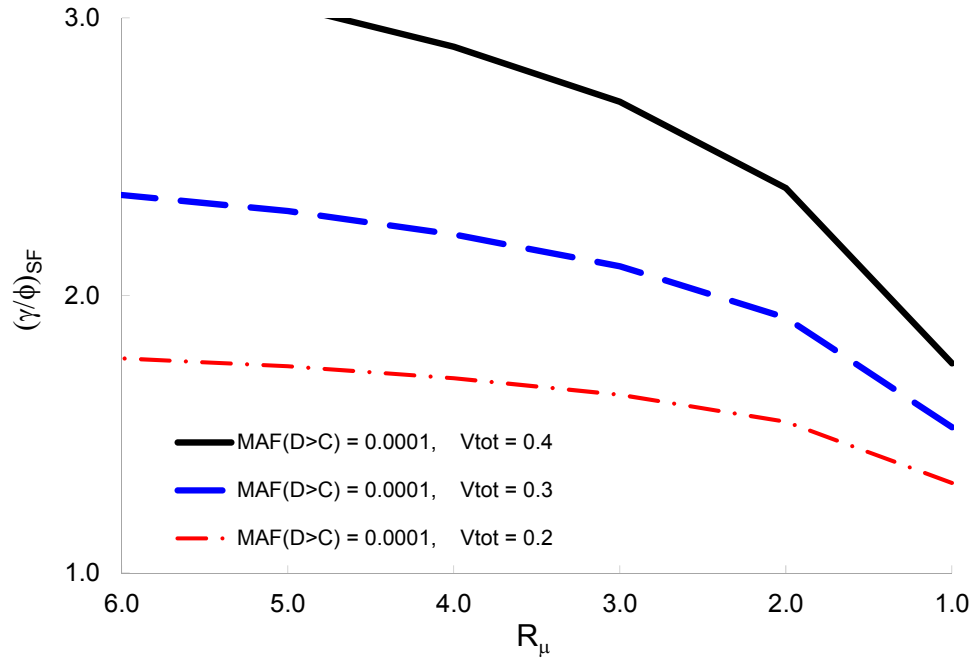
Figure 3-15: γ/ϕ-ratio sensitivity to R_μ and V_{tot} for frames located in San Francisco. C_m/C_n and $D_m/D_n = 1.0$
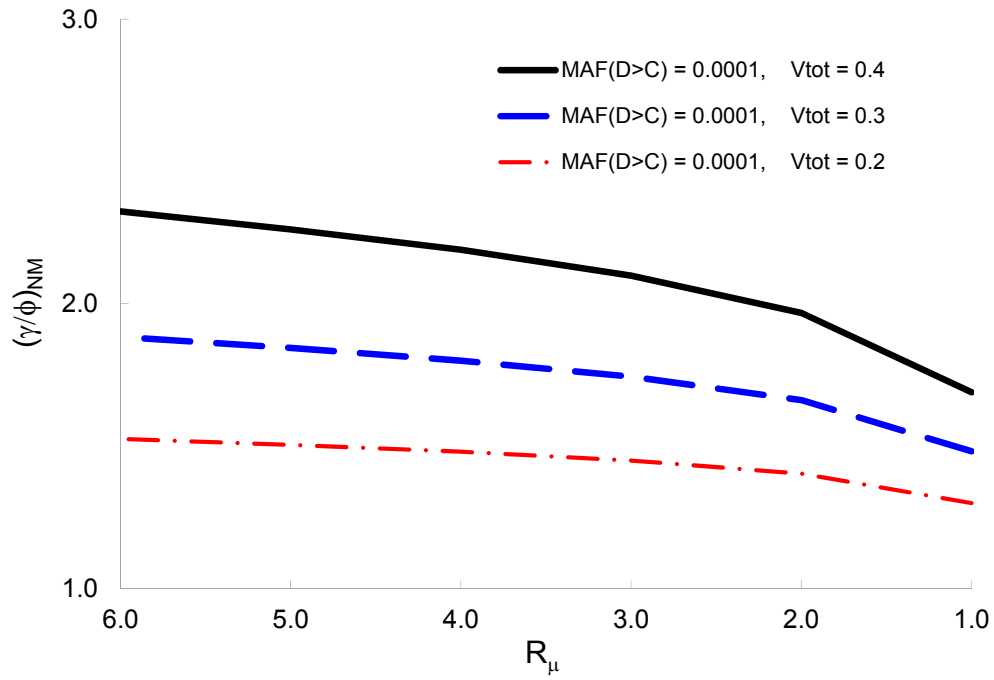
Figure 3-16: γ/ϕ-ratio sensitivity to R_μ and V_{tot} for frames located in New Madrid. C_m/C_n and $D_m/D_n =$ 1.0
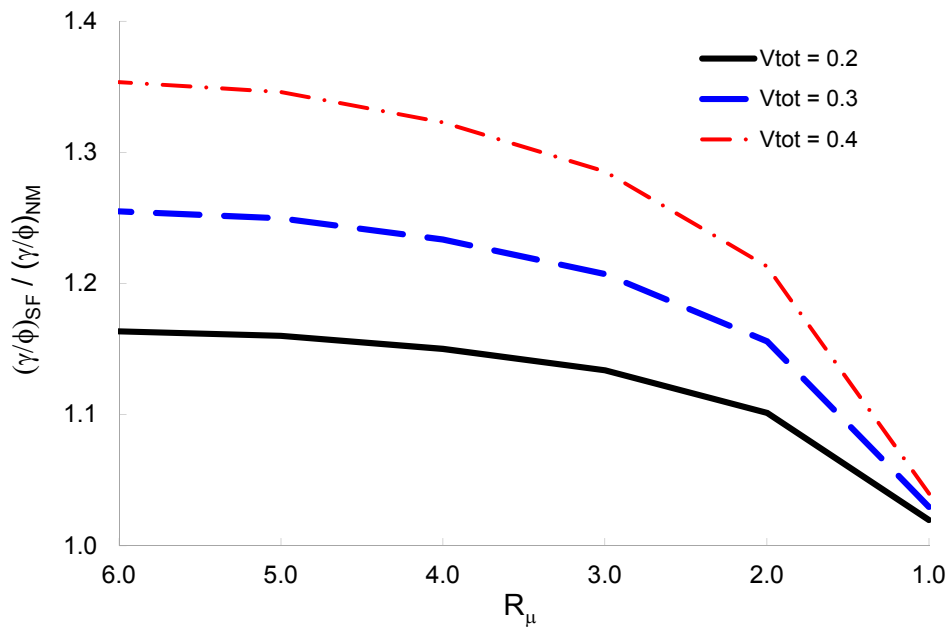
Figure 3-17: Ratio of calculated γ/ϕ-values calculated based on being located in San Francisco to those based on being located in New Madrid.

Capacity-Based Design in Single-Story Special Concentrically Braced Frames

4.1 Introduction

In Special Concentrically Braced Frames (SCBF), the braces are the deformation-controlled components, and the brace connections, beams and columns are the force-controlled components, whose required design strength is based on the brace strengths. Since the capacity-design principles dictate that connections should be stronger than the braces connected to them, connection failure is usually not modeled in nonlinear structural analysis. (NIST GCR 10-917-8, 2010). The objectives of this chapter are to investigate the demand on brace connections, their reliability and the potential consequences of brace connection failure on the seismic collapse safety of single-story SCBFs. The study entails nonlinear dynamic analyses of two single-story SCBF designs, results of which are interpreted using the reliability methodology developed in Chapter 3.

In the first portion of this study, the two single-story SCBF designs are analyzed through incremental dynamic analysis (Vamvatsikos & Cornell, 2002). These analyses are intended to represent the median model response, where the model parameters are based on the expected values of material strengths and element model parameters. As such, the analyses do not directly simulate connection failures. The two frames are designed for the same mass and seismic hazard, but they have different brace sizes so as to result in different values of overstrength and R_μ. It is of special interest to observe how the R_μ values of the frames, as calculated using guidelines from the methodology in Chapter 3, relate to the spectral accelerations at which the connection demand distributions reach peak values. Also, by including connection failures in the analysis, it

is of interest to observe how the frames' collapse fragility curves change and the subsequent change in annual probability of frame collapse.

In the second study of this chapter, Monte Carlo methods are combined with nonlinear analyses to simulate directly model uncertainties and connection failures. Aside from providing some insights into modeling uncertainties, the key goal of these analyses is to assess the conditional probability of system collapse due to connection failures, $P\left(Coll_{D>C}|D>C\right)$. A "full" modeling uncertainty analysis on a single story SCBF is performed, including variability in nonlinear brace properties and connection strengths.

4.2 *Dynamic Analysis of Median-Model Response of Single-Story Special Concentrically Braced Frames*

4.2.1 Description of Analysis

In this set of analyses, median models of the two single story SCBF designs are analyzed. One of the two frames is optimally designed according to ASCE 7-10 minimum design loads (ASCE, 2010), so as to have an R_μ as close as possible to the specified value of R = 6. In the second frame, the braces are significantly over-designed, with the resulting R_μ much less than the maximum specified R. Figure 4-1 shows the plan and elevation view of the frame models, and the key frame properties and design values are listed in Table 4-1. The braces selected for Frame 1 and HSS 6x6x5/16, which are the smallest braces that satisfy the design code requirements. Regardless, there is a significant overstrength in Frame 1 due to discrete member sizes, the resistance factor and differences in brace compression and tension strengths. In Frame 2, the brace areas are doubled with the use of HSS 6x6x5/8 members. The R_μ for Frame 1 is 2.5 while R_μ for Frame 2 is 1.4, both values significantly below R = 6.

The frames are idealized as two-dimensional plane frame models and analyzed using OpenSees (OpenSees, 2011). The models are developed to represent median conditions, where the expected (versus nominal) material strengths, section properties, and component model parameters are used. With the median models, the failure of capacity-

designed components is not modeled in the analysis since their median strengths are designed to exceed the brace median strengths. The braces are modeled using nonlinear force-based fiber elements. The beams and columns are modeled with elastic elements that have nonlinear rotational springs to model member hinging adjacent to the beam-column connections and column bases. The rotational behavior of the flexural hinge springs follows a bilinear hysteretic response based on the Modified Ibarra Krawinkler Deterioration Model (Ibarra et al. 2005, Lignos and Krawinkler 2009, 2010). Braces are assumed to have pinned end connections to the frame, and the two exterior columns are fixed at the base. The center elastic pin-ended column is included to exclude beam bending due to unbalanced brace forces. To capture the stiffening effect of the brace gusset plates, rigid offsets are used at the brace-to-frame connections and the effective length of the braces is 80% of the work-point-to-work-point length. The gravity system is idealized as a leaning column to simulate P-Delta effects and provides no lateral resistance. The gravity load (1080 kips) is applied to the leaning column as axial load. Rayleigh damping is assigned equal to 2% of critical damping at the first two vibration periods of the models ($T_1 = 0.39s$ and $T_2 = 0.17s$).

The hysteretic characteristics of the braces are modeled using a method developed by Uriz (2005). An illustration of the brace OpenSees model is shown in Figure 4-2. Each brace is subdivided into twelve nonlinear fiber members, each of which has three integration points along the length. Each fiber section is modeled with twenty fibers through its depth. To induce global buckling, initial camber in the middle of the braces is 0.1% (1/1000), as recommended by Uriz (2005). For these two-dimensional models, brace buckling is modeled to occur in-plane, but in concept the buckling response is equally indicative of buckling in- or out-of-plane. A Menegotto-Pinto material model (Steel02) with isotropic strain hardening is used for the brace fibers (Filippou et al., 1983).

To model low-cycle fatigue rupture of braces, the fatigue material developed by Uriz (2005), and implemented in OpenSees, is applied to the braces (uniaxialMaterial Fatigue). It tracks the strain history in each fiber and uses a modified rainflow cycle counting algorithm to determine the strain amplitudes. The fatigue material uses a Manson-Coffin relation calibrated to multiple brace tests characterizes low-cycle fatigue damage to each

fiber during each cycle, and Miner's rule determines whether the fatigue life had been exceeded. The fatigue material model in OpenSees wraps around the brace steel material model, and once the fatigue material reaches a damage level of 1.0, the stress of the steel material becomes zero. (Uriz, 2005)

To account for the non-simulated failure criteria of columns, 10% story drift limit is used following recommendations from the SCBF analysis in NIST GCR 10-917-8. Those recommendations are based on results from Newell and Uang (2006), which show that columns begin to lose their capacity after 7% to 9% story drift when subjected to cyclic axial and lateral loads.

The frames are subjected to the 44 ground motion records selected by and used in FEMA P695 *Quantification of Building Seismic Performance Factors* (FEMA, 2009). Unlike in the FEMA P695 study, where the ground motion set is scaled as a whole (based on the median of the set) to the spectral acceleration at the first mode period of the structure, in this study the ground motion records are scaled individually based on the spectral acceleration at the first mode period of the structure. This is done to systematically relate component demand to spectral acceleration, which can in return be related to frequencies of exceedance via the ground motion hazard curve for the site at that spectral period. The earthquake response spectra for the 44 ground motions as used in this analysis are plotted in Figure 4-3. The frames are analyzed using incremental time history analysis technique where each ground motion record is scaled up until frames collapse (Vamvatsikos & Cornell, 2002). During each dynamic analysis, the maximum axial forces developed in the braces, i.e. the maximum demand on the connections, are recorded. Connection fractures are not simulated directly in the analysis. Instead, the probability of brace connection failure is determined by comparing the maximum braced demand from each analysis to the probability distribution of connection strength. The probability of demand exceeding connection capacity at a given spectral acceleration is then calculated, i.e. $P(D > C|Sa)$. Based on the postulated consequences of connection fractures, specifically the probability of collapse given that the brace strength is

exceeded, $P(Coll_{D>C}|D > C)$, the total probability of frame collapse including connection fractures is calculated using Equation 3-12.

4.2.2 Brace Behavior

As described earlier, the braces are modeled using nonlinear fiber elements that can capture brace yielding and global buckling. A fatigue material is utilized to capture low-cycle fatigue fracture due to the combined effects of global and local buckling. Model parameters for the steel material and fracture models are based on calibration studies by Uriz for square HSS sections. (Uriz, 2005)

To check the cyclic response of the brace model, several braces were subject to far-field and near-field cycling loading protocols. The loading protocols were developed by Fell et al. (2006) by adjusting loading protocols from ATC-24 (ATC, 1992) to represent SCBF behavior. Table 4-2 shows the far-field loading protocol. For near-field loading (see Table 4-3_, both asymmetric compression and tension loading protocols were used. The brace axial deformations are related to the story drift angle by the following, Fell et al (2006):

$$\Delta_a = L_B \sqrt{1 + 2\theta \cos\alpha \sin\alpha + \theta^2 \sin^2\alpha} - L_B \qquad (4\text{-}1)$$

where Δ_a is the axial deformation, θ is the drift angle, α the brace angle and L_b the brace length. For α of 45° and L_b of 203in (80% of the work-point-to-work-point length in the two frames analyzed), the relationship between the axial deformation and the drift angle is:

$$\Delta_a / L_b \approx 0.50\theta \qquad (4\text{-}2)$$

Figures 4-4 to 4-9 show the brace hysteretic response as well as the loading history for the far-field, near-field tension and near-field compression loading protocols. In all cases the brace compression buckling, tensile yielding and eventually brace fracture due

to low-cycle fatigue can be observed. The peak tensile forces for the three loading protocols, far-field, near-field tension and near-field compression are 1.10, 1.15 and 1.09 times the expected brace yield strength and the corresponding compression forces are 1.25, 1.06 and 1.18 times the expected brace buckling strength.

4.2.3 Calculating R_μ

To estimate the spectral accelerations at which tensile yielding in the braces can be expected, $Sa_{y,exp}$, the procedure in Table 3-12 is used to calculate R_μ for each frame. By identifying the shaking intensity where the connection demands reach yield and begin to saturate, the $Sa_{y,exp}$, helps guide the choice of shaking intensities in the incremental dynamic analyses. Comparison of R_μ and $Sa_{y,exp}$, as calculated from the pushover analyses, also help confirm how well the procedure from Table 3-12 estimates R_μ and $Sa_{y,exp}$. The calculated values of R_μ and $Sa_{y,exp}$, based on the Table 3-12 procedures, are summarized in Table 4-4.

The calculated values of R_μ from Table 4-4 of 2.5 and 1.4 for Frames 1 and 2, respectively, corresponding to the $Sa_{y,exp}$ values of 0.4g and 0.7g. To further estimate the frames´ R_μ, a pushover analysis is also performed. Figures 4-10 and 4-11 show the pushover analyses results. In the figures, both the compression brace and tension brace response is shown along with the combined response. Based on the story shear forces when the tension braces yield, which represents the peak values in these cases, R_μ´s are 2.6 and 1.5 for Frames 1 and 2, respectively. A normalized story shear force of 1.0 equals the design force and R_μ of 6.0. The slight difference between R_μ calculated by pushover analysis and the Table 3-12 methodology arises because the tension and compression braces, as calculated by the pushover analysis, do not reach maximum strengths at the same story drifts. As shown in Figures 4-10 and 4-11, the compression brace typically reaches its peak buckling strength before the tension brace is fully yielded. This is in contrast to the behavior as assumed in the calculations in Table 4-4, where the two peaks are simply added together.

4.2.4 Nonlinear Dynamic Analysis Results

During each incremental dynamic analysis, the frame story drift ratios and the brace axial forces are recorded. Figures 4-12 to 4-15 show the recorded brace axial responses for Frame 1 when subjected to ground motion record No. 1 at ground motion intensities equaling, Sa_{T1} = 0.2g, 0.4g, 0.8g and 1.0g. The figures range from the demonstrating the elastic response of the braces in Figure 4-12, to the compression brace buckling and initiation of brace tensile yielding in Figure 4-13, to brace fracture after multiple inelastic cycles in Figures 4-14 and 4-15. The maximum story drift and the brace tensile forces for Frame 1 and ground motion record No. 1 are shown in Figure 4-16. From Figure 4-16a, it can be seen that the maximum story drift increases as the spectral acceleration increases, up to the point that the frame collapses. The collapsed point is shown in the figure as a cross with a dotted line connecting the last non-collapsed analysis point with the collapsed analysis point. Similarly, as demonstrated in Figure 4-16b, the maximum brace tensile force increases as the spectral acceleration increases. However, unlike the maximum story drift, the maximum developed brace force is limited by the brace strength capacity, which causes the maximum developed braces forces to saturate at the brace strength capacity. The maximum brace forces just before frame collapse is the cross in the figure.

The analysis process just described is then repeated for all other ground motion records, resulting in a distribution of story drift ratios and maximum brace tensile forces at Sa level. Figures 4-17 and 4-18 show the maximum story drift ratios and maximum brace tensile forces versus spectral acceleration for both frames. Figures 4-17a and 4-18a show that the increased elastic strength of Frame 2 causes large story drifts to occur at considerably higher spectral accelerations compared to Frame 1. Similarly, Figures 4-17b and 4-18b show that the brace tensile yielding occurs at higher spectral accelerations for Frame 2 than for Frame 1. The maximum brace forces are only recorded for the non-collapsed cases. Due to the brace strength capacity limiting the maximum forces that can be developed, the maximum brace forces for collapsed cases and non-collapsed cases are very similar. However, since later the brace forces are used to calculate the probability of connection failure and the probability of collapse due to connection failure of non-

collapsed cases, only the maximum brace forces from the non-collapsed cases are recorded. The variation in peak drifts and forces at each *Sa* level represents the record-to-record randomness. Using statistics from the collapse points, collapse fragility curves for each frame are then developed by fitting a lognormal distribution to the observed means and standard deviations and plotted as the dashed lines in Figure 4-19.

The incremental dynamic analysis was performed using the FEMA P695 ground motion records, each of which was linearly scaled up for each increment in the analysis. Linear scaling of the ground motion set results in conservative estimates of response and collapse safety at extreme ground motions as it does not account for the unique spectral shape of extreme ground motions and their effect on behavior (Baker and Cornell, 2006). The FEMA P695 methodology handles this issue by multiplying the median collapse point by a so-called spectral shape factor. The spectral shape factor is based on the building's fundamental period, its period-based ductility, and the applicable Seismic Design Category. For the frames analyzed here, the spectral shape factor is 1.3 based on Table 7-1b from FEMA P695 *Quantification of Building Seismic Performance Factors* (FEMA, 2009), ductility index of 6 and fundamental period below 0.5s. The solid collapse fragility curves shown in Figure 4-19 are calculated by shifting the original collapse fragility curves (shown dashed) by the FEMA P695 Spectral Shape Factor.

Since there are questions as to whether the FEMA P695 Spectral Shape Factor applies to these analyses of brace force demands (versus median collapse capacity), the results were checked by comparing collapse analysis results obtained using an alternative ground motion set that has the appropriate spectral shape. Appendix A and Appendix B contain results from this study on a similar single-story SCBF subjected to both the FEMA P695 ground motion set as well as a ground motion set selected to match the target response spectrum and variance, i.e. i.e. the conditional spectrum or CS. The CS ground motions were selected using an algorithm created by Jayaram et al. (2010). The analysis demonstrated that the demands on brace connections are not affected by which ground motion set is used, a consequence of both ground motion sets being similar at the lower spectral accelerations at which brace yielding initiates.

Figure 4-20 plots together the collapse fragility curve (top plot) as well as the normalized median brace tensile force (bottom plot) versus spectral accelerations for both frames. The figure demonstrates two key points. First, the median collapse capacity of Frame 2 exceeds the median collapse capacity of Frame 1 by 34%. This result was expected since Frame 2 is designed significantly stronger than Frame 1. Second, as compared to Sa_{MCE} of 1.10g, the braces in both frames reach their yield strength at relatively low spectral accelerations (on the order of Sa of 0.5g), and show only a modest increase in the maximum forces developed past that point (see Figure 4-20 and Table 4-5). The spectral accelerations at which yielding is expected, $Sa_{y,exp}$, are calculated in Table 4-4 and related to the R_μ as follows:

$$\text{Frame 1:} \qquad Sa_{y,exp} = \frac{\frac{2}{3} Sa_{MCE}}{R_\mu} = 0.40g$$

$$\text{Frame 2:} \qquad Sa_{y,exp} = \frac{\frac{2}{3} Sa_{MCE}}{R_\mu} = 0.70g$$

These calculated values compare well with the analysis results summarized in Table 4-5. For example, Table 4-5 shows that the median $P_{max}/P_{y,exp}$ for Frame 1 at 0.40g is 0.96 and 1.04 at 0.60g and then only a small increase passed that point, while for Frame 2, the median $P_{max}/P_{y,exp}$ is 0.97 at 0.60g and 1.01 at 0.80g. Note that in the proposed methodology, the brace force demand ratios are calculated at the MCE demands, which result in ratios of $P_{max}/P_{y,exp}$ equal to about 1.05 for these frames. While the braces continue to strain harden up to a ratio of 1.1, this occurs at large spectral accelerations with low frequencies of occurrence.

4.2.5 Probability of Brace Demand Exceeding Connection Capacity

The models used in this analysis are median models where the expected element properties (e.g. material strengths) are used. By using median models, the failure of brace connections is by default excluded in the analysis as their median strength capacities

exceed the braces median strength capacities. To calculate the probability of brace demand exceeding connection capacity and its possible influence on the overall frame collapse performance, the demand distribution developed by recording the maximum brace tensile forces in the dynamic analysis is used, along with an assumed probability distribution of connection capacity. With the demand and capacity distributions, the reliability index, which can be related to a probability of connection failure, is calculated by the following equation, assuming lognormal probability distributions:

$$\beta = \frac{\ln\left(\dfrac{\hat{C}_m}{\hat{D}_m}\right)}{\sqrt{V_C^2 + V_D^2 - 2\rho V_C V_D}} \qquad (4\text{-}3)$$

$$\left(\frac{\hat{C}_m}{\hat{D}_m}\right) = \left(\frac{D_n}{\hat{D}_m}\right)\left(\frac{\hat{C}_m}{C_n}\right)\frac{\gamma}{\phi} \qquad (4\text{-}4)$$

where $\hat{D}_m$ and $\hat{C}_m$, and D_n and C_n are the median and nominal values of the demand and capacity probability distributions, respectively, V_D and V_C are their lognormal standard deviations, and ρ is the correlation coefficient between demand and capacity, For this analysis, the correlation coefficient is assumed to be zero.

The dispersion around the brace connection demand recorded from the analysis is only due to the record-to-record randomness and does not reflect other uncertainties, such as material and fabrication variability. To include those additional uncertainties, an additional dispersion of 0.15 is added to the recorded analysis demand dispersion using the square root of the sum of the squares (SRSS), .e.g Equation 2-14. The initial dispersion varies from 0.20 at the low spectral acceleration to 0.02 at the high spectral acceleration, i.e. past brace yielding. The total dispersion at the high spectral accelerations is therefore 0.15, which compares well with collected statistics on brace forces from brace test results reported in Table 6-2. The analysis results are taken to represent the $\hat{D}_m / D_n$-ratio, where $\hat{D}_m$ is the true median demand and D_n the yield strength of the brace based on nominal material properties. For the connection capacity

distribution, $\hat{C}_m / C_n$ is set to 1.4 and $V_C = 0.15$. V_C is meant to capture the total dispersion of the brace connection capacity, including material, fabrication and connection model uncertainty and its value and $\hat{C}_m / C_n$ are based on observed connection capacity statistics of selected connection failure modes reported in Table 6-1 in Chapter 6. For this example, $\hat{C}_m$ is the true median capacity of a selected failure mode and C_n the nominal capacity of the same failure mode based on code design equation and nominal material properties. Given those statistical parameters, the probability of demand exceeding capacity is calculated for both frames vs. spectral acceleration for ϕ/γ-ratios of 0.75, 0.9 and 1.0. For comparison, the current AISC Seismic Provisions imply a ϕ/γ ratio of 0.75 for brace connections. The probability of brace demand exceeding connection capacity when $\phi/\gamma = 0.9$ is plotted in Figure 4-21 for both frames. As indicated, the probability of demand exceeding capacity saturates at about 0.05.

Figure 4-21 shows that the probability of brace demand exceeding connection capacity is negligible before $Sa_{y,exp}$ (0.40g and 0.70g for frames 1 and 2, respectively) and then increases sharply until it reaches its peak value. The probability of frame collapse including connection failures can be calculated by the following:

$$P(Coll|Sa) = P(Coll_{Sys}|Sa) + P(Coll_{D>C}|D>C) \times P(D>C|\overline{Coll}_{Sys}, Sa) \qquad (4\text{-}5)$$

where $P(Coll|Sa)$ is the total conditional collapse probability at a given spectral acceleration, $P(Coll_{Sys}|Sa)$ is the conditional probability of frame collapse as calculated directly from the incremental dynamic analysis, $P(Coll_{D>C}|D>C)$ is the conditional probability of frame collapse due to demand exceeding the capacity of capacity-designed components, and $P(D>C|\overline{Coll}_{Sys}, Sa)$ is the conditional probability of demand exceeding the capacity of capacity-designed components. By conservatively assuming $P(Coll_{D>C}|D>C) = 1.0$, the total collapse fragility curves for Frame 1 and Frame 2 are calculated for the three ϕ/γ-ratios. Figure 4-22 shows the results for $\phi/\gamma = 0.9$ where the increase in collapse probabilities at low spectral accelerations (around S_{aT1} of 0.5g) due to the inclusion of connection failures is evident.

To calculate the mean annual frequency of frame collapse for the different cases, the collapse fragility curves are integrated with site hazard curves. The hazard curve used for this example is from a downtown San Francisco site (Lat. 38.0, Lon. -121.7) with T of 1.02 seconds, see Figure 4-23. For reference, the spectral accelerations for exceedance probabilities of 2% and 10% in 50 years are 1.38g and 0.79g, respectively. The integration of the hazard curve with the frame collapse fragility is given by the following equation in continuous integral form:

$$MAF(D > C) = \int P(D > C | Sa = x) |dMAF(x)| \qquad (4\text{-}6)$$

In discrete form, the *MAF(Coll)* becomes:

$$MAF(D > C) = \sum_{all \ x_i} P(D > C | Sa = x_i) * MAF(Sa = x_i) \qquad (4\text{-}7)$$

The mean annual frequency of collapse can be converted into a probability of collapse in 50 years (making the typical assumption that *Sa* occurrences are Poissonian) using the following equation:

$$P(Collapse)_{50\,years} = 1 - e^{-50MAF(Coll)} \qquad (4\text{-}8)$$

The probabilities of collapse in 50 years for the two frames and three ϕ/γ-ratios are presented in Table 4-6 and plotted in Figure 4-24. Note that the value of ϕ/γ equal to 0 in Figure 4-24 corresponds to the case without connection failure. These data demonstrate that the probabilities of collapse of Frame 2 are considerably lower than of Frame 1 as well demonstrating that the impact of connection failures is considerably lower for Frame 2, a result of the braces developing the maximum demand at higher spectral accelerations for Frame 2 than for Frame 1. The probability of collapse in 50 years for Frame 1 excluding connection fractures is 2.0% compared to 0.5% for Frame 2, representing a 4 times larger risk or a 1.5% absolute increase in risk for Frame 1. When the ϕ/γ-ratio is 1.00, the collapse probabilities are 7.1% and 2.8%, for Frames 1 and 2, respectively. In this case, the connection failures increase the risk of collapse in Frame 1 by 3.6 times (a 5.1% absolute increase in collapse probability) and in Frame 2 by 5.6 times (a 2.3%

96

absolute increase in probability). Comparing the two frames, the 4.3% difference in absolute risk (between 7.1% and 2.8%) could be attributed to a difference of 1.5% due to the frame behavior (2.0% versus 0.5%) with the remaining2.8% difference due to connection fractures.

The probabilities of collapse in Table 4-6 are calculated based on collapse fragility curves that have not been adjusted for the ground motion spectral shape factor. Therefore, the collapse probabilities are larger than the actual values that would be calculated following the FEMA P695 procedures. The main points of the data are to demonstrate the relative effect of the connection failures on collapse and how these differ depending on the R_μ and ϕ/γ-ratios of the designs. If the median collapse points are adjusted with a spectral shape factor of 1.3, i.e. the median collapse points are now 2.35g and 3.16g, and the dispersions are kept the same; the probabilities of collapse in 50 years excluding connection fractures are 0.9% and 0.02% for Frame 1 and Frame 2, respectively. These are reduced from the collapse probabilities reported above of 2.0% and 0.5% without the spectral shape adjustment. When the connection effects are included for the ϕ/γ-ratio of 1.00, the resulting values of collapse probabilities are 6.2% and 2.5%, versus the values of 7.1% and 2.8% without the spectral shape shift. The absolute difference between the case without connection fractures and with a ϕ/γ-ratio of 1.00 is similar between the original and adjusted collapse fragility curves but the relative influence of connection failures is higher when the collapse fragility curves have been adjusted. Inclusion of connection failures increases the collapse probability by 6.9 times for Frame 1 (from 0.9% to 6.2%) and by 125 times for Frame 2 (from 0.02% to 2.5%). Of course, the large change ratio (125 times) for Frame 2 is due to the small probability for the basic case. In fact, the absolute increase in risk is much larger for Frame 1.

4.3 Monte Carlo Dynamic Analyses of Single-Story Special Concentrically Braced Frame Including Brace Connection Failure

4.3.1 Description of Analysis

In the previous analyses, neither modeling uncertainties nor brace connection failures were simulated directly in the nonlinear dynamic analyses. These effects were instead incorporated by post-processing the nonlinear dynamic analysis data. To evaluate the effect of connection failures on frame collapse, the prior analyses required an assumption as to the probability of collapse due to connection failures, i.e. $P(Coll_{D>C}|D>C)$. To evaluate this assumption, the analyses in this section incorporate connection failures directly in the nonlinear dynamic analysis. Since the likelihood of connection failure depends on both the connection strength and the force demands from the brace, assessing the connection failure requires that the analyses account for variability of both the brace and connection strength and modeling parameters.

To assess the probability of collapse due to connection failures, $P(Coll_{D>C}|D>C)$, dynamic analyses of Frame 1 are performed again, now with the possibility of brace fracture included. The analyses entail full treatment of modeling uncertainty, where the values of the main model parameters, as well as the brace connection strengths, are randomized. The results will assist in deciding what probability of collapse due to connection fractures, $P(Coll_{D>C}|D>C)$, to use in Equation 4-5. Furthermore, the analysis will evaluate the effects of modeling uncertainties on the frame's collapse capacity. The FEMA P695 (FEMA 2009) system reliability methodology incorporates modeling uncertainties when constructing frame collapse fragility curves by inflating the dispersion of the median models results while keeping the median collapse point constant. However, Liel et al. (2008) demonstrated that modeling uncertainties will in most cases both increase the dispersion of the collapse fragility curve as well as decrease the predicted median collapse point compared to the median model results. Therefore, simple inflation of the dispersion can result in unconservative probabilities of collapse. Liel et al.'s results were based on collapse risk assessments of ductile and non-ductile reinforced-concrete

moment frame buildings, where the median collapse capacities decreased by as much as 20% due to modeling uncertainties

Table 4-7 lists the model parameters, and their distributions, that are randomized in this study. The parameters randomized in this study are the input ground motion, the brace yield and ultimate stress, the brace gross area, the initial imperfection of the brace, the input parameters of the low-cycle fatigue material, the connection strength and the input parameters of the Modified Ibarra Krawinkler deterioration model. The distributions of the model parameters, central values and dispersions, are based on experimental results reported by multiple sources listed in Table 4-7. Based on the experimental results, lognormal probability distributions are assumed for most model parameters except the ultimate rotational capacity, θ_u, of the flexural hinge model and the input ground motion random variable, both cases where uniform distributions are assumed. One thousand model realizations of Frame 1 are created through Monte-Carlo simulation methods (Melchers, 1999; Rubinstein, 1981), and for each model realization, a ground motion record is randomly selected as well. For each set of simulated random variables the performance of the frame is assessed through dynamic analyses. Owing to the large number of model realizations, instead of a complete incremental dynamic analysis, the models are analyzed at selected spectral acceleration intensities to define the lower portion of the collapse fragility curve (up to just above the median collapse intensity).

In general, the model parameters listed in Table 4-7 are assumed to be independent from each other. A few exceptions are the θ_p, θ_{pc} and Λ parameters of the Modified Ibarra Krawinkler deterioration model and F_y and F_u of the brace steel material. The Modified Ibarra Krawinkler deterioration model defines the rotational behavior of the flexural hinge springs. The model is shown schematically in Figure 4-25 where all the model parameters are defined. θ_p, θ_{pc} and Λ are the pre-capping rotation capacity, post-capping rotation capacity and cyclic deterioration parameters. These three parameters are assumed correlated within the same element based on values from Lignos and Krawinkler (2009). The correlation between the parameters is shown in the correlation matrix in Table 4-8. F_y and F_u are the steel brace yield stress and ultimate stress, respectively, and a partial

correlation of 0.80 is assumed between them based on data from Liu (2003). The positive correlation between the parameters implies that if one of the variables is low or high, the other ones are likely to be low or high as well. This behavior is captured by simulating correlated random variables in the Monte-Carlo simulations.

To better quantify the how the connection failures affect the probability of collapse, all models are initially analyzed without connection fractures included and the probability of collapse calculated. The analyses are then performed again with connection fractures included. However, all one thousand simulations do not need to be re-run. Instead, the only analyses that are re-run are those where the frame has not collapsed in a sidesway mode (due to brace failure) and the calculated brace force demand exceeds the simulated connection strength. By using the method described above, the information the analyses give back is $P\!\left(Coll_{D>C}\middle|\overline{Coll}_{Syts}, D > C\right)$, not $P\!\left(Coll_{D>C}\middle|D > C\right)$. At the lower portion of the system collapse fragility curve, where the main focus of these analyses is, the difference between the two is negligible. Typically, this requires re-running of about 70 to 110 of one thousand analyses for each ground motion intensity level. The median brace connection strength is set intentionally low ($\phi/\gamma = 1.00$) to increase the instances of connection fractures. Presumably, this choice will provide a conservative estimate of the influence of connection failures on collapse risk.

The selected spectral accelerations of special interest are those between where the braces have already yielded in tension (at about Sa of 0.40g) and the MCE intensity (Sa_{MCE} of 1.10g). Based on the results from Section 4-2, the selected spectral accelerations for the second set of analyses are 0.40g, 0.80g, 1.25g, 1.50g and 2.00g. Table 4-9 lists the selected spectral accelerations, along with the probability of frame collapse at those accelerations and the median and dispersion of the normalized brace tensile forces. At $Sa = 0.40g$, probability of frame collapse is negligible (no observed collapses and negligible probability based on fitted distribution) but the normalized median brace force is already 0.96. Any additional collapses due to connection fractures at $Sa = 0.40g$ will have a large impact on the annual probability of frame collapse due to the high return periods at low spectral accelerations. At $Sa = 2.00g$, the probability of

collapse is 59% and the normalized median brace force is 1.09. The data from Table 4-9 and Figure 4-26 show both the probability of collapse (top plot) and the median of the normalized brace force (bottom plot) at the selected spectral accelerations.

4.3.2 Monte Carlo Dynamic Analysis Results

The Monte Carlo nonlinear analyses are initially performed with brace fracture excluded and the probability of brace demand exceeding the connection capacity is calculated for the non-collapsed cases. The median and dispersion of the brace demand are listed in Table 4-10. With the assumed median connection capacity of 1.35 times the median brace yield strength and dispersion of 0.15, the probability of demand exceeding capacity is calculated using component reliability methods described in Section 2.3 (Equation 2-8 and 2-11). The connection strengths of the realization are then incorporated in the model and the dynamic analyses are re-run for the cases where the connection capacity is less than the brace demand. The number of additional collapses due to connection failure is then incorporated in the results. The complete results are listed in Table 4-11 and shown in Figure 4-27 and 4-28.

As shown in Table 4-10, the probability of connection failure is fairly constant at around 11.0% to 13.0% for Sa_{T1} values of 0.80g, 1.25g, 1.50g and 2.00g, a result of brace forces having already saturated at 0.80g. However, as Table 4-11 and Figure 4-27 demonstrate, the added probability of collapse due to connection fractures $P\left(Coll_{D>C}\middle|\overline{Coll}_{Syts}, D > C\right)$ is not constant and it tends to increase with increasing ground motion intensity, Sa_{T1}. Referring to Table 4-11 and Figure 4-27, at $Sa_{T1} = 0.40$g the connection failures have no effect on collapse probability suggesting that at this ground motion intensity, the frame is robust enough that it can survive even if connections fracture. As the ground motion intensity increases, the frame's inherent collapse resistance decreases and $P\left(Coll_{D>C}\middle|\overline{Coll}_{Syts}, D > C\right)$ increases. Referring again to Figure 4-27, the increased probability of collapse due to connection failures increases up to about 0.2 to 0.3 at about 1g, approaching and belyond $S_{a,MCE}$. These results tend to agree

with conclusions from Luco and Cornell (2000) on the effects of brittle connection fractures on a 3-story Special Moment Resisting Frame, i.e. that the effect of connection fractures is less pronounced at lower ground motion intensities than at higher ones. These results greatly reduce the influence of brace connections on the system reliability as even if braces are likely to fracture at low spectral accelerations, i.e. close to $Sa_{y,exp}$, the probability of frame collapse is low. Figure 4-28 demonstrates the reduced influence of brace connection fractures on the frame's collapse fragility curve, where at the lower spectral accelerations, the probability of collapse with connection fractures (diamonds on the plot) and without connection fractures (squares on the plot) is nearly identical. The crosses on the plot represent the results if connection fractures had directly caused collapse, i.e., $P\left(Coll_{D>C}|D>C\right)$ equal to 1. Referring to Figure 4-27, at the spectral acceleration equal to the MCE demand, $P\left(Coll_{D>C}|\overline{Coll}_{Syts}, D>C\right) \approx 25\%$, though the absolute percentage is likely to depend on the system analyzed. The reduction in $P\left(Coll_{D>C}|\overline{Coll}_{Syts}, D>C\right)$ at high spectral accelerations, i.e. after $Sa_{TI} = 1.25g$ might seem counter intuitive at first. However, this is a result of conditioning at non-collapsed cases from the initial analyses. At the higher spectral accelerations, the non-collapsed cases are generally cases where the frames are subjected to ground motion records whose characteristics (e.g. frequency content, duration etc.) are such that they do not impose large deformation demands on the frames. As a result, the frames are less likely to collapse, with or without connection fractures.

4.3.3   Probability of Collapse Including Connection Fractures

With information on $P\left(Coll_{D>C}|D>C\right)$, the probability of collapse in 50 years can be re-calculated using Equations 4-7 and 4-8, and a site seismic hazard curve. The seismic hazard curve used for this example is again from a downtown San Francisco site (Lat. 38.0, Lon. -121.7, Figure 4-23). Table 4-12 lists the revised probabilities of collapse in 50 years for different ϕ/γ – ratios. Due to the frame's post-connection fracture capacity, the impact of brace connection fractures on the probability of collapse is significantly

reduced, allowing for the possibility to reduce the required design strength of connection, i.e. reducing the required ϕ/γ – ratios. Table 4-12 shows that the probability of collapse in 50 years for a ϕ/γ – ratio of 1.00 increases the probability of collapse excluding connection fractures by only 0.3% compared to 5.1% if connection fractures lead directly to collapse, a significant reduction in collapse probabilities. If a constant $P\left(Coll_{D>C}|D>C\right)$ of 0.20 at all spectral accelerations is used, the added probability of collapse in 50 years is 1.0% for a ϕ/γ – ratio of 1.00 and 0.4% for a ϕ/γ – ratio of 0.90. 0.4% probability of collapse due to connection fractures is of course a large addition to the total probability of collapse but the results reported here are for fairly weak connections, i.e. current ϕ/γ – ratio is 0.75, and are mainly meant to demonstrate that the limited impact of connection fractures at low intensities reduces the calculated probability of collapse in 50 years significantly compared to cases when connection fractures are believed to lead directly to system collapse. With the current ϕ/γ – ratio of 0.75, the added probability of collapse is small, or 0.002 for $P\left(Coll_{D>C}|D>C\right)$ of 1.00 and below 0.0004 for the other cases.

4.4 Conclusions

Capacity-based design is used as means to provide energy dissipation and a ductile response of seismic frames during earthquake ground motions. Global frame design values (e.g. R-factor) govern largely the minimum allowable size of deformation-controlled components and therefore both the demand on force-controlled components as well as the spectral acceleration at which yielding is expected to occur. For larger R-factors, yielding of deformation-controlled components is expected to occur at lower spectral accelerations than for smaller R-factors, due to smaller member sizes. The probability of experiencing large enough ground motions to experience member yielding is consequently higher for systems with large R-factors than for systems with small R-factors. Evidently, oversizing of members, which may occur in real structures for a number of reasons, counteracts this influence of the R-factor. Based on these observations, it is reasonable to assume that these same factors will influence the

reliability of force-controlled components and the methodology developed in Chapter 3 considers them when determining the required design strength of capacity-designed components, by including R_μ in the methodology which incorporates both the code R-factor as well as member oversizing.

To verify the influence of these factors and the applicability of the methodology, dynamic analyses of single-story SCBF´s were conducted. The first frame analyzed was an optimally designed frame according to ASCE 7-10 minimum design loads (ASCE, 2010), while the second one was significantly over-designed. The expected base (or story) shear yield strength of Frame 2 was 75% larger than that for Frame 1 and subsequently, R_μ for Frame 2 was 1.4 while 2.5 for Frame 1. The results demonstrated that it takes a considerably larger ground motions to cause yielding in the over-designed frames and that the spectral acceleration at which yielding occurs can be estimated fairly well with the predictive equations for $Sa_{y,exp}$ from Chapter 3 using calculated R_μ based on guidelines from Table 3-12. Consequently, when calculating the mean annual frequency of brace demand exceeding connection capacity, the values for Frame 1 were 2.5 to 4.0 times higher than for Frame 2 if designed according to the same criteria, i.e. the same γ/ϕ- ratio. This suggests that if consistent mean annual frequency is the objective, the γ/ϕ- ratio can be relaxed for Frame 2 to 0.90 compared to the current ratio of 0.75. Additionally, the overall probability of collapse for Frame 2 was considerably lower than for Frame 1, signifying an even further allowance for relaxing the γ/ϕ- ratio for Frame 2. The probability of collapse in 50 years, excluding the probability of connection fractures, was 2.0% and 0.5% for Frame 1 and Frame 2, respectively, and with γ/ϕ- ratio of 1.00, the probability was 7.1% and 2.8% for the two frames.

Connection fractures were not included in the first set of analyses so when relating the probability of connection fractures to the probability of frame collapse, the simplifying assumption was made that a connection fracture equals frame collapse, i.e. $P\left(Coll_{D>C} \middle| D > C\right) = 1.0$. To assess the probability of collapse due to connection fractures, as well as the influence of including modeling uncertainty in the analysis, the second set of analyses was a "full" modeling uncertainty analysis where connection fractures were

simulated directly in the dynamic analysis. The results from the analysis demonstrated that the probability of collapse due to connection fractures is not a constant, as assumed in the methodology from Chapter 3, but rather a function of the ground motion intensity, Sa_{T1}. The probability of collapse due to connection fractures was close to zero at spectral accelerations around $Sa_{y,exp}$ and then increased as Sa_{T1} increased. These finding suggest that connection fractures are likely to occur, even for relatively moderate ground motions, but that connection fractures are unlikely to cause system collapse. The low probability of collapse due to connection fractures at the lower spectral accelerations therefore greatly reduces the impact of connection fractures on the overall frame reliability and allows for the possibility to increase the tolerable probability of connection fractures, i.e. to reduce the required design strength of connections. These absolute values for $P\left(Coll_{D>C}\middle|D>C\right)$ are likely to be very sensitive to how well frames can re-distribute the load once a connection fractures, i.e. to redundancy and correlation within the system. The probabilities may also depend on factors such as ground motion duration effects, which are not explicitly considered in this study. However, the trend of low values at the low intensities with a gradual increase until the peak impact is reached is likely to be similar for other seismic resistant systems. Also, as the frame analyzed here only included a single pair of braces and accounted for no lateral stiffness from the gravity system, the results can be considered to give an upper bound on the likely influence of connection fractures.

Table 4-1: Properties of the two single-story braced frames investigated in Chapter 4

Properties	Frame 1	Frame 2
Width	30 ft	-
Height	15 ft	-
Seismic Weight	1040 kips	-
Code T_0	0.15 s	-
Design Base Shear	173 kips	-
Beam Section	W18x35	-
Beam: $F_{y,exp}$	55 kips	-
Columns Section	W12x72	-
Column: $F_{y,exp}$	55 kips	-
Brace Section	HSS 6x6x5/16	HSS 6x6x5/8
Brace: $F_{y,exp}$	60.3 kips	60.3 kips -
$\phi P_{n,c}$	158	266
$\phi P_{n,t}$	266	474
L/r	88	94
$F_{y,exp}A_g$	388	706
$F_{cr}A_g$	196	325
V_{RSA}	173	-
$V_{y,exp}$	413	729
$R_\mu = V_{DBE}/V_{y,exp}$	2.5	1.4

Table 4-2: Far-field loading protocol used to analyze brace behavior

Load Step	Number of Cycles	Peak θ (rads)	Peak Δ_a/L_b (rad)
1	6	0.00075	0.000375
2	6	0.0010	0.00050
3	6	0.0015	0.00075
4	4	0.0020	0.0012
5	2	0.01025	0.005
6	2	0.0185	0.009
7	2	0.02675	0.013
8	2	0.04	0.020
9	2	0.05	0.025

Table 4-3: Near-field tension and compression loading protocols used to analyze brace behavior

Load Step	Number of Cycles	Near-Field Tension		Near-Field Compression	
		Peak θ (rads)	Peak Δ_a/L_b (rad)	Peak θ (rads)	Peak Δ_a/L_b (rad)
1	6	0.00075	0.000375	0.00075	0.000375
2	½	0.0455	0.0228	0.0185	0.009
3	½	0.0415	0.0210	0.0605	0.030
4	1	0.0185	0.009	0.0185	0.009
5	2	0.0150	0.007	0.0150	0.007
6	4	0.01025	0.005	0.01025	0.005
7	6	0.0015	0.00075	0.0015	0.00075
8	4	0.0020	0.0012	0.0020	0.0012
9	2	0.01025	0.005	0.01025	0.005
10	2	0.0185	0.009	0.0185	0.009
11	2	0.02675	0.013	0.02675	0.013
12	2	0.04	0.020	0.04	0.020
13	2	0.05	0.025	0.05	0.025

Table 4-4: Estimation of R_μ for the two frames analyzed following guidelines from Table 3-12

Step 1		Step 2			Step 3	Step 4	Step 5	Step 6
Story	Brace	Tension [1] [kips]	Compression [2] [kips]	$V_{v,exp}$ [kips]	V_{RSA} [kips]	$V_{y,exp}/V_{RSA}$	$Sa_{y,exp}$ [g]	R_μ
1	HSS 6x6x5/16	388	196	413	173	2.4	0.38	2.5
2	HSS 6x6x5/8	706	325	729	173	4.2	0.67	1.4

1) $F_{y,exp} * A_g$

2) Column Strength Equation using expected material properties. The effective brace length is 80% of the work-point-to-work-point length

Table 4-5: Median and COV of normalized maximum brace forces, $P_{max}/P_{y,exp}$, from the Incremental Dynamic Analyses

Sa_{TI}	Frame 1		Frame 2	
[g]	Median	COV	Median	COV
0.10	0.37	0.20	0.21	0.22
0.20	0.72	0.12	0.43	0.20
0.30	0.89	0.08	0.63	0.16
0.40	0.96	0.05	0.84	0.10
0.60	1.04	0.03	0.97	0.06
0.80	1.05	0.02	1.01	0.03
1.00	1.06	0.02	1.05	0.02
1.25	1.07	0.02	1.07	0.02
1.50	1.08	0.02	1.07	0.02
2.00	1.09	0.02	1.08	0.02
2.50	1.10	0.02	1.09	0.02
3.00	1.10	0.02	1.10	0.02

Table 4-6: Calculated probabilities of collapse in 50 years for Frames 1 and 2 for variable ϕ/γ-ratios

P(Coll) in 50 years	Frame 1	Frame 2
Connection Failure Excluded	0.020	0.005
$\phi/\gamma = 0.75$	0.022	0.006
$\phi/\gamma = 0.90$	0.037	0.013
$\phi/\gamma = 1.00$	0.071	0.028

Table 4-7: Table of random model parameters

Random Variable	Central Value	Dispersion	Distribution	Source
Ground Motions				
GM #	Min: 1	Max: 44	Uniform Discrete	FEMA P695
Brace HSS6x6x5/16				
F_y	60.3	0.08	Lognormal	Liu (2003)
F_u	75.4	0.05	Lognormal	Liu (2003)
A_g	6.43	0.10	Lognormal	Ellingwood et al (1980)
Δ/L	0.25%	0.7	Lognormal	Uriz(2005),Galambos(2009)
m	0.500	0.20	Lognormal	Uriz (2005)
E_0	0.095	0.30	Lognormal	Uriz (2005)
Connection				
Strength	$1.35*P_{y,brace}$	0.15	Lognormal	Multiple (See Table 5-23)
Column W12x72				
$M_y/M_{y,p}$	1.17	0.21	Lognormal	Lignos & Krawinkler
M_c/M_y	1.11	0.05	Lognormal	(2009)
θ_p	0.034	0.43	Lognormal	
θ_{pc}	0.160	0.41	Lognormal	
Λ	2.0	0.43	Lognormal	
θ_u	Min: 0.05	Max: 0.06	Uniform	
Beam W18x35				
$M_y/M_{y,p}$	1.17	0.21	Lognormal	Lignos & Krawinkler
M_c/M_y	1.11	0.05	Lognormal	(2009)
θ_p	0.038	0.43	Lognormal	
θ_{pc}	0.130	0.41	Lognormal	
Λ	1.5	0.43	Lognormal	
θ_u	Min: 0.05	Max: 0.06	Uniform	

m: Slope of Coffin-Manson curve in log-log space

E_0: Value of strain at which one cycle causes failure

M_y: Effective yield moment

$M_{y,p}$: Nominal yield moment

M_c: Capping moment (w/strain hard.)

θ_p: Pre-capping rotation capacity

θ_{pc}: Post-capping rotation capacity

Λ: Cyclic deterioration parameter

θ_u: Ultimate rotation capacity

Δ/L: Brace initial imperfection

Table 4-8: Correlation matrix between parameters in the Modified Ibarra Krawinkler Deterioration Model

Random Variable	θ_p	θ_{pc}	Λ
θ_p	1.00	0.69	0.44
θ_{pc}	0.69	1.00	0.67
Λ	0.44	0.67	1.00

Table 4-9: Probability of collapse of the median model of Frame 1 at the spectral accelerations used in the modeling uncertainty analysis

Sa_{T1} [g]	Collapse Probability: Simulation Results	Collapse Probability: Fitted Distribution (Median = 1.81g, Disp = 0.45)	Median $P_{max}/P_{y,exp}$	COV $P_{max}/P_{y,exp}$
0.40	0/44 = 0.00	0.00	0.96	0.05
0.80	1/44 = 0.02	0.03	1.05	0.02
1.25	9/44 = 0.20	0.21	1.07	0.02
1.50	16/44 = 0.36	0.34	1.08	0.02
2.00	26/44 = 0.59	0.59	1.09	0.02

Table 4-10: Probability of brace demand exceeding connection capacity

Sa_{T1} [g]	D_m	V_D	C_m	V_C	$P(D>C)$
0.40	0.92	0.10	1.35	0.15	0.02
0.80	1.07	0.10	-	-	0.11
1.25	1.09	0.10	-	-	0.12
1.50	1.10	0.09	-	-	0.12
2.00	1.11	0.09	-	-	0.13

Table 4-11: Results for Frame 1 including modeling uncertainty and connection fracture

Sa_{T1} [g]	No. of Collapses (Connection Failures Excluded)	No. of Non-Collapsed Models w/Connection Failures	No. of Additional Collapses	$P(Coll_{D>C}|D>C,No\ Coll_{sys})$	$P(Coll)$
0.40	0 (0.0%)	17	0	0.0%	0.0%
0.80	35 (3.5%)	111	11	9.9%	4.6%
1.25	214 (21.4%)	114	36	31.6%	25.0%
1.50	402 (40.2%)	70	19	27.1%	42.1%
2.00	602 (60.2%)	65	14	21.5%	61.6%

Table 4-12: Calculated probabilities of collapse in 50 years for Frame 1 based on $P(Coll|D>C)$

$P(Coll)$ in 50 years	$P(Coll|D>C)$ = 1.0	$P(Coll|D>C)$ = 0.1	$P(Coll|D>C)$ = 0.2	$P(Coll|D>C)$ = Results from 4.3.2*
Connection Failure Excluded	0.020	0.020	0.020	0.020
$\phi/\gamma = 0.75$	0.022	0.020	0.020	0.020
$\phi/\gamma = 0.90$	0.037	0.021	0.024	0.021
$\phi/\gamma = 1.00$	0.071	0.025	0.030	0.023

* $P(Coll_{D>C}|D>C,No\ Coll_{sys})$ results from Section 4.3.2 (and listed in Table 4-11) are linearly interpolated between Sa levels and used with Equations 4-5, 4-7 and 4-8 to calculate probabilities of collapse in 50 years for Frame 1.

a)   b)
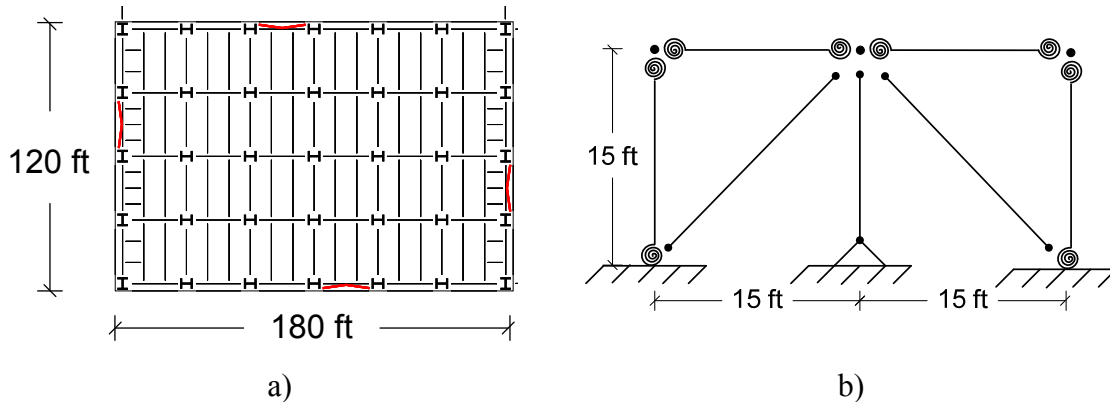
Figure 4-1: SCBF analyzed for this example a) Plan b) Elevation
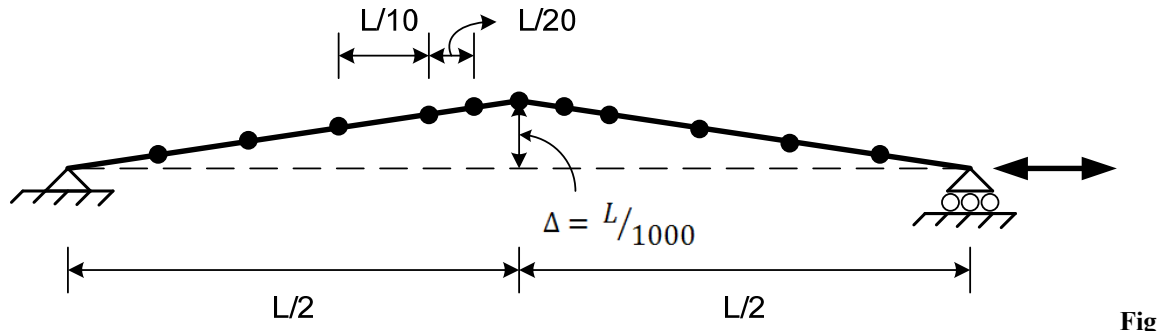
Figure 4-2: OpenSees model of braces.
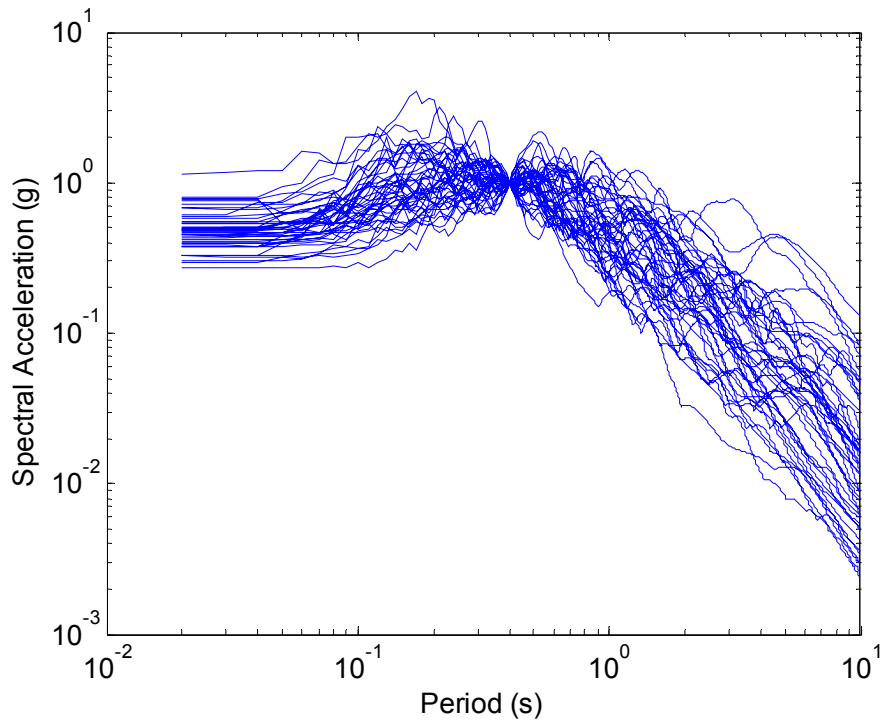
Figure 4-3: Earthquake response spectra for the 44 ground motions used for the Incremental Dynamic Analysis. The ground motions records are all scaled to have the same spectral acceleration at the first mode period of the frames.
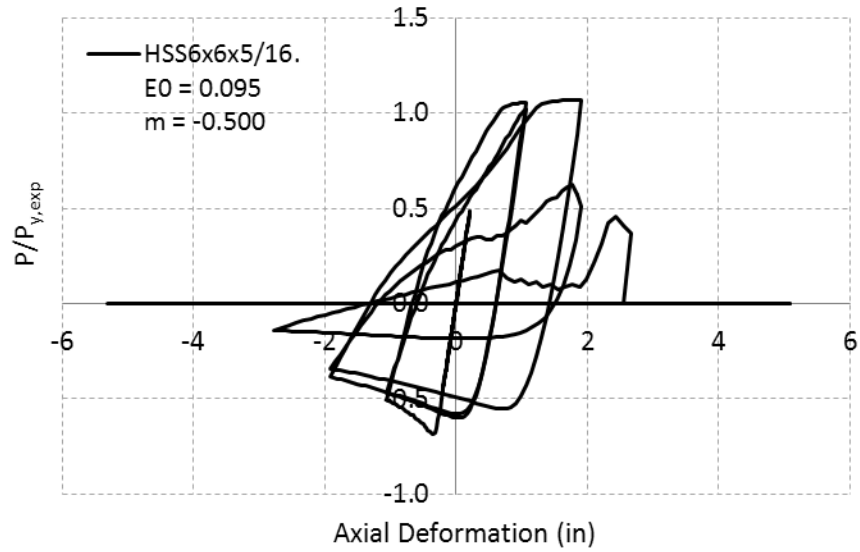
Figure 4-4: Response of the OpenSees model of a HSS6x6x5/16 brace section when subjected to a far-field loading protocol. E0 and m are parameters of the fatigue material used. Brace fracture occurs at relatively low axial deformations
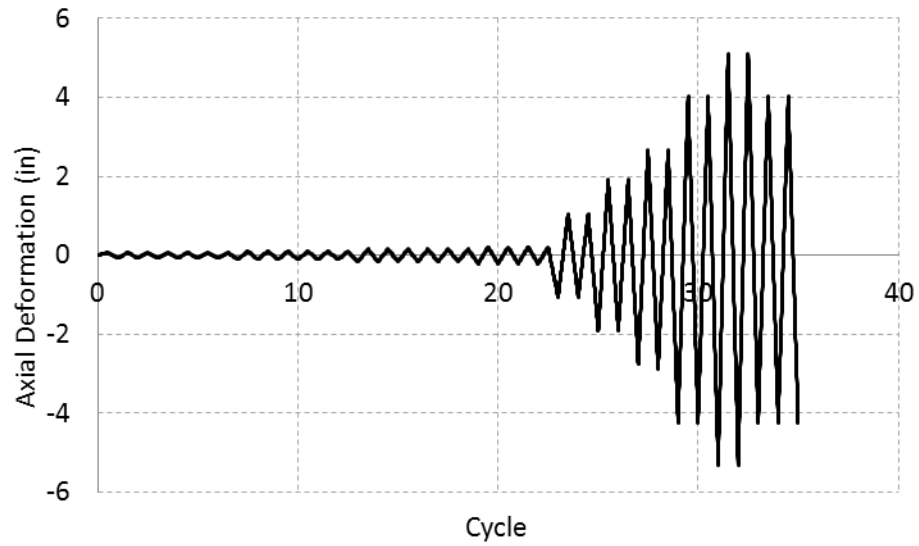
Figure 4-5: Far-field loading protocol developed by Fell et al (2006) and used to analyze brace behavior running dynamic analysis of SCBF frames
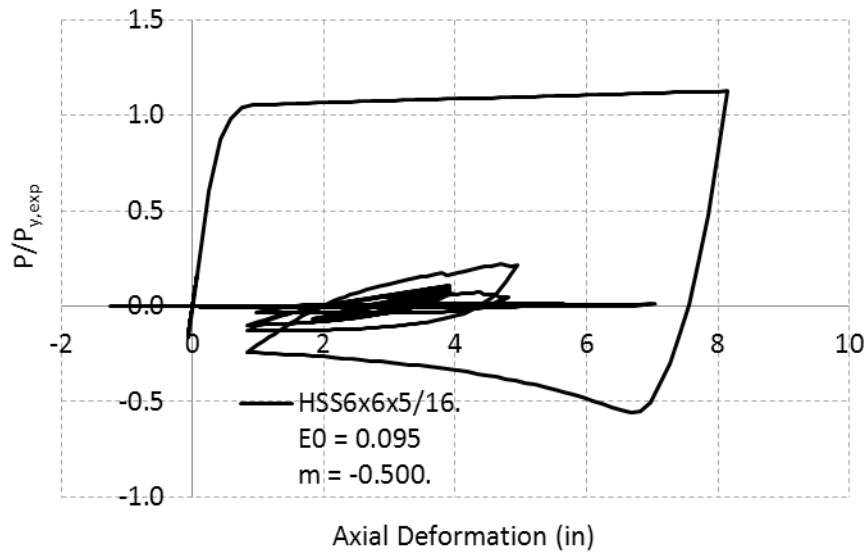
Figure 4-6: Response of the OpenSees model of a HSS6x6x5/16 brace section when subjected to a near-field tension loading protocol. E0 and m are parameters of the fatigue material used.
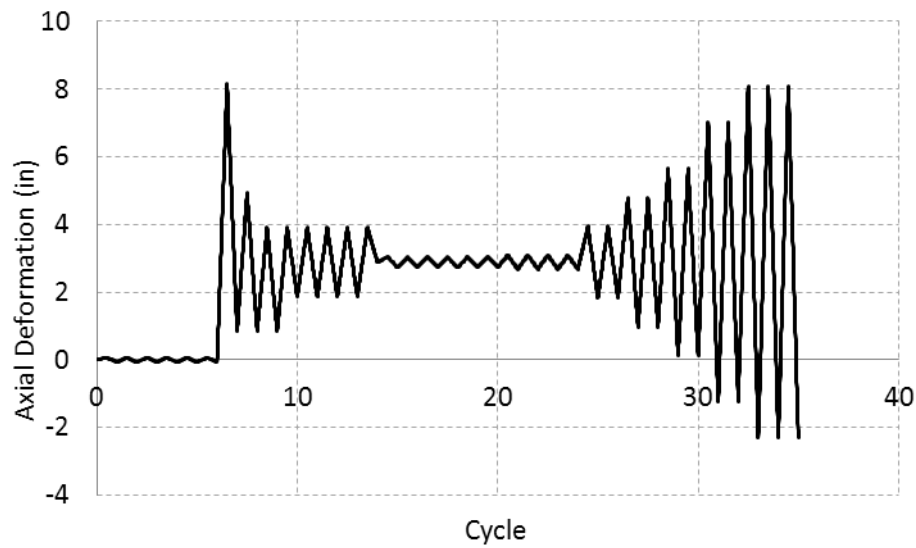
Figure 4-7: Near-field tension loading protocol developed by Fell et al (2006) and used to analyze brace behavior running dynamic analysis of SCBF frames
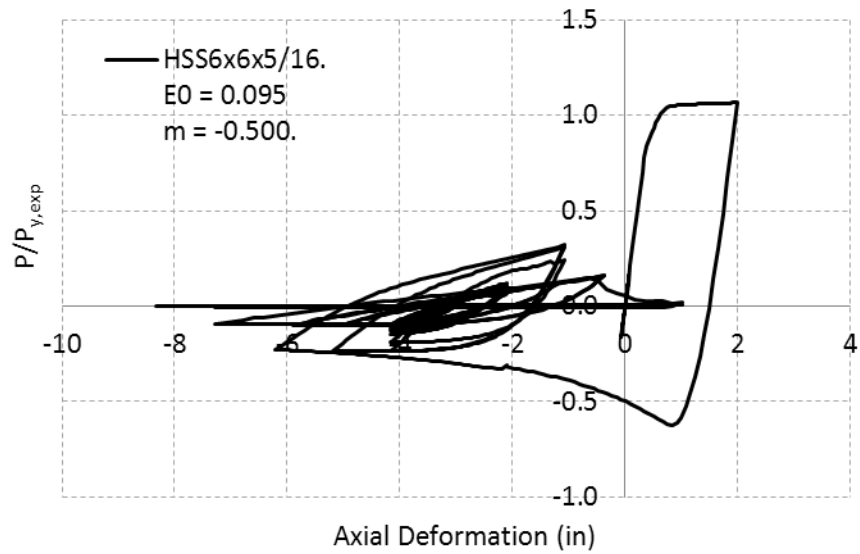
Figure 4-8: Response of the OpenSees model of a HSS6x6x5/16 brace section when subjected to a near-field compression loading protocol. E0 and m are parameters of the fatigue material used.
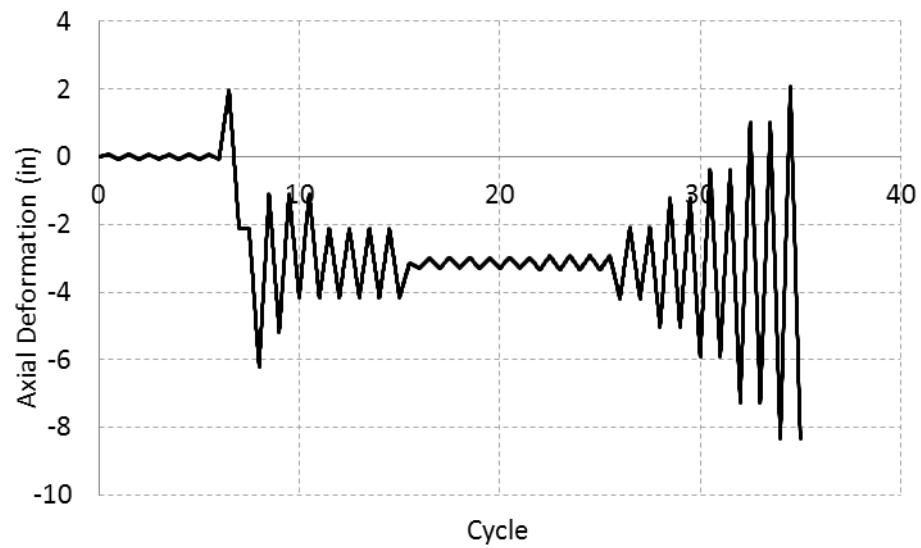
Figure 4-9: Near-field compression loading protocol developed by Fell et al (2006) and used to analyze brace behavior running dynamic analysis of SCBF frames
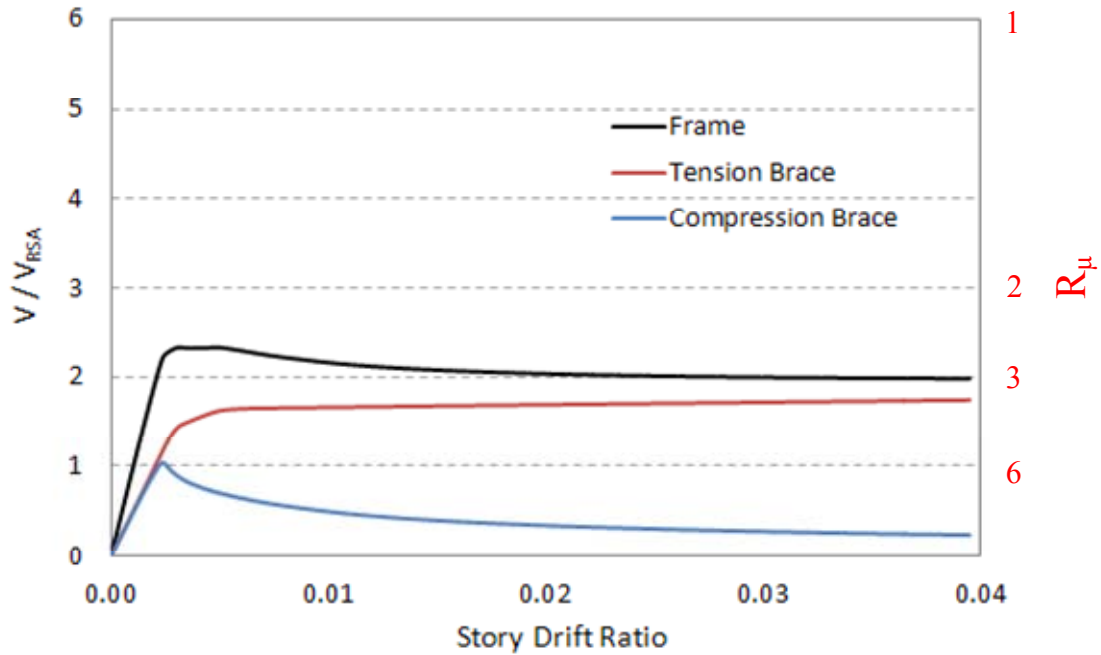
Figure 4-10: Results from pushover analysis on Frame 1 showing normalized base shear on the left y-axis, estimated R_μ on the right y-axis and story drift on the x-axis. The R_μ based on the pushover analysis is 2.6
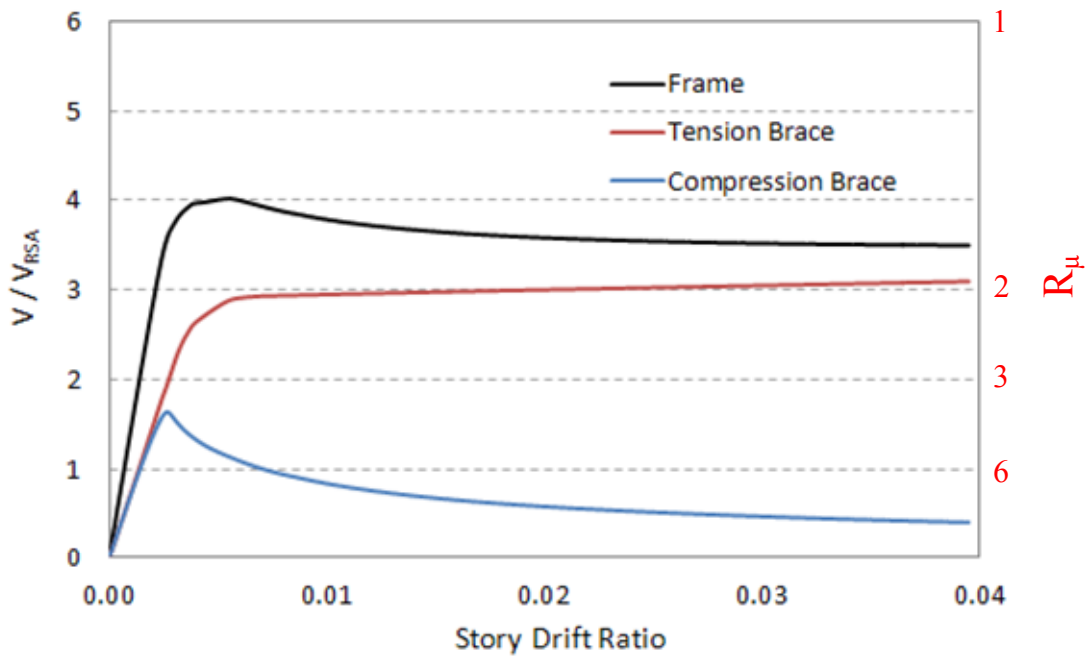
Figure 4-11: Results from pushover analysis on Frame 2 showing normalized base shear on the left y-axis, estimated R_μ on the right y-axis and story drift on the x-axis. The R_μ based on the pushover analysis is 1.5

a)

b)
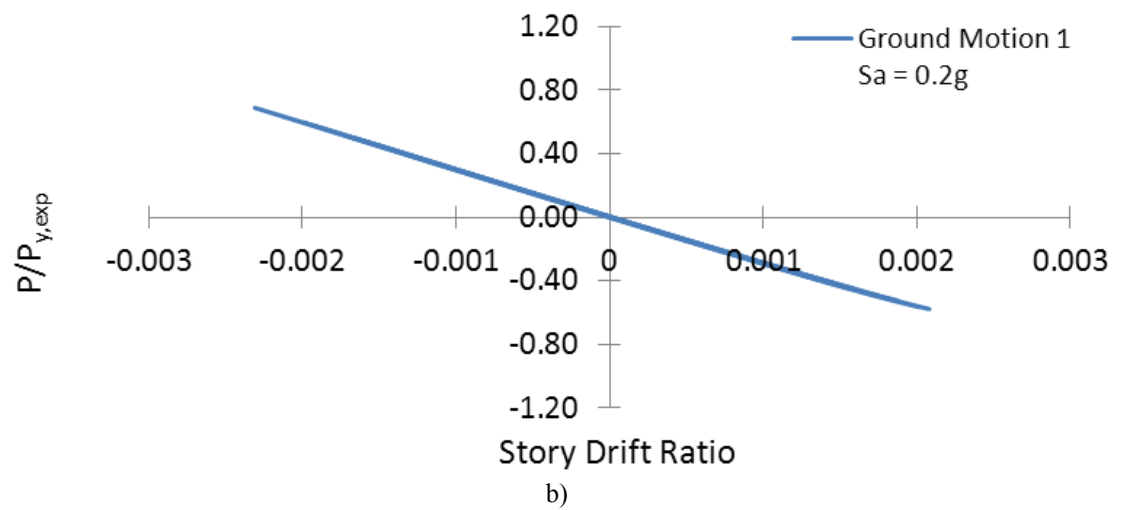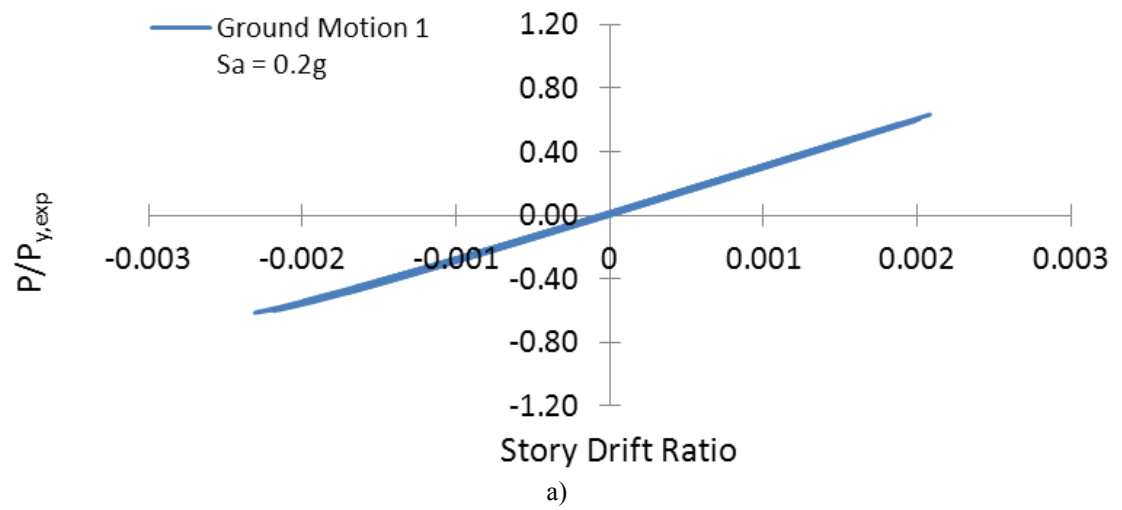
Figure 4-12: Hysteretic response of brace force demands versus induced story drift ratio for Frame 1 subjected to ground motion record No. 1 at Sa_{T1} = 0.2g. a) left brace b) right brace

a)

b)
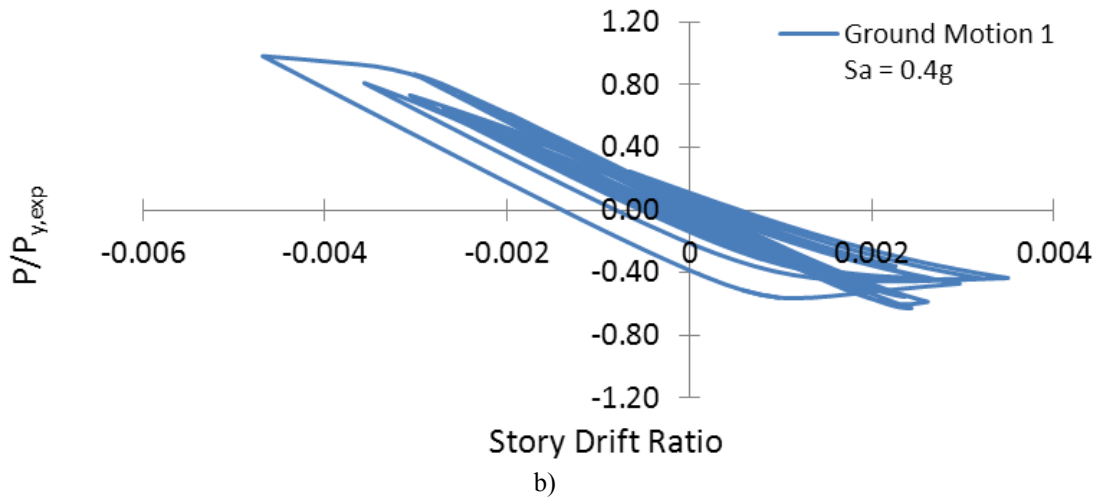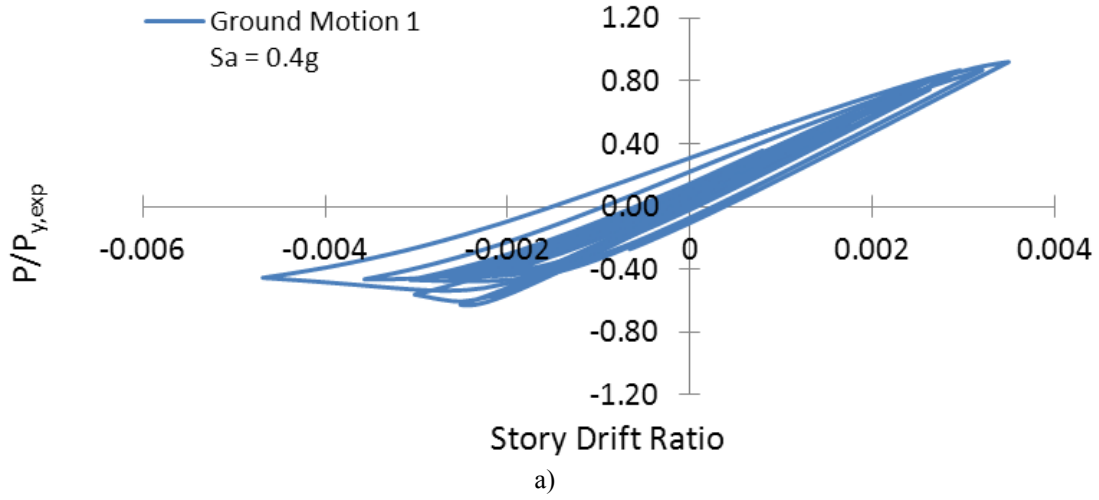
Figure 4-13: Hysteretic response of brace force demands versus induced story drift ratio for Frame 1 subjected to ground motion record No. 1 at $Sa_{T1} = 0.4g$. a) left brace b) right brace

118
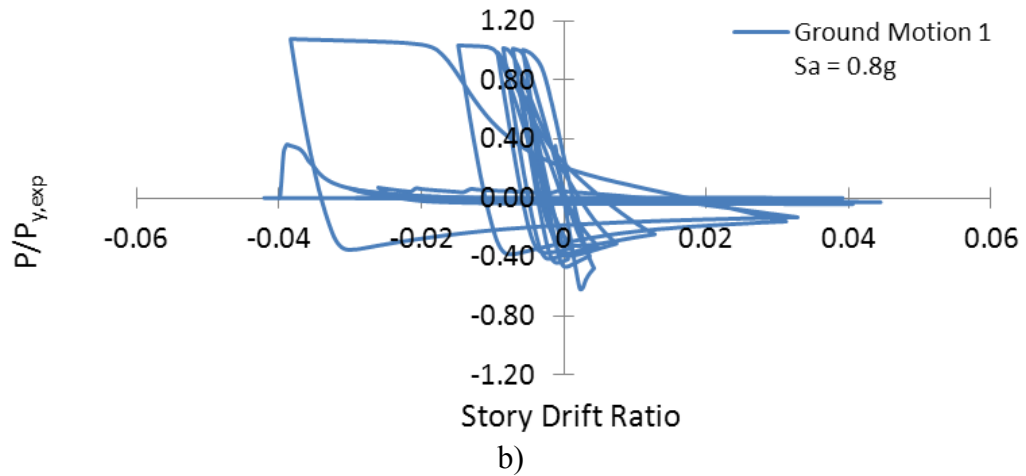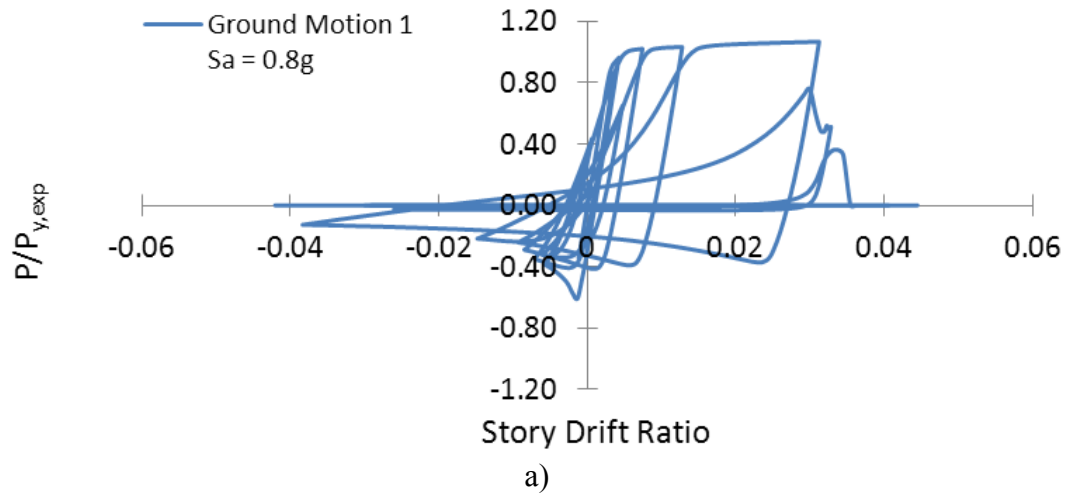
Figure 4-14: Hysteretic response of brace force demands versus induced story drift ratio for Frame 1 subjected to ground motion record No. 1 at Sa_{T1} = 0.8g. a) left brace b) right brace
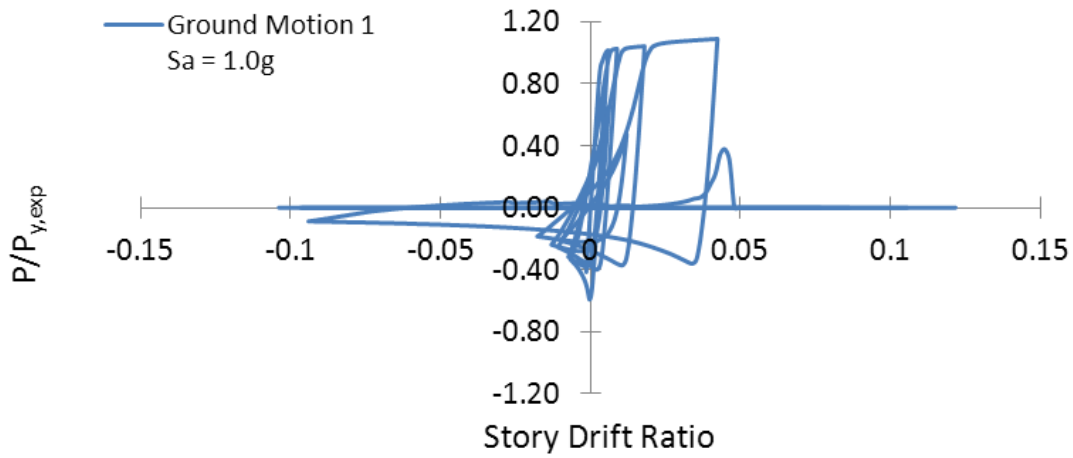
a)
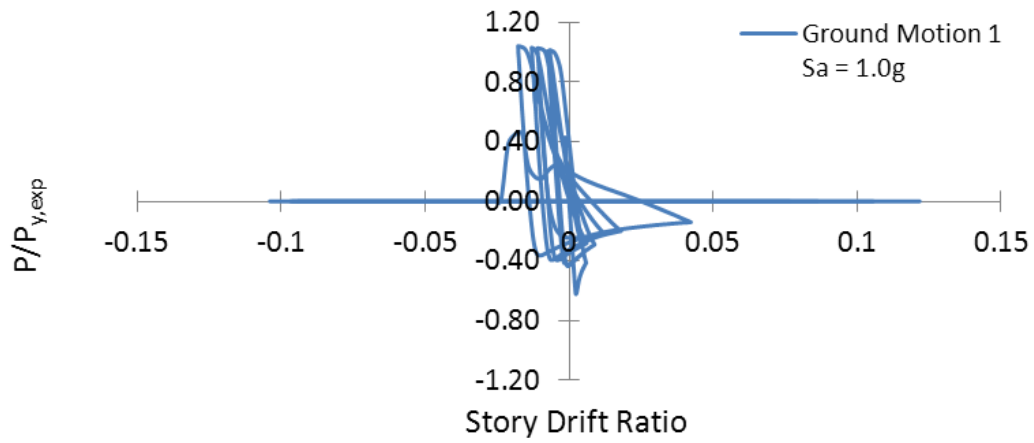
b)

Figure 4-15: Hysteretic response of brace force demands versus induced story drift ratio for Frame 1 subjected to ground motion record No. 1 at $Sa_{T1} = 1.0$g. a) left brace b) right brace

a)

b)
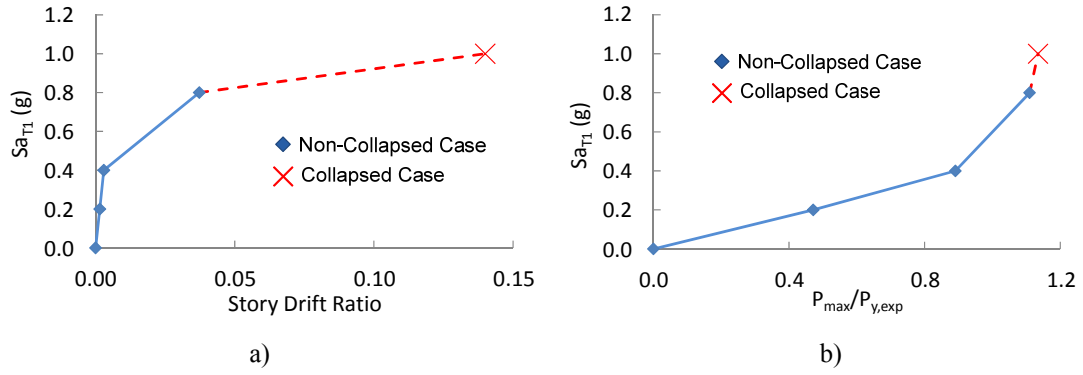
Figure 4-16: The maximum story drift ratio and maximum tensile brace force in Frame 1 when subjected to ground motion record No. 1 at Sa_{T1} = 0.2g, 0.4g, 0.8g and 1.0g.

a)

b)
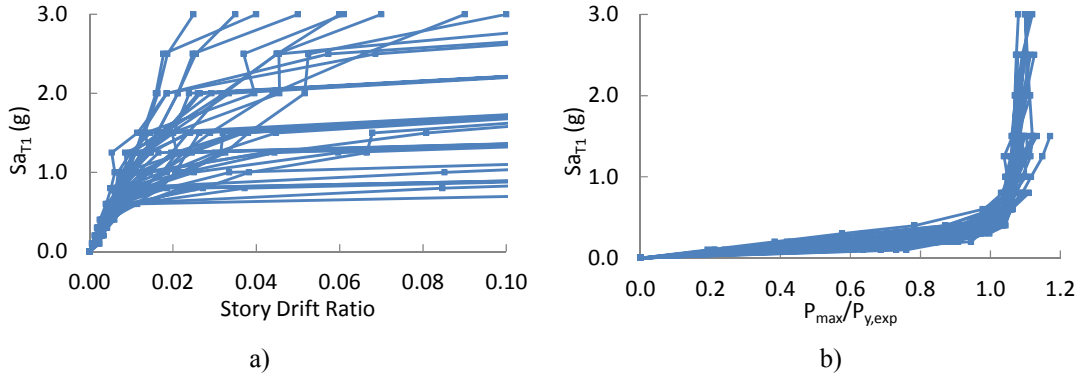
Figure 4-17: Incremental dynamic analysis for Frame 1 a) Maximum story drift ratio vs. Sa_{T1} b) Normalized maximum brace tensile force vs. Sa_{T1}

a)

b)
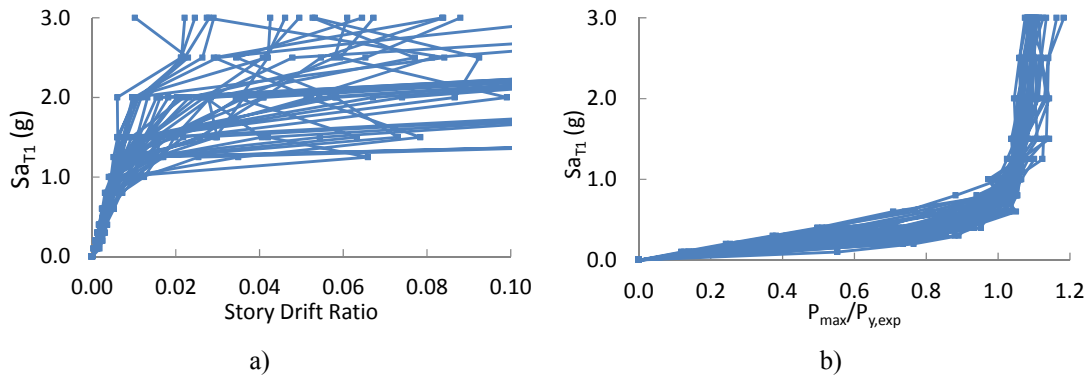
Figure 4-18: Incremental dynamic analysis for Frame 2 a) Maximum story drift ratio vs. Sa_{T1} b) Normalized maximum brace tensile force vs. Sa_{T1}

121
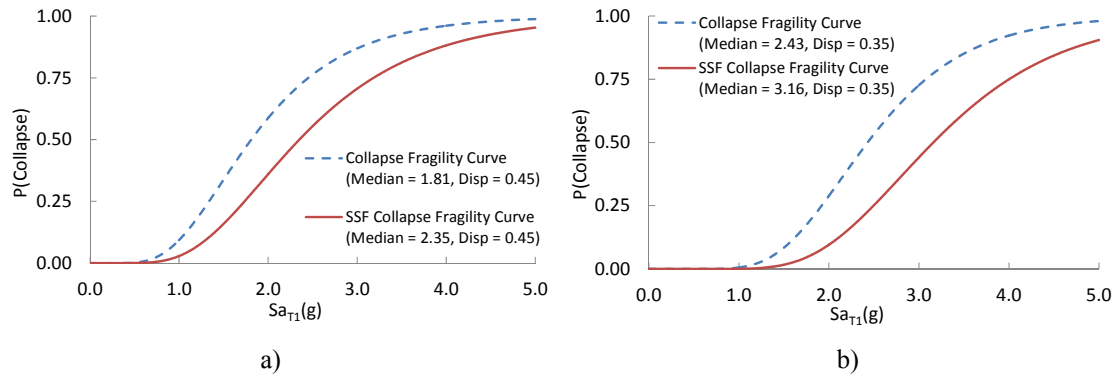
Figure 4-19: Collapse fragility curves from incremental dynamic analysis with and without the spectral shape factor shift, a) Frame 1 b) Frame 2
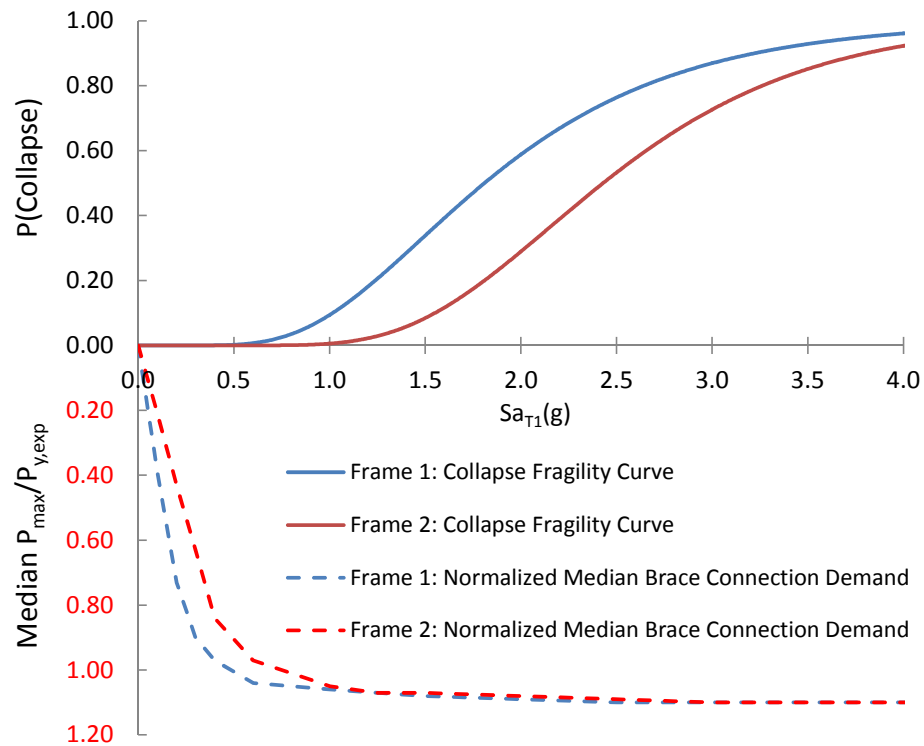
Figure 4-20: Frame 1 and 2 collapse fragility curves (above) and the median of the normalized maximum brace tensile forces vs. Sa_{T1} (below)
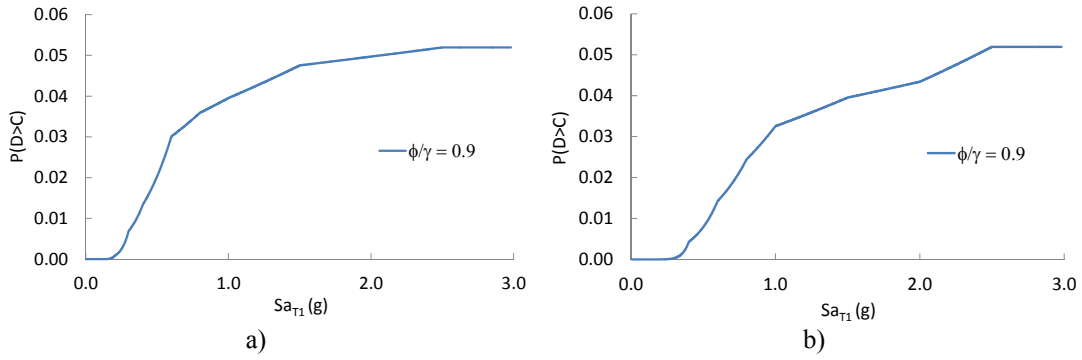
Figure 4-21: The probability of brace demand exceeding connection capacity based on brace demand distributions from the Incremental Dynamic Analyses when $\phi/\gamma = 0.9$, $C_m/C_n = 1.4$ and $V_c = 0.15$ for a) Frame 1 and b) Frame 2.
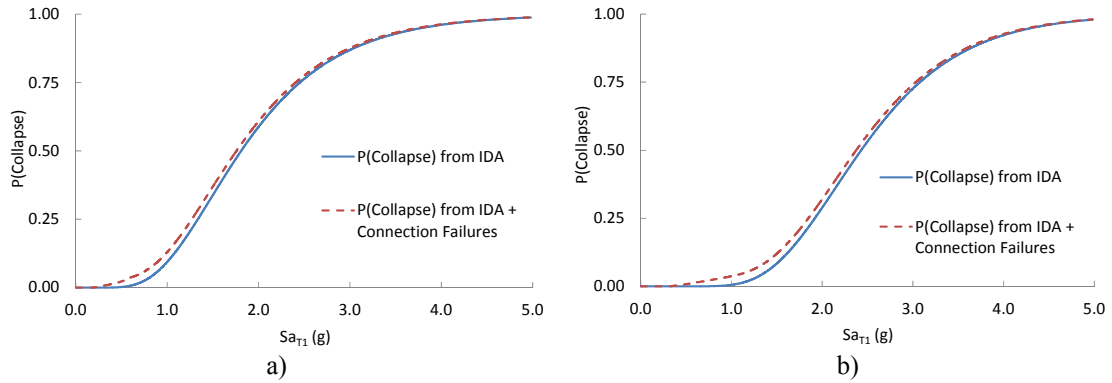
Figure 4-22: The collapse fragility curves for a) Frame 1 and b) Frame 2 both including ($\phi/\gamma = 0.9$) and excluding connection failures.
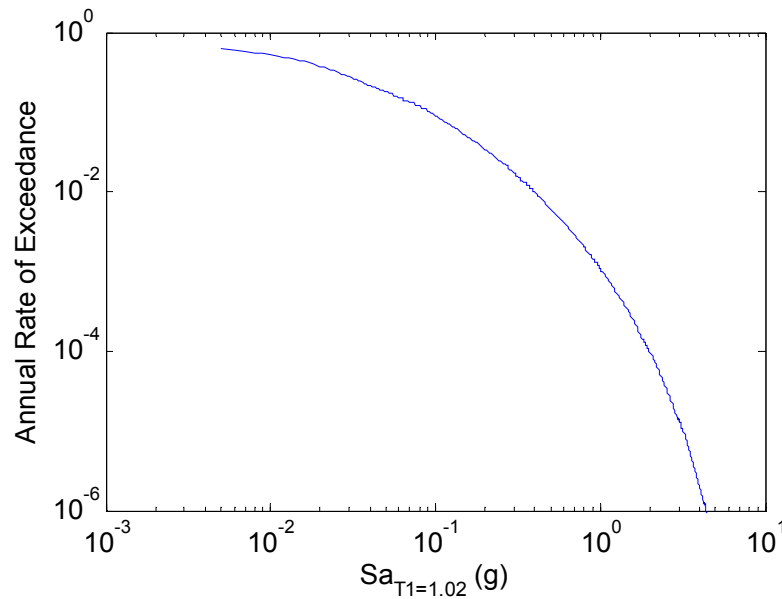
Figure 4-23: Site ground motion hazard curve used in this example to calculate mean annual frequencies of collapse is a San Francisco hazard curve (Lat 38.0, Long -121.7)
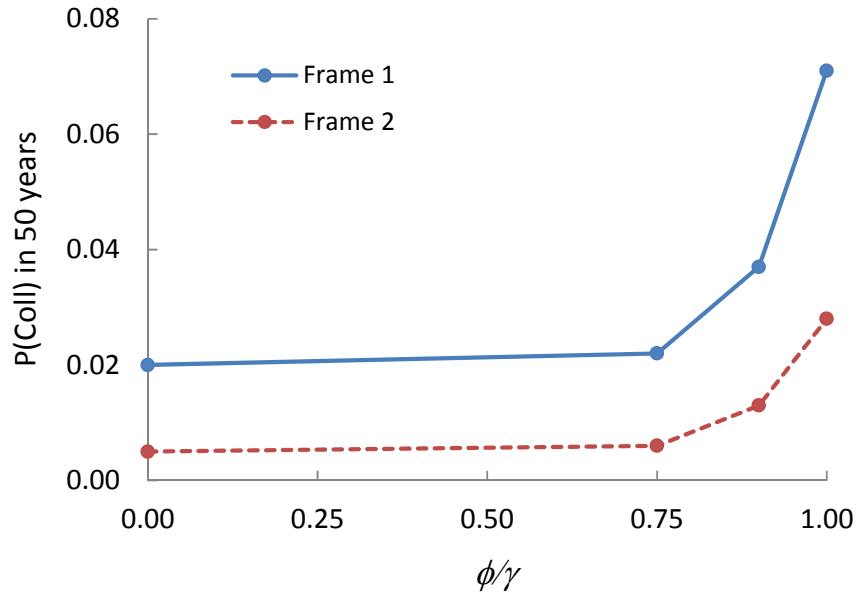
Figure 4-24: Calculated probabilities of collapse in 50 years for Frame 1 and Frame 2 versus ϕ/γ-ratio, i.e. the connection strength.

- M_y and θ_y: Effective yield strength and rotation
- $K_e = M_y/\theta_y$: Effective stiffness
- $(M_c$ and $\theta_c)$: Capping strength and associated rotation for monotonic loading
- θ_p: Pre-capping rotation capacity for monotonic loading
- θ_{pc}: Post-capping rotation capacity
- $M_r = \kappa M_y$: Residual strength
- θ_u: Ultimate rotation capacity
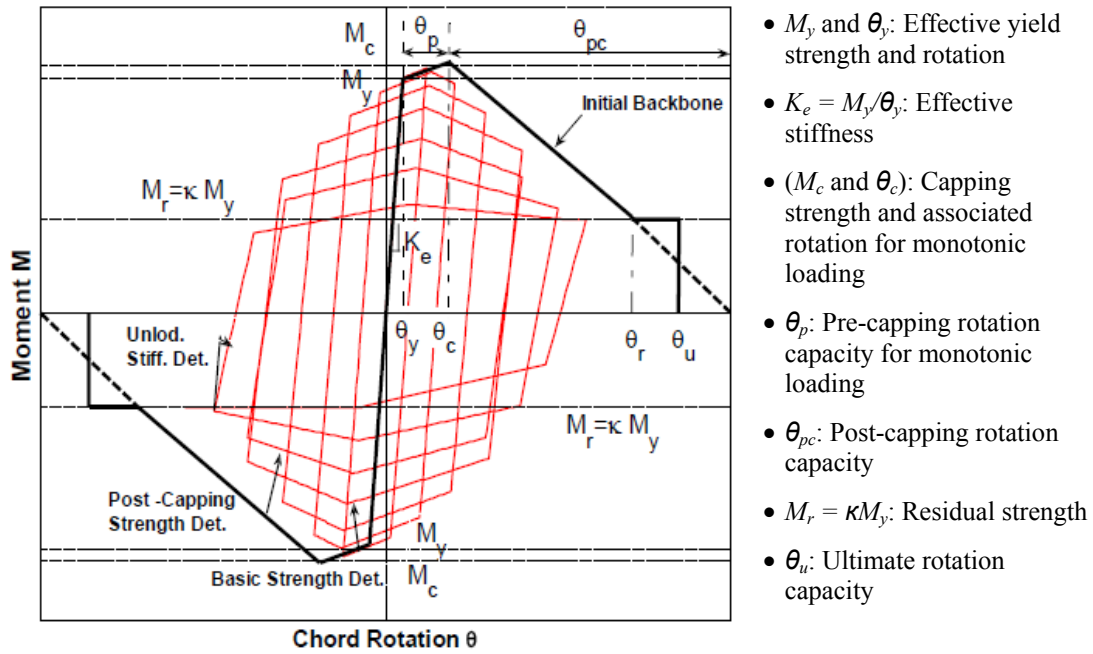
Figure 4-25: Modified Ibarra Krawinkler Deterioration Model (Image from Lignos & Krawinkler, 2009)
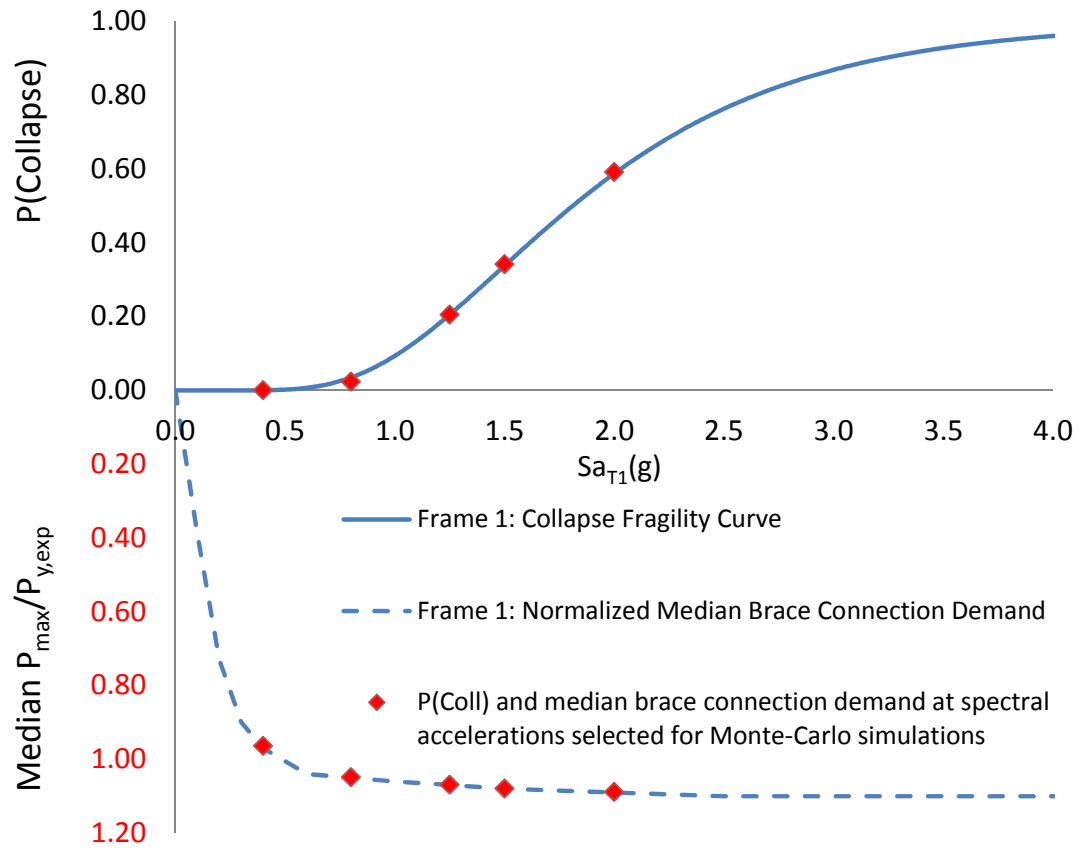
Figure 4-26: The collapse fragility curve (above) based on the median model, the median of the normalized maximum brace tensile forces vs. Sa_{T1} (below) and the representative values of Sa_{T1} where the full uncertainty analysis is performed
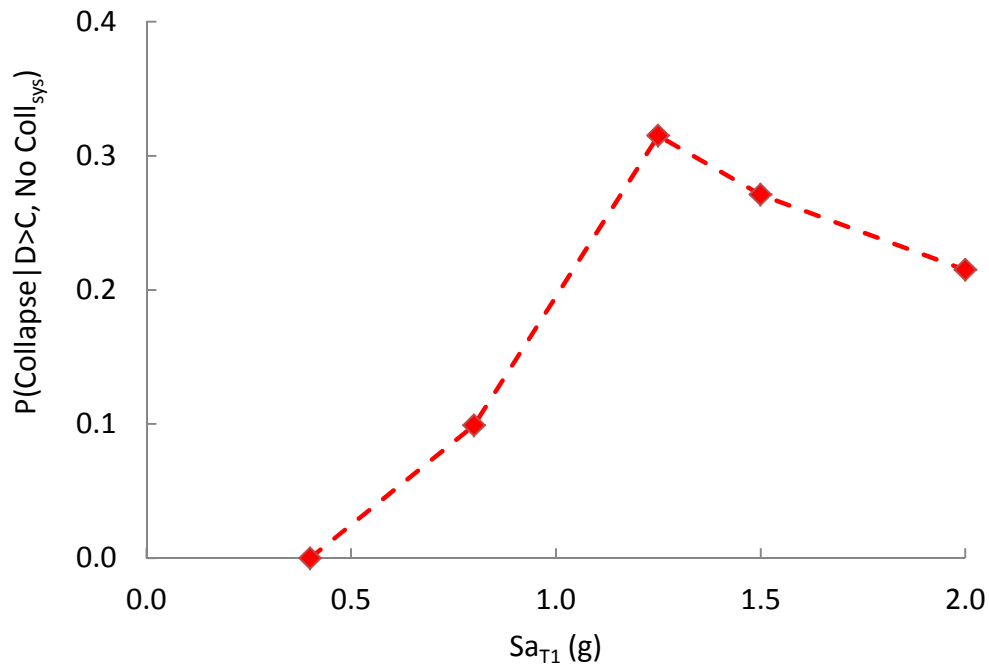
Figure 4-27: Probability of collapse due to brace connection fracture for Frame 1
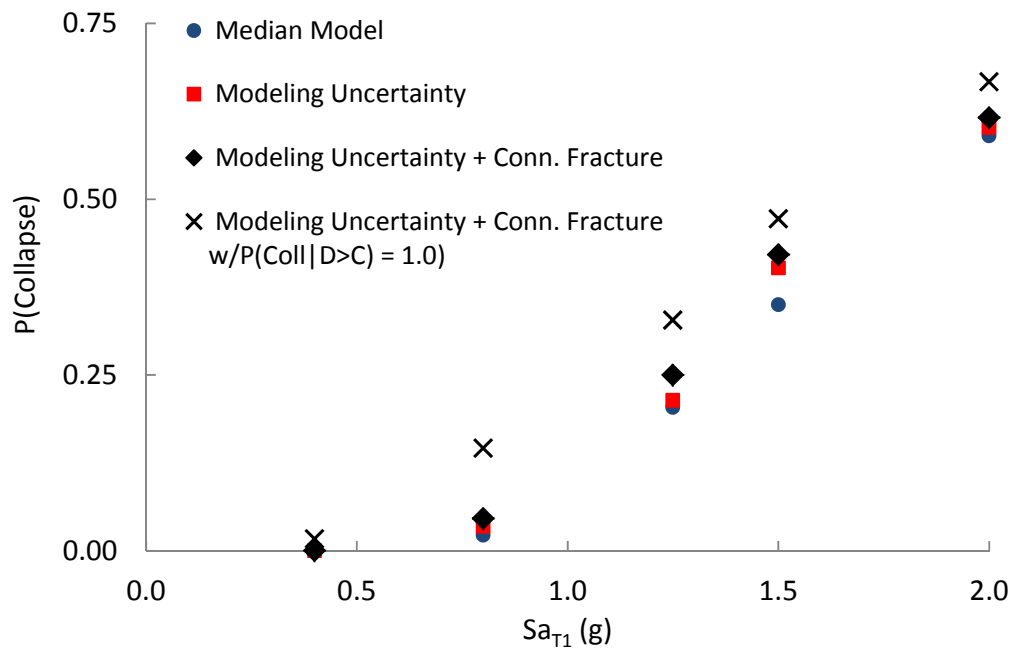
Figure 4-28: Probabilities of collapse for Frame 1 including the influence of modeling uncertainty and connection failures

Chapter 5

Capacity-Based Design in Multi-Story Special Concentrically Braced Frames

5.1 Introduction

In this chapter, dynamic analyses of multi-story Special Concentrically Braced Frames are conducted with goals to (1) demonstrate the applicability of the methodology developed in Chapter 3 for multi-story systems, (2) calculate the conditional probability of collapse caused by connection failure, (3) investigate the demand distribution on columns in braced frames, and (4) use the findings to recommend capacity design factors for selected failure modes in brace connections.

Median models of 6- and 16-story SCBF′s are studied through incremental dynamic analysis to investigate the effects of building height and the quantity of deformation-controlled components in a system on the force demands on brace connections and columns. Of particular interest is to confirm whether the R_μ values, as calculated using guidelines from the methodology in Chapter 3, predict well the spectral accelerations at which the demand distributions on capacity-designed components reach their peak values. The analyses further demonstrate how well simplified methods of establishing required connection design strengths, as proposed in Chapter 3, compare with those obtained though full integration of the seismic hazard curve with the probability of force demands exceeding capacities.

In a second set of analyses, incremental dynamic analyses are performed on a median model of an alternative design of a 6-story SCBF with identical braces up the building height. This is intended to represent a case where the frame is over-designed for all stories above the first one. Since many of the braces are larger than required by the minimum design requirements and may not yield under large ground motions, this design

raises the question of whether the same stringent capacity design criteria need to be applied to the connections and columns of this frame. Thus, the main objective of this study is to examine whether the force demand distributions on capacity-designed components can be relaxed or otherwise revised in braced frames with some over-designed braces.

To investigate the influence of connection failure on frame collapse, nonlinear dynamic analyses are re-run on the initial 6-story frame, including the possibility of connection failures. The analysis approach is similar to analysis from Chapter 4 on the single story frame.

5.2 *Dynamic Analysis of a 6-Story and a 16-Story Special Concentrically Braced Frames*

5.2.1 Description of Analysis

In this first set of analyses, models of 6-Story (Design 1) and 16-Story SCBF´s are investigated through incremental dynamic analysis. The frame designs are from the SCBF study in NIST GCR 10-917-8 *"Evaluation of the FEMA P-695 Methodology for Quantification of Building Seismic Factors"* (2010). The beam, brace and column sizes of the two frames are listed in Table 5-1. The analysis models are based on median component properties, implying that the failure of capacity-designed brace connection and column components is not directly simulated in the analysis since their median strengths exceed the median force demands from the braces. Modal Response Spectrum Analyses are also performed to determine values of R_μ and $Sa_{y,exp}$, following the procedure outlined in Table 3-12. From the nonlinear dynamic analyses, the maximum force demands on the capacity-designed connections and columns are recorded and used to evaluate a) accuracy of $Sa_{y,exp}$, as calculated by the simplified methods proposed in Table 3-12, to the observed brace yielding b) the demand distributions on connections in multi-story frames relative to those in single-story frames, c) required connection design strengths, and d) required axial column design strengths in multi-story braced frames.

The frame models for this analysis are idealized two-dimensional plane frame models, implemented in OpenSees (OpenSees, 2011). Figure 5-1 shows the plan and elevation view of the frame models. The models are developed to represent median conditions, where the expected (versus nominal) material strengths, section properties, and component model parameters are used. The braces are modeled using nonlinear force-based fiber elements which captures both global buckling and low-cycle fatigue rupture of the braces. The effective length of the braces is 80% of the work-point-to-work-point length. The beams and columns are modeled with elastic elements that have nonlinear rotational springs to model member hinging adjacent to the beam-column connections and column bases. The beam-column connections where there are no braces connecting to the frames are assumed to have no rotational stiffness. The rotational behavior of the flexural hinge springs follows a bilinear hysteretic response based on the Modified Ibarra Krawinkler Deterioration Model (Ibarra et al. 2005, Lignos and Krawinkler 2009, 2010). Braces are assumed to have pinned end connections to the frame, and the columns are fixed at the base. The gravity system is idealized as leaning columns to simulate P-Delta effects and provides no lateral resistance. The gravity load (1056 kips per floor and 794 kips roof) is applied to the leaning column as axial load. Rayleigh damping is assigned equal to 2% of critical damping at the first two vibration periods of the models. The OpenSees modeling and dynamic analysis procedure for the two frames follows the procedure for the single-story SCBF analyses described in Chapter 4.

5.2.2 Brace Behavior

The brace behavior is critical in the response of SCBFs. The braces are modeled using nonlinear fiber elements where each brace is subdivided into 12 nonlinear fiber sections with 3 integration points along the length of each section. 20 fibers are used across the depth of the cross section and an initial imperfection of the braces is 0.1%. Before running the dynamic analysis, the brace behavior is analyzed by subjecting an OpenSees model of them to far-field and near-field cycling loading protocols. The description of the loading protocols and examples of the brace responses when subjected to cyclic loading protocols can be found in Chapter 4.

5.2.3 Calculating R_μ

The following is a summary of the step-by-step procedure to calculate $Sa_{y,exp}$ and R_μ for the 6-story frame following the procedure in Table 3-12. Results for both the 6- and 16-story frames are then summarized in Tables 5-5 to 5-8. Values calculated by the Table 3-12 method are then verified by comparison to data from dynamic analyses to assess the accuracy of the simplified method works for multi-story frames.

Step 1: Design a frame according to code specification

The frame used for these calculations was designed as a part of NIST GCR 10-917-8 *"Evaluation of the FEMA P-695 Methodology for Quantification of Building Seismic Factors"* (2010). The frame was designed using the Equivalent Lateral Force procedure in ASCE 7-05 for Seismic Design Category D_{max} and Soil Site Class D. The resulting brace sizes are listed in Table 5-1.

Step 2: Calculate the expected yield shear force for each story, $V_{y,exp}$, using expected material properties. $V_{y,exp}$ is calculated as the sum of the horizontal projection of the expected tensile and compression strengths of each pair of braces. The braces in this example are inclined at a 45° angle. The calculation results are listed in Table 5-2.

Step 3: Perform a Modal Response Spectrum Analysis using the design response spectrum divided by the response modification factor, R, and record the story shear forces, V_{RSA}. The RSA is performed following the procedure in ASCE 7-10 using SAP 2000. Figure 5-2 shows the design response spectrum and Table 5-3 summarizes the results.

Step 4: Calculate the minimum ratio of $V_{y,exp}/V_{RSA}$

The calculation results are listed in Table 5-4. Here the minimum $V_{y,exp}/V_{RSA}$-ratio is 2.42. The $V_{y,exp}/V_{RSA}$-ratio is fairly constant between stories, suggesting a balanced and optimal design.

Step 5: Calculate the spectral acceleration at which yielding is expected, $Sa_{y,exp}$

$$Sa_{y,exp} = Sa_{T1} * V_{y,exp}/V_{RSA} = 0.122g * 2.42 = 0.30g$$

Step 6: Calculate the frame's R_μ.

$$Sa_{MCE} = 1.10g$$

$$\mathbf{R_\mu = 2/3 * Sa_{MCE}/Sa_{y,exp} = 2/3*1.10g/0.30g = 2.5}$$

The effective R-factor of 2.5 is considerably smaller than the code R-factor of 6, despite the frame being fairly optimally designed. However, assuming an average overstrength of 2.0 for SCBFs, a value close to 3.0 ($R/\Omega_0 = 6/2 = 3.0$) could be expected, even for optimal designs. The R/R_μ-ratio for this frame is 2.4, which can be explained by the following factors (1) overdesign due to discrete member sizes, (2) the required ϕ-factor of 0.9, (3) the difference between nominal and expected material properties ($R_y = 1.4$), (4) the difference between brace tensile and compression strength (here the tensile strength is 1.6 to 2.0 times larger than the compressive strength), and (5) the smaller calculated design force demands from modal response spectrum analysis as compared to the equivalent lateral force procedure forces used in the design. The ratio of 2.4 is almost fully explained by the combined effects of the ϕ-factor ($1/0.9 = 1.1$), the expected versus nominal material properties (factor of 1.4), and the difference between brace tensile and compressive strengths (factor of 1.6 to 2.0).

Following standard building code provisions, the nominal story shear strength can be written as:

$$V_{nom} = 2 \times F_{cr,nom} \times A_{brace} \times \cos(\theta_{angle})$$ (5-1)

where $F_{cr,nom}$ is the nominal critical strength in compression members using nominal material properties (e.g., as specified in ANSI/AISC 360-10) and θ_{angle} is the brace angle with the horizontal.

The expected story shear yield strength is as follows:

$$V_{y,exp} = (F_{y,exp} + \alpha F_{cr,exp}) \times A_{brace} \times \cos(\theta_{angle})$$ (5-2)

where $F_{y,exp}$ is the expected yield stress, $F_{cr,exp}$ the expected critical strength of compression members using expected material properties (assuming the same compression strength equation as in 5-1 this ignores any conservatism in the compression strength equation) and α is a factor to account for the fact that the tension brace and compression brace not reach peak values at the same drift (see Figure 5-3). The ratio between the expected yield shear strength and the design shear strength is:

$$\frac{V_{y,exp}}{V_{nom}} = \frac{F_{y,exp}}{2 \times F_{cr,nom}} + \frac{\alpha F_{cr,exp}}{2 \times F_{cr,nom}}$$ (5-3)

Figure 5-4 shows the ratio for the expected tensile yield stress over the nominal critical stress as a function of the slenderness ratio. The figure shows clearly that the $F_{y,exp}/F_{cr,nom}$ ratio increases sharply as the slenderness ratio increases. Figure 5-5 shows the ratio between the expected critical stress and the nominal critical stress as a function of the slenderness ratio. In this case the $F_{cr,exp}/F_{cr,nom}$ ratio decreases as the slenderness ratio increases until it reaches a value of 1.0. This is due to reduced impact of the yield stress as the slenderness ratio increases. Figure 5-6 finally shows the combined results of Figures 5-4 and 5-5. As demonstrated in Figure 5-6, the ratio between the expected yield shear strength and the nominal shear strength is very dependent on the slenderness ratio. For slenderness ratios of 60, 80 and 100 and α of 1.0, the ratios between the expected

132

yield shear strength and the nominal shear strength are 1.3, 1.5 and 1.7 for HSS circular sections.

In the previous calculations, the elastic design force demands are based on the design spectrum, which may or may not match the elastic force demands from specific ground motions. To investigate the significance of this, the R_μ calculations are repeated using the median response spectrum of the 44 ground motions used in the time history analysis. The calculated results for the 6- and 16-story frames are summarized in Tables 5-6 to 5-8. The calculated R_μ for the 6-story frame is 2.7 using the median response spectra compared to 2.5 for the design response spectra. For the 16-story frame, the calculated R_μ is 1.1 using the median response spectra and 1.0 using the design response spectra. The difference between the design spectra and median response spectra is due to differences in the spectra values at periods less than the fundamental periods, i.e. in the spectra values used for higher mode effects calculations. Shown in Figure 5-7 is a comparison of the two spectra, anchored at the respective periods ($T_1 = 0.82$s and 1.71s) for the two frames. For both frames, large differences at periods less than the fundamental period is evident, e.g. from Figure 5-7b it can be seen that the median response spectra is up to 70% higher than the design response spectra at periods between 0.2s and 0.6s for the 16-story frame. The nonlinear analysis results will show that using the median ground motion response spectra calculates R_μ and $Sa_{y,exp}$ more accurately, not surprising since those best represent the analysis input.

5.2.4 Nonlinear Dynamic Analysis: Force Demands on Brace Connections

Results from the incremental dynamic analysis of the 6-story Design 1 and the 16-story frames are presented in this section, including story drift ratios and force demands on brace connections. Figure 5-8 shows the maximum store drift ratio versus Sa_{T1} and Figure 5-9 the collapse fragility curves for both frames. For the 6-story frame, the calculated median collapse spectral acceleration is 1.67g. With Sa_{MCE} = 1.10g, the calculated collapse margin ratio, CMR, is 1.52. Based on FEMA P-695 (FEMA, 2009), the spectral shape factor, SSF, is 1.21 and the adjusted collapse margin ratio, ACMR, is 1.84. For the 16-story frame, the calculated median collapse point is 1.02, the CMR is 1.93 and ACMR is 2.32. Based FEMA P695 minimum acceptance criteria, ACMR´s equal to 1.56 and 1.46 for the 6-story and 16-story frames, both frames pass. However, the ACMR values calculated in this study are considerably lower those reported in NIST GCR 10-917-8 *Evaluation of the FEMA P-695 Methodology for Quantification of Building Seismic Factors"* (2010) where the ACMR values for the two frames are 2.64 and 3.20. The difference between the results is likely due to the difference in modeling the beam-column connections. The models in NIST GCR 10-917-8 did not capture all of the deterioration models associated with beam plastic hinging and as result, the models often had considerable lateral force capacity, even after all of the braces at a given story had lost all their capacity in both tension and compression. Although proper modeling of the beam-column hinges is extremely important when calculating collapse risk, the main objective of this study is to investigate demand on and reliability of capacity-designed components within multi-story systems, not calculating collapse risk. The results will demonstrate that the area of interest for those factors is at lower earthquake intensities where the probability of collapse is small and the details of beam-column hinge modeling are not a major concern.

The maximum brace tensile forces per story, P_{max}, normalized by the expected yield strength, $P_{y,exp}$, are plotted versus spectral acceleration for the 6-story frame in Figure 5-11. Two points are worth mentioning from the plots. First, no story remains elastic throughout all ground motions and all intensities, a result of a fairly balanced design. This is evident by observing that the $P_{max}/P_{y,exp}$ exceeds 1.0 for all stories at the higher spectral

accelerations, i.e. passed 0.3s. Second, the braces in story 5 and story 6 yield at the lowest spectral accelerations, closely followed by other stories. These trends follow those evident in Table 5-6 where stories 5 and 6 have the largest R_μ values and therefore the lowest $Sa_{y,exp}$. Tables 5-9 and 5-10 list the median and the dispersion of the brace forces per story and the maximum for the whole frame and Figure 5-17 plots the results. The R_d calculations from Section 5.2.3 predicted an R_μ of 2.7 and a $Sa_{y,exp}$ of 0.27g and based on the analysis results, those predictions are fairly accurate, i.e. the median $P_{max}/P_{y,exp}$ for story 6 is 0.97 at $Sa_{T1} = 0.30$s with a limited increase at higher spectral accelerations (Table 5-9).

The median of the maximum brace tensile forces for each story of the 16-story frame are plotted in Figure 5-14. From 5-14a, corresponding to a low intensity shaking of Sa_{T1} = 0.30g, it can be seen that brace yielding occurs first in stories 3 and 13. As reported in Table 5-8, these two stories had the highest calculated R_μ, equal to 1.1 and 1.0 for stories 3 and 13, respectively; and the expected spectral accelerations at yield in these stories is 0.33g and 0.36g. The member overstrength was not as consistent between stories in the 16-story frame as compared to the 6-story frame. For the 16-story frame, the calculated R_μ ranged from 0.6 to 1.1, implying that some stories may remain elastic while others yield. Figure 5-14c shows that the median of the normalized maximum brace forces for stories 8 and 16 are well below 1.0, even at $Sa_{T1} = 1.00$g which is the median collapse point. Stories 8 and 16 also have the lowest R_μ, or 0.6. The dispersion in the stories that remain essentially elastic is considerably higher than the yielding stories, since for the elastic members small differences in deformations causing large differences in brace forces. As pointed out above, the R_μ predictions in Table 5-8 proved to be fairly accurate. The stories with the lowest and highest R_μ, story 16 and story 3, envelope response from all other stories when normalized median brace forces and the dispersion are plotted versus spectral acceleration. (Figure 5-12a and 5-12b)

The median of the normalized story brace force demand is lower in a given story in multi-story systems than in single-story systems. This is a result of large inelastic deformations, and thus large brace connection demands, concentrating in different stories for different ground motions in multi-story systems and therefore bringing the median for

a given story down. While the median within a story decreases for multi-story systems, the record-to-record variability increases. This phenomenon becomes more pronounced as the number of stories in a frame increases. This can be seen when comparing the median and dispersion of the brace forces for the 6-story frame (Tables 5-9 and 5-10) to the 16-story frame (Tables 5-11 and 5-12). The maximum normalized median brace force in a given story in the 6-story frame is 1.02 with a dispersion of 0.03 while for the 16-story frame the corresponding values are 0.93 and 0.13. However, when comparing the median of the maximum for all stories in a given analysis, the results for the 6-story frame and 16-story frame approach those from the single-story frame, i.e. the normalized maximum of all stories is 1.04 for the 6-story frame (Table 5-9), 1.10 for the 16-story frame (Table 5-11) and 1-10 for both single-story frames (Table 4-5).

5.2.5 Nonlinear Dynamic Analysis: Required Design Strength of Brace Connections

To assess how well the proposed simplified method of establishing required connection design strengths compares with a full integration of the probability of demand exceeding capacity with a seismic hazard curve, both methods are used and the results compared. To calculate the probability of brace demand exceeding connection capacity, the brace connection demands from the dynamic analyses are used along with an assumed connection strength distribution. The dispersion around the brace connection demand recorded from the analysis is only due to the record-to-record randomness and does therefore not include dispersion due to other uncertainties, such as material and fabrication variability. To include those additional uncertainties, the total demand dispersion is inflated by 0.15. The nonlinear analysis results are taken to represent the $\hat{D}_m / D_n$-ratio and for the simplified method, the demand distribution corresponding to the maximum considered earthquake ground motion intensity is used. For the connection capacity distribution, $\hat{C}_m / C_n$ is set to 1.4 and $V_C = 0.15$. Zero correlation is assumed between the demand and capacity. The tolerable mean annual frequency of demand exceeding capacity in a given story is assumed to be 0.002% or 0.1% in 50 years.

Using the parameters that we just described, the ϕ/γ-ratios are calculated by using Equation 5-4, which is the methodology's basic equation (simplified ϕ/γ-ratio calculations), as well as by using equation 5-5 where the ϕ/γ-ratios are varied until the tolerable mean annual frequency of demand exceeding capacity is met (detailed ϕ/γ-ratio calculations). The hazard curve used for this example is from a downtown San Francisco site (Lat. 38.0, Lon. -121.7).

$$\frac{\gamma}{\phi} = \frac{\hat{D}_m}{D_n}\frac{C_n}{\hat{C}_m}\exp\left(\beta_{R,Ha}\sqrt{V_C^2 + V_D^2 - 2\rho V_C V_D}\right) \tag{5-4}$$

$$MAF(D > C) = \sum_{Sa} P(D > C|Sa) * MAF(Sa) \tag{5-5}$$

The calculated ϕ/γ-ratios are reported in Tables 5-13 and 5-14, and the ratios calculated by the two different methods are plotted against each other in Figure 5-22. For comparison, the current ϕ/γ-ratio for brace connections in AISC 2010 (AISC, 2010a) is 0.75. The calculated ϕ/γ-ratios range from 0.72 to 0.81 for the 6-story frame and from 1.25 to 1.77 for the 16-story frame. The absolute values of the calculated ϕ/γ-ratios were not of primary concern in this analysis, but rather to assess how well the simplified method compares with the full integration method. The large difference between the calculated ϕ/γ-ratios for the 6-story frame and the 16-story frame can be explained by (a) the large overstrength in the 16-story frame compared to the 6-story frame, i.e. lower R_μ, and (b) the lower median demand per story in the 16-story frame compared to the 6-story frame. Since large inelastic deformations tend to concentrate in different stories for different ground motions, taking advantage of the lower median demand per story as the number of stories increases can lead to unconservative results. It would therefore be more appropriate to use the maximum of all stories statistics to calculate the ϕ/γ-ratios. Regardless, from Tables 5-13 and 5-14 as well as Figure 5-16, it can be observed that the simplified method and the detailed integration method compare quite well, especially for the 6-story frame where the overstrength between stories is similar. The results using the simplified method are unconservative for most cases due to the step-function simplification (see Figure 3-5), which ignores the possibility of demand exceeding

capacity at spectral accelerations below $Sa_{y,exp}$. The difference between the simplified method and the detailed integration method ranges from -3.0% to 31.0%. The unconservatism using the simplified method is more pronounced in stories which are significantly over-designed compared to others within the same frame. In those instances, that over-designed story may stay elastic for all ground motions and at all earthquake intensities. As a result, the median demand never stabilizes and dispersion stays high causing the step-function simplification not to capture the true behavior. Figure 5-17 shows the strong relationship between R_μ and the ϕ/γ-ratios where a lower R_μ results in higher ϕ/γ-ratio.

5.2.6 Nonlinear Dynamic Analyses: Axial Force Demands on Columns

Column axial force demands from the 6 and 16-story frames' dynamic analyses are presented in this section. Based on the 2010 AISC *Seismic Provisions*, the required design strength of columns in SCBF´s is the maximum of forces from either one of two following analyses:

i) An analysis in which all braces are assumed to resist forces corresponding to their expected strength in compression or in tension.

ii) An analysis in which all braces in tension are assumed to resist forces corresponding to their expected strength and all braces in compression are assumed to resist their expected post-buckling strength.

However, the required design strength of columns does not need to exceed any of the following:

a) The forces determined using design loads, including amplified seismic load (Ω_0), applied to a frame model in which all compression braces have been removed.

b) The forces corresponding to the resistance of the foundation to overturning uplift.

c) Forces determined from nonlinear analysis.

The determination of the required design strength of columns in SCBF´s in the 2010 *Seismic Provisions* has become significantly more elaborate than in the 2005 version, especially with the inclusion and exclusion of the compression braces in the analysis.

Richards (2009) demonstrated that the column axial demands can easily exceed elastic design demand by more than the Ω_0-factor of 2.0, especially for low rise frames and in the upper stories in high-rise frames, due to force redistribution after brace buckling. To account for the force redistribution, Richards (2009) suggested an amplification factor, A_x, for axial column loads at story x which accounts for the force redistribution in story x when the compression brace at that story is removed:

$$A_x = 1 + \frac{\sum_{i=x}^{n} F_i h_x}{\sum_{i=x+c}^{n} F_i \sum_{j=x+c}^{n} h_j} \qquad (5\text{-}6)$$

where F_i = lateral force at the floor above story i, h_x, h_j = story height of story x or j, n the number of stories in the frame, and $c = 1$ if story x has chevron brace or $c = 0$ if story x has V-bracing. The A_x amplification factor is largest for low-rise frames and in the upper-stories of high-rise frames and then slowly decreases as the number of stories above story x increases. However, as pointed out by Richards (2009), Equation 5-6 might not capture the maximum column demands as both the possible brace compression capacity overdesign and the inevitable brace tension capacity overdesign can cause the maximum column demands to far exceed the elastic design demands, even the when amplified by A_x. Therefore, capacity design provisions where these factors are accounted for are required to capture the theoretical maximum column demands.

Capacity-design concepts for high-rise frames, which assume all braces reach their maximum capacities simultaneously, can cause columns in the lower-stories to be excessively overdesigned. Studies on Eccentrically Braced Frames taller than 9 stories demonstrated that simultaneous yielding of all links never occurred and that the column demands at the base were as low as 60% of the theoretical maximum force (Koboevic and Redwood, 1997; Richards, 2004). On the other hand, the conclusions from nonlinear dynamic analyses on 2-, 4-, 8- and 12-story chevron braced steel frames by Tremblay and

Robert (2001) are that column compression force must be determined assuming that all compression braces carry their buckling strength simultaneously and that the square root of the sum of the squares (SRSS method) for accumulating brace compression loads is un-conservative. However, the dispersion in the column demand at the lower stories of both the 8-story and the 12-story frames is considerable. For example, the column demand for the bottom stories in the 12-story frame ranges from 50% of what capacity-design provisions suggest up to close to 100% of what they suggest.

The column seismic axial demand for the 6-story and 16-story frames is plotted in Figures 5-18 through 5-27, described below. In all cases, C_{max} is the maximum seismic axial demand in a column for a given ground motion record. The demand is normalized by two different design rules. C_{exp} is the expected column demand based on capacity design principles, as given by the maximum of either design rule i) or ii) above. $C_{elastic,AISC}$ is the elastic design demand using design rule a) above calculated without Ω_0. Starting from the 1st level, C_{exp} for the 6-story frame is [2466, 2466, 1151, 1168, 324, 274] kips and for the 16-story frame it is [9852, 9852, 8039 8039 6511, 6511, 4984, 4984, 3584, 3584, 2286, 2286, 1264, 1264, 424, 424] kips. Similarly, $C_{elastic,AISC}$ for the 6-story frame is [1520, 1520, 833, 833, 274, 274] kips and for the 16-story frame it is [2498, 2498, 2074, 2074, 1655, 1655, 1250, 1250, 873, 873, 540, 540, 269, 269, 82, 82] kips.

The median and the dispersion of C_{max}/C_{exp} are plotted for both frames in Figures 5-18, 5-21 and 5-24 to 5-27. The general trend for both frames is that the median demand decreases as the number of stories above it increases and the dispersion increases. The median demand for the 1st-story of the 6-story frame is approximately 90% of what capacity design rules suggest, even at the MCE demand ($Sa_{T1} = 1.10g$). For the 16-story frame, the 1st-story demand is approximately 50% of what capacity design rules suggest at the MCE demand. ($Sa_{T1} = 0.53g$). On distinct difference between the column demand and the brace connection demand is that the influence of R_μ on the shape of the demand curve decreases as the number of stories increases. The results for the 16-story frame show this very clearly. For the top stories, the demand at $Sa_{y,exp}$ is close to the demand at Sa_{MCE} but for the bottom stories, there is a considerable difference between those two values and the demand continues to increase even past Sa_{MCE}. For example, at the 1st

story, the median demand at $Sa_{y,exp}$ is 50% of the demand at Sa_{MCE}, and at the median collapse point, the median demand is 20% higher than the demand at Sa_{MCE}. This is a consequence of the likelihood of simultaneous yielding decreasing as the number of deformation-controlled components increases as well as a considerable difference in $Sa_{y,exp}$ between stories. In the cases where multiple deformation-controlled components cause the demand, capacity design principles do not explain well the expected demand on capacity-designed components, rather the maximum demand that theoretically can be delivered to them (see Figures 5-19 and 5-22).

Based on the AISC 2010 Seismic Provisions, the required design demand on columns does not need to exceed elastic design demand, $C_{elastic,AISC}$. Figures 5-20 and 5-23 plot the column axial demand normalized by $C_{elastic,AISC}$ for both the frames (Ω_0.exluded). For the 6-story frame, whose design was force-controlled and the member overstrength in yielding capacity was approximately 2.5 (see Table 5-6), limiting the required design demand not to exceed $C_{elastic,AISC}$ is justified. However, for the 16-story frame, whose design was drift-controlled, this limit on the required design demand underestimates the demand in the upper stories significantly. Table 5-8 shows that the member overstrength in yielding goes from approximately 6 in the lower stories to approximately 10 at the top. Therefore, using a fixed over-strength factor, $\Omega_0 = 2.0$, irrelevant of the design causes the demand to be greatly under-estimated as now the capacity has been increased.

According to guidelines published by the Pacific Earthquake Engineering Center´s (PEER) Tall Building Initiative (TBI; 2010), axial forces in columns are listed under "force-controlled critical actions". Force-controlled actions, which have been referred to as force-controlled or capacity-designed components in this thesis, are those in which inelastic deformation capacity cannot be assumed and force-controlled critical actions are those in which "the failure mode poses severe consequences to structural stability under gravity and/or lateral loads". Following the terminology in the reliability methodology from Chapter 3, this would imply that for force-controlled critical actions $P(Coll_{D>C}|D>C)$ approaches 1.0.

The PEER TBI guidelines specify that the expected design axial strength of columns, based on expected material properties $\phi P_{n,exp}$, shall exceed 1.5 times the mean demand from 7 nonlinear response history analyses at the Maximum Considered Earthquake shaking. The 1.5 factor is meant to represent the mean plus one standard deviation in force-demands based on past studies, such as those by Zareian and Krawinkler (2007) on steel moment resisting frames and Yang and Moehle (2008) on reinforced concrete shear walls systems. These and other studies indicate that the dispersion (roughly equivalent to a coefficient of variation) to be approximately 0.4 due to record-to-record variability. The amplification factor of 1.5 is directly specified since little confidence is given to the computed standard deviation from only 7 analyses. Further, while the 1.5 factor is based on only the record-to-record variability, other uncertainties (modeling, material, fabrication) would presumably not increase the overall standard deviation significantly. Based on these requirements, the implied tolerable probability of exceeding the design axial strength of columns at the MCE level is 16%, i.e., one standard deviation about the mean. If the true distribution is in fact lognormal with a dispersion of 0.4, the mean is 1.084 times the median. Using 7 analyses, the coefficient of variation around the predicted mean is 0.16 ($\approx 0.4/\sqrt{7}$) and the probability of exceeding the design demand is 12.3% (see Figure 5-28 for overlap region of the two distribution).

The following discussion will be based on probability of exceeding the design axial strength for the 1st story column in the 16-story frame where the reduction in design axial strength compared to full capacity design would be the greatest. It should be kept in mind that of course exceeding the design axial strength does not necessarily equate to complete column failure.

As has been demonstrated with the brace connections, conditioning on rare events such as the MCE demand can provide a false sense of safety when applied to capacity-designed components as the peak demands might develop at much more frequent events. However, as the discussion above pointed out and Figure 5-21 demonstrated, the demand versus Sa_{T1} curve of base columns in multi-story frames does not follow the same bi-linear shape as it does in the top stories. To investigate what this means for the 1st story columns in the 16-story frame, the axial force demand distribution from the nonlinear

analysis is used to calculate the probability of exceeding the TBI design force demand. To calculate the mean and variance of the TBI design distribution, random samples of the 44 recorded demands at the MCE level are created and the mean and the variance of the sample calculated. The probability of exceeding the design distribution is then calculated at other spectral accelerations Figure 5-29 shows the axial force demand distributions and their overlap with the TBI design distribution for $Sa_{y,exp}$, Sa_{MCE} and the median collapse point. Figure 5-30 shows the calculated probability of the axial force demand distribution exceeding the TBI design distribution at the same spectral accelerations.

Figure 5-36 reveals that the probability of exceeding the design demand is 4.6% at the MCE demand and about 0.3% at $Sa_{y,exp}$. These are positive results for the practice of conditioning at the MCE demand. However, the demand continues to increase past the MCE demand and the probability of exceeding the design demand at the median collapse point is 10.6%, or more than twice that of the MCE demand. That is of course counteracted by much lower frequencies of occurrence of earthquake intensities associated with the median collapse point. For example, based on Project 07's definition of the MCE demand and a collapse fragility curve dispersion of 0.8, the ratio between the frequency of occurrence of the MCE demand to the one associated with the median collapse point is 188 for a San Francisco site hazard curve (Lat. 38.0, Lon. -121.7, T = 1.0s)

5.3 Dynamic Analysis of an Alternative Design of a 6-Story Special Concentrically Braced Frame

5.3.1 Description of Analysis

In the next set of analyses, the median model of an alternative design of a 6-Story SCBF (Design 2) is investigated. This alternative SCBF design is similar to the original design, except that the 1st-story brace sizes are used through the building height, and the capacity-designed columns are re-designed accordingly. The main objective of these analyses is to investigate the demand distributions on capacity-designed components in over-designed stories and how they compare to those in optimally-designed stories. The frame member sizes are listed in Table 5-15.

As in the previous studies, Modal Response Spectrum Analyses are performed to determine the R_μ and $Sa_{y,exp}$, values, following the procedure outlined in Table 3-12 and used in Section 5.2.3. The results are listed in Table 5-16 and 5-17. During each nonlinear dynamic analysis, the maximum demands on the capacity-designed connections and columns are recorded and used to a) compare the spectral acceleration at which braces begin to yield in tension to $Sa_{y,exp}$ calculated through simplified methods proposed in Table 3-12, b) compare the demand distributions on connections in over-designed frames to the ones in optimally designed frames, c) calculate the required connection design strengths, and d) investigate the demand distribution on columns in multi-story braced frames

144

5.3.2 Nonlinear Dynamic Analyses: Force Demands on Brace Connections

The simulation results from the incremental dynamic analysis of Design 2 of the 6-Story SCBF are presented in this section. During each dynamic analysis, the frame's story drift ratios and the brace and column axial forces are recorded. Figure 5-31a shows the maximum story drift ratio versus Sa_{T1} and Figure 5-31b the collapse fragility curve. The median collapse point is 1.66g, which is almost identical to the median collapse point for Design 1 of the 6-story SCBF. The dispersion of the collapse fragility curve for Design 2 is however reduced compared to Design 1, or 0.52 compared to 0.58. Figure 5-34 compares the collapse fragility curves for the two frames. The smaller dispersion for Design 2 is a result of the inelastic deformations occurring only in the bottom two stories and therefore the frame's collapse capacity is solely based on the their capacities (see Table 5-18 for location of collapses). This point is further illustrated in Figure 5-32, which compares the maximum story drift results for the two designs. Figure 5-32 shows that at low spectral accelerations, the story drift dispersion for Design 2 are lower than that of Design 1. This results in lower probability of collapse at the low spectral accelerations for Design 2 than for Design 1. However, with the median collapse capacity equal, the end result is a lower dispersion in the collapse fragility curve. Figure 5-33 compares the maximum story drift ratio in story 1 versus the spectral accelerations for the two 6-story frames and it clearly shows the increased deformation demands in story 1 of Design 2 compared to story 1 of Design 1 due to the concentration of inelastic deformations in the lower stories.

The maximum brace tensile forces per story normalized by expected yield strength of the braces are plotted in Figure 5-36. The plot shows that brace tensile yielding occurs almost exclusively in story 1 and story 2 while the braces in the other stories experience limited tensile yielding throughout the incremental dynamic analysis. This was expected based on the considerable member overstrength in the upper stories. However, as the braces in the upper stories have generally not yielded in tension, the dispersion around the maximum brace forces is high as small differences in story drift ratios result in large differences in the brace forces developed. Tables 5-19 and 5-20 list the median and the dispersion of the brace forces per story and the maximum for the whole frame and Figure

5-37 plots the results. The R_μ calculations from Section 5.2.3 predicted an R_μ of 2.5 and a $Sa_{y,exp}$ of 0.30g and based on the analysis results, those predictions are fairly accurate.

5.3.3 Nonlinear Dynamic Analysis: Required Design Strength of Brace Connections

To assess how well simplified methods of establishing required connection design strengths proposed by the methodology match with those when a full integration of the probability of demand exceeding capacity and a seismic hazard curve is performed, the ϕ/γ-ratios are calculated following the same technique as described in Section 5.2.4. The calculated ϕ/γ-ratios are reported in Tables 5-21 and Figure 5-38 plots the ratios calculated through the two different methods against each other, including the results from the other 2 previously analyzed frames. Again, the simplified method and the detailed integration method compare quite well, especially for stories which do experience inelastic deformations. The calculated ϕ/γ-ratio for the 6th story in Design 2 using the simplified method is noticeably unconservative compared to the integration method, or 19% larger. The 6th story stays essentially elastic for all ground motions at all earthquake intensities and as a result, the median demand never stabilizes and dispersion stays high causing the step-function simplification not to capture the true behavior. (Figure 5-40) Figure 5-39 shows the strong relationship between R_μ and the ϕ/γ-ratios where the ϕ/γ-ratio decreases as R_μ increases.

5.3.4 Nonlinear Dynamic Analyses: Axial Force Demands on Columns

The seismic axial demands from the dynamic analysis of 6-story Design 2 SCBF are presented in this section. Similar to what was done in 5.2.5, the demand is normalized by two different design rules. C_{exp} and $C_{elastic,AISC}$, which have been described previously. Starting from the 1st level, C_{exp} is [3561, 3561, 2147, 2147, 732, 732] kips and $C_{elastic,AISC}$ is [1520, 1520, 833, 833, 274, 274] kips.The median and the dispersion of C_{max}/C_{exp} are plotted in Figures 5-41, 5-44 and 5-45. The general trend for the demand is the opposite

146

of the other 2 frames analyzed, i.e. it the normalized median demand increases as the number of stories above it increases and the dispersion decreases, i.e. the dispersion is the highest in the top stories. This is due to the overdesign of the upper stories which causes the braces not to develop their full capacity and to remain essentially elastic. Therefore small differences in story drift ratios result in large differences in the brace forces developed. This also causes the demand to continue to increase past the frames $Sa_{y,exp}$. The median demand at the base of the frame is approximately 80% of what capacity design rules suggest at the MCE demand (Sa_{TI} = 1.10g) with a 10% dispersion but 67% at $Sa_{y,exp}$ with a dispersion of 10%.

Based on the AISC 2010 Seismic Provisions, the required design strength of columns does not need to exceed elastic design demand, $C_{elastic,AISC}$. Figure 5-43 plots the column axial demand normalized by $C_{elastic,AISC}$ (Ω_0 excluded). It can be seen that this elastic design rule causes un-conservative estimates of the demand. This could be expected as the design rule does not take into consideration the true member overstrength. Even if the first stories of Design 1 and Design 2 have similar member overstrength, the upper stories in Design 2 are significantly over-designed (see Table 5-17), thus creating the capacity to develop larger forces. Therefore, similar to the observations for the 16-story frame, using a fixed over-strength factor, Ω_0, irrelevant of the design causes the demand to be greatly under-estimated.

5.4 Probability of Collapse Including Connection Failures

To assess the probability of collapse due to connection failures, $P\left(Coll_{D>C}|D>C\right)$, dynamic analyses of the 6-story SCBF – Design 1 are performed again, now with the possibility of brace fracture included. Unlike the analysis on the single-story frame in Chapter 4 where brace fracture was modeled in a full Monte Carlo analysis that included variability in all nonlinear model parameters, the only random variables in this analysis are the brace connection strengths. A total of 880 models are created by generating realization of the brace connection strengths using Monte-Carlo simulation methods (Melchers, 1999; Rubinstein, 1981). The median connection strength is 1.4 times the

expected yield strength, $P_{y,exp}$, of the connected brace connected and the brace strength dispersion is 0.18. The brace connection strength is intentionally low ($\phi/\gamma = 1.00$ instead of 0.75) to increase the instances of connection fractures. The brace connection strengths are assumed to be statistically independent from each other, except the brace connections on either end of the same brace are assumed to be fully correlated. Each frame model is then matched with a ground motion such, such that each ground motion is used 20 times. To better quantify the added probability of collapse due to connection failures only, all models are initially analyzed without connection fractures included. This requires only 44 dynamic analyses (the previously performed incremental dynamic analysis), since with the connection fractures excluded, all of the model realizations are identical, and the only difference between different simulations is the ground motion record. For the resulting non-collapsed analysis cases, where the maximum demand from the dynamic analysis exceeds the previously simulated connection strength, the dynamic analysis is re-run, now including possible connection fractures and the number of additional collapses is recorded.

The spectral accelerations of special interest are the relatively low ones where the braces have already yielded in tension and the frequency of exceedance is still high, i.e. Sa_{T1} between $Sa_{y,exp}$ and Sa_{MCE}. The selected spectral accelerations for the analyses are from 0.40 to 2.50g. The trends observed in these analyses general agree with those from the single-story analyses of Chapter 4. Where connection fractures occur at low spectral accelerations, they have a low probability of causing collapse (practically zero probability at an impose intensity of $Sa_{y,exp}$)At higher intensities, the probability of collapse due to connection failure increases to maximum of about 25.6%. Thus, as in the single-story example, these analyses indicate that the consequence of connection failures on system collapse is relatively low. Table 5-22 and Figures 5-47 to 5-49 show the results of the analyses. The circles in Figure 5-47 represent the probability of collapse of the median model at the specified spectral accelerations. The same values are shown in column 2 of Table 5-22. The number of frame models where connection failures occurred, but the systems did not collapse in the first set of dynamic analysis, are shown in column 3 of Table 5-22. If a connection failure equaled frame collapse, those could be directly added

to the frame models which collapsed in the initial analysis. The diamonds on Figure 5-47 show the change in the collapse fragility curve if that was the case. However, when the dynamic analyses are re-run with the possibility of connection failures included, only a fraction of the models collapse during the dynamic analyses. The result of the second set of dynamic analysis is shown in column 4 of Table 5-22. The probability of collapse given connection failure and that the system has not otherwise collapsed is calculated in column 5 of Table 5-22 and shown visually in Figure 5-48. Eventually, the total probability of collapse is calculated and presented in column 6 of Table 5-22 and the values represented by the squares in Figure 5-47. Fitted distributions of these three different cases are plotted in Figure 5-55.

5.5 Conclusions

The main objectives of this chapter are (1) to demonstrate the applicability of the methodology developed in Chapter 3 for multi-story systems, (2) to calculate the probability of system collapse given connection failure, (3) to investigate the differences between multi-story and single-story systems with respect to the proposed methodology, and (4) to investigate the demand on columns in braced frames. To meet these objectives, dynamic analyses of two 6-story and one 16-story SCBF´s were conducted.

Modal Response Spectrum Analyses were performed for each of the frames to assess the R_μ and $Sa_{y,exp}$, values, following the procedure outlined in Table 3-12. The Modal Response Spectrum Analyses were performed using both the design response spectrum as well as using the median response spectrum of the 44 ground motions used in the dynamic analyses. Similar to the single-story systems, the spectral acceleration at which braces began to yield in tension for all frames compared well with the with the previously calculated $Sa_{y,exp}$, except for the 16-story frame when the design response spectrum was used. This was due to higher mode effects playing a larger role in the 16-story frame and a significant difference between the design response spectrum and the median ground motion response spectrum at periods less than the fundamental period, suggesting that care needs to be given to which response spectrum are used for taller buildings. For best

results, a ground motion response spectrum that best represents the given site conditions should be used in the Modal Response Spectrum Analysis.

For balanced designs, such as the 6-story Design 1 SCBF, no story can be expected to remain elastic throughout all ground motions and all intensities. Capacity-designed components therefore need to be designed to resist the demand from deformation-controlled components as they undergo inelastic deformations. The calculated ϕ/γ-ratios for the 6-story Design 1 frame demonstrated this where the difference between stories is minimal. However, compared to single-story frames, the median brace connection demand per story decreases and the variability increases with increased number of deformation-controlled components. This is due to concentration of large inelastic deformations in different stories for different ground motions, thus shielding the other ones from large deformations. This effect becomes more pronounced as the number of stories increases. Nevertheless, for all three multi-story frames analyzed, the maximum normalized brace tensile force for the whole frame versus spectral acceleration curves compare well with the same curve for the single-story frames, since inelastic deformations will occur somewhere within a frame when subjected to large enough earthquake ground motions. Therefore, for ϕ/γ-ratio calculations in balanced designs where inelastic deformations are as likely to occur in one story as the next, it is not appropriate to take advantage of this decrease in the median demand as it will result in weaker connections. Instead, the maximum normalized brace tensile force statistics should be used.

When member overstrength varies significantly between stories, as was the case for both the 6-story Design 2 frame and the 16-story frame, some stories may remain elastic, or close to elastic, throughout all dynamic analyses. The 6-story Design 2 frame was specifically designed to study this case. All braces up the height of the frame were identical, and therefore the member overstrength in the upper stories was significant. The dynamic analysis results demonstrated that inelastic deformation occurred almost exclusively in story 1 and story 2. As a consequence, the calculated ϕ/γ-ratio for each story varies significantly, or by 72% between story 1 and story 6. For this case, requiring the margin between the brace connection strengths and the brace yield strengths to be the

same for both stories is conservative. Caution should be taken though when some stories are significantly over-designed compared to others within the frame as the demand dispersion can be significant due the members still behaving elastically and therefore small increase in deformation demands will cause a large increase in brace forces. Those are cases where the capacity-design concept does not apply as well since the deformation-controlled components do not necessarily reach their full capacity. As a result, the simplified method proposed in Chapter 3 to establish the ϕ/γ-ratio, resulted in quite unconservative values as the step-function assumption it makes does not capture the probability of demand exceeding capacity curve accurately.

The demand on columns in braced frames is a complex matter. As the results from the three braced frame studies demonstrated, capacity design principles do not explain well the expected demand on columns, rather the maximum theoretical demand that can be delivered to them. For columns where there are only a few stories above them, the expected demand is this theoretical maximum demand, at least for balanced designs. Given the column capacity distribution and the consequences of exceeding column capacities, the simplified method proposed by the methodology to establish the required column strength can be used. However, for columns with multiple stories above them, the maximum demand predicted by capacity design principles rarely develops and the demand on the columns continues to increase passed $Sa_{y,exp}$ and even up to the median collapse point. Therefore, if risk-consistent column strength guidelines are the goal, the simplified method proposed by the methodology will not suffice but a full integration of the probability of exceeding the column capacity and a seismic ground motion hazard curve is required. However, full integration is not a practical solution. Fortunately, for design guidelines such as those in TBI (2010) which condition the design checks at the MCE ground motion intensity, this means that the column demand at the MCE ground motion intensity is considerably larger than the column demand at lower intensities. Unfortunately, it also means that the MCE demand might not capture the maximum column demand that can be developed. However, as the frequency of experiencing those large demands associated with the maximum column demand becomes very small, that is not of a great concern. Conditioning the reliability calculations, or design checks, at the

MCE demand is therefore as valid as it is for the simplified method proposed by the methodology, but the margin between demand and capacity at the MCE demand needs be adjusted to account for the different shape of the probability of demand exceeding capacity curve.

The AISC 2010 *Seismic Provisions* include a limit on the maximum required design strength of columns. The required design strength does not need to exceed the forces determined using design loads, including amplified seismic load (Ω_0), applied to a frame model in which all compression braces have been removed. However, this study showed that the use of a fixed overstrength factor, Ω_0, irrelevant of the design causes the demand to be greatly under-estimated.

The dynamic analyses of the 6-story SCBF – Design 1 where the possibility of brace connection fractures was included demonstrated, similar to a similar analysis in the single-story frame, that the probability of collapse given connection failure is not a constant as assumed in the methodology but that it rather gradually increases until it reaches its peak values around 25% at the MCE demand. This greatly reduces the influence of connection fractures on the system reliability as the main contribution of connection fractures to the mean annual frequency of collapse would be at the low intensities with high frequencies of occurrence. These results agree with similar conclusions on the impact of connection fractures on system behavior in Luco and Cornell (2000).

Table 5-1: Member sizes for the 6-Story and 16-Story SCBFs

Story	6-Story Frame[1]			16-Story Frame		
	Beams[2]	Braces[3]	Columns[2]	Beams[2]	Braces[3]	Columns[2]
16	-	-	-	W18x65	HSS9-5/8x3/8	W12x45
15	-	-	-	W18x35	HSS9-5/8x3/8	W12x45
14	-	-	-	W18x71	HSS8-5/8x1/2	W14x82
13	-	-	-	W18x35	HSS8-5/8x1/2	W14x82
12	-	-	-	W18x86	HSS11-1/4x1/2	W14x120
11	-	-	-	W18x35	HSS11-1/4x1/2	W14x120
10	-	-	-	W18x86	HSS10x5/8	W14x176
9	-	-	-	W18x35	HSS10x5/8	W14x176
8	-	-	-	W18x97	HSS11-1/4x5/8	W14x233
7	-	-	-	W18x35	HSS11-1/4x5/8	W14x233
6	W18x97	HSS7-1/2x5/16	W14x68	W18x97	HSS11-1/4x5/8	W14x283
5	W24x104	HSS9-5/8x3/8	W14x68	W18x35	HSS11-1/4x5/8	W14x283
4	W24x131	HSS9-5/8x1/2	W14x176	W21x93	HSS11-1/4x5/8	W14x342
3	W18x76	HSS11-1/4x1/2	W14x176	W18x35	HSS11-1/4x5/8	W14x342
2	W24x146	HSS12-1/2x1/2	W14x342	W24x146	W12x96	W14x370
1	W21x62	HSS12-1/2x1/2	W14x342	W18x35	W12x96	W14x370

1) 6-Story Frame – Design 2 has HSS12-1/2x1/2 at all floors ($F_{y,exp}$ = 60.3 kips)

2) ASTM A992 ($F_{y,exp}$ = 55 kips)

3) ASTM A500 Grade B ($F_{y,exp}$ = 55 kips)

Table 5-2: Expected story shear yielding force, $V_{y,exp}$

Story	Expected Brace Strength			$V_{y,exp}$ [kips]
	Brace	Tension[1] [kips]	Compression[2] [kips]	
6	HSS7-1/2x5/16	388	221	431
5	HSS9-5/8x3/8	600	428	727
4	HSS9-5/8x1/2	788	557	951
3	HSS11-1/4x1/2	929	724	1169
2	HSS12-1/2x1/2	1035	847	1331
1	HSS12-1/2x1/2	1035	847	1331

1) $F_{y,exp} * A_g$
2) Column Strength Equation using expected material properties
   The effective brace length is 80% of the work-point-to-work-point length

Table 5-3: Design story shear forces from Modal Response Spectrum Analysis

Story	V_{RSA} [kips]
6	171
5	301
4	383
3	469
2	519
1	526

Table 5-4: The $V_{y,exp}/V_{RSA}$-ratio for each story

Story	V_{RSA} [kips]	$V_{y,exp}/V_{RSA}$
6	171	2.53
5	301	2.42
4	383	2.49
3	469	2.49
2	519	2.56
1	526	2.53

Table 5-5: Summary of calculations performed to calculate the 6-Story Design 1 frame's R_μ using the design response spectrum

Step 1		Step 2			Step 3	Step 4	Step 5	Step 6
Story	Brace	Tension [kips]	Compression [kips]	$V_{y,exp}$ [kips]	V_{RSA} [kips]	$V_{y,exp}/V_{RSA}$	$Sa_{y,exp}$ [g]	R_μ
6	HSS 7-1/2x5/16	388	221	431	171	2.53	0.31	2.4
5	HSS 9-5/8x3/8	600	428	727	301	2.42	0.30	2.5
4	HSS 9-5/8x1/2	788	557	951	383	2.49	0.30	2.4
3	HSS 11-1/4x1/2	929	724	1169	469	2.49	0.30	2.4
2	HSS 12-1/2x1/2	1035	847	1331	519	2.56	0.31	2.3
1	HSS 12-1/2x1/2	1035	847	1331	526	2.53	0.31	2.4

Table 5-6: Summary of the calculations performed to calculate the 6-story Design 1frame´s R_μ using the ground motion set´s median response spectrum

Step 1		Step 2			Step 3	Step 4	Step 5	Step 6
Story	Brace	Tension [kips]	Compression [kips]	$V_{y,exp}$ [kips]	V_{RSA} [kips]	$V_{y,exp}/V_{RSA}$	$Sa_{y,exp}$ [g]	R_μ
6	HSS 7-1/2x5/16	388	221	431	194	2.22	0.27	2.7
5	HSS 9-5/8x3/8	600	428	727	317	2.30	0.28	2.6
4	HSS 9-5/8x1/2	788	557	951	385	2.47	0.30	2.4
3	HSS 11-1/4x1/2	929	724	1169	468	2.50	0.30	2.4
2	HSS 12-1/2x1/2	1035	847	1331	526	2.53	0.31	2.4
1	HSS 12-1/2x1/2	1035	847	1331	539	2.47	0.30	2.4

Table 5-7: Summary of the calculations performed to calculate the 16-story frame´s R$_\mu$ using the design response spectrum

Step 1		Step 2			Step 3	Step 4	Step 5	Step 6
Story	**Brace**	**Tension [kips]**	**Compression [kips]**	**V$_{y,exp}$ [kips]**	**V$_{RSA}$ [kips]**	**V$_{y,exp}$/V$_{RSA}$**	**Sa$_{y,exp}$**	**R$_\mu$**
16	HSS9-5/8x3/8	600	428	727	49.7	14.6	0.86	0.4
15	HSS9-5/8x3/8	600	428	727	92.1	7.9	0.47	0.8
14	HSS8-5/8x1/2	700	452	815	111.9	7.3	0.43	0.8
13	HSS8-5/8x1/2	700	452	815	123.1	6.6	0.39	0.9
12	HSS11-1/4x1/2	929	724	1169	124.0	9.4	0.56	0.6
11	HSS11-1/4x1/2	929	724	1169	131.4	8.9	0.53	0.7
10	HSS10x5/8	1011	730	1231	131.4	9.4	0.55	0.6
9	HSS10x5/8	1011	730	1231	144.3	8.5	0.50	0.7
8	HSS11-1/4x5/8	1147	889	1439	150.3	9.6	0.56	0.6
7	HSS11-1/4x5/8	1147	889	1439	171.1	8.4	0.50	0.7
6	HSS11-1/4x5/8	1147	889	1439	181.7	7.9	0.47	0.8
5	HSS11-1/4x5/8	1147	889	1439	208.9	6.9	0.41	0.9
4	HSS11-1/4x5/8	1147	889	1439	220.2	6.5	0.39	0.9
3	HSS11-1/4x5/8	1147	889	1439	241.5	6.0	0.35	1.0
2	W12x96	1551	1086	1864	252.3	7.4	0.44	0.8
1	W12x96	1551	1086	1864	258.8	7.2	0.42	0.8

Table 5-8: Summary of the calculations performed to calculate the 16-story frame´s R_μ using the ground motion set´s median response spectrum

Step 1		Step 2			Step 3	Step 4	Step 5	Step 6
Story	Brace	Tension [kips]	Compression [kips]	$V_{y,exp}$ [kips]	V_{RSA} [kips]	$V_{y,exp}/V_{RSA}$	$Sa_{y,exp}$	R_μ
16	HSS9-5/8x3/8	600	428	727	69	10.6	0.62	0.6
15	HSS9-5/8x3/8	600	428	727	118	6.2	0.36	1.0
14	HSS8-5/8x1/2	700	452	815	131	6.2	0.37	1.0
13	HSS8-5/8x1/2	700	452	815	134	6.1	0.36	1.0
12	HSS11-1/4x1/2	929	724	1169	129	9.1	0.54	0.7
11	HSS11-1/4x1/2	929	724	1169	135	8.7	0.51	0.7
10	HSS10x5/8	1011	730	1231	138	8.9	0.53	0.7
9	HSS10x5/8	1011	730	1231	149	8.3	0.49	0.7
8	HSS11-1/4x5/8	1147	889	1439	154	9.3	0.55	0.6
7	HSS11-1/4x5/8	1147	889	1439	168	8.6	0.51	0.7
6	HSS11-1/4x5/8	1147	889	1439	181	8.0	0.47	0.8
5	HSS11-1/4x5/8	1147	889	1439	209	6.9	0.41	0.9
4	HSS11-1/4x5/8	1147	889	1439	231	6.2	0.37	1.0
3	HSS11-1/4x5/8	1147	889	1439	259	5.6	0.33	1.1
2	W12x96	1551	1086	1864	286	6.5	0.38	0.9
1	W12x96	1551	1086	1864	292	6.4	0.38	0.9

Table 5-9: Median of the normalized maximum brace tensile force vs. Sa_{T1} for 6-story SCBF – Design 1

Sa_{T1} [g]	Story 1	Story 2	Story 3	Story 4	Story 5	Story 6	Max All
0.10	0.52	0.47	0.44	0.44	0.55	0.59	0.64
0.20	0.82	0.77	0.76	0.78	0.88	0.92	0.94
0.30	0.91	0.86	0.86	0.86	0.95	0.97	0.98
0.40	0.93	0.94	0.92	0.92	0.97	0.98	0.99
0.60	0.95	0.98	0.94	0.97	0.98	0.99	1.01
0.80	0.97	0.99	0.98	0.98	0.99	1.00	1.02
1.00	0.98	1.00	0.98	0.98	0.99	0.99	1.03
1.25	0.99	1.01	0.98	0.99	0.99	0.99	1.03
1.50	0.99	1.01	0.99	0.99	0.99	1.00	1.03
2.00	0.99	1.02	0.99	1.00	0.98	1.00	1.04

Table 5-10: Dispersion of the normalized maximum brace tensile force vs. Sa_{T1} for 6-story SCBF – Design 1

Sa_{T1} [g]	Story 1	Story 2	Story 3	Story 4	Story 5	Story 6	Max All
0.10	0.21	0.19	0.18	0.17	0.25	0.29	0.26
0.20	0.10	0.11	0.12	0.13	0.09	0.11	0.07
0.30	0.09	0.09	0.08	0.10	0.06	0.07	0.03
0.40	0.04	0.08	0.09	0.08	0.06	0.06	0.03
0.60	0.05	0.07	0.07	0.07	0.05	0.04	0.02
0.80	0.04	0.07	0.05	0.06	0.04	0.03	0.02
1.00	0.04	0.05	0.03	0.06	0.03	0.03	0.03
1.25	0.04	0.04	0.03	0.05	0.02	0.03	0.03
1.50	0.05	0.03	0.04	0.04	0.02	0.04	0.03
2.00	0.04	0.03	0.03	0.03	0.04	0.02	0.03

Table 5-11: Median of the normalized maximum brace tensile force vs. Sa_{T1} for 16-story SCBF

Story	Sa_{T1} [g]						
	0.15	**0.30**	**0.45**	**0.60**	**0.90**	**1.35**	**1.80**
1	0.55	0.73	0.78	0.81	0.83	0.82	0.86
2	0.50	0.65	0.71	0.77	0.82	0.86	0.90
3	0.67	0.85	0.87	0.90	0.92	0.89	0.90
4	0.59	0.81	0.88	0.92	0.92	0.91	0.93
5	0.57	0.74	0.79	0.83	0.86	0.84	0.85
6	0.49	0.69	0.75	0.84	0.85	0.81	0.83
7	0.48	0.66	0.70	0.74	0.76	0.73	0.72
8	0.43	0.61	0.67	0.73	0.70	0.74	0.79
9	0.46	0.64	0.72	0.77	0.79	0.80	0.81
10	0.43	0.64	0.69	0.78	0.80	0.76	0.79
11	0.52	0.68	0.75	0.78	0.82	0.81	0.77
12	0.46	0.64	0.68	0.76	0.75	0.76	0.76
13	0.66	0.84	0.88	0.87	0.88	0.89	0.86
14	0.61	0.81	0.89	0.92	0.91	0.82	0.84
15	0.68	0.82	0.83	0.84	0.85	0.83	0.83
16	0.50	0.65	0.69	0.73	0.73	0.72	0.69
All	0.73	0.96	0.98	1.01	1.03	1.07	1.10

Table 5-12: Dispersion of the normalized maximum brace tensile force vs. Sa_{T1} for 16-story SCBF

Story	Sa_{T1} [g]						
	0.15	**0.30**	**0.45**	**0.60**	**0.90**	**1.35**	**1.80**
1	0.25	0.16	0.14	0.13	0.15	0.20	0.12
2	0.26	0.19	0.20	0.18	0.18	0.13	0.16
3	0.24	0.10	0.11	0.09	0.12	0.16	0.13
4	0.26	0.16	0.13	0.10	0.15	0.16	0.13
5	0.22	0.12	0.13	0.15	0.18	0.23	0.19
6	0.23	0.17	0.19	0.16	0.16	0.22	0.19
7	0.24	0.17	0.15	0.15	0.18	0.22	0.23
8	0.28	0.22	0.20	0.17	0.19	0.23	0.17
9	0.33	0.21	0.20	0.19	0.15	0.16	0.15
10	0.31	0.25	0.23	0.18	0.16	0.17	0.19
11	0.27	0.20	0.18	0.18	0.15	0.18	0.21
12	0.26	0.19	0.20	0.16	0.18	0.21	0.21
13	0.26	0.14	0.11	0.17	0.15	0.17	0.21
14	0.32	0.17	0.13	0.08	0.14	0.20	0.19
15	0.28	0.16	0.14	0.13	0.13	0.19	0.20
16	0.40	0.27	0.24	0.19	0.22	0.23	0.23
All	0.27	0.06	0.03	0.04	0.04	0.05	0.06

Table 5-13: φ/γ-ratios for 6-Story SCBF - Design 1 calculated by both full integration and by simplified method proposed in the methodology

Story	Brace	$V_{y,exp}/V_{RSA}$	$Sa_{y,exp}$ [g]	R_μ	Detailed φ/γ	Simplified φ/γ
6	HSS 7-1/2x5/16	2.22	0.27	2.7	0.72	0.78
5	HSS 9-5/8x3/8	2.30	0.28	2.6	0.76	0.79
4	HSS 9-5/8x1/2	2.47	0.30	2.4	0.80	0.81
3	HSS 11-1/4x1/2	2.50	0.30	2.4	0.81	0.81
2	HSS 12-1/2x1/2	2.53	0.31	2.4	0.80	0.78
1	HSS 12-1/2x1/2	2.47	0.30	2.4	0.79	0.80

Table 5-14: φ/γ-ratios for 16-Story SCBF calculated by both full integration and by simplified method proposed in the methodology

Story	Brace	$V_{y,exp}/V_{RSA}$	$Sa_{y,exp}$ [g]	R_μ	Detailed φ/γ	Simplified φ/γ
16	HSS9-5/8x3/8	10.58	0.62	0.6	1.46	1.92
15	HSS9-5/8x3/8	6.17	0.36	1.0	1.25	1.55
14	HSS8-5/8x1/2	6.20	0.37	1.0	1.30	1.52
13	HSS8-5/8x1/2	6.07	0.36	1.0	1.29	1.50
12	HSS11-1/4x1/2	9.08	0.54	0.7	1.77	1.83
11	HSS11-1/4x1/2	8.65	0.51	0.7	1.59	1.70
10	HSS10x5/8	8.92	0.53	0.7	1.75	1.76
9	HSS10x5/8	8.27	0.49	0.7	1.67	1.74
8	HSS11-1/4x5/8	9.33	0.55	0.6	1.84	1.90
7	HSS11-1/4x5/8	8.56	0.51	0.7	1.74	1.85
6	HSS11-1/4x5/8	7.97	0.47	0.8	1.70	1.65
5	HSS11-1/4x5/8	6.89	0.41	0.9	1.54	1.63
4	HSS11-1/4x5/8	6.22	0.37	1.0	1.40	1.51
3	HSS11-1/4x5/8	5.56	0.33	1.1	1.30	1.29
2	W12x96	6.52	0.38	0.9	1.65	1.63
1	W12x96	6.39	0.38	0.9	1.53	1.69

Table 5-15: Member sizes for the 6-Story SCBF – Design 2

Story	Beams	Braces	Columns
6	W18x97	HSS12-1/2x1/2	W14x99
5	W24x104	HSS12-1/2x1/2	W14x99
4	W24x131	HSS12-1/2x1/2	W14x193
3	W18x76	HSS12-1/2x1/2	W14x193
2	W24x146	HSS12-1/2x1/2	W14x398
1	W21x62	HSS12-1/2x1/2	W14x398

Table 5-16: Summary of calculations performed to calculate the 6-story Design 2 frame's R_μ using the design response spectrum

Step 1		Step 2			Step 3	Step 4	Step 5	Step 6
Story	Brace	Tension [kips]	Compression [kips]	$V_{y,exp}$ [kips]	V_{RSA} [kips]	$V_{y,exp}/V_{RSA}$	$Sa_{y,exp}$ [g]	R_μ
6	HSS 12-1/2x1/2	1035	847	1331	165	8.07	0.98	0.7
5	HSS 12-1/2x1/2	1035	847	1331	302	4.41	0.54	1.4
4	HSS 12-1/2x1/2	1035	847	1331	392	3.39	0.41	1.8
3	HSS 12-1/2x1/2	1035	847	1331	476	2.79	0.34	2.2
2	HSS 12-1/2x1/2	1035	847	1331	526	2.53	0.31	2.4
1	HSS 12-1/2x1/2	1035	847	1331	536	2.48	0.30	2.4

Table 5-17: Summary of the calculations performed to calculate the 6-story Design 2 frame´s R_μ using the ground motion set´s median response spectrum

Step 1		Step 2			Step 3	Step 4	Step 5	Step 6
Story	Brace	Tension [kips]	Compression [kips]	$V_{y,exp}$ [kips]	V_{RSA} [kips]	$V_{y,exp}/V_{RSA}$	$Sa_{y,exp}$ [g]	R_μ
6	HSS 12-1/2x1/2	1035	847	1331	185	7.18	0.88	0.8
5	HSS 12-1/2x1/2	1035	847	1331	318	4.18	0.51	1.4
4	HSS 12-1/2x1/2	1035	847	1331	397	3.35	0.41	1.8
3	HSS 12-1/2x1/2	1035	847	1331	475	2.80	0.34	2.1
2	HSS 12-1/2x1/2	1035	847	1331	531	2.51	0.31	2.4
1	HSS 12-1/2x1/2	1035	847	1331	547	2.43	0.30	2.5

Table 5-18: Story location of collapsed cases.
Comparison between the two 6-Story SCBFs

Story	Design 1	Design 2
5 &6	11	-
3 & 4	5	-
1 & 2	22	36

Table 5-19: Design 2 - Median values of the normalized maximum brace tensile force vs. Sa_{T1}

Sa_{T1}	Median $P_{max}/P_{y,exp}$						
[g]	Story 1	Story 2	Story 3	Story 4	Story 5	Story 6	Max All
0.10	0.54	0.47	0.38	0.33	0.31	0.18	0.55
0.20	0.90	0.82	0.68	0.61	0.55	0.35	0.88
0.30	0.96	0.94	0.81	0.74	0.60	0.38	0.96
0.40	0.97	0.97	0.86	0.79	0.69	0.43	0.98
0.60	0.98	0.99	0.90	0.85	0.76	0.50	1.00
0.80	0.99	1.00	0.93	0.88	0.81	0.49	1.01
1.00	1.00	1.01	0.93	0.91	0.84	0.54	1.03
1.25	1.00	1.02	0.96	0.94	0.81	0.57	1.04
1.50	0.98	1.00	0.97	0.95	0.86	0.57	1.03
2.00	1.01	1.02	0.97	0.97	0.89	0.62	1.05

Table 5-20: Design 2 - Dispersion of the normalized maximum brace tensile vs. Sa_{T1}

Sa_{T1}	COV of $P_{max}/P_{y,exp}$						
[g]	Story 1	Story 2	Story 3	Story 4	Story 5	Story 6	Max All
0.10	0.28	0.23	0.23	0.19	0.29	0.34	0.26
0.20	0.11	0.13	0.15	0.15	0.21	0.26	0.09
0.30	0.05	0.08	0.10	0.13	0.19	0.24	0.03
0.40	0.05	0.06	0.09	0.13	0.19	0.27	0.02
0.60	0.04	0.03	0.12	0.13	0.19	0.31	0.03
0.80	0.04	0.03	0.07	0.11	0.14	0.28	0.02
1.00	0.04	0.05	0.12	0.09	0.17	0.25	0.04
1.25	0.03	0.07	0.07	0.07	0.18	0.25	0.04
1.50	0.09	0.11	0.08	0.11	0.15	0.29	0.05
2.00	0.04	0.10	0.06	0.06	0.14	0.22	0.04

Table 5-21: φ/γ-ratios for 6-Story SCBF - Design 2 calculated by both full integration and by simplified method proposed in the methodology

Story	Brace	$V_{y,exp}/V_{RSA}$	$Sa_{y,exp}$ [g]	R_μ	Detailed φ/γ	Simplified φ/γ
6	HSS 12-1/2x1/2	7.18	0.88	0.8	1.00	1.19
5	HSS 12-1/2x1/2	4.18	0.51	1.4	0.83	0.82
4	HSS 12-1/2x1/2	3.35	0.41	1.8	0.80	0.78
3	HSS 12-1/2x1/2	2.80	0.34	2.1	0.78	0.75
2	HSS 12-1/2x1/2	2.51	0.31	2.4	0.72	0.71
1	HSS 12-1/2x1/2	2.43	0.30	2.5	0.71	0.73

Table 5-22: Results for Design 1 including brace connection fracture

Sa_{T1} [g]	No. of Collapses (Connection Failures Excluded)	No. of Models w/Connection Failures (and didn't collapse)	No. of Additional Collapses	$P(Coll_{D>C}|D>C,No\ Coll_{Sys})$	$P(Coll)$
0.40	20 (2.3%)	92	0	0.0%	2.3%
0.60	20 (2.3%)	99	5	5.1%	2.8%
0.80	80 (9.1%)	114	10	8.8%	10.2%
1.00	160 (18.2%)	129	24	18.6%	20.9%
1.25	260 (29.5%)	117	30	25.6%	33.0%
1.50	380 (43.2%)	78	19	24.4%	44.3%
2.00	560 (63.6%)	74	18	23.1%	65.7%
2.50	640 (72.7%)	39	5	12.8%	73.3%
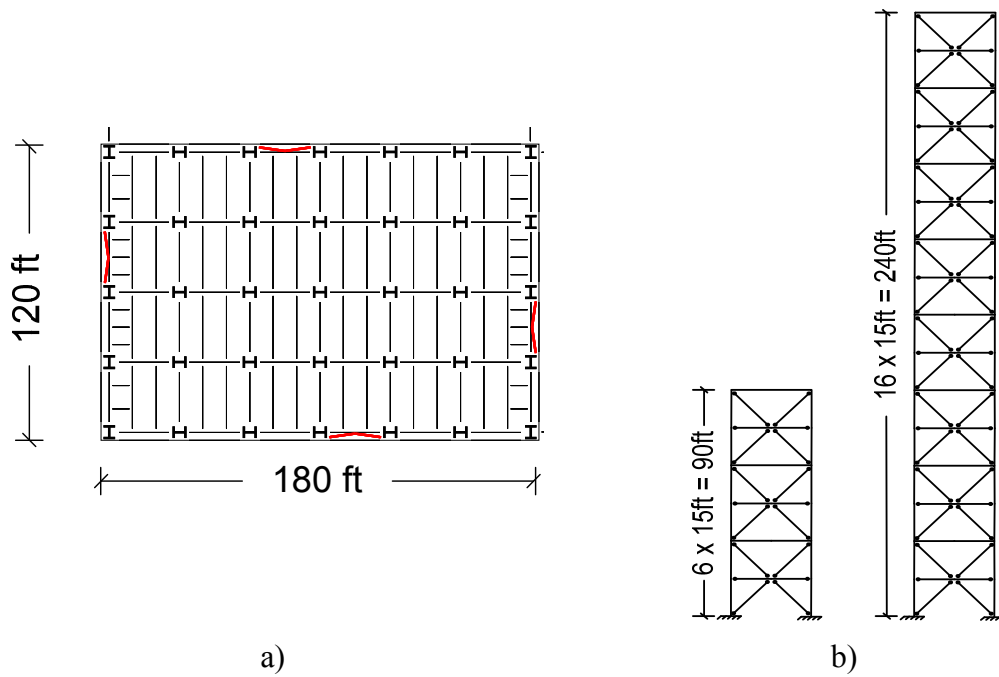
Figure 5-1: Plan and elevation of 6- and 16-story frames analyzed.
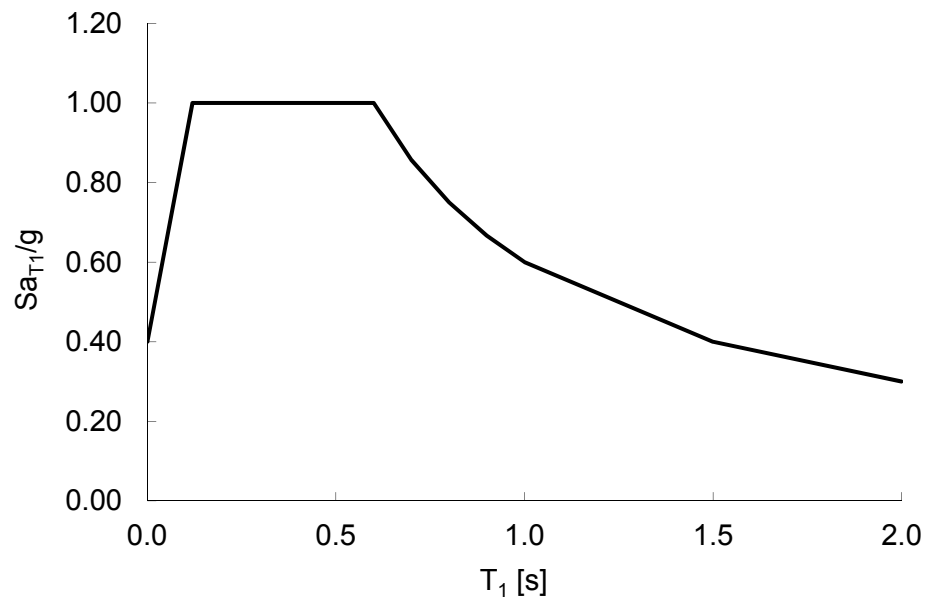
Figure 5-2: Design response spectrum used in Modal Response Spectrum Analysis
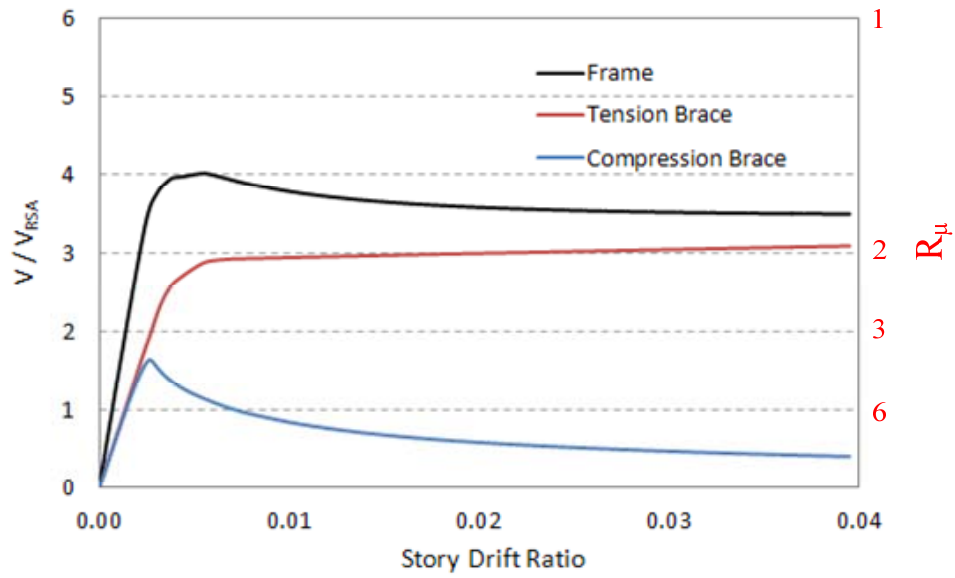
Figure 5-3: Pushover analysis results from Frame 2 used in IDA analysis described in Chapter 4.
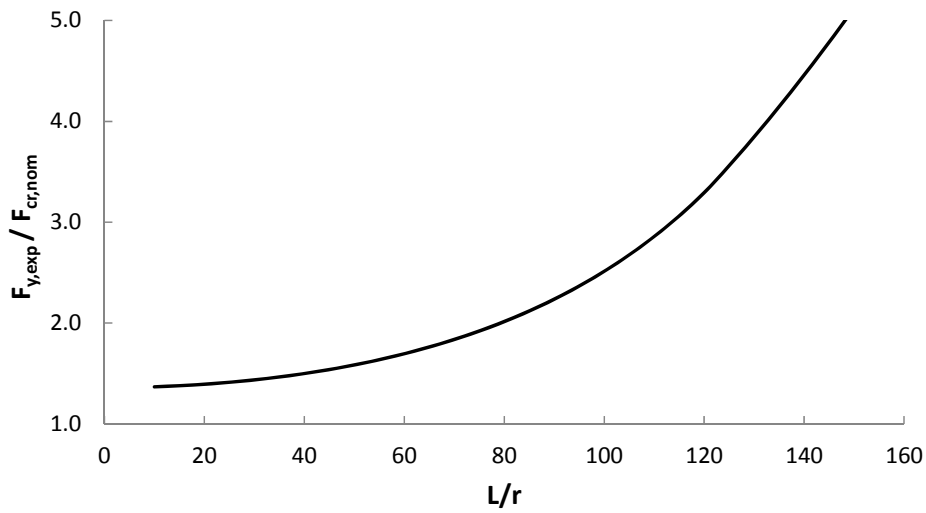
Figure 5-4: The ratio of the expected tensile yield stress over the nominal critical stress vs. the slenderness ratio in HSS circular section.
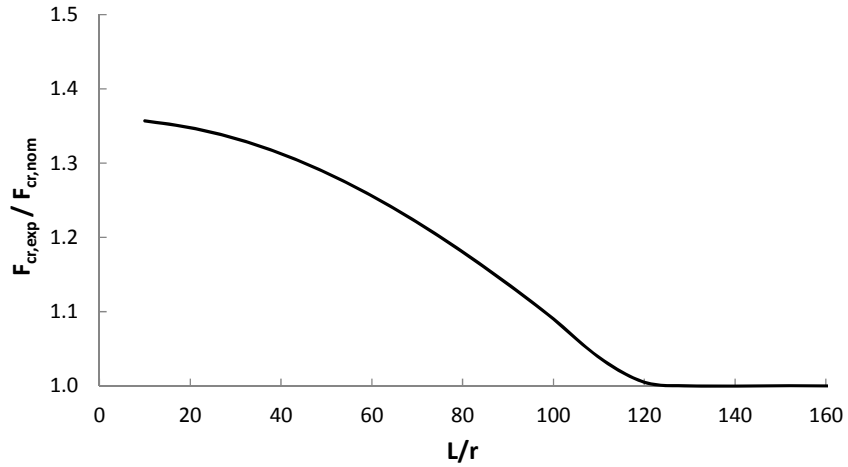
Figure 5-5: The ratio between the expected critical stress and the nominal critical stress vs. the slenderness ratio in HSS circular section.
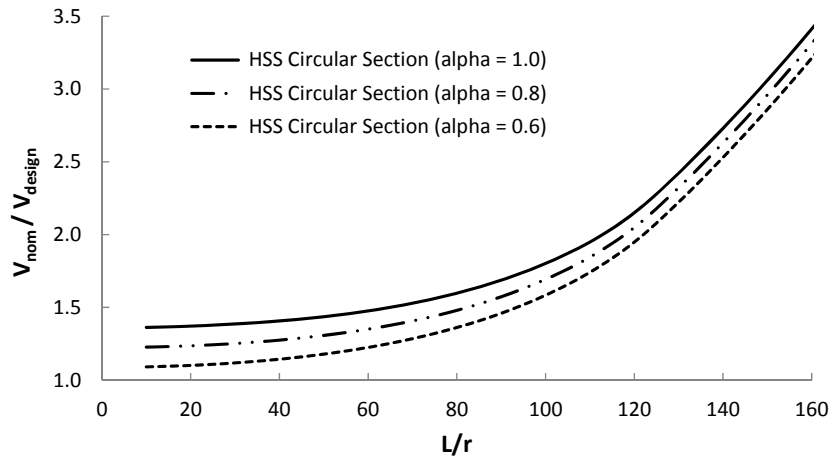
Figure 5-6: The ratio between the expected yield shear strength and the nominal shear strength vs. the slenderness ratio in HSS circular section.
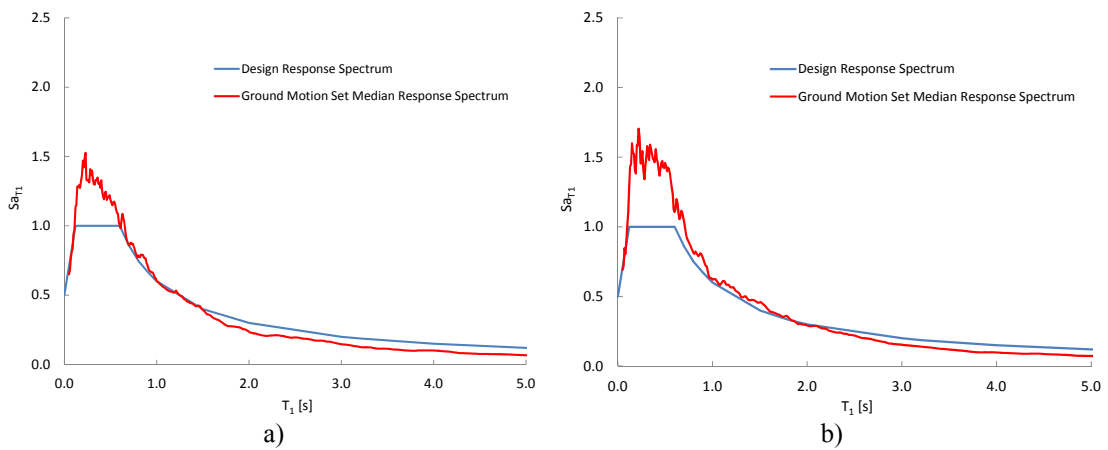
Figure 5-7: Comparison of design response spectrum and ground motion median response spectrum for a) 6-Story SCBF – Design 1 b) 16-Story SCBF

167
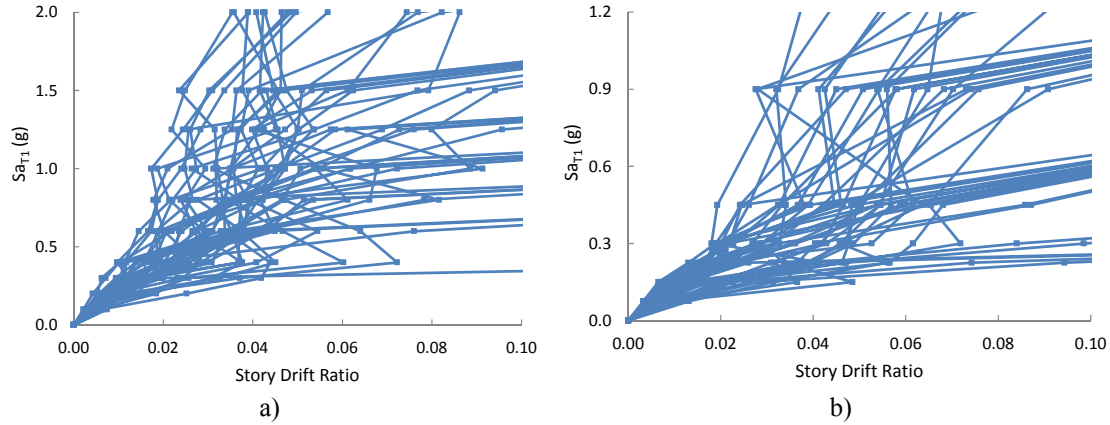
Figure 5-8: Maximum story drift ratio vs. Sa_{T1} for a) 6-story SCBF - Design 1 b) 16-story SCBF
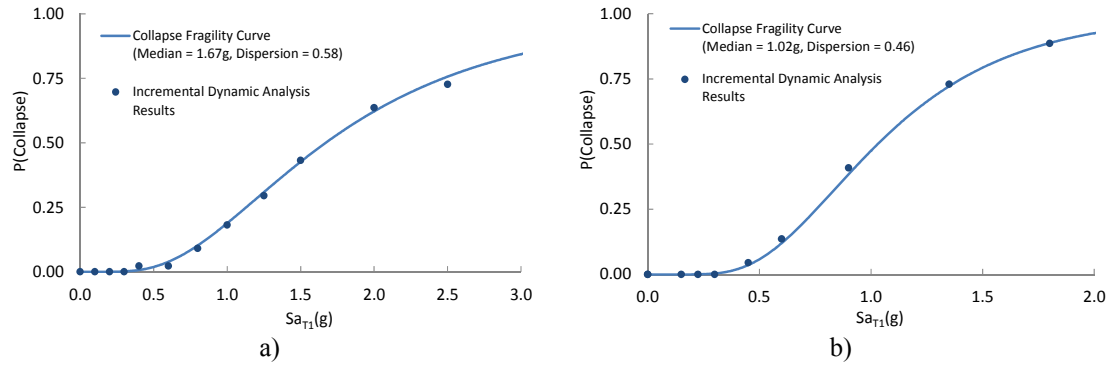
Figure 5-9: The collapse fragility curve, developed directly from incremental dynamic analysis results, for a) 6-story SCBF – Design 1 b) 16-story SCBF
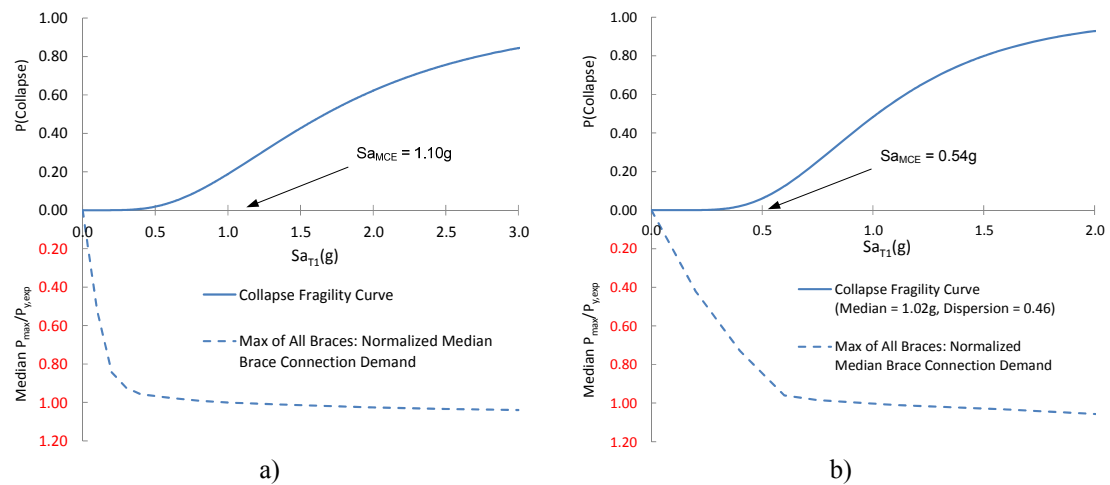
Figure 5-10: The collapse fragility curve (above) and the median of the normalized maximum brace tensile forces vs. Sa_{T1} (below) for a) 6-story SCBF – Design 1 b) 16-story SCBF
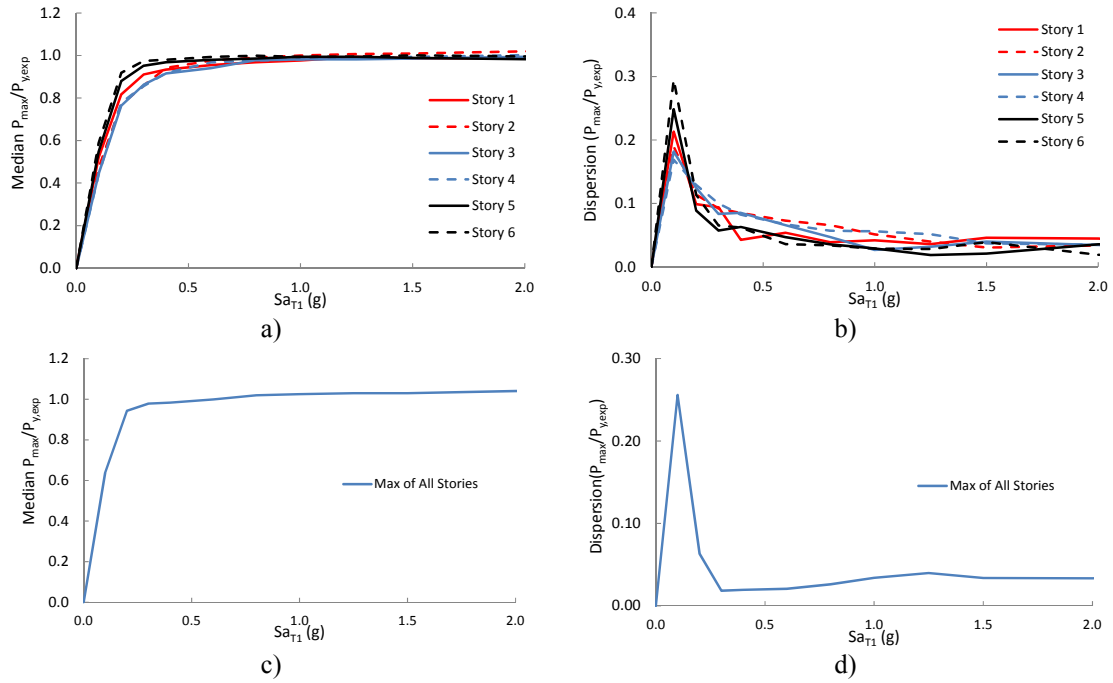
Figure 5-11: 6-Story – Design 1 incremental dynamic analysis results. a) Median of the normalized maximum brace tensile force vs. Sa_{T1}. b) COV of the normalized maximum brace tensile force vs. Sa_{T1}. c) Median of the normalized maximum brace tensile force for entire frame vs. Sa_{T1}. d) COV of the normalized maximum brace tensile force for entire frame vs. Sa_{T1}
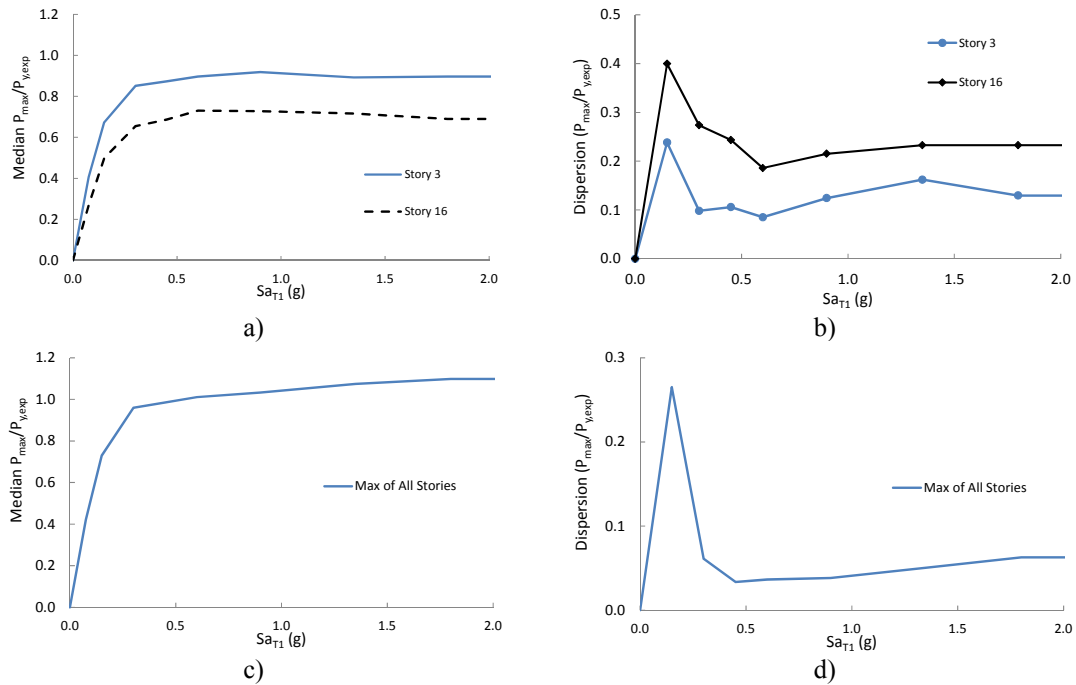
Figure 5-12: 16-story incremental dynamic analysis results. a) Median of the normalized maximum brace tensile force vs. Sa_{T1}. b) COV of the normalized maximum brace tensile force vs. Sa_{T1}. c) Median of the normalized maximum brace tensile force for entire frame vs. Sa_{T1}. d) COV of the normalized maximum brace tensile force for entire frame vs. Sa_{T1}

169
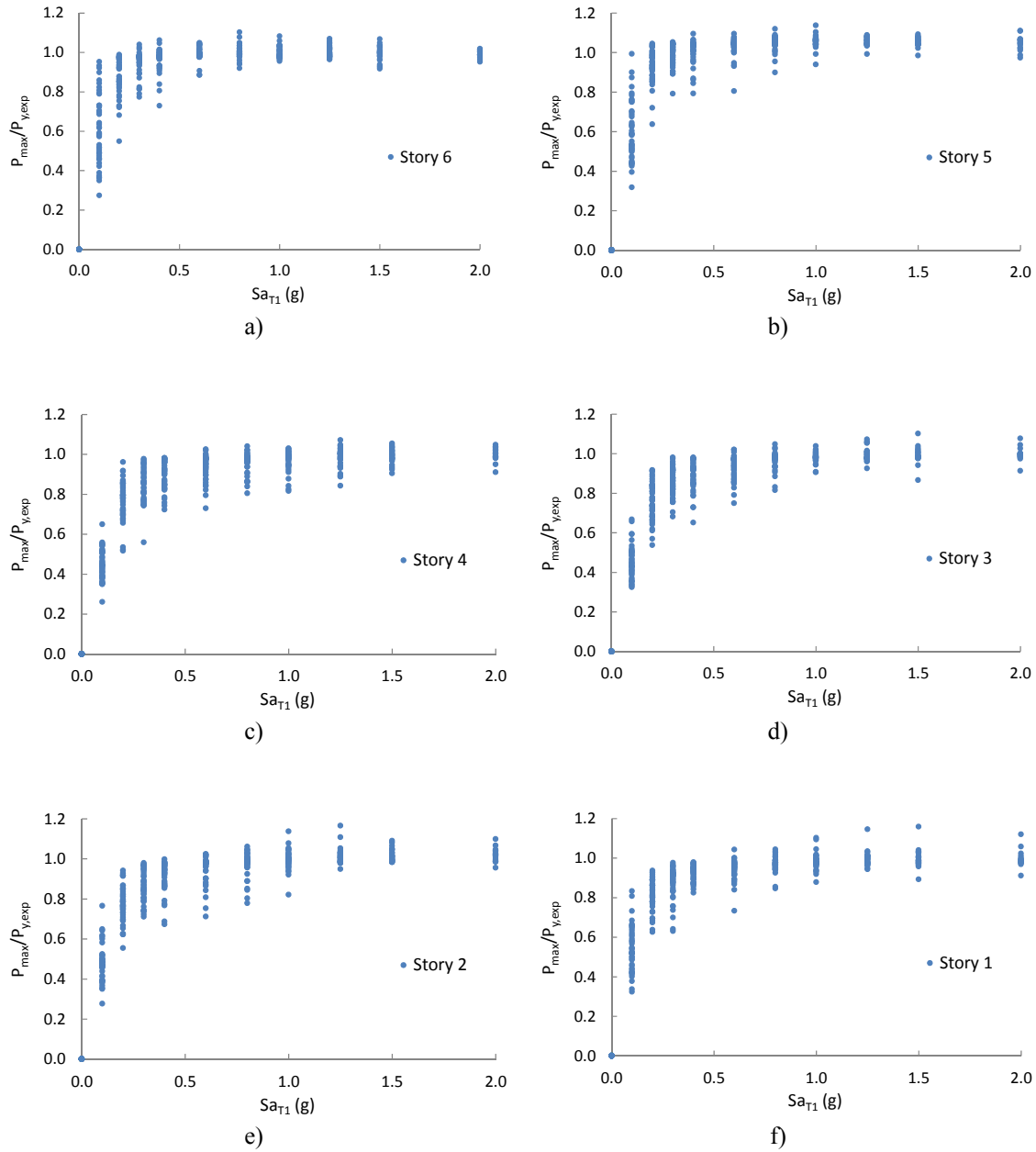
Figure 5-13: 6-story SCBF – Design 1 IDA results. Normalized maximum brace tensile force vs. Sa_{T1} for non-collapsed cases.
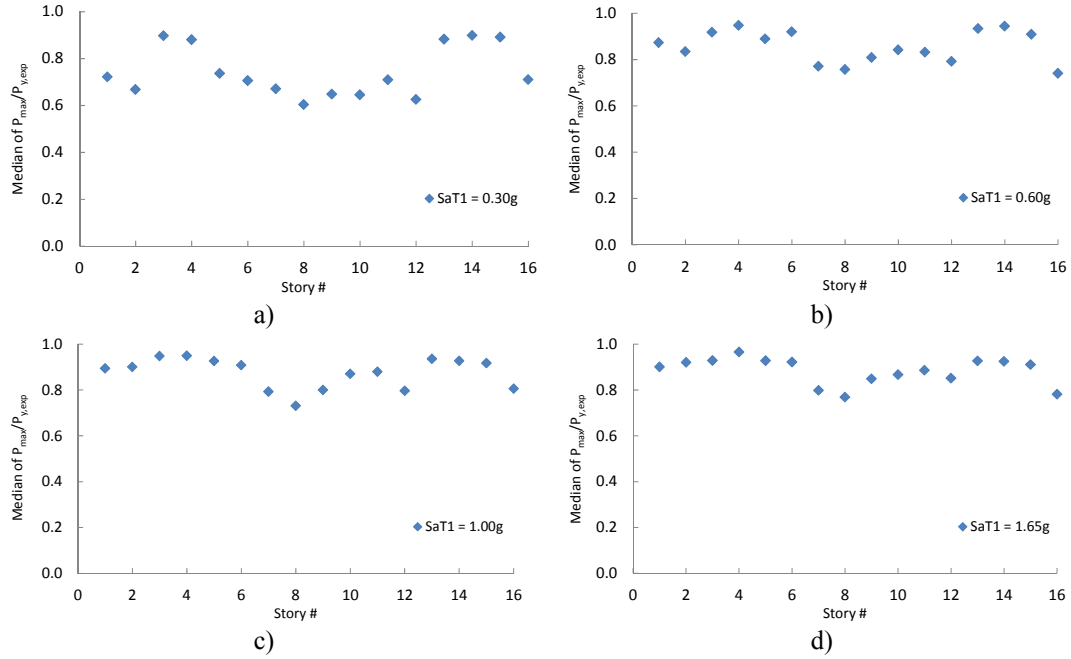
Figure 5-14: Median of the maximum brace tensile demand normalized by the expected brace strength for 16-Story SCBF
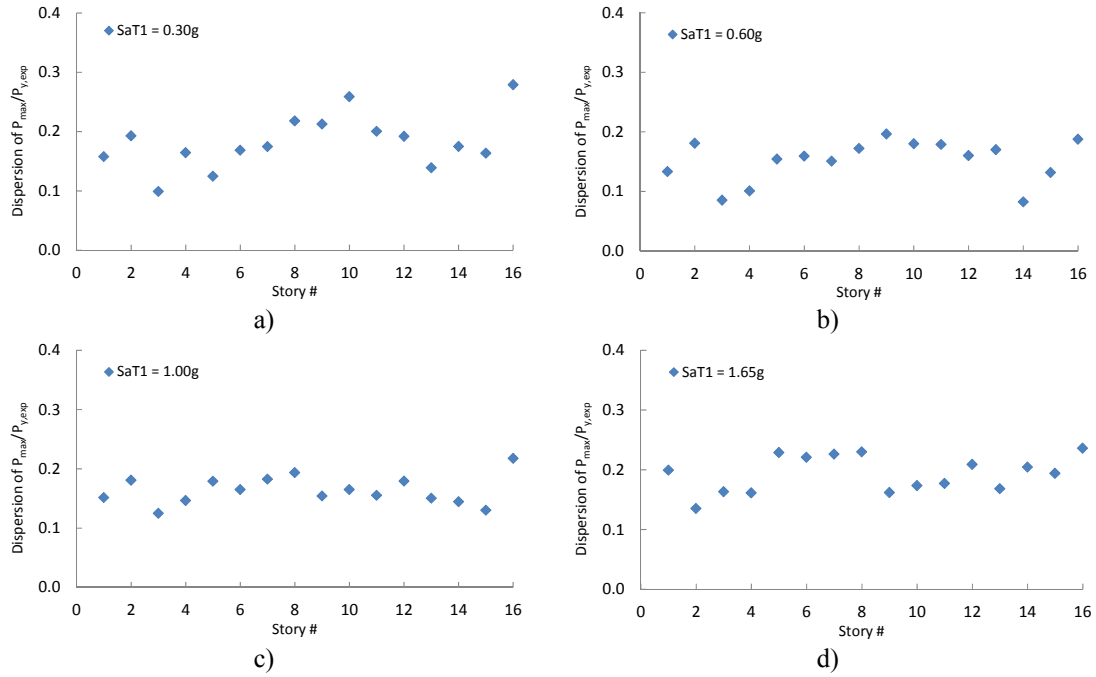
Figure 5-15: Dispersion of the maximum brace tensile demand normalized by the expected brace strength for 16-Story SCBF
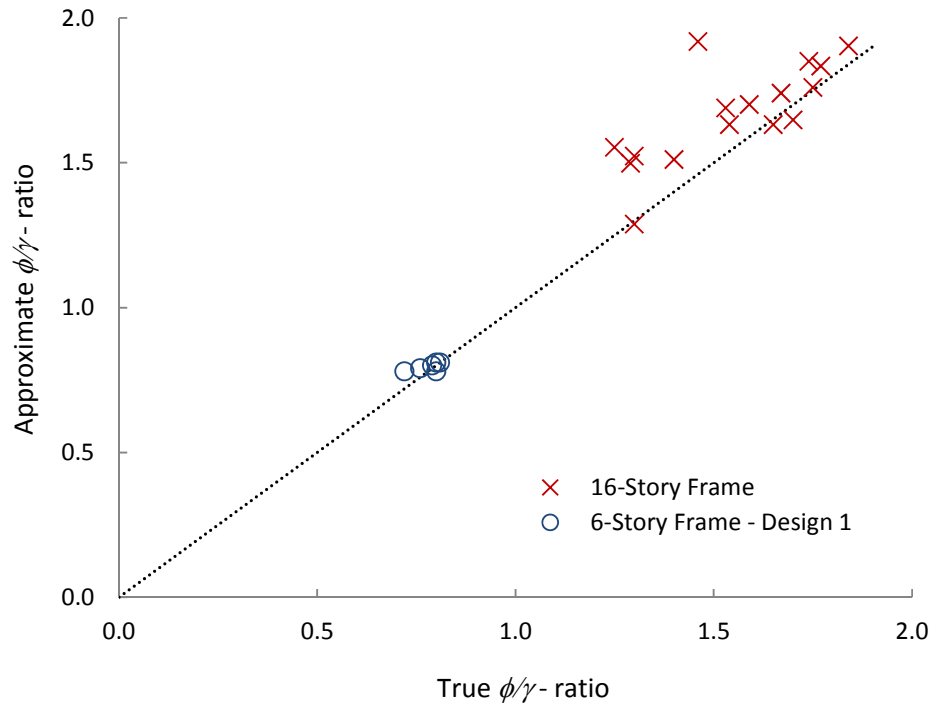
Figure 5-16: ϕ/γ-ratios calculated through simplified method vs. ϕ/γ-ratios calculated through integration of dynamic analysis results for the 6-story and the 16-story frames
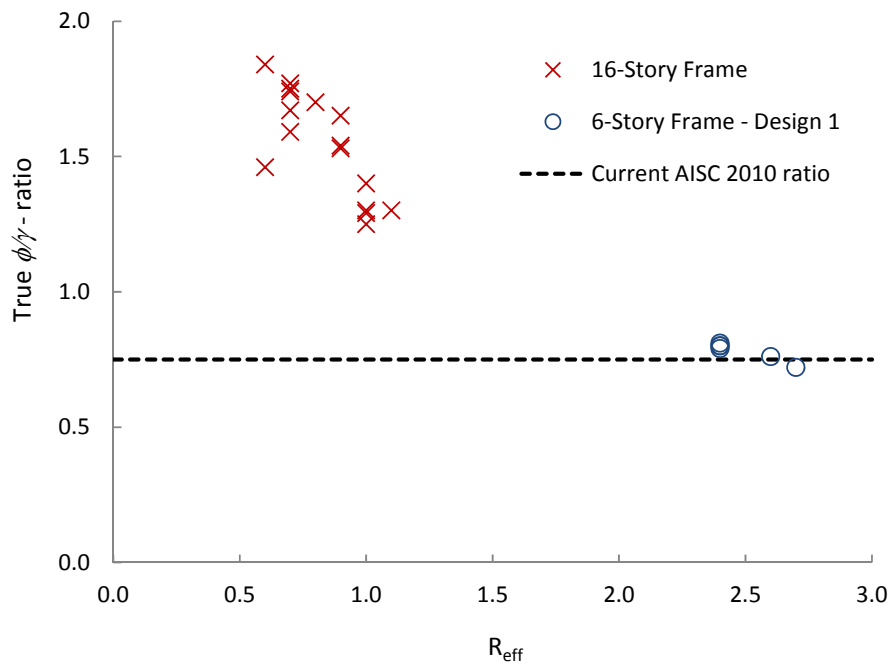
Figure 5-17: Calculated ϕ/γ-ratios vs. R_μ based on incremental dynamic analysis results for the 6-story and the 16-story frames.

172
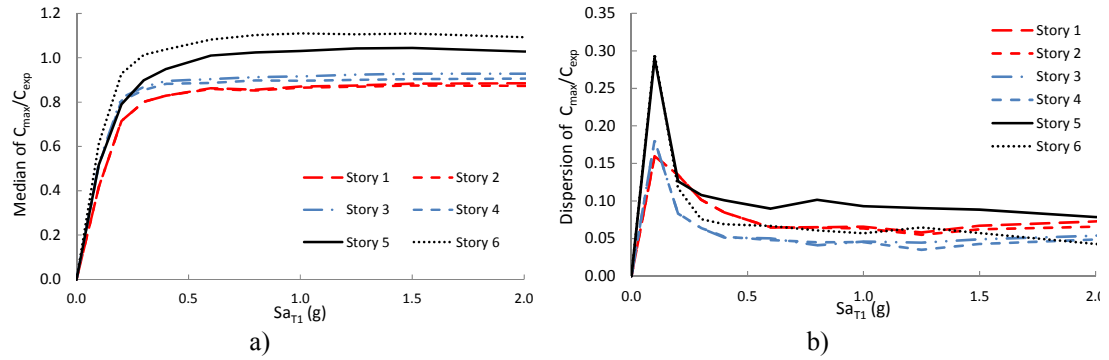
Figure 5-18: 6-story SCBF – Design 1 a) Median of column axial force demand normalized by expected demand vs. Sa_{T1}. b) Dispersion of column axial force demand normalized by expected demand vs. Sa_{T1}.
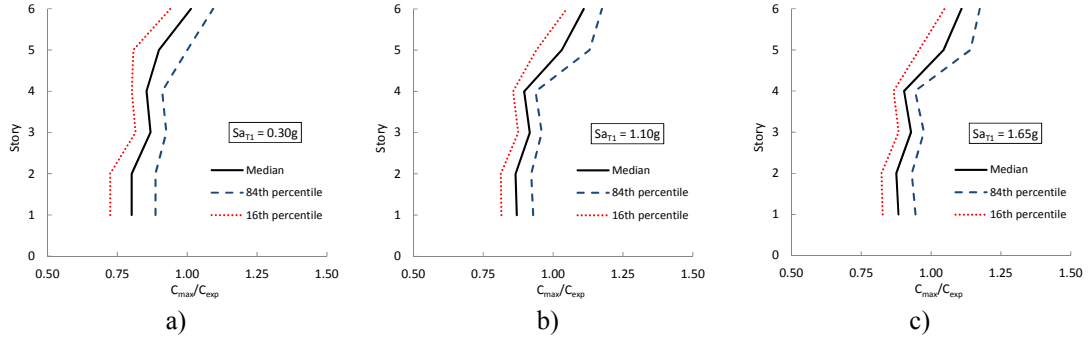
Figure 5-19: 6-story SCBF – Design 1. Seismic axial demand in columns normalized by expected demand using capacity design principles
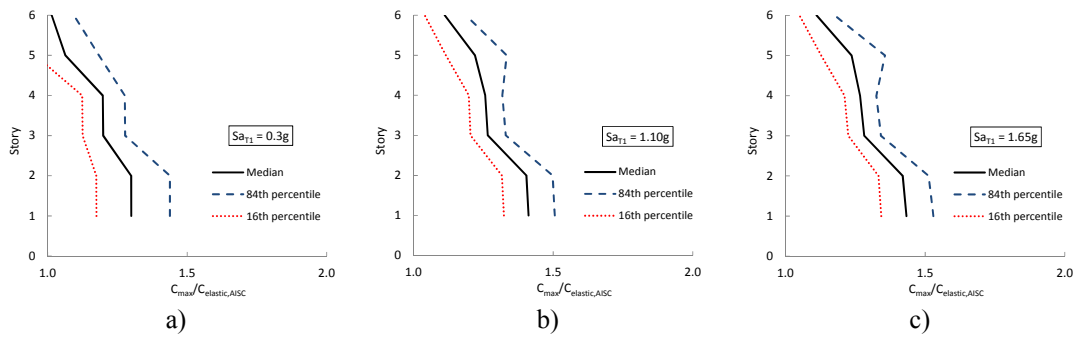
Figure 5-20: 6-story SCBF – Design 1. Seismic axial demand in columns normalized by maximum design strength as per AISC 2010 *Seismic Provisions*
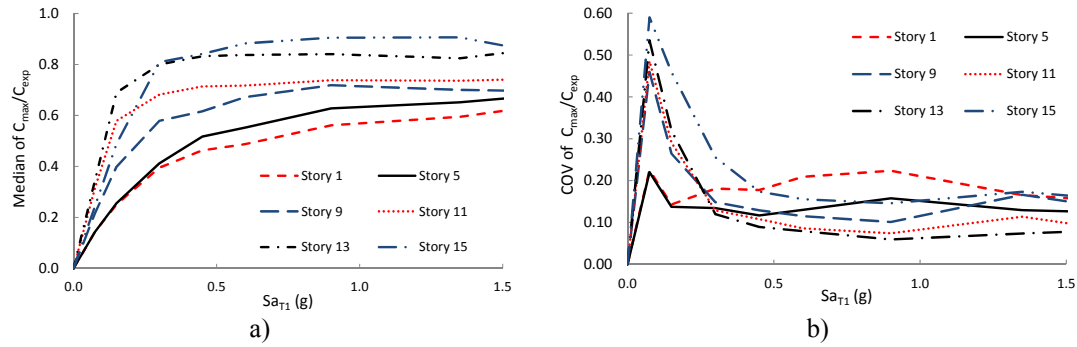
Figure 5-21: 16-story SCBF a) Median of column axial force demand normalized by expected demand vs. Sa_{T1}. b) Dispersion of column axial force demand normalized by expected demand vs. Sa_{T1}.
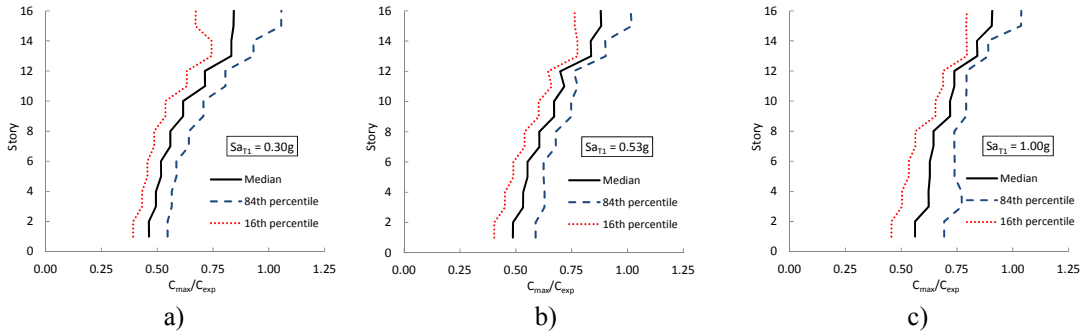
Figure 5-22: 16-story SCBF. Seismic axial demand in columns normalized by expected demand using capacity design principles
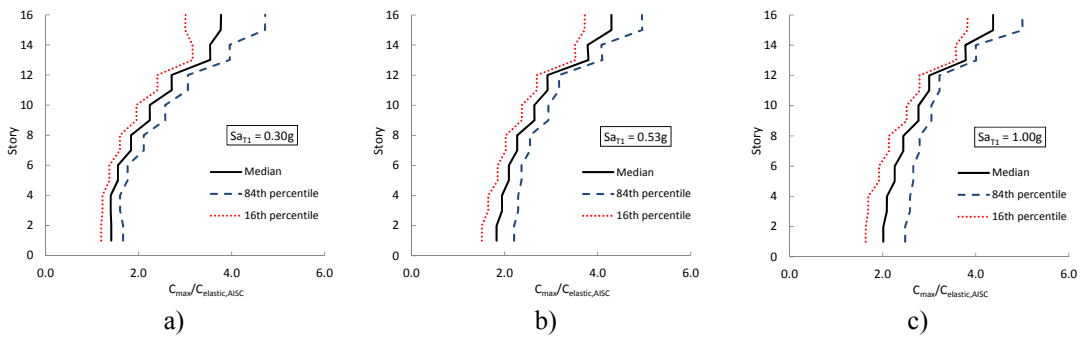
Figure 5-23: 16-story SCBF. Seismic axial demand in columns normalized by maximum design strength as per AISC 2010 *Seismic Provisions*
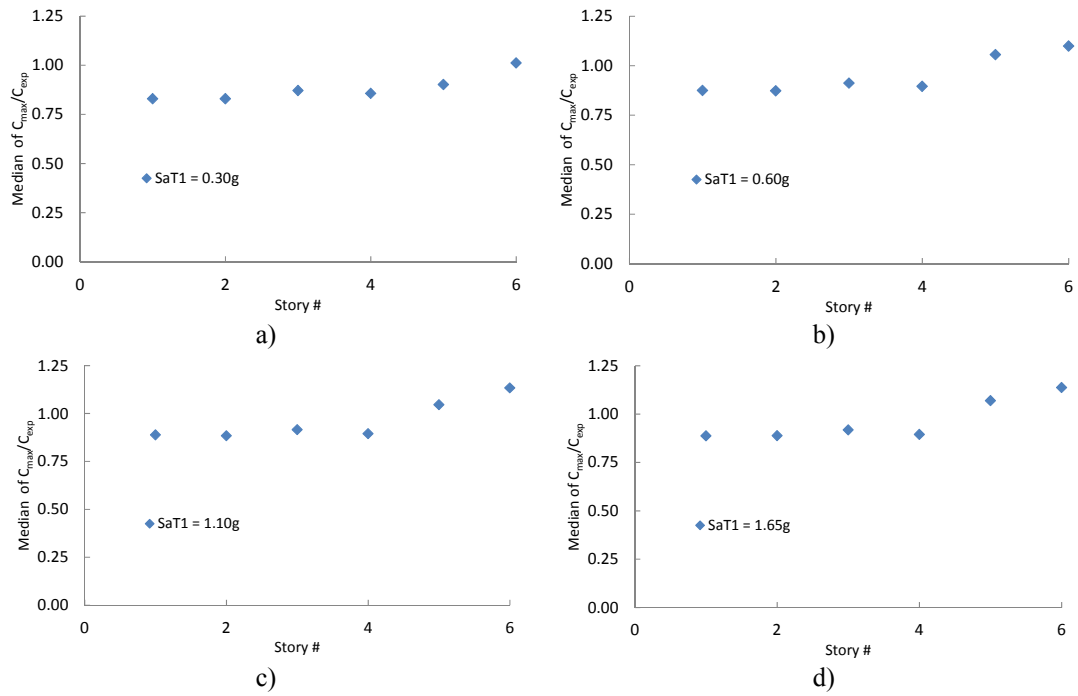
Figure 5-24: Median of the maximum column axial demand normalized by the expected column demand for 6-Story SCBF – Design 1
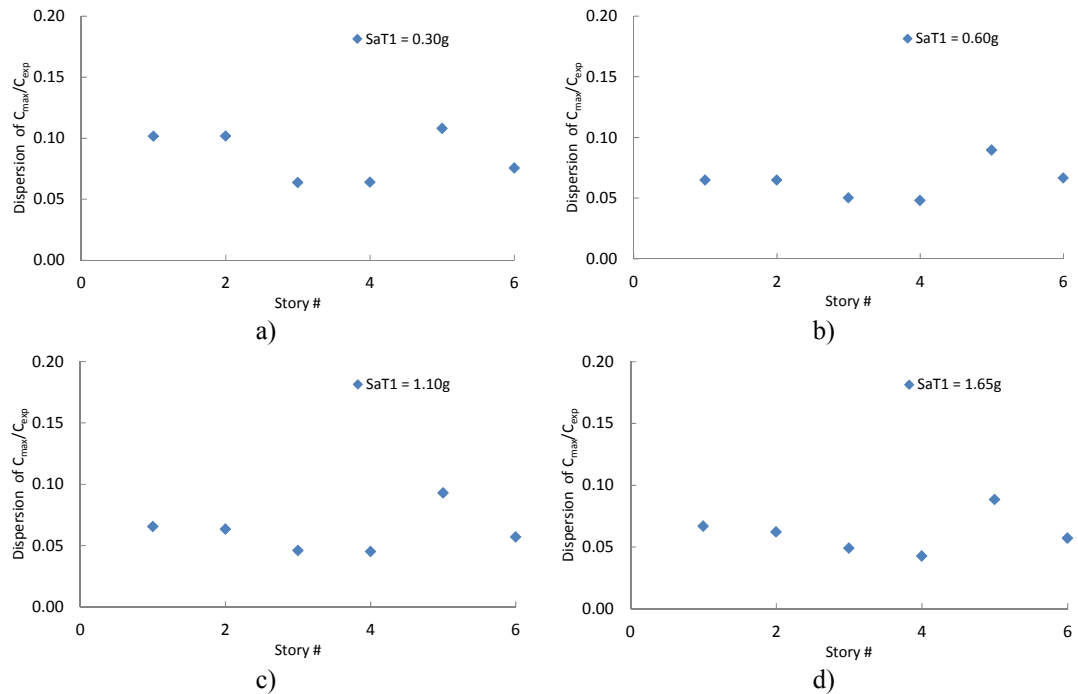
Figure 5-25: COV of the maximum column axial demand normalized by the expected column demand for 6-Story SCBF – Design 1

175
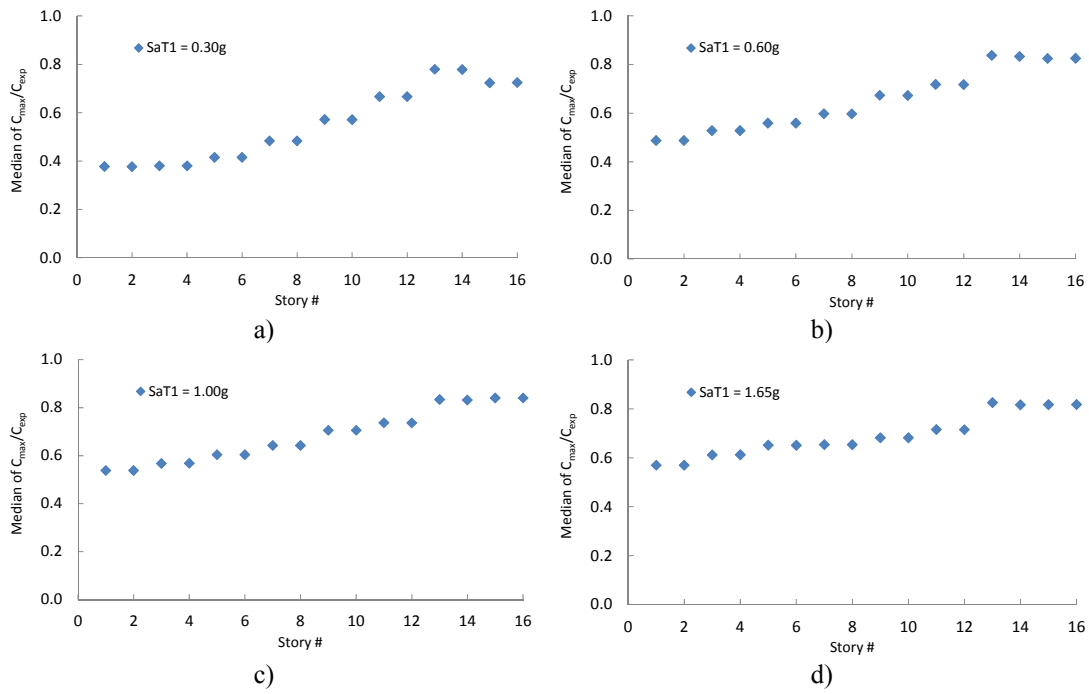
Figure 5-26: Median of the maximum column axial demand normalized by the expected column demand for 16-Story SCBF
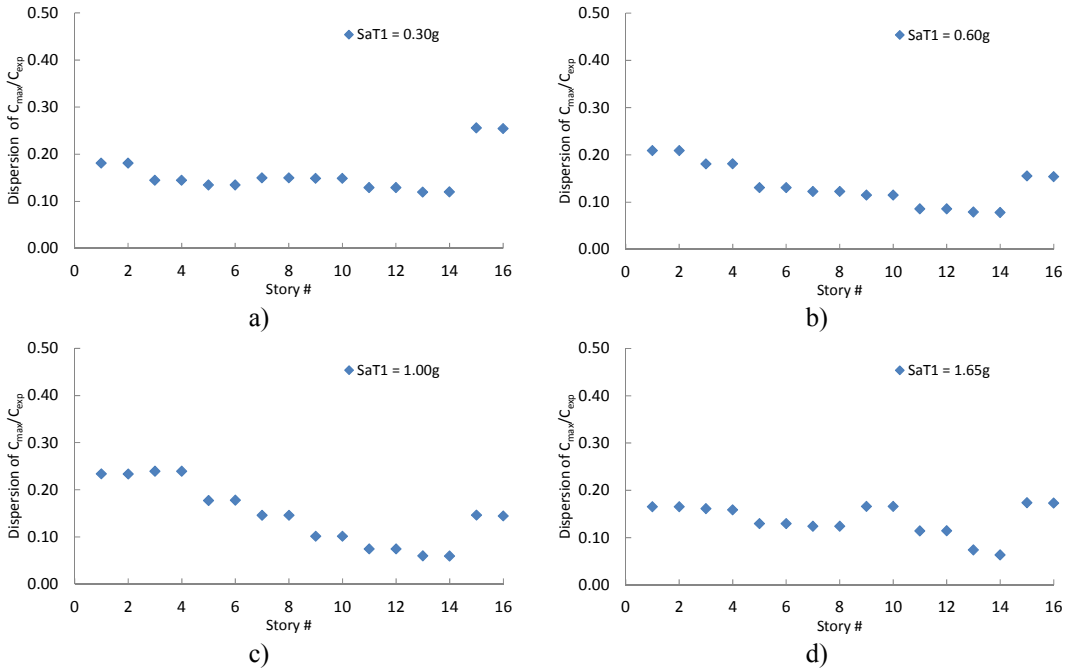
Figure 5-27: Dispersion of the maximum column axial demand normalized by the expected column demand for 16-Story SCBF

176
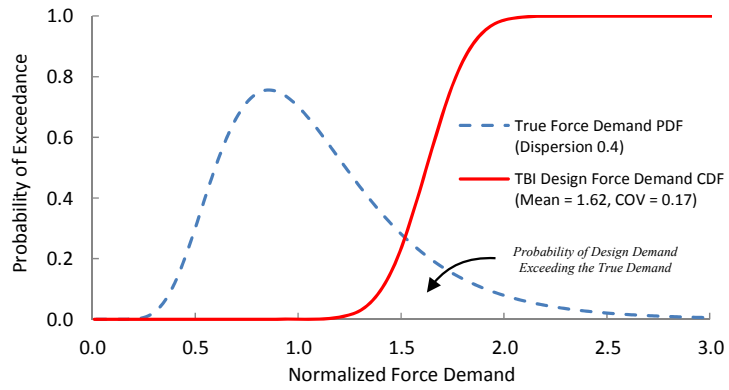
Figure 5-28: Overlap of the TBI design force demand and the true force demand

a)

b)

c)

d)

e)

f)
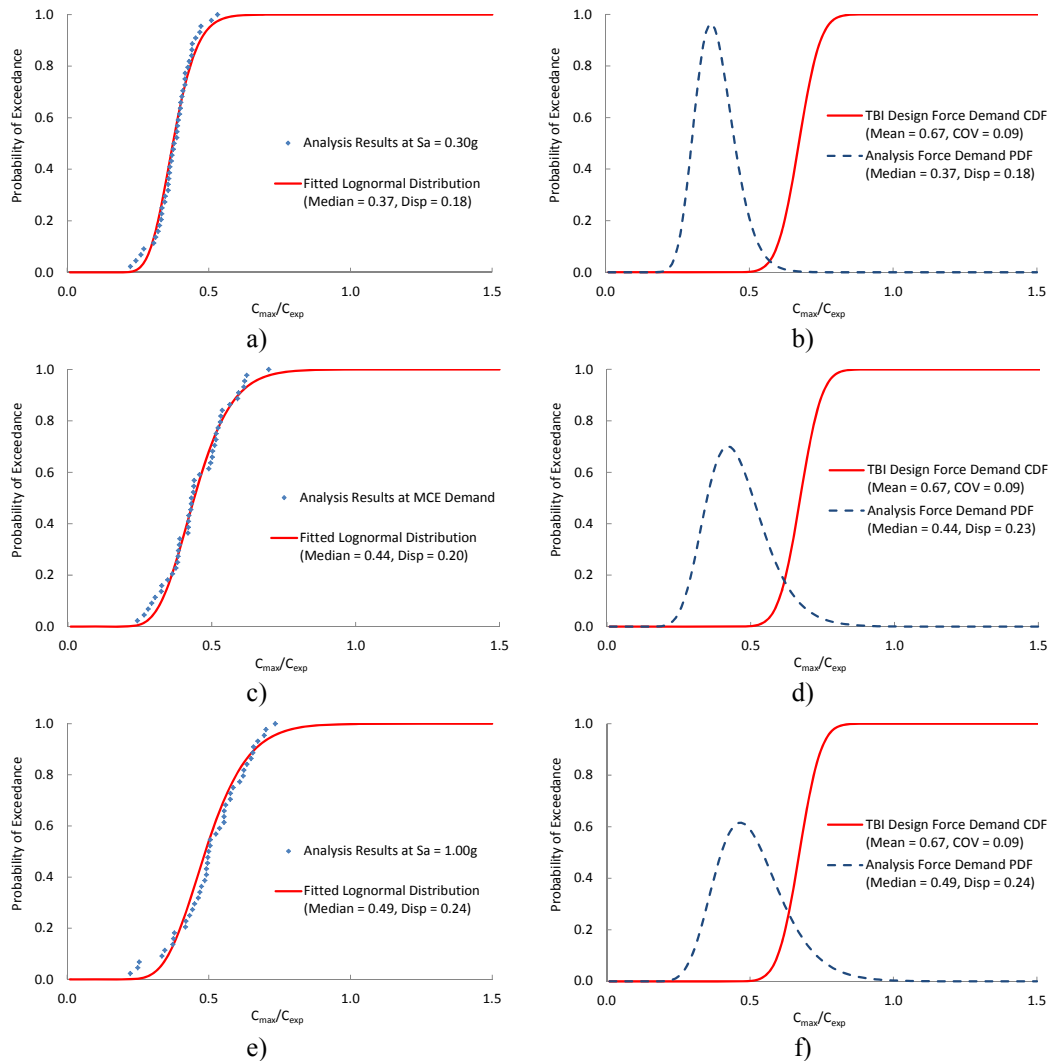
Figure 5-29: 16-story SCBF. Axial force demand and the probability of exceeding the TBI design demand in the 1st story columns at a-b) $Sa_{y,exp}$, c-d) Sa_{MCE}, e-f) Median collapse point
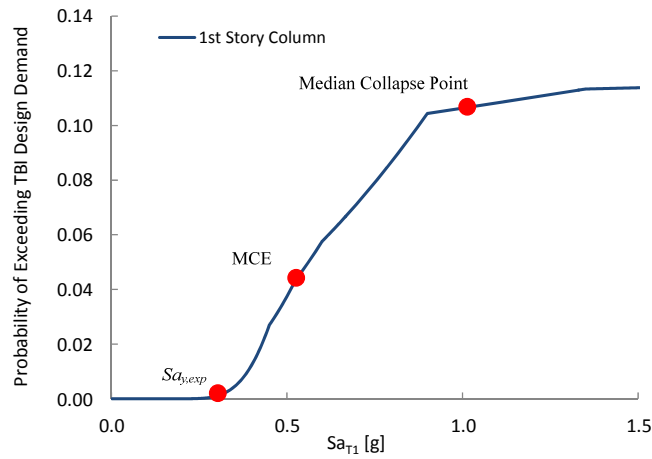
Figure 5-30: 16-story SCBF. Probability of exceeding the TBI design demand in the 1st story columns vs. Sa_{T1}

a)   b)
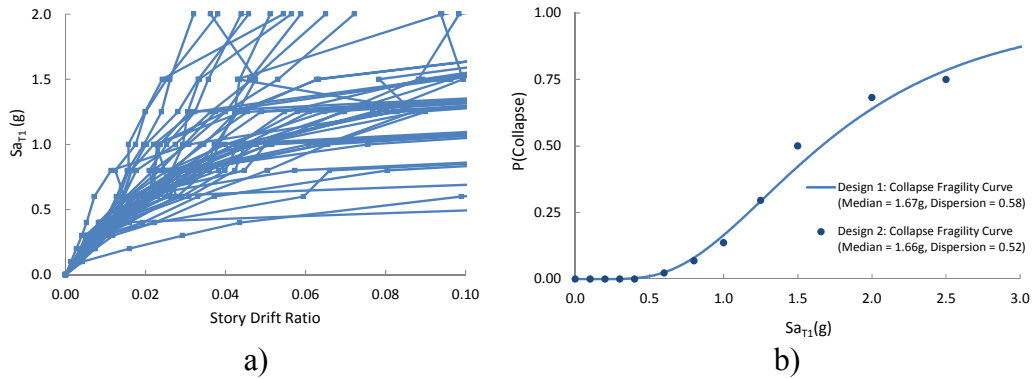
Figure 5-31: 6-story SCBF - Design 2 a) Maximum story drift ratio vs. Sa_{T1} b) The collapse fragility curve developed directly from Incremental Dynamic Analysis results

a)   b)
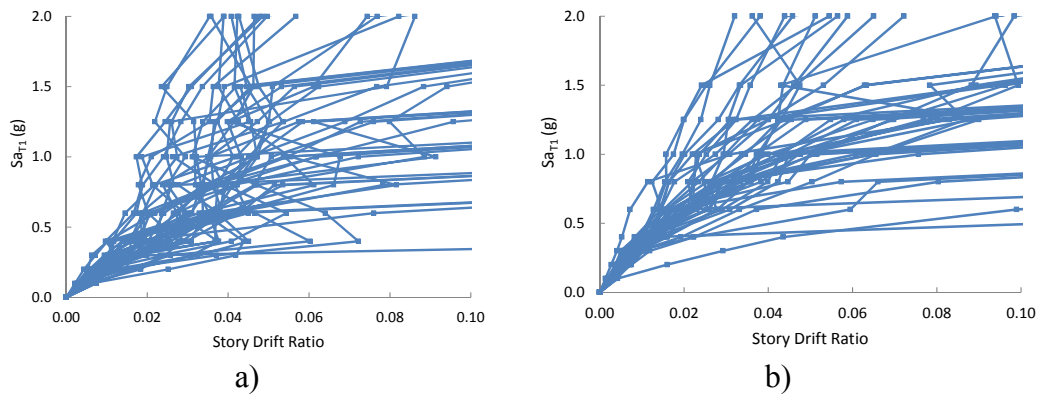
Figure 5-32: Comparison of the maximum story drift ratio vs. Sa_{T1} for the two 6-story SCBF's analyzed a) Design 1 and b) Design 2.

a)   b)
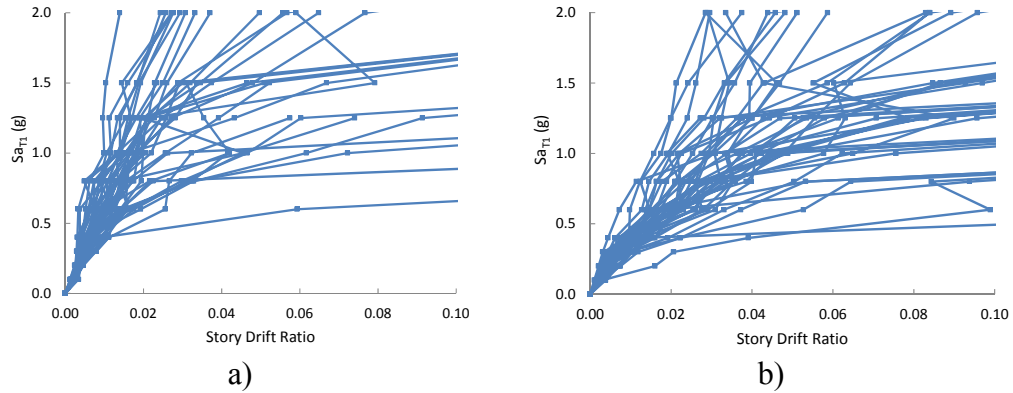
Figure 5-33: Comparison of the maximum story drift ratio in story 1 vs. Sa$_{T1}$ for the two 6-story SCBF's analyzed a) Design 1 and b) Design 2
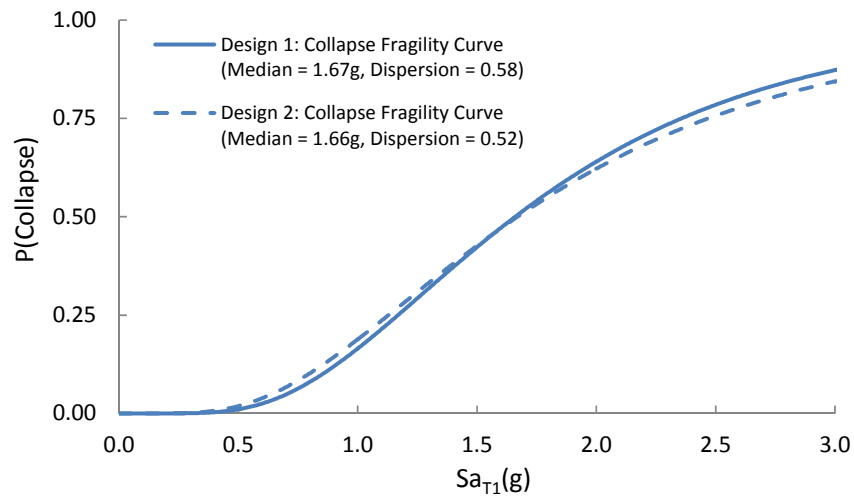
Figure 5-34: Collapse fragility curves for the two 6-Story SCBFs.
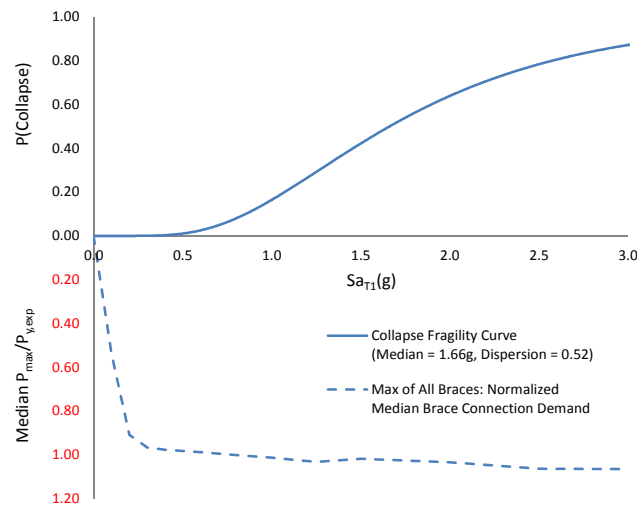
Figure 5-35: The collapse fragility curve (above) and the median of the normalized maximum brace tensile forces vs. Sa$_{T1}$ (below) for the 6-Story SCBF – Design 2
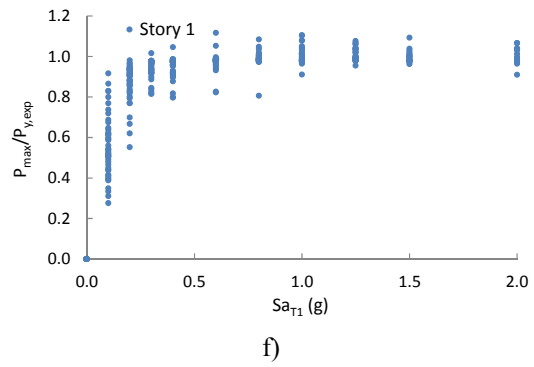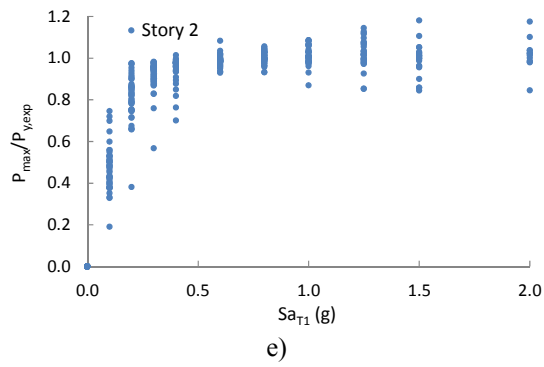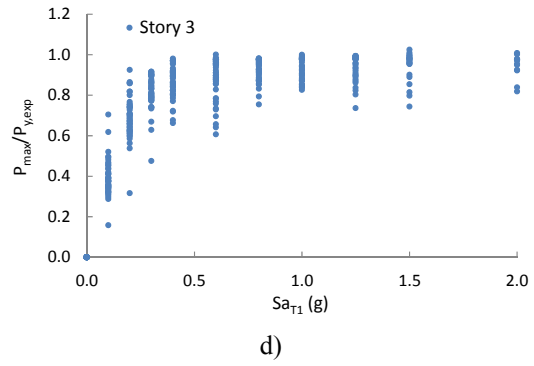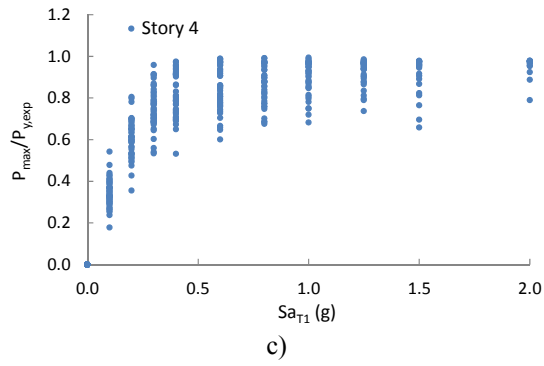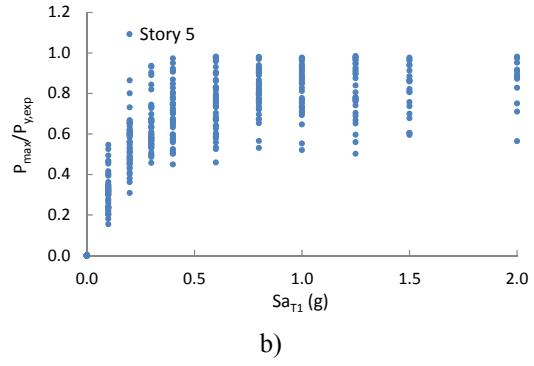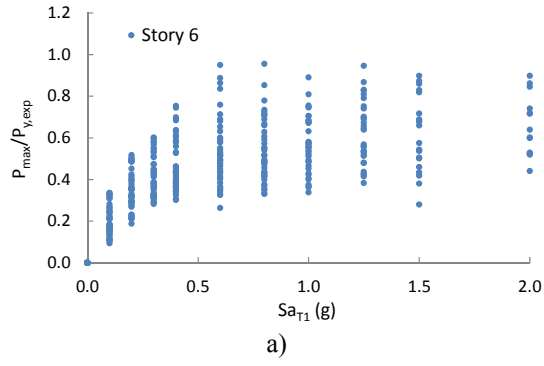
Figure 5-36: 6-story SCBF – Design 2 IDA results. Normalized maximum brace tensile force vs. Sa$_{T1}$ for non-collapsed cases.
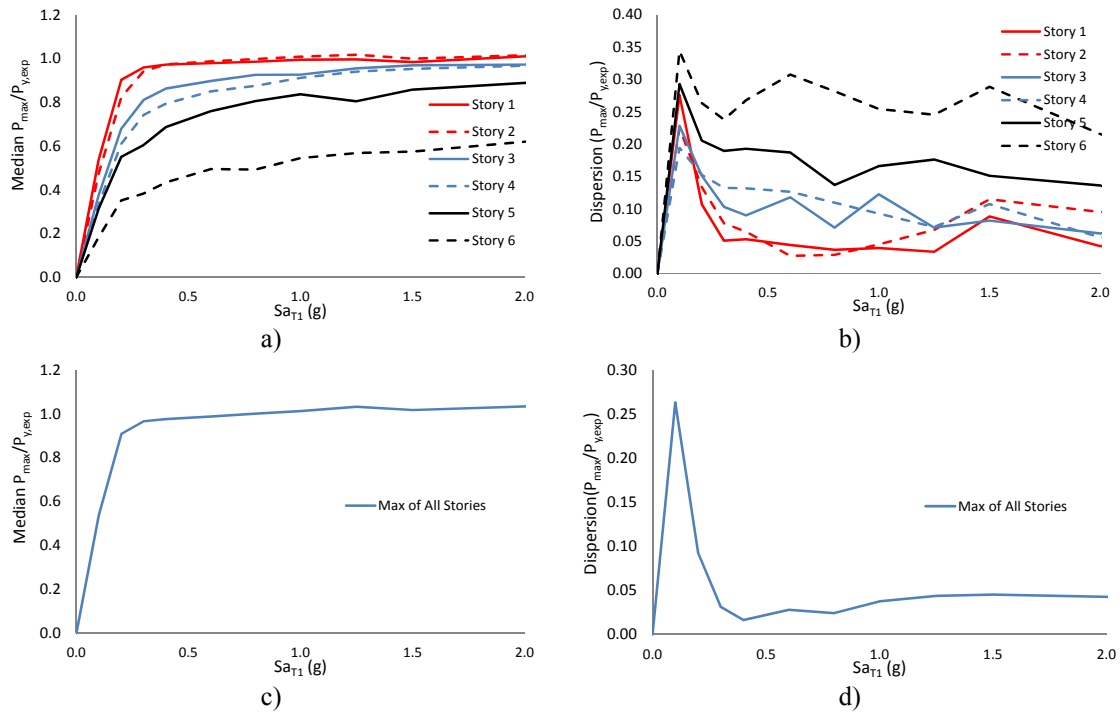
Figure 5-37: 6-Story SCBF – Design 2 Incremental Dynamic Analysis results. a) Median of the normalized maximum brace tensile force vs. Sa_{T1}**. b) COV of the normalized maximum brace tensile force vs.** Sa_{T1}**. c) Median of the normalized maximum brace tensile force for entire frame vs.** Sa_{T1}**. d) COV of the normalized maximum brace tensile force for entire frame vs.** Sa_{T1}
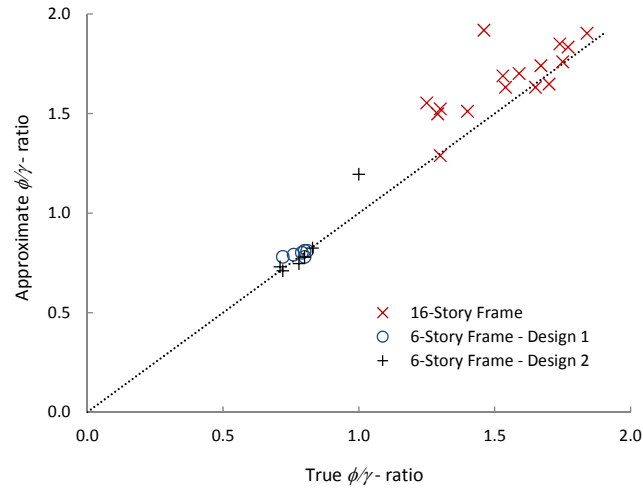
Figure 5-38: ϕ/γ-ratios calculated through simplified method vs. ϕ/γ-ratios calculated through integration of dynamic analysis results for all 3 frames
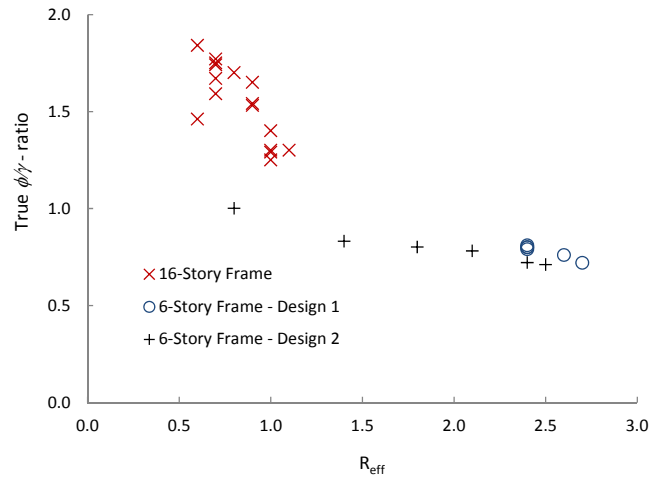
Figure 5-39: Calculated ϕ/γ-ratios vs. R_μ based on incremental dynamic analysis results for all 3 frames

a)   b)
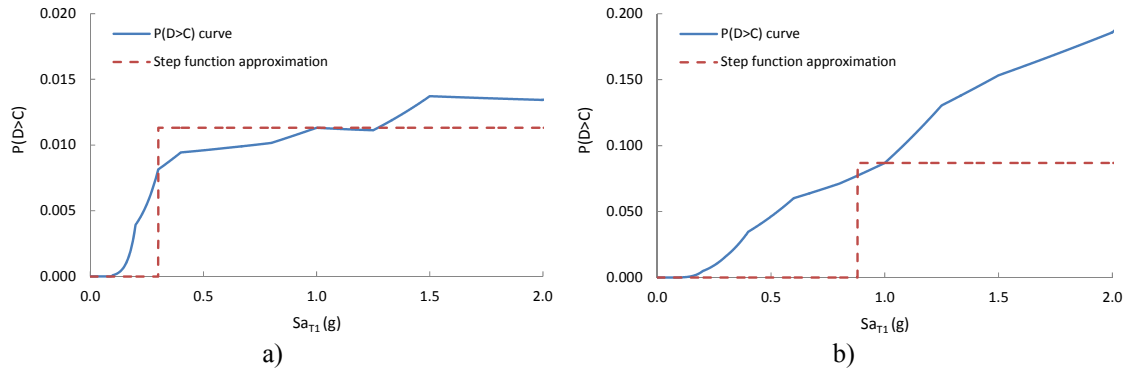
Figure 5-40: The probability of demand exceeding capacity curve and the step function approximation for a) Story 1 b) Story 6
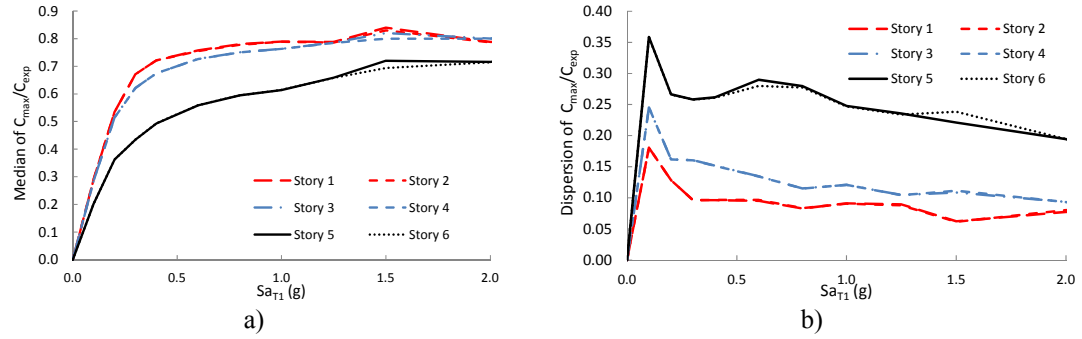
Figure 5-41: 6-story SCBF – Design 2 a) Median of column axial force demand normalized by expected demand vs. Sa_{T1}. b) COV of column axial force demand normalized by expected demand vs. Sa_{T1}.
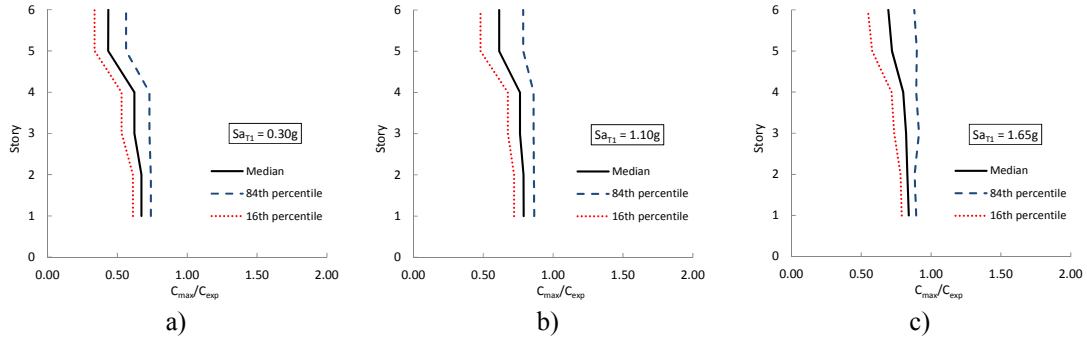
Figure 5-42: 6-story SCBF – Design 2. Seismic axial demand in columns normalized by expected demand using capacity design principles
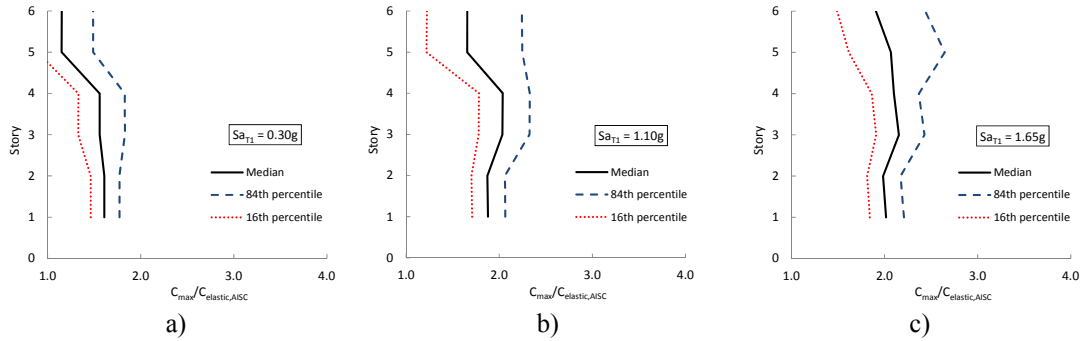
Figure 5-43: 6-story SCBF – Design 2. Seismic axial demand in columns normalized by maximum design strength as per AISC 2010 *Seismic Provisions*
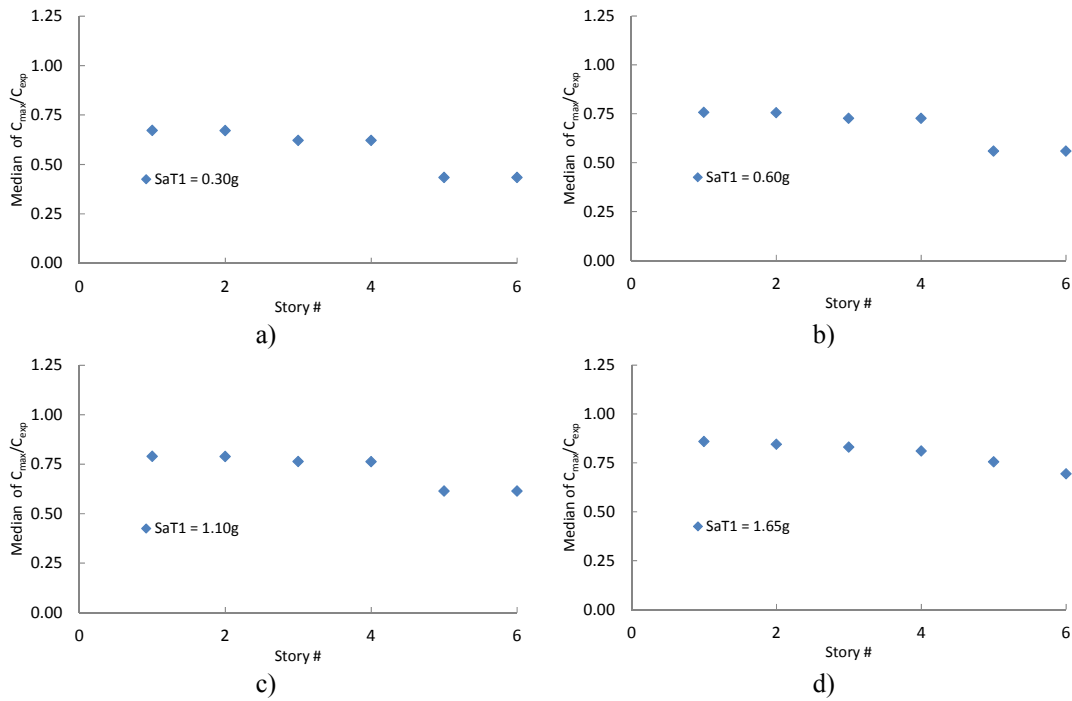
Figure 5-44: Median of the maximum column axial demand normalized by the expected column demand for 6-Story SCBF – Design 2
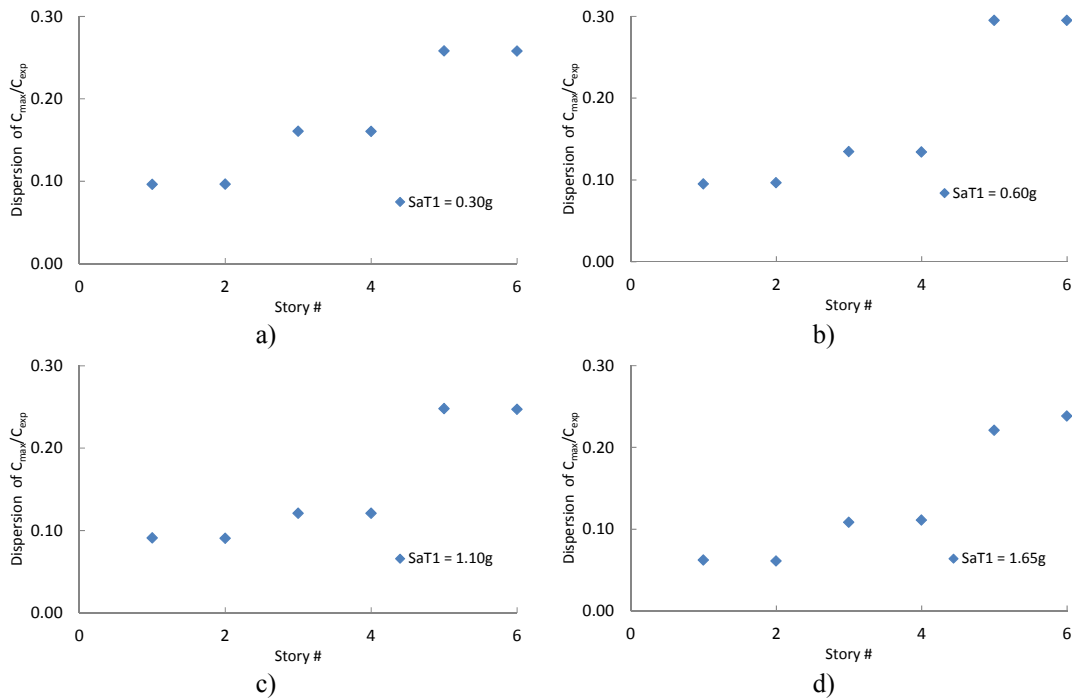
Figure 5-45: Dispersion of the maximum column axial demand normalized by the expected column demand for 6-Story SCBF – Design 2

184
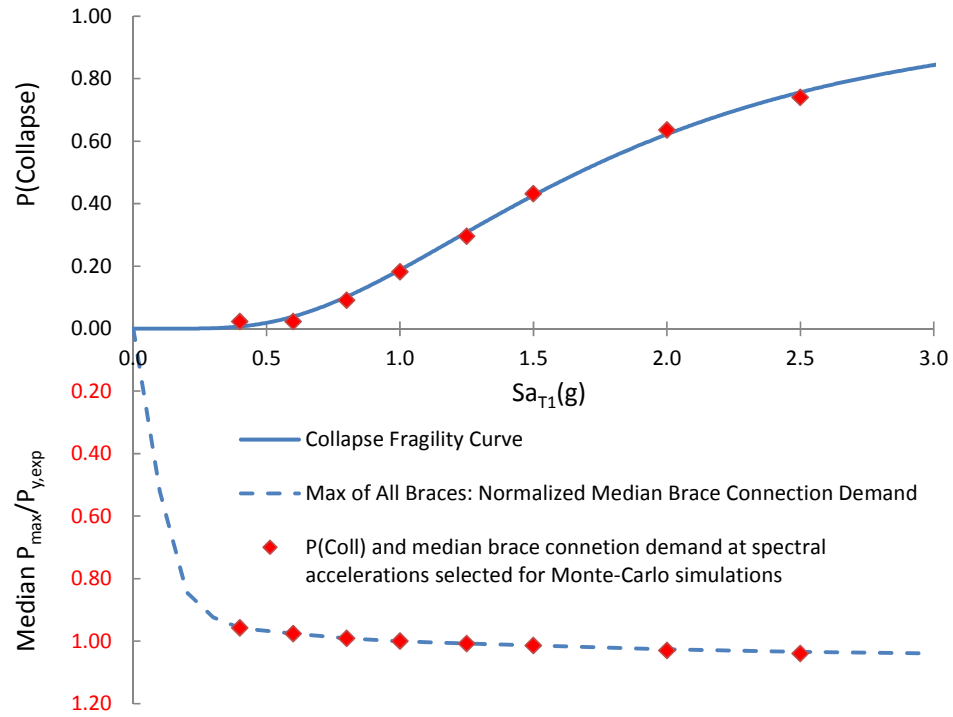
**Figure 5-46: The collapse fragility curve (above), the median of the normalized maximum brace tensile forces vs. Sa_{T1} (below) and the representative values at the Sa_{T1} where the Monte-Carlo simulations are performed.**
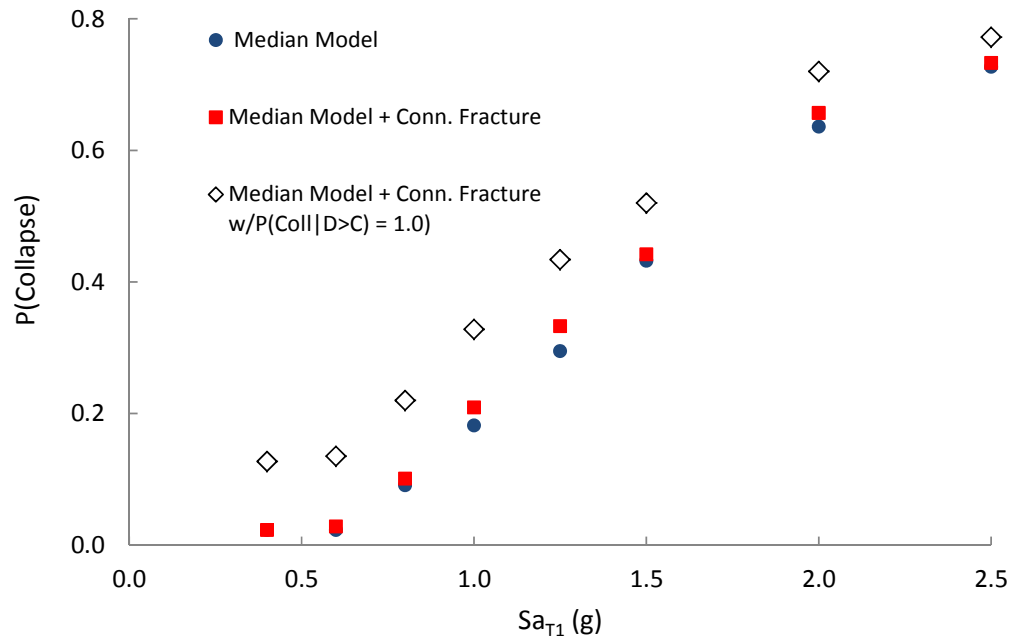
Figure 5-47: Probabilities of collapse for the 3 different models of Design 1
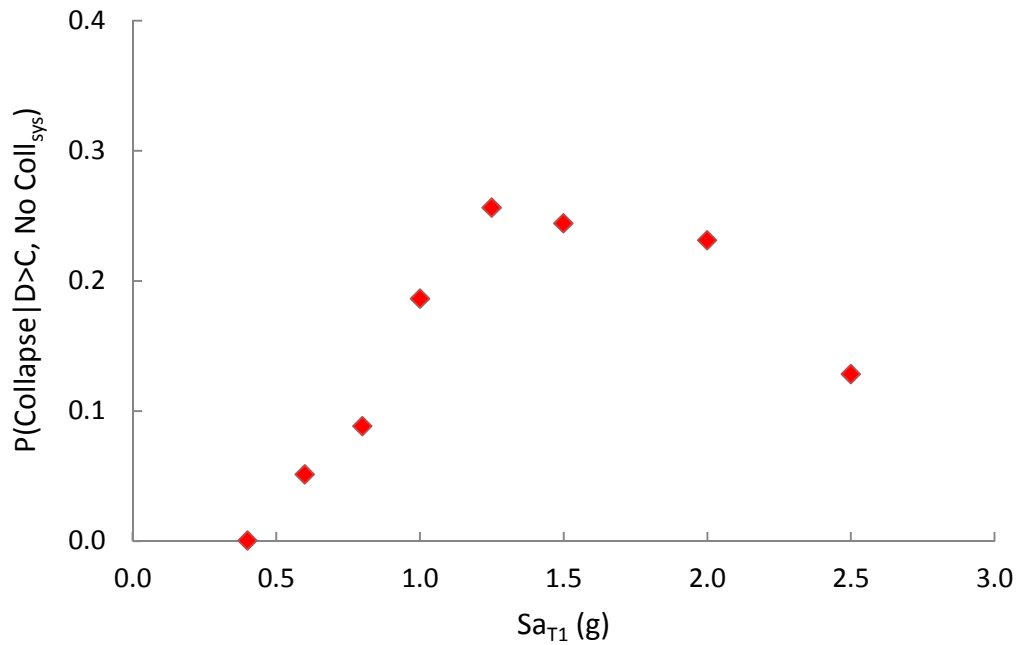
Figure 5-48: Collapse fragility curve after brace connection fracture for Design 1
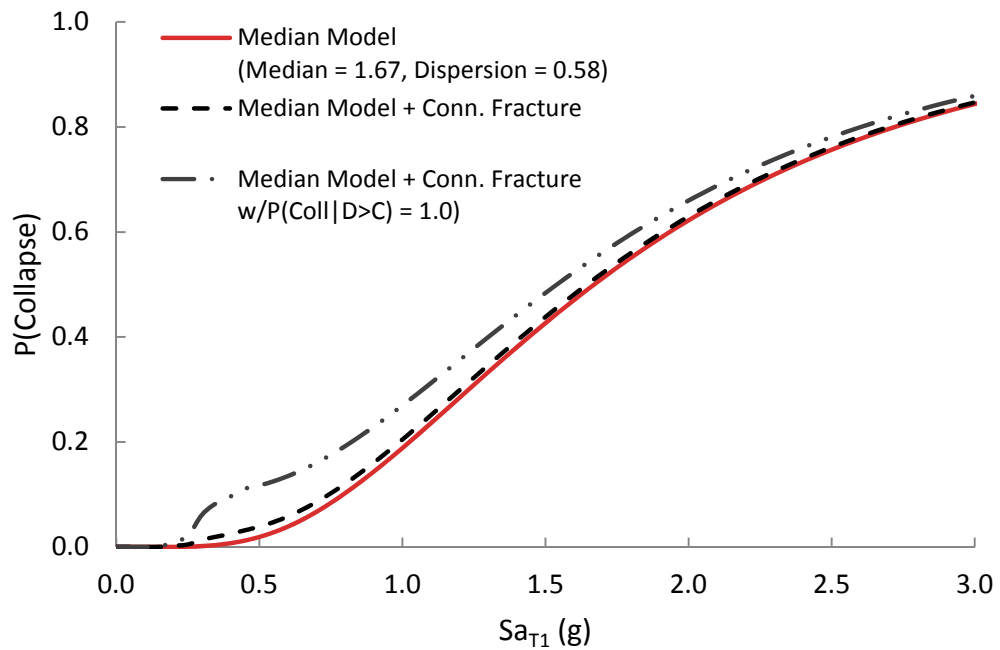
Figure 5-49: Collapse fragility curves for Design 1. Comparison between the model with and without brace connection fractures included in the analysis

Chapter 6

Application of Capacity Design Factor
Methodology

6.1 Introduction

In this chapter the proposed Capacity Design Factor methodology is summarized and then applied to selected brace connection failure modes to demonstrate its use and provide guidance on its application. Capacity design factors are calculated for the selected failure modes, based on collected statistical data on brace connection demand and capacity as well as collapse behavior and other force-demand data from the SCBF analyses in Chapters 4 and 5. In these examples, the medians and dispersions of the force demands are combined with data to characterize the statistical variation of force demands and capacities in the force-controlled connections.

The calculations of capacity design factors are carried out using two methods. First is the simplified method proposed in Chapter 3 that allows for a closed form solution of the target reliability index, $\beta_{R,Ha}$, and capacity design factors. Second is an integration method that allows for relaxing some of the assumptions required for the closed form solution in the simplified method, most notably the fixed probability of frame collapse given a component failure. The results of two methods are then compared.

6.2   Digest of Proposed Methodology

The proposed Capacity Design Factor methodology is a component reliability methodology that incorporates system reliability effects through definition of the load demands and the target reliability index. It calculates the required design strength of capacity-designed components such that the reliability is consistent between different components, systems and seismic regions. Design equations for capacity-designed components generally take on the following form:

$$\phi C_n \geq \gamma D_n \tag{6-1}$$

where D_n and C_n are the respective nominal values of demand, D, and capacity, C, as specified in design codes, and γ and ϕ are the demand and capacity factors (load and resistance factors) meant to account for the uncertainties inherent in determination of the nominal values of demand and capacity. The required design strength of capacity-designed components is set by adjusting the demand and capacity factors, γ and ϕ, until the desired reliability is achieved. When demand and capacity probability distributions are lognormal, the basic equation to calculate the ratio between capacity design factors is:

$$\frac{\gamma}{\phi} = \frac{\hat{D}_m}{D_n} \frac{C_n}{\hat{C}_m} \exp\left(\beta_{R,Ha} \sqrt{V_C^2 + V_D^2 - 2\rho V_C V_D}\right) \tag{6-2}$$

where $\hat{D}_m$ and $\hat{C}_m$, are the respective median values of the demand and capacity probability distributions, V_D and V_C their lognormal standard deviations, and ρ the correlation between demand and capacity. Equation 6-2 is based on the first-order second-moment (FOSM) reliability method, and the capacity design reliability index, $\beta_{R,Ha}$, provides a measure of probability of demand exceeding capacity of capacity-designed components. The relationship between the reliability index, $\beta_{R,Ha}$, and the probability of demand exceeding capacity is shown in Equation 6-3 where Φ^{-1} is the inverse cumulative standard normal distribution function.

$$\beta_{R,Ha} = \Phi^{-1}\left(P(D > C)\right) \tag{6-3}$$

To apply the methodology, quantification of the demand and capacity of components is required together with a target reliability index, $\beta_{R,Ha}$.

Capacity: The capacity is generally the strength limit state of capacity-designed components. To quantify the capacity, the median ($\hat{X}$) and dispersion (V) of the random variables are required, as determined from experimental test results, analysis, and/or judgment. The following is a summary of the normalized random capacity variables: material strength variable (x_1), fabrication variable (x_2) and component model variable (x_3), which calculates the ratio of expected strength capacity to the nominal strength capacity. The normalized median capacity and dispersion can be calculated using the following equations:

$$\frac{\hat{C}_m}{C_n} = \hat{X}_1 \times \hat{X}_2 \times \hat{X}_3 \tag{6-4}$$

$$V_C = \sqrt{\sum_{i=1}^{3} V_{x_i}^2} \tag{6-5}$$

Demand: For capacity-based design, the demand is based on the strength capacity of the deformation-controlled components and on the deformation demands in the structure. The calculated reliability index therefore varies based on the earthquake-induced deformation demands in the structure, which in turn can be related to the input ground motion intensity. Here, the spectral acceleration at the fundamental period of a structure is typically used to describe the ground motion intensity. The methodology establishes demands on capacity-designed components for the MCE ground motion intensity, Sa_{MCE}, but with consideration of how the demand accumulates at lower intensities. The risk of demands exceeding capacity at intensity lower than the MCE is controlled through the target reliability index. The demand associated with the MCE ground motion intensity is quantified through the median ($\hat{X}$) and dispersion (V) of the normalized random variables listed below. The values are determined from a combination of experimental tests, nonlinear structural analysis, and/or judgment. The normalized variables include: load model parameter (x_4), material strength (x_5), fabrication (x_6) and record-to-record

variable (x_7). The resulting normalized median demand and dispersion are then calculated by combining the constituent parts by the following equations:

$$\frac{\hat{D}_m}{D_n} = \hat{X}_4 \times \hat{X}_5 \times \hat{X}_6 \times \hat{X}_7 \qquad (6\text{-}6)$$

$$V_D = \sqrt{\sum_{i=4}^{7} V_{x_i}^2} \qquad (6\text{-}7)$$

When there is correlation between demand and capacity random variables, the total dispersion is calculated using the following equation,

$$\sqrt{V_C^2 + V_D^2 - 2\rho V_C V_D} = \sum_{i=1}^{7} \sum_{j=1}^{7} a_i a_j \rho_{i,j} V_{x_i} V_{x_j} \qquad (6\text{-}8)$$

where a_i is +1 if x_i is a capacity random variable and -1 if x_i is a demand random variable and $\rho_{i,j}$ is the correlation coefficient between random variable x_i and x_j.

Target $\beta_{R,Ha}$: Determining a target reliability index, $\beta_{R,Ha}$, is somewhat subjective, since judgment plays a factor in determining some of the factors involved. The methodology takes into consideration the many factors that influence the reliability of capacity-designed components and results in risk consistency between capacity-designed components. This requires both understanding of the demand in capacity-based design and approximations in assessing the impact of component failure on system reliability. A common characteristic of the demand in capacity-based design is that it increases quickly at low spectral accelerations, where the deformation-controlled components behave elastically. However, once deformation-controlled components yield, the demand increase is much more gradual with spectral acceleration, and demand is even approximately constant in many cases. The result is that the probability of demand exceeding capacity is small prior to yielding of deformation-controlled components but then increases quickly until it saturates. The spectral acceleration at which components are expected to begin yielding is referred to as $Sa_{y,exp}$. The proposed methodology makes the assumption that the probability of demand exceeding capacity versus spectral

acceleration can be represented by a step function that is zero at spectral accelerations below $Sa_{y,exp}$ and a constant non-zero value beyond $Sa_{y,exp}$. The probability of demand exceeding capacity beyond $Sa_{y,exp}$ is based on the probability at the MCE demand. Figure 6-1 illustrates the step-function approximation.

The step-function approximation allows for the closed-form solution of the reliability index shown in Equation 6-9 that results in a consistent mean annual frequency of demand exceeding capacity, $MAF(D>C)$. $Sa_{y,exp}$ can be calculated using Equation 6-10 and $MAF(Sa>Sa_{y,exp})$ is read directly from a site ground motion hazard curve. R_μ is here defined as the yield response modification factor as it relates the deformation-controlled components elastic demand to its expected yield strength.

$$\beta_{R,Ha} = \Phi^{-1}\left(\frac{MAF(D>C)}{MAF\left(Sa>Sa_{y,exp}\right)}\right) \qquad (6\text{-}9)$$

$$Sa_{y,exp} = \frac{\frac{2}{3}Sa_{MCE}}{R_\mu} \qquad (6\text{-}10)$$

Equation 6-9 allows for choosing a reliability index that results in consistent mean annual frequency of demand exceeding capacity. The challenge then becomes deciding upon the tolerable mean annual frequency. For a consistent basis, the methodology suggests relating the impact of component failure to the system reliability through Equation 6-11:

$$P(Coll|Sa) = P(Coll_{Sys}|Sa) + P(Coll_{D>C}|D>C) \times P\left(D>C|\overline{Coll}_{Sys},Sa\right) \qquad (6\text{-}11)$$

where $P(Coll\,|\,Sa)$ is the total probability of collapse given Sa and $P(Coll_{Sys}\,|\,Sa)$ is the probability of frame collapse at a given spectral acceleration, as calculated from incremental dynamic analysis procedures but excluding consideration of failures of capacity-designed components. $P(Coll_{D>C}\,|\,D>C)$ is the probability of frame collapse due to demand exceeding the capacity of capacity-designed components and $P(D>C\,|\,\overline{Coll}_{Sys},Sa)$ is the probability of demand exceeding the capacity of a

capacity-designed component. As a default value, $P(Coll_{Sys}|Sa)$ is assumed to be a lognormal collapse fragility curve with a dispersion of 0.8, and when integrated with a site ground motion hazard curve, the probability of collapse is 1.0% in 50 years. The methodology then proposes that, when the total collapse fragility curve, $P(Coll|Sa)$, is integrated with a site ground motion hazard curve, the probability of collapse does not exceed 1.1% in 50 years, or in other words that the added probability of collapse due to failure of capacity-designed components does not exceed 0.1% in 50 years.

To allow for a closed-form solution, the methodology´s simplified method proposes using a constant $P(Coll_{D>C}|D>C)$ at all spectral accelerations. However, based on the SCBF studies from Chapter 4 and Chapter 5, $P(Coll_{D>C}|D>C)$ does vary with ground motion intensity and is close to zero at low spectral accelerations. When integrated with a site ground motion hazard curve, a small difference in the probability of collapse at low spectral accelerations can cause a large difference in the calculated probability of collapse in 50 years. Consequently, use of a constant $P(Coll_{D>C}|D>C)$ curve leads to conservative results. It is therefore proposed that when a probability of collapse curve and a site ground motion hazard curve are integrated, that the $P(Coll_{D>C}|D>C)$ curve be allowed to be represented by a bi-linear curve as shown in Figure 6-2 that goes from zero to a representative value (20% in the figure) at the Sa_{MCE} and is then constant beyond Sa_{MCE}.

Figure 6-3 illustrates how sensitive the total probability of collapse in 50 years is to the value of the collapse fragility curves at the low spectral accelerations. The bottom curve is a collapse fragility curve excluding component failures while the other two curves are based on different assumptions regarding the form of $P(Coll_{D>C}|D>C)$ curve, i.e. bi-linear (integration method) or constant (simplified method). For both curves, $P(Coll_{D>C}|D>C)$ = 20% at Sa_{MCE}. At first glance, the collapse fragility curve associated with the simplified method appears to result in lower annual probability of collapse. However, at the low spectral accelerations it exceeds the probability of collapse of the fragility curve associated with the integration method and the result is that the

192

collapse risk is the same for the two collapse fragility curves when integrated with a San Francisco site (Lat = 38.0, Long = -121.7) ground motion hazard curve. As shown in Figure 6-4, the tolerable probability of demand exceeding capacity at spectral accelerations larger than $Sa_{y,exp}$ is 2.7 times larger for the integration method than for the simplified method due to the introduction of the bi-linear form of $P(Coll_{D>C} \mid D > C)$ curve. This example is for illustration purposes only. The probability of collapse for the default collapse fragility curve is 1.0% in 50 years and 3.0% in 50 years for the other two collapse fragility curves, or well above the suggested maximum value of 1.1% in 50 years.

6.3 Required Design Strength of Brace Connections

To illustrate the proposed reliability framework for establishing the required design strength of capacity-designed components, six failure modes in brace connections subjected to tensile brace forces are used, and capacity design factors recommended for those failure modes. The selected failure modes are: 1) Net section failure, 2) Block shear of welded gusset plate 3) Weld failure (SMAW) 4) Weld failure (FCAW) 5) Shear bolt failure (A325 and A490) and 6) Block shear of bolted gusset plate. Figure 6-5 shows examples of typical brace connections, e.g. bolted channel or angle, welded hollow rectangular section or pipe with net-section reinforcement and bolted and welded W-shape connected through web. Figure 6-6 illustrates typical connection details for a welded hollow rectangular section with net-section reinforcement and possible failure modes for this detail.

According to the AISC *Seismic Provisions* (AISC, 2010), the required design strength of a brace connection in SCBFs has to exceed the expected brace yield strength, $R_yF_yA_g$. The design equation for brace connections has the following form:

$$\phi C_n \geq \gamma D_n \qquad (6\text{-}12)$$

where γ- and ϕ-factors are the capacity design factors, currently equal to $\gamma = 1.00$ and $\phi = 0.75$, C_n is the nominal strength (capacity) of the brace connection as specified by the *Seismic Provisions* and D_n is:

$$D_n = R_y F_y A_g \qquad (6\text{-}13)$$

where R_y is the ratio of expected yield stress to specified minimum yield stress, F_y is the specified minimum yield stress and A_g the brace gross area.

From the methodology´s application guidelines listed in Table 3-13 in Chapter 3, the first steps are to collect statistical data on component demand and capacity. For the selected failure modes, statistical data was collected from multiple experimental test results. For capacity, the variables of interest are the material, fabrication and connection modeling variables. The median and dispersion of the connection capacities are listed in Table 6-1 along with the sources. Table 6-2 lists the median and dispersion of the brace demand based on loading protocol and deformation collected from cyclic experimental test results. The values for the record-to-record variable on the demand side are based on observations from the SCBF analyses in Chapters 4 and 5. The only failure mode where demand and capacity are assumed to be correlated is the Net-section failure of welded connections. The correlation coefficient between the demand and capacity material variables is 0.60 based on values from Liu (2003) and the correlation coefficient between the demand and capacity fabrication variables is set to 0.70 to account for the brace and brace connection in this example being the same member. With the collected statistical data, Equation 6-14 is used to calculate the capacity design factors, the γ/ϕ-ratios, suggested by the methodology.

$$\frac{\gamma}{\phi} = \frac{\hat{D}_m}{D_n} \frac{C_n}{\hat{C}_m} \exp\left(\beta_{R,Ha}\sqrt{V_C^2 + V_D^2 - 2\rho V_C V_D}\right) \qquad (6\text{-}14)$$

The reliability index, $\beta_{R,Ha}$, is based on R_μ, $P(Coll_{D>C})$ in 50 years of 0.1% for each failure mode, $P(Coll_{D>C}|D>C)$, site ground motion hazard curve, and which method is used. For this example, a San Francisco site (Lat = 38.0, Long = -121.7) and a New Madrid site (Lat = 35.2, Long = -89.9) ground motion hazard curves at T = 0.2s are used.

Brace forces associated with 4% cyclic loading are considered to represent the demand on connections at the MCE ground motion intensity and used in the reliability calculations. The methodology is based on using demands associated with the MCE demand and Table 6-2 shows that at 4% cyclic loading, the median brace forces are 8% above the yield brace forces. These results compare well with the developed median brace forces at the MCE demand from the SCBF dynamic analyses from Chapters 4 and 5 which ranged from 1% to 8% above the yield brace forces.

The results for the selected failure modes in bracing connections using the simplified method are shown in Tables 6-3 and 6-4. The results are represented as the required demand factor, γ, given a capacity factor, $\phi = 0.75$ with a 0.1% probability of collapse in 50 years due to connection failures. All the failure modes selected are tensile failure modes but the same method can easily be applied to compression or flexural failure modes. The computed γ–factors are based on the reliability of a single connection and a single failure mode and does not include the presence of multiple connections and failure modes. The inclusion of multiple connections in the reliability calculations might increase the calculated γ–factors. However, given the observed tendency of deformation demands to localize in a few stories in the SCBF analyses from Chapter 4 and Chapter 5, this effect is mitigated as other stories will in turn experience lower deformation demands and the brace connections lower force demands. Zooming in on the results when $P(Coll_{D>C}|D>C)$ is set to 20% and $R_{\mu} = 4$, the range of recommended γ-factors for the San Francisco site is from 0.84 to 0.98. Due to lower seismic hazard at the seismic design level in New Madrid compared to San Francisco, the recommended γ-factors are lower. The range of γ-factors for the same conditions in New Madrid is from 0.69 to 0.85. The target reliability index, $\beta_{R,Ha}$, is 2.7 for the San Francisco site and 2.0 for the New Madrid site.

The same calculations were also performed where $P(Coll_{D>C}|D>C)$ is not set as a constant at all spectral accelerations, but rather as a function of the spectral acceleration. For these calculations, a bi-linear function is used to represent the $P(Coll_{D>C}|D>C)$ versus spectral acceleration curve. $P(Coll_{D>C}|D>C)$ is set as zero at spectral acceleration of 0.0g and increases linearly until Sa_{MCE} and is a constant passed that point. Figure 6-2

shows the bi-linear plot and the difference between the two methods. The range of recommended γ-factors for $P(Coll_{D>C}|D>C)$ = 20% at the MCE demand is now from 0.74 to 0.88 for the San Francisco site, compared to 0.84 to 0.98, and for the New Madrid site it is 0.62 to 0.79, compared to 0.69 to 0.85. The target reliability index, $\beta_{R,Ha}$, is 2.2 for the San Francisco site and 1.6 for the New Madrid site.

The difference between the calculated γ-factors for the two methods is approximately 10% for the case analyzed. The difference is due to the performance goal being a constant increase in the probability of collapse due to connection failures. Since the integration method uses a bi-linear curve to represent the $P(Coll_{D>C}|D>C)$ versus spectral acceleration curve instead of a constant value, it decreases the impact of connection failures on the probability of collapse at the low spectral accelerations where the frequency of exceedance is high. As a consequence, since the demand and capacities at the MCE demand are the same, regardless of which method is used, this implies a higher tolerable probability of demand exceeding capacity at the MCE demand for the integration method than the simplified method.

6.4   Conclusions

To demonstrate the methodology, capacity design factors are recommended for selected failure modes in brace connections. The recommended capacity design factors are based on learnings from the SCBF analyses in Chapters 4 and 5 and collected statistical data on connection capacity distributions. The capacity design factors are calculated using both a simplified method that offers a closed-form solution as well as using a method that requires integration with site ground motion hazard curves. The sites used for the calculations are a San Francisco site and a New Madrid site and the tolerable added probability of collapse due to connection failures is 0.1% in 50 years. The probability of collapse due to connection failures is assumed to be 20% at all ground motion intensities for the simplified method while for the integration method it increases linearly from zero at 0.0g to 20% at the MCE ground motion intensity. The calculated γ-factors for San Francisco (R_μ = 4) range from 0.84 to 0.98 using the simplified method

196

and 0.74 to 0.88 using the integration method. The corresponding target reliability indices, $\beta_{R,Ha}$'s, are 2.7 and 2.2. For New Madrid ($R_\mu = 4$), the calculated γ- factors are 0.69 to 0.85 using the simplified method and 0.62 to 0.79 using the integration method with $\beta_{R,Ha}$'s of 2.2 and 1.6.

The results suggest that the requirements for the capacity design factors for brace connections in SCBF's can be relaxed from the current values of 1.00. The recommended γ-factors are 0.9 and 0.8 for the Western US and the Central and Eastern US respectively.

Table 6-1: Brace connection capacity data used in reliability analysis

Brace Connection Capacity		Material X_1	Fabrication X_2	Connection Model X_3	$X_{m,1}*X_{m,2}*X_{m,3}$ $\mathbf{sqrt(\Sigma V_{xi}^2)}$
Net Section Failure – Welded Connection[1]	$X_{m,i}$ V_{xi}	1.02 0.09	1.00 0.07	1.29 0.06	1.32 0.13
Block Shear of Welded Gusset[2]	$X_{m,i}$ V_{xi}	1.14 0.08	1.00 0.05	1.26 0.04	1.44 0.10
Weld Failure (SMAW)[3]	$X_{m,i}$ V_{xi}	1.40 0.14	1.00 0.10	1.17 0.16	1.64 0.23
Weld Failure (FCAW)[3]	$X_{m,i}$ V_{xi}	1.66 0.14	1.00 0.10	1.17 0.17	1.94 0.24
Shear Bolt Failure (A325)[4]	$X_{m,i}$ V_{xi}	1.41 0.05	1.00 0.05	1.00 0.05	1.41 0.10
Shear Bolt Failure (A490)[4]	$X_{m,i}$ V_{xi}	1.25 0.02	1.00 0.05	1.00 0.05	1.25 0.08
Block Shear of Bolted Gusset[5]	$X_{m,i}$ V_{xi}	1.14 0.08	1.00 0.05	1.19 0.05	1.36 0.11

1) Material values are based on data from Liu (2003)
   Fabrication values are based on recommendations from Ravindra and Galambos (1978)
   Connection model values are based on test results from Yang and Mahin (2005), Willibald et al. (2006), Fell et al. (2006), Cheng et al. (1998)
   Correlation between X_1 and X_4 (ρ_{14}) is 0.60 and between X_2 and X_5 (ρ_{25}) is 0.70
2) Material values are based on data from Liu (2003)
   Fabrication values are based on recommendations from Ravindra and Galambos (1978)
   Connection model values are based on results from Topkaya (2006)
3) Values are based on recommendations from Fisher et al. (1978), Ng. et al. (2002), Ng, Driver and Grondin (2004), Lesik and Kennedy (1990) and Deng (2003)
4) Values are based on recommendations from Kulak, Fisher and Struik (1987)
5) Material values are based on data from Liu (2003)
   Fabrication values are based on recommendations from Ravindra and Galambos (1978
   Connection model values are based on test results from Hardash and Bjorhovde (1984), Rabinovitch and Cheng (1993), Udagawa and Yamada (1998), Nast et al. (1999), Aalberg and Larsen (1999), Huns et al (2002) and Mullin (2005)

Table 6-2: Brace connection demand data used in reliability analysis

Brace Connection Demand[1]		Material X_1	Fabrication X_2	Load Model X_3	Record-to-Record X_7	$X_{m,4}*X_{m,5}*X_{m,6}*X_{m,7}$ sqrt(ΣV_{xi}^2)
Brace Yield	$X_{m,i}$	0.95	1.00	1.00	1.00	0.95
	V_{xi}	0.11	0.05	0.05	0.05	0.14
2% Cyclic	$X_{m,i}$	-	-	1.07	1.00	1.02
	V_{xi}	-	-	0.05	0.05	0.14
4% Cyclic	$X_{m,i}$	-	-	1.08	1.00	1.03
	V_{xi}	-	-	0.06	0.05	0.14
4% Monotonic[2]	$X_{m,i}$	-	-	1.17	1.00	1.11
	V_{xi}	-	-	0.10	0.05	0.16

1) Material values are based on data from Liu (2003)
   Fabrication values are based on recommendations from Ravindra and Galambos (1978)
   Cyclic values are based on cyclic brace tests by Fell et al. (2006), Yang and Mahin (2005), Black et al. (1981), Shaback (2001), Lehman et. al (2008), Han et al. (2007) and Elchalakani et al. (2003)
2) Monotonic load model parameter values are based on test results that show that at 4% story drift, braces have developed about 90% of their ultimate strength

Table 6-3: Recommended γ-factors based on R_μ and $P(Coll_{D>C})$ in 50 years of 0.1% for selected connection failure modes in SCBF's located in San Francisco. $\phi = 0.75$

Failure Modes	$R_\mu = 1$ $P(Coll_{D>C}\|D>C)$			$R_\mu = 2$ $P(Coll_{D>C}\|D>C)$			$R_\mu = 4$ $P(Coll_{D>C}\|D>C)$		
	40%	20%	10%	40%	20%	10%	40%	20%	10%
Net Section Failure - Welded	0.75	0.71	0.67	0.83	0.80	0.77	0.88	**0.86**	0.83
Block Shear of Welded Gusset	0.73	0.69	0.64	0.82	0.79	0.75	0.89	**0.86**	0.82
Weld Failure (SMAW)	0.76	0.69	0.62	0.92	0.85	0.79	1.04	**0.98**	0.91
Weld Failure (FCAW)	0.65	0.59	0.52	0.79	0.73	0.67	0.89	**0.84**	0.78
Shear Bolt Failure (A325)	0.73	0.69	0.64	0.82	0.79	0.75	0.89	**0.85**	0.82
Shear Bolt Failure (A490)	0.82	0.77	0.72	0.92	0.88	0.84	0.98	**0.95**	0.91
Block Shear of Bolted Gusset	0.78	0.73	0.68	0.88	0.84	0.79	0.95	**0.91**	0.87

Table 6-4: Recommended γ-factors based on R_μ and $P(Coll_{D>C})$ in 50 years of 0.1% for selected connection failure modes in SCBF's located in New Madrid. $\phi = 0.75$

Failure Modes	$R_\mu = 1$ $P(Coll_{D>C}\|D>C)$			$R_\mu = 2$ $P(Coll_{D>C}\|D>C)$			$R_\mu = 4$ $P(Coll_{D>C}\|D>C)$		
	40%	20%	10%	40%	20%	10%	40%	20%	10%
Net Section Failure - Welded	0.74	0.71	0.66	0.78	0.74	0.71	0.81	**0.77**	0.74
Block Shear of Welded Gusset	0.72	0.68	0.63	0.76	0.72	0.68	0.80	**0.76**	0.72
Weld Failure (SMAW)	0.75	0.68	0.60	0.81	0.75	0.68	0.87	**0.80**	0.74
Weld Failure (FCAW)	0.64	0.57	0.51	0.69	0.64	0.58	0.74	**0.69**	0.63
Shear Bolt Failure (A325)	0.72	0.68	0.63	0.76	0.72	0.68	0.79	**0.76**	0.72
Shear Bolt Failure (A490)	0.81	0.76	0.71	0.85	0.81	0.76	0.89	**0.85**	0.80
Block Shear of Bolted Gusset	0.77	0.72	0.67	0.81	0.77	0.72	0.85	**0.81**	0.76

Table 6-5: Recommended γ-factors based on R_μ and $P(Coll_{D>C})$ in 50 years of 0.1% for selected connection failure modes in SCBF's located in San Francisco. $\phi = 0.75$

Failure Modes	$R_\mu = 1$ $P(Coll_{D>C}\|D>C,MCE)$			$R_\mu = 2$ $P(Coll_{D>C}\|D>C,MCE)$			$R_\mu = 4$ $P(Coll_{D>C}\|D>C,MCE)$		
	40%	20%	10%	40%	20%	10%	40%	20%	10%
Net Section Failure - Welded	0.74	0.70	0.66	0.80	0.77	0.73	0.83	**0.80**	0.77
Block Shear of Welded Gusset	0.71	0.67	0.62	0.79	0.75	0.71	0.83	**0.79**	0.75
Weld Failure (SMAW)	0.73	0.66	0.59	0.85	0.79	0.72	0.93	**0.87**	0.80
Weld Failure (FCAW)	0.62	0.56	0.50	0.73	0.67	0.61	0.80	**0.74**	0.68
Shear Bolt Failure (A325)	0.72	0.67	0.62	0.79	0.75	0.71	0.83	**0.79**	0.76
Shear Bolt Failure (A490)	0.80	0.75	0.70	0.88	0.84	0.79	0.92	**0.88**	0.84
Block Shear of Bolted Gusset	0.76	0.71	0.65	0.84	0.79	0.75	0.88	**0.84**	0.80

Table 6-6: Recommended γ-factors based on R_μ and $P(Coll_{D>C})$ in 50 years of 0.1% for selected connection failure modes in SCBF's located in New Madrid. $\phi = 0.75$

Failure Modes	$R_\mu = 1$ $P(Coll_{D>C}\|D>C,MCE)$			$R_\mu = 2$ $P(Coll_{D>C}\|D>C,MCE)$			$R_\mu = 4$ $P(Coll_{D>C}\|D>C,MCE)$		
	40%	20%	10%	40%	20%	10%	40%	20%	10%
Net Section Failure - Welded	0.73	0.69	0.64	0.75	0.72	0.68	0.77	**0.73**	0.69
Block Shear of Welded Gusset	0.70	0.66	0.60	0.73	0.69	0.64	0.75	**0.71**	0.66
Weld Failure (SMAW)	0.72	0.64	0.56	0.76	0.70	0.62	0.79	**0.72**	0.65
Weld Failure (FCAW)	0.61	0.55	0.48	0.65	0.59	0.53	0.67	**0.62**	0.55
Shear Bolt Failure (A325)	0.71	0.66	0.61	0.73	0.69	0.65	0.75	**0.71**	0.67
Shear Bolt Failure (A490)	0.79	0.74	0.69	0.82	0.78	0.73	0.84	**0.79**	0.75
Block Shear of Bolted Gusset	0.75	0.70	0.64	0.78	0.73	0.68	0.80	**0.75**	0.70
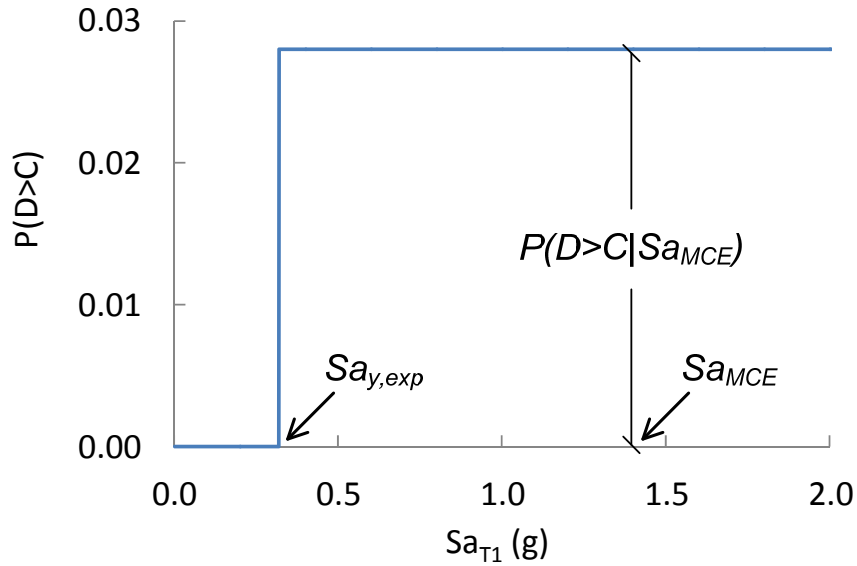
Figure 6-1: Probability of imposed demand on a component exceeding its capacity is approximated by a step function whose height depends on the calculated probability at Sa_{MCE}.
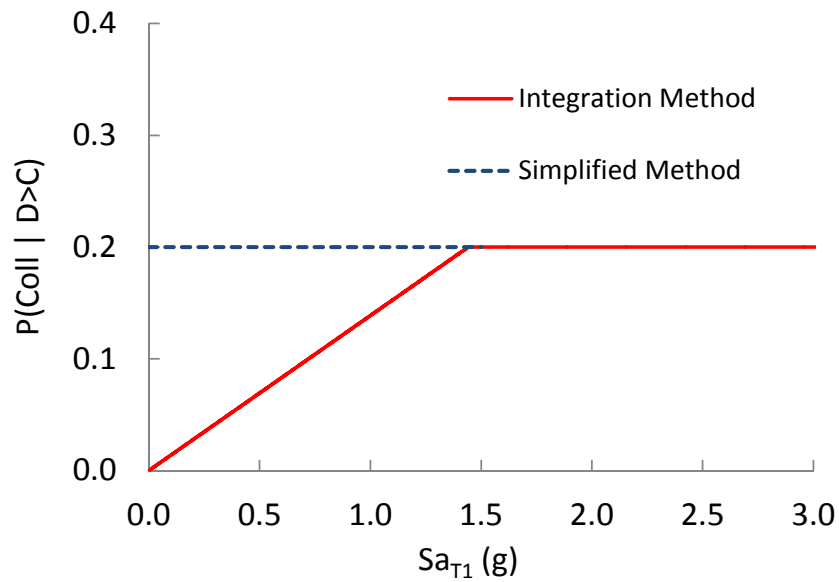
Figure 6-2: The difference between the probability of collapse given component failure between the integration method and the simplified method
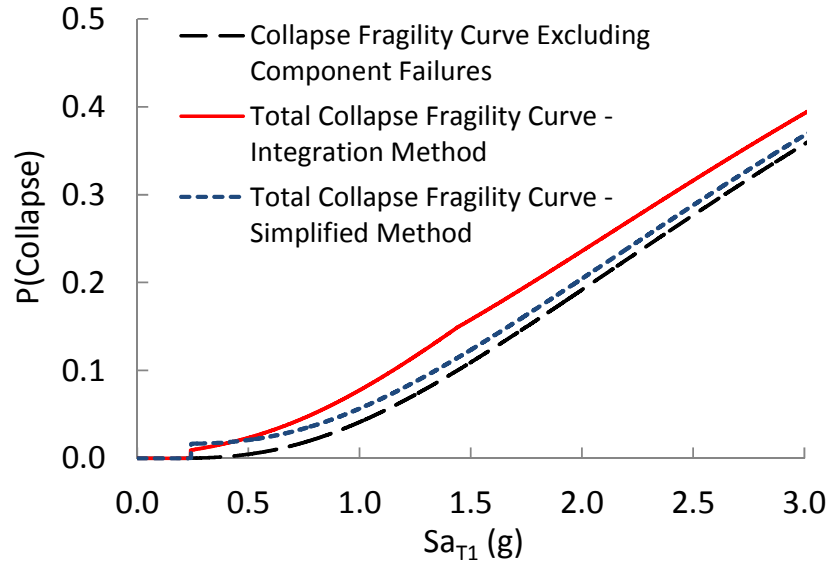
Figure 6-3: Difference in constant risk total collapse fragility curves between the integration method and the simplified method
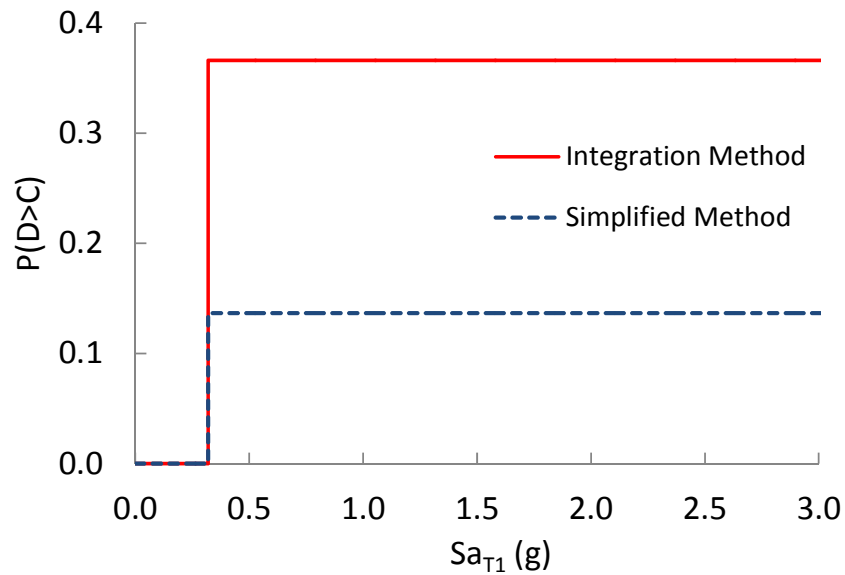
Figure 6-4: The difference between the probability of demand exceeding capacity between the integration method and the simplified method
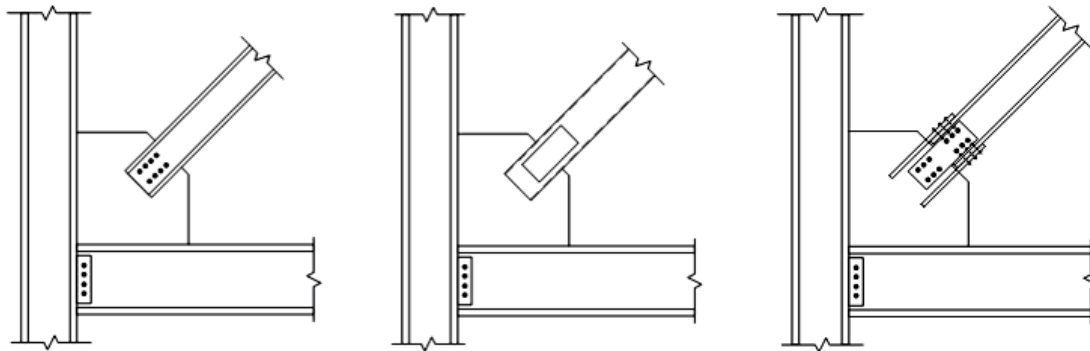
Figure 6-5: Examples of common SCBF brace connections a) Bolted channel or angle b) Welded hollow rectangular section or pipe with net-section reinforcement c) Bolted and welded W-shape connected through web

$P_{ye}*$ = Required Strength

$P_{ye}* < Rn*$

Rn* (mode of failure)

1 weld rupture

2 block shear

3 weld rupture

4 net section rupture

* implies a random variable
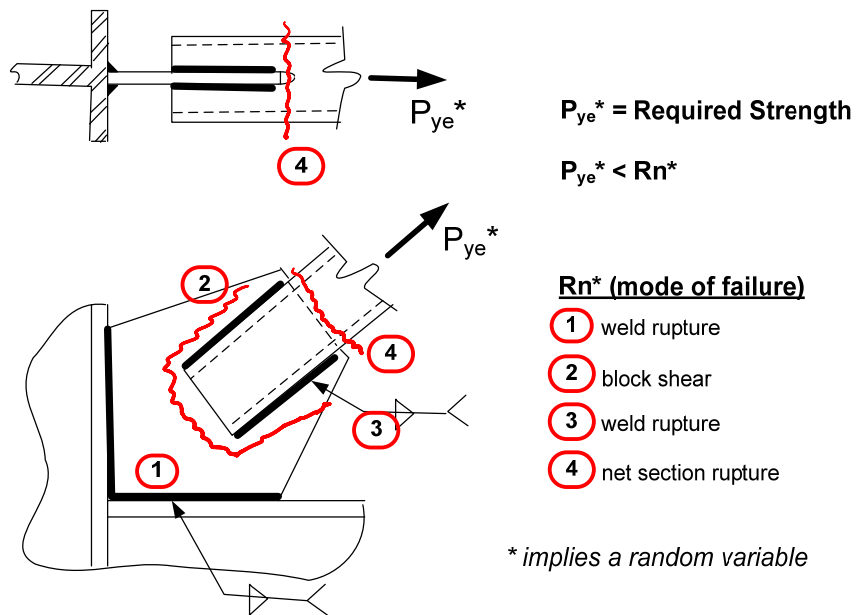
Figure 6-6: Braced Frame Connection Detail

206

Summary, Conclusions, Limitations and Future Work

7.1 Summary and Conclusions

Capacity design provisions are a vital part of most modern seismic building codes. For both economic reasons as well as to provide ductile response and energy dissipation capacity, seismic resisting systems are designed for only a fraction of the earthquake forces that can be delivered to them during large seismic events. In US structural design codes this is achieved through ASCE 7-10's response modification factor, R, which reduces the design seismic forces. (ASCE, 2010) As a consequence, in the event of an earthquake, inelastic deformations can be expected. To control which components deform inelastically, the design strengths of selected components (deformation-controlled components), are deliberately lower than those of others (force-controlled or capacity-designed components). To achieve this, capacity design provisions in building codes have capacity-designed components specifically designed to be stronger than the strength capacity of the deformation-controlled components. Given the inherent uncertainties in both local component strengths and overall system response, capacity design factors, ϕ and γ, are used by building codes to ensure a high probability that the desired behavior is achieved, effectively adjusting the margin between the expected capacities of the capacity-designed components and the expected demands from the deformation-controlled components such that the probability of demand exceeding capacity is small.

However, rigorous treatment of the uncertainties involved and understanding of the overall system behavior and its relationship with the demand on capacity-designed components has been generally neglected when capacity design factors have been established. This has resulted in inconsistencies in the way they are established for

different seismic force resisting systems. The primary objectives of this research were to explore which uncertainties and system behavior aspects are important for the reliability of capacity-designed components in seismic resistant systems and to develop a systematic way to treat them.

The reliability-based methodology developed incorporates the main factors believed to influence the reliability of capacity-designed components and it allows for making informed decisions on their required design strengths. The factors considered are, the system response modification factor (R-factor), member overstrength, site ground motion seismic hazard curve and postulated consequences of capacity-designed components failure on system behavior. The end result is a framework for establishing the required design strength of capacity-designed components such that the tolerable probability of frame collapse due to component failure is consistent between different components. The calculated ϕ/γ-ratios for the 6-story and 16-story SCBFs in Chapter 5, using both the methodology's approximate method and direct integration of the probability of demand exceeding capacity curve and a ground motion seismic hazard curve showed that the approximate method provided very comparable results. Despite addressing numerous factors that influence the reliability of capacity-designed components, applying the methodology is straightforward once necessary statistical data has been collected. Digest of the methodology and example application for selected brace connection failure modes were provided in Chapter 6. Detailed conclusions corresponding to the objectives outlined in Chapter, 1 along with conclusions from the analyses of the two capacity-designed components, are summarized below.

7.1.1 Expected Demand on Capacity-Designed Components

The expected demand on capacity-designed components in seismic resistant systems is the demand from deformation-controlled components as they undergo inelastic deformations. The demand therefore depends on the deformation demands in the structure, which in return can be related to the ground motion intensity it is subjected to. Here, the spectral acceleration at the fundamental period of a structure is used to describe

the ground motion intensity. Some strain hardening can be expected but it depends on members, materials and the system involved and its impact on the reliability is often not the most critical concern as the probability of experiencing large enough ground motions to cause significant strain hardening decreases quickly compared to the resulting increase in demand. The demand associated with components' initial yielding is, however, critical as even for moderate ground motions, the capacity-designed components are likely to be subjected to that demand, and the higher the R_μ, the lower the spectral accelerations at which yielding is expected, $Sa_{y,exp}$ becomes and the higher is the probability of experiencing that demand.

When a single deformation-controlled component causes the demand, force-controlled components, e.g. brace connections, can be expected to experience their demand associated with inelastic deformations. As the number of stories in a frame increases, the expected demand on a given component decreases while the dispersion increases. This is a result of inelastic deformations concentrating in different stories for different ground motion records, and thus, for a specific ground motion record, only a few stories might experience large inelastic deformations, and therefore large force demands on capacity-designed components, while the other stories experience modest deformations. These observations are based on the braced frame studies, and the reduction in the expected demand decreases considerably as the number of stories increases. Braced frames tend to concentrate inelastic deformations in only a few stories and the results might differ for systems that are able to distribute inelastic deformations within the system more evenly. Of course, if overstrength between stories varies significantly, this behavior might change, i.e. if inelastic deformations are designed to occur only in specific stories, as was the case for the 6-story SCBF – Design 2. In that case the braces up the height of the frame were identical and the expected demand for the bottom two stories was higher than for the same stories in the 6-story SCBF that was optimally designed. For all multi-story frames analyzed, the maximum normalized brace tensile force for the whole frame versus spectral acceleration curves compare well with the same curve for single-story frames, since inelastic deformations will occur somewhere within a frame when subjected to large enough earthquake ground motions.

When multiple deformation-controlled components are causing the demand on capacity-designed components, such as on columns in multi-story braced frames, the likelihood of all deforming inelastically decreases as the number of deformation-controlled components increases. Likewise, the impact of R_μ on the demand versus spectral acceleration curve diminishes as well with increased number of deformation-controlled components. As a result, capacity design principles do not explain well the expected demand on columns, rather the maximum theoretical demand that can be delivered to them.

7.1.2 System Design Factors and Member Overstrength

The ASCE 7-10 response modification factor, the R-factor, and overstrength of deformation-controlled components have a great impact on the expected demand on and the reliability of capacity-designed components as well as impacting the system reliability. In this thesis, these two factors have been combined into one factor, named here R_μ, which is the R-factor divided by member overstrength in its yielding capacity. R_μ is a factor that relates the MCE spectral acceleration, Sa_{MCE}, to the spectral acceleration at which components are expected to yield $Sa_{y,exp}$. R_μ, or $Sa_{y,exp}$, is not unique for the whole structure as it is based on components' over-design, which varies from one component to the next and between stories. For systems with high R_μ's, the deformation-controlled components can be expected to yield at relatively low earthquake intensities, i.e. at low spectral accelerations, compared to systems with lower R_μ's. This results in systems having potentially large differences in the annual probabilities of experiencing member yielding and thus in capacity-designed components experiencing large demands. Therefore, for otherwise identical systems, as R_μ's increase, the ductility demands on the systems to achieve tolerable collapse probabilities increases and consequently the importance of capacity-designed components increases. In addition, for similar systems with different R_μ's, the systems with lower R_μ's tend to have an overall lower probability of collapse compared to systems with higher R_μ's, a consequence of over-design.

An important aspect of these findings is that they make it possible to consider requiring less strength for capacity-designed components within systems that rely less on inelastic deformation to achieve set performance goals, such as the tolerable probability of collapse. For most structures, i.e. R_μ's>1.0 and P(D>C)<1.0% in 50 years, it is not being suggested that the expected strength of capacity-designed components be less than the expected demand the deformation-controlled components exert on them when deforming inelastically in any case, but rather that the margin between demand and capacity can be reduced for systems with low R_μ's, i.e. the probability of demand exceeding capacity can be increased due to the low probability of experiencing that demand. The results from Section 3.2.3 demonstrated that the reduction in required design strengths can become quite significant when R_μ's <2.0.

7.1.3 Seismic Hazard Curve

The influence of R_μ and $Sa_{y,exp}$ on the component reliability is a result of deformation-controlled components yielding and reaching maximum capacities at ground motion intensities with varying frequencies of occurrence. Therefore, the ground motion seismic hazard curve is very influential in the reliability of capacity-designed components, as it reports the frequency of occurrence of a given earthquake intensity at a given site. R_μ explains the difference in the probabilities of deformation-controlled components yielding between similar systems with different R_μ located in the same area, and it was demonstrated in an example in Chapter 3 that the probabilities can vary significantly based on R_μ. The example showed that for a frame with $R_\mu = 6$ in San Francisco, there is 90.9% probability in 50 years that the frame will experience a large enough earthquake ground motions for its components to yield, while for a frame with $R_\mu = 2$ that probability is down to 27.8%. This large difference is due to the steepness of the seismic hazard curve in San Francisco, i.e. the probability of experiencing the earthquake intensities corresponding to $R_\mu = 6$ is much higher than the intensities corresponding to $R_\mu = 2$. For Central and Eastern US geographic locations where the seismic hazard curves are not as steep as the ones in the Western US, the difference is less or for the same example the

probabilities would be 24.8% and 10.5% if the systems are located in the New Madrid area. These two examples also demonstrated that even for an identical system located in different geographic locations, the difference can be significant, and suggesting that the required design strengths of capacity-designed components can justifiably vary based on location. How much the required design strength can vary depends heavily on the dispersion around the median demand and capacity. The results from Section 3.2.3 demonstrated that for a total dispersion of components´ demand and capacity distributions between 0.2 and 0.3, the difference in calculated required design strengths between the two locations using the proposed methodology ranges from 10% to 25%.

The difference between different geographic locations was reduced somewhat with the introduction of the risk-targeted MCE target, as now the spectral acceleration of the maximum considered earthquake in the Central and Eastern US generally decreases, and therefore its frequency increases, while the reverse is generally the case in the Western US. All the results presented here were based on the new risk-targeted MCE target.

7.1.4   Component and System Reliability

Most methods used to analyze reliability of structural systems, e.g. FEMA P695, do not explicitly account for the failure of capacity-designed components within the reliability assessment. This is justified by stating that capacity-designed components are specifically designed to be stronger than deformation-controlled components and will thus not fail (NIST GCR 10-917-8, 2010) (which is a very deterministic thinking within a probabilistic framework) and through the "Quality Rating of Index Archetype Models" in FEMA P-695 which increases the variance of the collapse probability distribution to account for failure modes that are not modeled in the analysis. (FEMA P695, 2009) Fortunately, the probability of failure of capacity-designed components is generally low so the above justification is likely to be reasonable in most cases. In addition, redundancy within systems will also decrease the adverse consequences of components failing. However, to determine the required design strengths of capacity-designed components, or

any other components, the consequences of component failure on the overall system reliability needs to be quantified.

Non-simulated collapse modes in FEMA P695 incorporate component failures that are difficult to simulate directly, e.g. shear and axial failure in reinforced concrete columns, fracture in connections or hinge regions of steel moment frame components, or failure of tie-downs in light-frame wood shear walls, through limit state checks in post-processing of analyses results. If a limit state is exceeded, the assumption made in FEMA P695 is that it leads to a system collapse, i.e. $P(Coll_{D>C}|D>C) = 1.0$. This is a conservative approach that tends to shift the collapse fragility curve to lower values. Many of the non-simulated collapse modes checked for are related to exceeding a specific deformation, drift or rotation limit, often related to a deterioration mechanism, and are therefore likely to occur at somewhat high spectral accelerations. Therefore, even if exceeding those limit states is assumed to lead directly to collapse, the overall conservatism in the collapse risk might be reasonable compared to the reduction in the overall computational effort by neglecting those failure modes in the dynamic analysis. However, if the same procedure is applied to account for failure of capacity-designed components, which are force-based limit states, the conservatism in the collapse risk might be significant if exceeding the limit states is assumed to equal system collapse. The SCBF analyses demonstrated this clearly. Due to braces approaching peak strength capacities at relatively low spectral accelerations, the brace connections begin to fail at those low spectral accelerations as well. If brace connection failures equal system collapse, it can have an un-proportional effect on the collapse risk due to the high frequency of occurrence of the spectral accelerations where brace connections begin to fail. The single-story SCBF analysis in 4.3 and the 6-story SCBF analysis in 5.4, where connection fractures were directly simulated in the analyses, demonstrated that connection fracture does not necessarily equal collapse. Further, analyses results demonstrated that the probability of collapse given connection fracture depends on the ground motion intensity. At spectral accelerations close to the MCE demand, the probability of collapse due to connection fractures was 25%-30% for the cases studied.

Regardless of impact on system reliability, conditional reliability calculations of capacity-designed components need to be done with awareness that the reliability of many capacity-designed components is fairly constant beyond the point of deformation-controlled components yielding and reaching maximum strengths. Therefore, even if the system does not collapse, failure of capacity-designed components can be expected, even at low spectral accelerations.

7.1.5 Capacity-Based Design of Brace Connections in SCBF´s

Many of the observations made on the nature of the reliability of capacity-designed components were inferred from the single-story SCBF analyses where frames with different member overstrengths, i.e. varying R_μ´s, were analyzed, observations that were later verified through analyses of multi-story SCBFs. Through simulation of connection strengths using Monte Carlo methods and comparison of simulated strengths with developed brace forces from dynamic analyses, it became evident that connection failures begin to occur at relatively low spectral accelerations, and that those can be related to R_μ. For systems with lower R_μ, the connection fractures initiate at higher spectral accelerations than for systems with high R_μ The spectral acceleration at which connection fractures initiate is where the braces begin to yield in tension, $Sa_{y,exp}$ which is defined as two-thirds the MCE spectral accelerations divided by R_μ. Due to very limited strain hardening in braces in SCBFs when cyclically loaded, the demand on the connections is fairly constant from the point where the braces initially yield in tension up until much higher larger deformations. The probability of demand exceeding connection capacity is therefore somewhat constant beyond that point. Integrating these results with a site seismic hazard curve, the system with higher R_μ will require a larger margin, i.e. higher ϕ/γ-ratio, than a system with lower R_μ, if the objective is consistent annual probability of connection failures between the two systems. Based on the SCBF examples analyzed in this thesis, R_μ of 3, collected statistical information on brace connection capacities, the current ϕ/γ-ratio of 0.75 appears conservative and a new ϕ/γ-ratio of 0.90 recommended.

7.1.6 Capacity-Based Design of Columns in SCBF´s

The demand on columns in braced frames is a complex matter. It is very system, height and configuration dependent which causes challenges when attempting to develop general guidelines. The maximum demand that can be delivered to them is bounded by the capacity of the braces above them and the AISC 2010 *Seismic Provisions* have done well to capture the maximum demand. However, unless there are only a couple of braces exerting demand on columns, capacity design principles overestimate the expected demand on them and the difference increases as the number of stories increases. This is caused by the low likelihood of simultaneous yielding of all braces, different member overstrength between stories and further complicated in the case of SCBF's with the differences in brace tension and compression strength capacities.

The AISC 2010 *Seismic Provisions* have included a limit on the maximum required design strength of columns based on an amplified seismic load and the exclusion of all compression braces in the analysis. The amplified seismic load is the design load multiplied by the overstrength factor, Ω_0. However, this study showed that this limit in the *Seismic Provisions* can greatly under-estimate the demand, for instance by a factor of 2.5 for the 16-story frame, as it is based on a fixed overstrength factor and does therefore not consider possible over-design beyond that.

7.1.7 Column Demand in Tall Building Initiative

The Pacific Earthquake Engineering Center´s (PEER) Tall Building Initiative (TBI; 2010) approach to the issue of column demands in multi-story seismic resistant frames is to use the results of 7 nonlinear dynamic analyses of the structure being analyzed under MCE ground motion demand to calculate the required design strength of columns. The TBI guidelines therefore incorporate the relevant system, height and configuration effects on the demand. With concerns about overloading the columns, a factor of 1.5 is multiplied to the mean value of the analysis results. The 1.5 factor is meant to represent the mean plus one standard deviation of the design demand. For the 1st story columns in the 16-story frame, the probability of exceeding the TBI design demand is 4.6% at the

MCE demand but only 0.3% at $Sa_{y,exp}$. These are positive results for the practice of conditioning at the MCE demand. However, the demand continues to increase past the MCE demand and the probability of exceeding the design demand at the median collapse point is 10.6% or more than twice that at the MCE demand. However, as the frequency of experiencing those large demands associated with the maximum column demand becomes very small, that is not of a great concern. Conditioning the reliability calculations, or design checks, at the MCE demand is therefore as valid as it is for the simplified method proposed by the methodology, but the margin between demand and capacity at the MCE demand needs be adjusted to account for the different shape of the probability of demand exceeding capacity curve.

7.2 Limitations and Future Work

The limitations of this research and possible areas for future research include the following:

1. **Consequences of exceeding component limit states**: An integral part of the methodology is relating component reliability to system reliability. Although a very complex matter, the proposed methodology addresses this by multiplying the probability of exceeding the component limit state with an assumed probability of component failure leading to collapse, i.e. $P(Coll_{D>C}|D>C)$, which in the simplified method proposed in Chapter 3 is assumed to be independent of the ground motion intensity. The methodology therefore allows for differentiating between those components whose failure is assumed to have limited consequence on the system behavior to those whose failure is assumed to have severe consequences, e.g. the force-controlled non-critical actions and the force-controlled critical actions in the Tall Building Initiative (TBI, 2010). The examples in Chapters 4 and 5 showed the probability of collapse given connection failure for the single-story and the 6-story SCBF's analyzed is not independent of the ground motion intensity. Rather than being constant, it was negligible at low ground motion intensities (before $Sa_{y,exp}$) and reached

216

approximately 25% - 30% at the MCE demand. These results agree with results from Luco and Cornell (2000) on connection failures in SMRF where the impact of connection failure on the system response was modest at the lower ground motion intensities but increased as the intensity increased. However, these results are based on only two braced frame studies and are possibly very system dependent. Therefore, to justifiably take advantage of the post-component failure system behavior, future research is needed on more structures and different capacity-designed components to further quantify and understand this behavior. Possible avenues to investigate in this regard are gravity system effects, random variable interaction and correlation and redundancy.

a. **Gravity system effects**: The possible beneficial contribution of the gravity system is not included in the dynamic analyses of the SCBF frames in this thesis. Although the contributions of the gravity system to the system collapse capacity might be limited at high ground motion intensities, its contribution at the lower ground motion intensities might be significant. As this research has demonstrated, failures of capacity-designed components are likely to occur at low ground motion intensities compared to the MCE demands, ground motion intensities with relatively high return periods. Therefore, proper modeling of the gravity system and its inclusion in the models can reduce the probability of collapse due to the failure of capacity-designed components and consequently greatly reduce the annual probability of collapse due to component failure.

b. **Random variable interaction**: The probability of collapse given connection failure calculations in Chapter 5 for the 6-story frame were based on varying only the connection strengths and therefore ignores the effects of possible variable interaction, e.g. weak connections but strong beam-column connections etc. In Chapter 4, both a full uncertainty analysis and an analysis where only the connection capacities were

217

varied was conducted and it demonstrated that the results are not identical between the two methods, although comparable; suggesting that although the latter method can give a reasonable estimate, for more accurate results, varying the random variables together is required.

    c. **Correlations and redundancy**: Despite its importance, correlation and redundancy is a consistently ignored aspect of structural reliability due to the challenges of quantifying correlation between structural components. Regardless, with increased computational power, studies on the effects of correlations and redundancy within a structural system on its behavior are worth the effort, even if simply parametric studies to investigate the possible influence and identify which parameters are most important in this regard.

2. **Influence of R_μ on system reliability**: The influence of R_μ on the development of maximum demands on capacity-designed components and therefore their reliability is a central part of the methodology. It was demonstrated that as R_μ increases, the frequency of capacity-designed components experiencing large demands increases and likewise does the mean annual frequency of their failure. Ignoring the effect R_μ has on the reliability of capacity-designed components, the frames analyzed in this thesis with low R_μ's, i.e. the single-story SCBF – Frame 2 and the 16-story SCBF both had a lower annual probability of collapse compared to the other frames with higher R_μ's, thus suggesting that if consistent risk between the systems is the goal, the capacity design requirements on the low R_μ frames can be reduced beyond what only consistent component reliability suggests. To take advantage of the possible reduction in frame collapse probabilities due to decreased R_μ's, further studies are required. A limit on how low R_μ can become must also be considered since the goal of the R-factor is to help ensure a ductile response and energy dissipation capacity in seismic resisting systems and increased member overstrength counteracts that goal and the overall design philosophy.

3. **Column reliability in seismic force-resistant systems**: Much work has been done to quantify the demand on columns in seismic resistant systems with the general consensus that full capacity design of columns at the base of tall buildings is conservative, as simultaneous yielding and/or strain hardening of all deformation-controlled components above is unlikely. However, attempting to develop guidelines or code provisions that allow for taking advantage of the decreased likelihood of simultaneous yielding as the number of stories increases is challenging for several reasons. First, the column demand is very system, height and configuration dependent, which causes challenges when attempting to develop general guidelines. Second, the capacity is present to develop simultaneous yielding and studies have shown significant dispersion in the column demand at the base of buildings (Tremblay and Robert, 2001) where close to simultaneous yielding of deformation-controlled components occurs in some cases and due to a natural conservatism when dealing with columns, this can cause resistance to relax the column design requirements. Third and maybe most important reason is that these studies deal mainly with the demand on columns and neither considers the column capacity nor the consequences of overloading the columns. The need for accurate modeling of column behavior in structural models, including the uncertainty around the parameters controlling the column behavior is therefore pivotal if consistent column design requirements are to be developed. The Tall Building Initiative (TBI, 2010) approach to this issue is perhaps the most logical one as the design demand is based on nonlinear analysis results of the structure being designed, therefore incorporating the relevant system, height and configuration effects on the demand. However, with the consequences of overloading the columns fairly unknown, but considered severe, a factor of 1.5 is multiplied with the mean value of the analysis results to represent the mean plus one standard deviation. The analysis results are based on only 7 ground motion records and therefore little confidence is given to the calculated standard deviation and instead a fixed value used.

4. **Full modeling uncertainty analysis of multi-story frames**: To incorporate all the topics mentioned above and to accurately include their effects on the probability of system collapse, full modeling uncertainty analyses of a suite of multi-story frames is needed. However, to try to capture the influence of specific design requirements or components on the system reliability, not just to assess the overall impact of modeling uncertainty on the system behavior, a systematic approach is required, e.g. where additional uncertainties are incorporated step-by-step, similar to what was done with the introduction of the connection fracture to the frame models in Chapter 4 and 5.

5. **Alternative seismic force-resistant systems**: This research was focused on Special Concentrically Braced Frames and the methodology was developed based on findings from dynamic analyses results of braced frames. Although most of the methodology's concepts are general in nature and apply to most seismic force-resistant systems, i.e. the effect of the R-factor and member overstrength, future work is needed on other systems to verify the applicability there.

7.3   Concluding Remarks

The framework developed in this thesis serves to quantify the reliability of capacity-designed components in seismic resistant systems and allows for making informed decisions on their required design strengths. The development of the framework was based on results from nonlinear dynamic analyses of Special Concentrically Braced Frames subjected to multiple recorded earthquake ground motions. However, the main concepts of the framework are general in nature and should apply to capacity-designed components in a variety of seismic resistant systems. Given the importance of the consequences of component failure on system reliability to establish the required component design strength, further research in that area appears warranted.

Notation List

A_g	Gross area of a member
$ACMR$	Adjusted collapse margin ratio which adjusts the CMR due to the spectral shape of extreme ground motions.
b	Regression coefficient for linear regression of drift demand D on intensity Sa in logarithmic space (SAC-DCFD)
b_f	Flange width of a member
C	Capacity variable
C_m	Mean capacity
$\hat{C}_m$	Median capacity
C_n	Nominal capacity
C_d	Deflection amplification factor of seismic force resisting systems
C_{pr}	Factor in the AISC *Prequalified Connection Requirements* to account for peak connection strength, including strain hardening. The factor is based on a stress demand equal to the average between F_y and F_u
CDF	Cumulative distribution function
CMR	Collapse margin ratio defined in FEMA P695 as the median collapse spectral acceleration level divided by the MCE spectral acceleration
D	Demand variable
D_m	Mean demand
$\hat{D}_m$	Median demand
$\hat{D}^{P_0}$	Median drift demand under ground motion of intensity $P_{0,Sa}$. (SAC-DCFD)
D_n	Nominal demand on a member
DBE	Design basis earthquake
DR	Story drift ratio
DR_{NSC}	Story drift ratio of a non-simulated collapse mode
DR_{SC}	Story drift ratio of a simulated collapse mode
F_{cre}	Specified minimum critical compressive stress
F_u	Specified minimum tensile stress
F_y	Specified minimum yield stress
f_y	Specified minimum yield stress of reinforcing steel
H	Height of story
Ha	Site ground motion hazard curve
IDA	Incremental dynamic analysis
IDR	Inter-story drift ratio
k	Coefficient for linear regression of hazard H(Sa) on intensity Sa in proximity of region of interest in logarithmic space (SAC-DCFD)
L_h	Distance between plastic hinge locations
M_n	Nominal flexural strength
M_{nc}	Nominal flexural strength of columns
M_{nb}	Nominal flexural strength of beams

M_p	Nominal plastic flexural strength
M_{pc}	Nominal plastic flexural strength of columns
M_{pr}	Maximum probable flexural strength
MAF	Mean annual frequency
MCE	Maximum considered earthquake
MAF(Sa)	The derivative of the ground motion hazard curve at Sa
P_0	Specific value for annual probability of performance level not being met (SAC-DCFD)
P_{ysc}	Axial yield strength of steel core
$P(Coll_{Sys}\|Sa)$	Probability of frame collapse at a given spectral acceleration calculated through incremental dynamic analysis, including the failure of non-simulated collapse modes
$P(Coll_{D>C}\|D>C)$	Probability of frame collapse due to demand exceeding the capacity of capacity-designed components
$P(Collapse)_{50years}$	Probability of frame collapse in 50 years
Q	Load random variable used in LRFD
Q_n	Nominal load in LRFD
R	Resistance random variable used in LRFD
R	Frame code response modification factor used in seismic design
R_n	Nominal resistance in LRFD
R_y	Ratio of expected yield stress to specified minimum yield stress, F_y, as specified in the AISC *Seismic Provisions*
R_t	Ratio of expected tensile stress to specified minimum tensile stress, F_u, as specified in the AISC *Seismic Provisions*
R_μ	Yield response modification factor relating frame's elastic story or base shear demand (V_{DBE}) to its expected story or base shear yield strength ($V_{y,exp}$)
Sa_{T1}	Spectral acceleration of the fundamental period of a structure
Sa_{MCE}	Spectral acceleration of the maximum considered earthquake
Sa_{DBE}	Spectral acceleration of the design basis earthquake
Sa_{design}	Spectral acceleration used for the design of frames
$Sa_{y,exp}$	Spectral acceleration at which yielding of members is expected to begin
S_e	Minimum required design strength of connections
S_n	Probable strength at intended yield locations
$S_{T(NSC)}$	Spectral acceleration of a non-simulated collapse mode
$S_{T(SC)}$	Spectral acceleration of a simulated collapse mode
SSF	Spectral Shape Factor
t_f	Flange thickness of a member
V	Coefficient of variation of statistical parameters used in the LRFD reliability methodology. For lognormally distributed parameters with $V < 0.3$, it is approximately equal to the dispersion/lognormal standard deviation
V	Design story or base shear
V_C	Dispersion of capacity variables as used in the Capacity Design Factor methodology

V_D	Dispersion of demand variables as used in the Capacity Design Factor methodology
V_{DBE}	Elastic story or base shear demand
V_e	The design shear force (ACI 318-08)
V_n	Nominal story or base shear strength
V_R	LRFD resistance dispersion
V_Q	LRFD load dispersion
$V_{gravity}$	Beam shear force resulting from gravity forces
V_{tot}	Total dispersion, i.e. dispersion due to both demand and capacity
$V_{y,exp}$	Expected story or base shear yield strength
$V_{u,exp}$	Expected story or base shear ultimate strength
Z_x	Plastic section modulus of a member
β	Compression strength adjustment factor (BRBF´s)
β	LRFD reliability index, which is a relative measure of reliability
β_C	Dispersion measure for drift capacity C (SAC-DCFD)
$\beta_{D|Sa}$	Dispersion measure for drift demand D at given *Sa* level (SAC-DCFD)
$\beta_{R,Ha}$	Capacity design factor reliability index which incorporates the frame's R-factor and site ground motion hazard curve such that different failure modes in different systems have a consistent reliability
γ	Load/Demand factor
ϕ	Resistance/Capacity factor
ϕ_d	Resistance/Capacity factor for ductile limit states as specified in AISC 358
ϕ_n	Resistance/Capacity factor for non-ductile limit states as specified in AISC 358
ρ	Correlation coefficient
Ω_0	System overstrength factor
$\Omega_{y,exp}$	Story or base shear yield over-strength
Φ	Standard normal cumulative distribution function
$\Delta P(Coll_{D>C})_{50years}$	Added probability of frame collapse in 50 years due to failure of capacity-designed components
Δ	Story drift
Δ_{in}	Inelastic story drift
ω	Strain hardening adjustment factor

References

Aalbert, A. and Larse, P.K. (1999) *Strength and Ductility of Bolted Connections in Normal and High Strength Steels.* Department of Structural Engineering, Norwegian University of Science and Technology, Trondheim, Norway.

ACI 318 (2010) Building Code Requirements for Structural Concrete and Commentary. American Concrete Institute, Farmington Hills, MI.

American Institute of Steel Construction Inc. (AISC). (2010a). Seismic Provisions for Structural Steel Buildings. American Institute of Steel Construction.

American Institute of Steel Construction Inc. (AISC) (2010b) *Prequalified Connections for Special and Intermediate Steel Moment Frames for Seismic Applications*, ANSI/AISC 358-10. Draft.

American Institute of Steel Construction Inc. (AISC) (2010c) *Specification for Structural Steel Buildings*.

American Society of Civil Engineers (ASCE). (2010). ASCE-7-10: Minimum Design Loads for Buildings and Other Structures, Reston, VA.

ATC (1992). ATC-24, Guidelines for Cyclic Seismic Testing of Components of Steel Structures, Applied Technology Council.

Baker, J.W. (2005). *Vector-Valued Ground Motion Intensity Measures For Probabilistic Seismic Demand Analysis.* PhD Dissertation, Department of Civil Engineering, Stanford University, Stanford, CA.

Baker, J.W. and C.A. Cornell (2006). "Spectral shape, epsilon and record selection," *Earthquake Engineering & Structural Dynamics*, Vol. 34, No. 10, pp. 1193-1217.

Bartels, P.A. (2000) *Net Section Rupture in Tension Members with Connection Eccentricity.* PhD.Dissertation. Department of Civil Engineering, West Virginia University, Morgantown, WV.

Benjamin, J. R., & Cornell, C. A. (1970). *Probability, Statistics, and Decisions for Civil Engineering*: McGraw-Hill Book Co., New York.

Black, G.R., Wenger, B.A. and Popov, E.P. (1980) *Inelastic Buckling of Steel Struts Under Cyclic Load Reversals.* UCB/EERC-80/40, Earthquake Engineering Research Center, Berkeley, CA.

Cornell, C.A. Jalayer, F, Hamburger, R.O. Foutch, D.A. (2002), "The Probabilistic Basis for the 2000 SAC/FEMA Steel Moment Frame Guidelines." *Journal of Structural Engineering*, ASCE, Vol. 128, No. 4, pp. 526-533.

Cheng, J.J. Roger, Kulak G.L. and Khoo, H-A.. (1998) "Strength of slotted tubular tension members." *Canadian Journal of Civil Engineering*. Vol. 25, pp. 982-991.

Choi, S.W. and Park, H.S. (2009) "Evaluation of the Minimum Column-to-Beam Strength Ratios to Prevent the Formation of Plastic Hinges on the Column Parts Consisting of Joints in Special Steel Moment Frames" *International Conference on Civil and Environmental Engineering, ICCEE-2009.* Pukyong National University.

Deng, K. (2003). "The Effect of Loading Angle on the Behavior of Fillet Welds" Masters Thesis. Department of Civil and Environmental Engineering, University of Alberta, Edmonton, Alta.

Dexter, R.J., Melendrez, M.I. (2000) "Through thickness properties of columns flanges in welded moment connections" *Journal of Structural Engineering.* Vol. 126, No. 1, pp. 24-31.

Dolsek, M. (2009) "Incremental dynamic analysis with consideration of modeling uncertainties" *Earthquake Engineering and Structural Dynamics.* Vol. 38, No. 6 pp. 805 - 825

Elchalakani, M., Zhao, X.L., Grzebieta, R. (2003) "Test of Cold-Formed Circular Tubular Braces under Cyclic Axial Loading" *Journal of Structural Engineering.* Vol. 129. pp.507-514.

Ellingwood, B., Galambos, T.V., MacGregor, J.G., Cornell, C.A. (1980). "Development of a Probability Load Criterion for American National Standard A58." *National Bureau of Standards*. Publication 577.

Ellingwood, B., MacGregor, J.G., Galambos, T.V. and Cornell, C.A. (1982) "Probability Based Load Criteria: Load Factors and Load Combinations." *Journal of the Structural Division.* Vol 108, pp. 978-997.

Engelhardt M. D., Venti M. J. (2000) *Behavior and Design of Radius Cut Reduced Beam Section Connections*. Report No. SAC/BD-00/17, SAC Joint Venture.

Fell, B. V. (2008). *Large-Scale Testing and Simulation of Earthquake-Induced Ultra Low Cycle Fatigue in Bracing Members Subjected to Cyclic Inelastic Buckling.* Ph.D. Dissertation, University of California at Davis, Davis, CA.

Fell B.V., Kanvinde A.M., Deierlein G.G., Myers A.T, Fu X. (2006) "Buckling and fracture of concentric braces under inelastic cyclic loading." *SteelTips Series*, Structural Steel Education Council, Moraga, CA.

FEMA P695 (2009). *Quantification of Building Seismic Performance Factors.* Federal Emergency Management Agency.

Filippou, F. C., Popov, E. P., Bertero, V. V. (1983). *Effects of Bond Deterioration on Hysteretic Behavior of Reinforced Concrete Joints.* Report EERC 83-19, Earthquake Engineering Research Center, University of California, Berkeley.

Fisher, J.W., Ravindra, M.K., Kulak, G.L., Galambos, T.V. (1978) "Load and Resistance Factor Design Criteria for Connectors" *Journal of Structural Division.* Vol. 104, pp. 1427-1441.

Galambos, T.V. (1990) "System Reliability and Structural Design" *Structural Safety,* Vol. 7, Issue 2-4, March 1990, pp. 101 – 108.

Galambos, T.V. (2004). "Reliability of the Member Stability Criteria in the 2005 AISC Specifications." *International Journal of Steel Structures.* Korean Society of Steel Construction. Vol. 4, pp 223-230.

Galambos, T.V. (2009) *Reliability of Steel Beam-Columns,* Personal Communication

Galambos T.V., Ellingwood, B., MacGregor, J.G. and Cornell, C.A. (1982). "Probability-Based Load Criteria: Assessment of Current Practice." *Journal of the Struct. Division*, ASCE 108 (ST5), pp. 959-977.

Galambos, T.V., Ravindra, M.K. (1978). "Properties of Steel for Use in LRFD." *Journal of the Struct. Division.* ASCE, 104(ST9), pp. 1459-1468.

Gilton C., Chi B., and Uang C. M.(2000) *Cyclic Response of RBS Moment Connections: Weak-Axis Configuration and Deep Column Effects.* Report No. SAC/BD-00/23, SAC Joint Venture.

Han, S.W., Kim, W.T. and Foutch, D.A. (2007) "Seismic Behavior of HSS Bracing Members according to Width-Thickness Ratio under Symmetric Cyclic Loading" *Journal of Structural Engineering*. Vol. 133, No.2, pp. 264-273.

Hardash, S.G. and Bjorhovde, R. (1984) *Block Shear Behavior of Coped Steel Beams.* Structural Engineering Report No. 244. Department of Civil and Environmental Engineering, University of Alberta, Edmonton, Alta.

Haselton, C. B. (2006) *Assessing Seismic Collapse Safety of Modern Reinforced Concrete Moment Frame Building.* PhD Dissertation, Department of Civil Engineering, Stanford University, Stanford, CA.

Huns, B.B., Grond, G.Y., Driver, R.G. (2002) *Block Shear Behaviour of Bolted Gusset Plates.* Structural Engineering Report No. 240. Department of Civil Engineering, University of Alberta, Edmonton, Alta.

Huns, B.B., Grondin, G.Y., Driver, R.G. (2006) "Tension and shear block failure of bolted gusset plates." *Canadian Journal of Civil Engineering.* Vol. 33. pp. 395-408

Ibarra, L. (2003). *Global Collapse of Frame Structures under Seismic Excitations* PhD Dissertation, Department of Civil Engineering, Stanford University, Stanford, CA.

Ibarra, L. F., and Krawinkler, H. (2005). *Global collapse of frame structures under seismic excitations*. Technical Report 152, The John A. Blume Earthquake Engineering Research Center, Department of Civil Engineering, Stanford University, Stanford, CA.

Ibarra, L. F., Medina, R. A., and Krawinkler, H. (2005). "Hysteretic models that incorporate strength and stiffness deterioration," *Earthquake Engineering and Structural Dynamics*, Vol. 34, 12, pp. 1489-1511.

Jayaram, N., Lin, T., and Baker, J. W. (2010). "A computationally efficient ground-motion selection algorithm for matching a target response spectrum mean and variance" *Earthquake Spectra*, (in press).

Koboevic, S. and Redwood, R. (1997). "Design and seismic response of shear critical eccentrically braced frames." *Canadian Journal of Civil Engineering,* Vol. 21, No. 1, pp. 761-771.

Kulak, G.L., Fisher, J.W., and Struik, J.H.A. (1987) *Guide to Design Criteria for Bolted and Riveted Joints.* Second Edition. New York. John Wiley & Sons.

Kulak, G.L. Wu, E.Y. (1997) "Shear lag in bolted angle tension members." *Journal of Structural Engineering*. Vol. 123, No. 9. September 1997. pp.1144-1152

Lehman, D.E., Roeder, C.W., Herman, D., Johnson, S., Kotulka, B. (2008) "Improved Seismic Performance of Gusset Plate Connections" Journal of Structural Engineering. Vol. 134, pp. 840-901

Lesik, D.F. and Kennedy, D.J.L. (1990) "Ultimate Strength of Fillet Welded Connections Loaded in Plane." *Canadian Journal of Civil Engineering*. Vol. 17, No. 1. pp. 55-67.

Liel, A.B. (2008). *Assessing the Risk of California′s Existing Reinforced Concrete Frame Structures: Metrics for Seismic Safety Decisions.* PhD Dissertation, Department of Civil Engineering, Stanford University, Stanford, CA.

Liel, Abbie B., Curt B. Haselton, Gregory G. Deierlein, and Jack W. Baker. (2009) "Incorporating modeling uncertainties in the assessment of seismic collapse risk of buildings." *Structural Safety,* Vol. 31, pp 197-211.

Lignos, D.G. (2008). *Sidesway Collapse of Deteriorating Structural Systems under Seismic Excitations.* PhD Dissertation, Department of Civil Engineering, Stanford University, Stanford, CA.

Lignos, D. G., and Krawinkler, H. (2009). *Sidesway Collapse of Deteriorating Structural Systems under Seismic Excitations.* Technical Report 172, The John A. Blume Earthquake Engineering Research Center, Department of Civil Engineering, Stanford University, Stanford, CA.

Lignos, D. G., and Krawinkler, H. (2011). "Deterioration Modeling of Steel Beams and Columns in Support to Collapse Prediction of Steel Moment Frames," *ASCE, Journal of Structural Engineering* (in press).

Ling, T.W., Zhao, X.L., Al-Mahaidi, R., Packer, J.A. (2007). "Investigation of Block Shear Tear-Out Failure in Gusset-Plate Welded Connections in Structural Steel Hollow Sections and Very High Strength Tubes." *Engineering Structures.* Vol. 29, 2007, p. 469-482.

Liu, J. (2003), "Examination of Expected Yield and Tensile Strength Ratios," Draft Addendum Report, AISC, Chicago, IL.

Luco, N. and Cornell, C.A. (1998) "Effects of random connection fractures on demands and reliability for a 3-story pre-Northridge SMRF structure." *Proceedings of the 6th U.S. National Conference on Earthquake Engineering.* Paper No. 244. EERI: El Cerrito, CA. Seattle, WA, pp. 1-12

Luco, N. and Cornell, C.A. (2000) "Effects of connection fractures on SMRF seismic drift demands". *ASCE Journal of Structural Engineering.* Vol 126, pp. 127-136.

Luco, N., Ellingwood, B.R., Hamburger, R.O., Hooper, J.D., Kimball, J.K., Kircher, C.A., (2007). "Risk-Targeted versus Current Seismic Design Maps for the Conterminous United States" Proc. SEAOC 2007 Annual Conference, 13 pgs.

Medina, R.A. and Krawinkler, H. (2005) "Strength Demand Issues Relevant for the Seismic Design of Moment-Resisting Frames" *Earthquake Spectra,* Vol. 21, Issue 2, pp. 415-439.

Melchers, R.E. (1999) *Structural Reliability Analysis and Prediction.* Second Edition. New York. John Wiley & Sons, Inc.

Mullin, D. (2005) *Gusset Plates as Energy Dissipaters in Seismically Loaded Structures.* Ph.D. Dissertation, Department of Civil and Environmental Engineering, University of Alberta, Edmonton, Alta.

Nakashima, M., and Sawaizumi, S. (2000) "Column-to-beam strength ratio required for ensuring beam-collapse mechanisms in earthquake responses of steel moment frames" *Proceedings, 12th World Conference on Earthquake Engineering*, New Zealand Society for Earthquake Engineering, paper No. 1109, Auckland, New Zealand, 8 pp

Nast, T.E., Grondin, G.Y. and Cheng, J.J.R. (1999) *Cyclic Behavior of Stiffened Gusset Plate-Brace Member Assemblies,* Structural Engineering Report 229, Department of Civil and Environmental Engineering, University of Alberta, Edmonton, Alta.

Newell, J. and Uang, C.M., (2006) *Cyclic Behavior of Steel Columns with Combined High Axial Load and Drift Demand*, Report No. SSRP-06/22, Structural Systems Research Project, Department of Structural Engineering, University of California, San Diego, California.

NIST GCR 10-917-8 (2010) *Evaluation of the FEMA P-695 Methodology for Quantification of Building Seismic Performance Factors.* National Institute of Standards and Technology, Gaithersburg, MD 208999-8600

Ng, A.K:F., Driver, R.G. and Grondin, G.Y. (2002). *Behavior of Transverse Fillet Welds*. Structural Engineering Report 245, Department of Civil and Environmental Engineering, University of Alberta, Edmonton, Alta.

Ng, A.K:F., Driver, R.G. and Grondin, G.Y. (2004). "Behavior of Transverse Fillet Welds: Parametric and Reliability Analyses". *Engineering Journal*. Second Quarter. pp 55-67.

OpenSees (2011). *Open System for Earthquake Engineering Simulation.* Pacific Earthquake Engineering Research Center. University of California, Berkeley. Online at http://opensees.berkeley.edu/

Paulay, T. (1986) "A critique of the special provisions for seismic design of the building code requirements for reinforced concrete (ACI 318-83)", *ACI Journal*. Vol. 83, Issue 2, pp. 274-283.

Petersen, M. D., Frankel, A. D., Harmsen, S. C., Mueller, C. S., Haller, K. M., Wheeler, R. L., Wesson, R. L., Zeng, Y., Boyd, O. S., Perkins, D. M., Luco, N., Field, E. H., Wills, C. J., and Rukstales, K. S. (2008). *Documentation for the 2008 Update of the United States National Seismic Hazard Maps: U.S. Geological Survey Open-File Report 2008–1128*.

Pinto, P.E., Giannin, R., & Franchin, P. (2004). *Seismic reliability analysis of structures.* Pavia, Italy, IUSS Press.

Porter, K.A., Kennedy, R., Bachman, R. (2007), "Creating Fragility Functions for Performance-Based Earthquake Engineering," *Earthquake Spectra*, Vol 23, Issue 2, pp. 471-489

Porter, K.A., Beck, J.L., Shaikhutdinov, R.V. (2002) "Sensitivity of building loss estimates to major uncertain variables" *Earthquake Spectra*. Vol. 18, Issue. 4, pp. 719-743.

Rabinovitch, J.S. and Cheng, J.J.R. (1993) *Cyclic Behavior of Steel Gusset Plate Connections*. Structures Report No. 191, Department of Civil and Environmental Engineering, University of Alberta, Edmonton, Alta.

Rajashekhar, M.R. and Ellingwood B.R. (1993) "A new look at the response surface approach for reliability analysis" *Structural Safety*. Vol. 12, Issue 3, pp. 205-220.

Ravindra, M.K., Cornell, C.A., and Galambos, T.V. (1978), "Wind and Snow Load Factors for Use in LRFD." *Journal of the Struct. Division.* ASCE 104(ST9), Proc. Paper 14006, 9/1978, pp. 1443-1457.

Ravindra, M.K., Galambos, T.V. (1978) "Load and resistance factor design for steel." *Journal of the Structural Division*, ASCE 1978; 104(STD9): pp. 1337-1353.

Richards, P.W. (2004) *Cyclic stability and capacity design of steel eccentrically braced frames*. PhD Dissertation, Department of Civil Engineering, University of California, San Diego, La Jolla, CA.

Richards, P.W. (2009) "Seismic Column Demands in Ductile Braced Frames" *Journal of Structural Engineering,* ASCE 2009, Vol. 135. No. 1, pp. 33-41

Ricles, J. M., Zhang X., Lu, L,, Fisher, J. (2004) *Development of Seismic Guidelines for Deep-Column Steel Moment Connection.* ATLSS Report No. 04-13. June, 2004.

Rubinstein, R.Y. (1981) *Simulation and the Monte Carlo Method.* New York, John Wiley and Sons.

Sabelli, R., Mahin, S., Chang, C. (2003) 'Seismic demands on steel braced frame buildings with buckling-restrained braces" *Engineering Structures*. Vol. 25, Issue 5, pp. 655 - 666

SEAOC Seismology Committee (2008) "A Brief Guide to Seismic Design Factors" *Structure Magazine*, September 2008, pp. 30 – 32.

Shaback, J.B. (2001) *Behavior of Square HSS Braces with End Connections under Reversed Cyclic Axial Loading.* Masters Thesis. Department of Civil Engineering, University of Calgary, Calgary, Alta.

Song Yu, Q., Gilton, C. & Uang, C.-M. (2000) *Cyclic Response of RBS Moment Connections: Loading Sequence and Lateral Bracing Effects.* Report No. SAC/BD-00/22, SAC Joint Venture.

TBI (2010). *The Tall Building Initiative*, Pacific Earthquake Engineering Research Center, http://peer.berkeley.edu/tbi/

Topkaya, C. (2007). "Block Shear Failure of Gusset Plates with Welded Connections." *Engineering Structures*. Vol 29. pp. 11-20

Tremblay, R. and Robert, N. (2001) "Seismic performance of low- and medium-rise chevron braced steel frames" *Canadian Journal of Civil Engineering,* Vol. 28, No. 4, pp. 699-714.

Udagawa, K. and Yamada, T. (1998) "Failure Modes and Ultimate Tensile Strength of Steel Plates Joined with High-Strength Bolts." *Journal of Structural Construction Engineering,* AIJ, No. 505, pp. 115-122.

Uriz, P. (2005). *Towards Earthquake Resistant Design of Concentrically Braced Steel Structures.* Ph.D. Dissertation, University of California, Berkeley.

Uriz, P. and Mahin, S.A. (2004) "Seismic Performance Assessment of Concentrically Braced Steel Frames." Proceedings of the 13th World Conference on Earthquake Engineering.

Vamvatsikos, D. and Cornell, C.A. (2002) "Incremental Dynamic Analysis." *Earthquake Engineering and Structural Dynamics*, Vol. 31, Issue 3, pp. 491-514.

Vamvatsikos, D. and Cornell, C.A. (2004) "Applied Incremental Dynamic Analysis." *Earthquake Spectra*. Vol 30, Issue 2, pp. 523-553

Willibald, S., Packer, J.A and Martinez-Saucedo, G. (2006) "Behavior of gusset plate connections to ends of round and elliptical hollow structural section members." *Canadian Journal of Civil Engineering.* Vol. 33, pp 373-383.

Yang, F., and Mahin, S.A. (2005) "Limiting Net Section Fracture in Slotted Tube Braces." *SteelTips Series*, Structural Steel Education Council, Moraga, CA.

Yang, T.Y., Moehle, J.P. (2008). "Shear in Walls," unpublished presentation at the 2008 meeting of the Los Angeles Tall Building Structural Design Council, Los Angeles.

Yun, S-Y., Hamburger, R. O., Cornell, C.A., and Foutch, D.A. (2002). "Seismic Performance for Steel Moment Frames." *Journal of Structural Engineering.* Vol. 128, Issue 4, pp. 534-545.

Zareian, F. (2006). *Simplified Performance-Based Earthquake Engineering*. PhD Dissertation, Department of Civil Engineering, Stanford University, Stanford, CA.

Zareian, F., Krainkler, H. (2007) "Assessment of probability of collapse and design for collapse safety." *Earthquake Engineering and Structural Dynamics,* Vol. 36, Issue 13, pp. 1901 – 1914.

Incremental Dynamic Analysis of Low - Redundancy Single-Story SCBF

This appendix contains dynamic analysis results on low-redundancy single-story SCBFs. The objective of the analysis is to investigate the influence of connection failures on the reliability of single story SCBFs. The analysis is similar to the one from Chapter 4 except brace fracture is not simulated in the analysis and the beam-column hinges provide no lateral resistance. To investigate the influence of connection failures on frame capacity, two models of single story SCBFs are created. The frames are subjected to 44 ground motions and analyzed through incremental dynamic analysis. Connection failure is simulated through post-processing of the results.

A.1   Description of Analysis

The frame models for this analysis are idealized two-dimensional plane frame models of single story SCBFs with pinned connections at beam-column joints. Therefore, the braces provide all lateral resistance of the frame. Figure A-1 shows the plan and elevation view of the frame models. The models are median models where the expected strengths of members are used. By using median models, the failure of capacity-designed components is by default excluded in the analysis as their median strength capacities exceed the braces median strength capacities. Connection fractures are therefore not simulated directly in the analysis. The gravity system is idealized as leaning columns and provides no lateral resistance. The frames are modeled with elastic beams and columns and the braces are fiber sections which capture global buckling, but not local buckling or fracture. 2.0% Rayleigh damping is applied to the models. The key difference between the two frames is that Frame 2 is very over-designed, .i.e. the braces are stronger than

necessary, and therefore the R_μ of Frame 2 is smaller than that of Frame 1. The braces in Frame 1 are HSS 6x6x5/16 compared to HSS 6x6x1/2 in Frame 2. The main frame properties are listed in Table A-1. Figure A-2 shows pushover analysis results for the two frames. The over-design of Frame 2 is obvious where the base shear is more than seven times the design base shear. For Frame 1, the base shear is approximately two times the design base shear.

Similar to previous braced frame studies, the frames are subjected to the 44 ground motion records selected by and used in FEMA P695 *Quantification of Building Seismic Performance Factors* (FEMA, 2009). Unlike in the FEMA P695 study, where the ground motion set is scaled as a whole (based on the median of the set) to the spectral acceleration at the first mode period of the structure, in this study the ground motion records are scaled individually based on the spectral acceleration at the first mode period of the structure. This is done to systematically relate component demand to spectral acceleration, which can in return be related to frequencies of exceedance via the ground motion hazard curve for the site at that spectral period. The frames are analyzed using incremental time history analysis technique where each ground motion record is scaled up until frames collapse (Vamvatsikos & Cornell, 2002). The frames are analyzed using OpenSees (OpenSees, 2011).

A.2 Simulation Results

During each dynamic analysis, the maximum drift and the maximum tensile force in the braces are recorded. The results of the incremental dynamic analyses are illustrated in Figure A-3 and Table A-4. In Figure A-3, the story drift and the maximum brace axial forces are plotted versus the spectral acceleration of the fundamental period of the frames, Sa_{T1}. Figure A-3 and Table A-4 show that the maximum brace axial forces saturate at low spectral accelerations for both frames analyzed, although not at the same spectral accelerations for the two frames.

Using Equation 3-4, the spectral acceleration at which yielding is expected, $Sa_{y,exp}$, can be calculated based on the frame design properties from Table A-1:

Frame 1: $\qquad Sa_{y,\exp} = \dfrac{\sfrac{2}{3}\,Sa_{MCE}}{R_\mu} = \dfrac{1.0g}{2.5} = 0.40g$

Frame 2: $\qquad Sa_{y,\exp} = \dfrac{\sfrac{2}{3}\,Sa_{MCE}}{R_\mu} = \dfrac{1.0g}{1.7} = 0.59g$

Table A-2 and Figure A-4a show that the calculated R_μ predicts the spectral acceleration at which yielding is expected well. It was expected that Frame 2 would have a higher $Sa_{y,exp}$ as it was considerably over-designed. Next step is to investigate if this effects the brace connections at all and if so, how. Figure A-4b shows that yielding occurs at similar story drifts for both frames, as expected, being a function of frame geometry.

A.3 Probability of Brace Demand Exceeding Connection Capacity

Connection failures are not simulated in the analyses directly. To analyze the influence of connection failures on the overall frame performance, connection strengths are simulated during post-processing of the results and compared to axial forces developed in the braces during the analysis. The connection strengths are simulated by using Equation A-1 to determine the median connection strength that yields a fixed mean annual frequency (MAF) of connection failures. The end result is a median connection capacity that is some constant of the median demand.

$$C_m = D_m e^{\beta\sqrt{V_C^2 + V_D^2}} \qquad\qquad (A\text{-}1)$$

The values for D_m, and V_D are from the IDA results for brace forces shown in Table A-2. V_C is assumed to be 0.15 for this study. For these simulations, a single connection failure mode is deemed to be the controlling failure mode.

For each time history analysis, at each ground motion intensity one million Monte Carlo simulations are run with varying connection strengths, using the median connection strength calculated from Equation A-1 and the connection strength variance. If the axial

forces developed in the braces at any point in time in the analyses exceeded the simulated connection strength, connection failure is recorded. For these single-story frames, connection failure is assumed to represent frame collapse. Using the simulation results, new collapse fragility hazard curves are created; fragility curves that include the failure of brace connections. The new fragility curves are plotted in Figures A-6 and A-8 for Frame 1 and Frame 2, respectively. The connection strengths are based on a fixed mean annual frequency of connection failure. Due to the difference in the probability of connection failure versus spectral acceleration curve between the two frames, for the same mean annual frequency of connection failure, the median connection strength is higher for Frame 1 than for Frame 2. To investigate the increased mean annual frequency of frame collapse due to connection failures, the new collapse fragility curves are integrated with a site ground motion hazard curve. The hazard curve used for this example is a downtown San Francisco site (Lat 38.0, Long -121.7) shown in Figure A-5. The tabulated results from the simulations can be found in Tables A-3 and A-4. Figures A-7 and A-9 show the contributions of a given spectral acceleration to the mean annual frequency of collapse. Due to the high seismic hazard at low spectral acceleration, small probabilities of collapse at the low spectral accelerations contribute significantly to the total probability of collapse.

The results from the analysis show a few different things worth discussing. First is that conditioning the brace reliability calculations at fixed intensity levels will result in different mean annual frequency of brace connection failures for the two frames. Figure A-10 demonstrates this clearly. For $P(Conn\ Failure|MCE) = 0.10$, the mean annual frequency of failure is 0.0009 for Frame 1 while it is 0.0005 for Frame 2. Looking at it the other way, if the mean annual frequency of connection failures is fixed, the connections in Frame 2 can be allowed to have a larger conditional probability of failure than the connections in Frame 1. As a result, the ϕ/γ-ratio are different for the two frames. Figures A-10 and A-11 demonstrate this. If the mean annual frequency is fixed at 0.0005, the tolerable probability of connection failure at MCE is 0.05 for Frame 1 while for Frame 2 it is 0.10. Based on Figure A-11, this represents maximum ϕ/γ-ratio of 0.70 for Frame 1 but 0.80 for Frame 2. This is due to the different $Sa_{y,exp}$ of the frames, as they

236

both end up developing the same demands, only for Frame 1 the demand develops earlier, i.e. at higher intensities, and therefore the mean annual frequency of failure is higher if both connections are designed with consistent conditional probability of failure.

Second point worth discussing is if the mean annual frequency of frame collapse is the variable that should be fixed? Frame 2 is over-designed and has a lower mean annual frequency of frame collapse then Frame 1 when connection failures are excluded. Could Frame 2 therefore be allowed to have higher mean annual frequency of connection failures such that the end result is equal mean annual frequency of frame collapse for both frames? Figure A-12 plots the mean annual frequency of collapse against the mean annual frequency of connection failure. The figure demonstrates that for a fixed mean annual frequency of collapse, Frame 2 can be allowed a higher mean annual frequency of connection failure. For example, if the mean annual frequency of collapse is fixed at 0.002, the tolerable mean annual frequency of connection failure is 0.014 for Frame 1 and 0.018 for Frame 2. Consequently, as demonstrated in Figure A-13, this allows for a higher ϕ/γ-ratio for Frame 2 compared to Frame 1, or for a mean annual frequency of collapse of 0.002, ϕ/γ-ratio of 0.84 for Frame 1 and 0.90 for Frame 2.

The dynamic analyses of the two frames described here were the preliminary frame analyses of the ones described in Chapter 4. As such, the major conclusions are quite similar. The objective was to investigate the influence of connection failures on the reliability of single story SCBFs. The results demonstrated that since connections can fail at relatively low spectral accelerations, their failure can have a significant impact on the probability of frame collapse if their failure causes collapse directly, and that the influence increases as R_{μ} increases.

Table A-1: Frame properties

Properties	Frame 1	Frame 2
Brace Section	HSS 6x6x5/16	HSS 6x6x1/2
$\phi P_{n,c}$	158	230
$\phi P_{n,t}$	266	403
L/r	88	91
$F_{y,exp}A_g$	388	623
$F_{cr}A_g$	196	286
V_{RSA}	180	180
$V_{y,exp}$	413	630
$R_\mu = V_{DBE}/V_{y,exp}$	2.5	1.7

Table A-2: Median and COV of normalized maximum brace forces, $P_{max}/P_{y,exp}$, from analysis

Sa_{T1}	Frame 1		Frame 2	
[g]	Median	COV	Median	COV
0.10	0.25	0.12	0.16	0.12
0.20	0.50	0.12	0.33	0.13
0.30	0.75	0.09	0.50	0.13
0.40	0.92	0.06	0.67	0.111
0.50	1.01	0.04	0.84	0.09
0.60	1.04	0.03	0.97	0.07
0.70	1.06	0.02	1.04	0.05
0.80	1.07	0.02	1.07	0.03
0.90	1.07	0.02	1.08	0.02
1.00	1.08	0.02	1.08	0.02
1.50	1.09	0.02	1.10	0.02
2.00	1.10	0.02	1.11	0.02

Table A-3: MAF's for Frame 1 and various connection strengths

Connections			Frame		
MAF_{conn}	P(Fail) in 50 years	P(Fail|MCE)	MAF_f	P(Coll) in 50 years	$MAF_f/MAF_{f,no\ CF}$
0	-	-	0.00057	0.028	1.00
0.00001	0.001	0.002	0.00058	0.029	1.01
0.0001	0.005	0.015	0.00066	0.032	1.16
0.001	0.048	0.117	0.00157	0.075	2.76
0.002	0.095	0.212	0.00260	0.122	4.56
0.005	0.221	0.440	0.00554	0.242	9.74
0.01	0.393	0.704	0.01055	0.411	18.56

Table A-4: MAF's for Frame 2 and various connection strengths

Connections			Frame		
MAF_{conn}	P(Fail) in 50 years	P(Fail|MCE)	MAF_f	P(Coll) in 50 years	$MAF_f/MAF_{f,no\ CF}$
0	-	-	0.00032	0.016	1.00
0.00001	0.001	0.002	0.00033	0.016	1.02
0.0001	0.005	0.022	0.00042	0.021	1.28
0.001	0.048	0.182	0.00128	0.062	3.94
0.002	0.095	0.331	0.00226	0.107	6.96
0.005	0.221	0.671	0.00527	0.232	16.22
0.01	0.393	0.948	0.01046	0.407	32.18

2 Idealized Single Story Frames

- Area = 180 ft x 120 ft
- Weight = 100 psf x 21600 = 2160 kips
- Story Height = 15 ft, Bay Width = 30 ft
- V_{design} = 173 kips
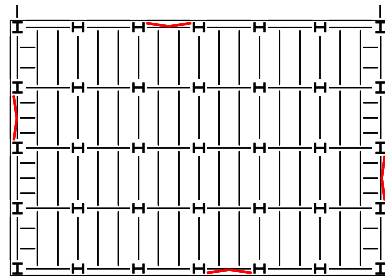
1-bay or 4-bays
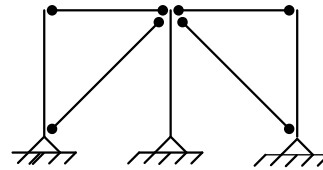
Figure A-1: SCBF analyzed for this example

a)   b)
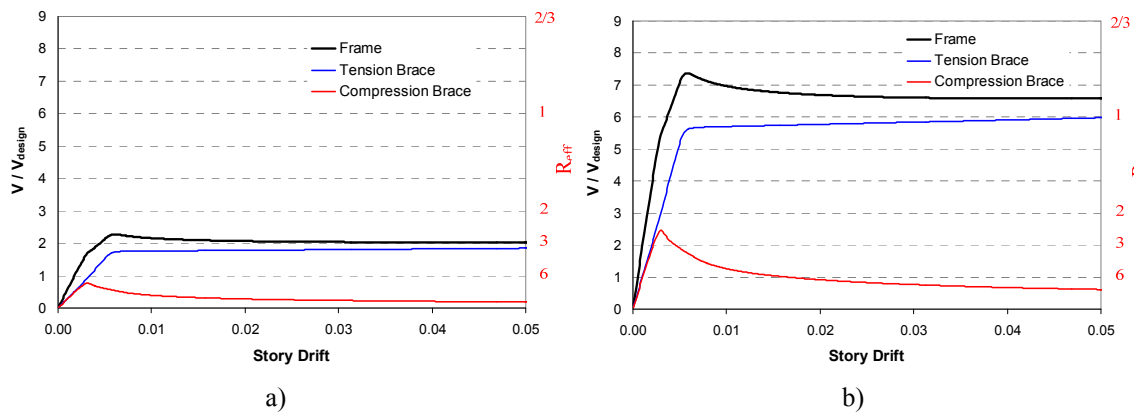
Figure A-2: Results from pushover analysis showing normalized base shear on the left y-axis, estimated R_μ on the right y-axis and story drift on the x-axis. a) Frame 1 b) Frame 2
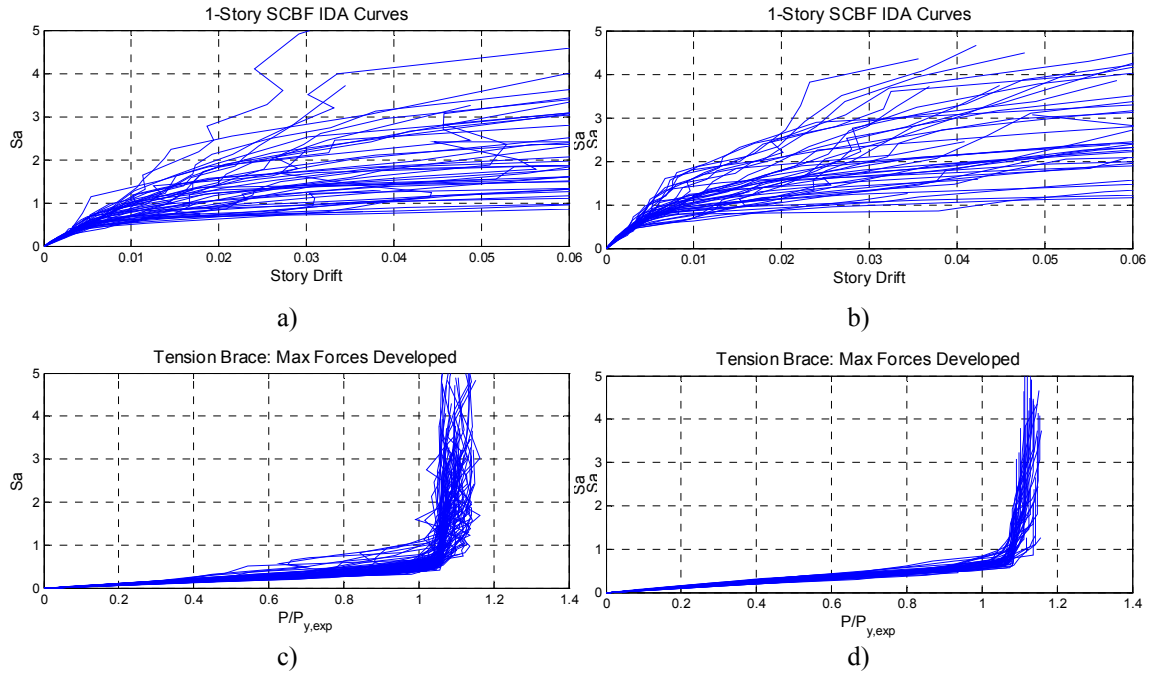
Figure A-3: Frame maximum story drift and brace axial forces vs. spectral acceleration for a) Frame 1: maximum story drift b) Frame 2: maximum story drift c) Frame 1: maximum brace axial forces d) Frame 2: maximum brace axial forces
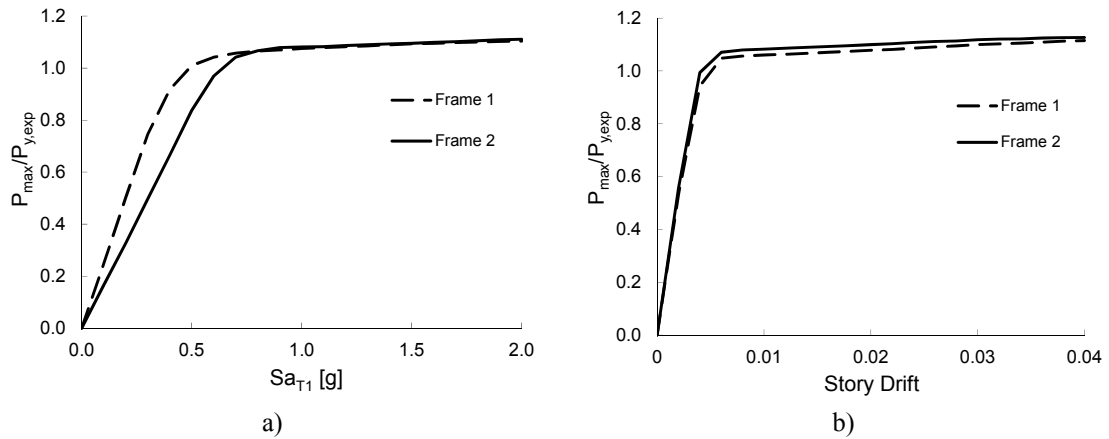
Figure A-4: a) Median of brace maximum axial forces vs. spectral acceleration and b) Median of brace maximum axial forces vs. story drift.
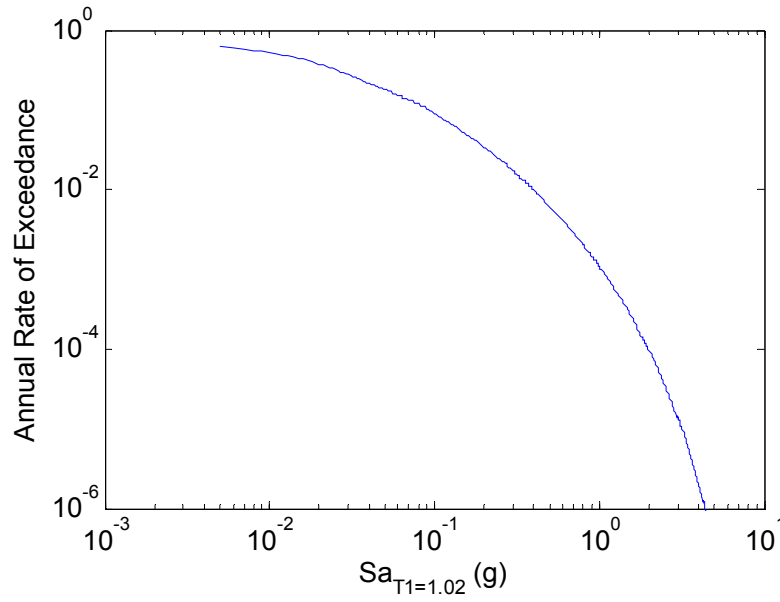
Figure A-5: Site ground motion hazard curve used in this example to calculate mean annual frequencies of collapse is a San Francisco hazard curve (Lat 38.0, Long -121.7)
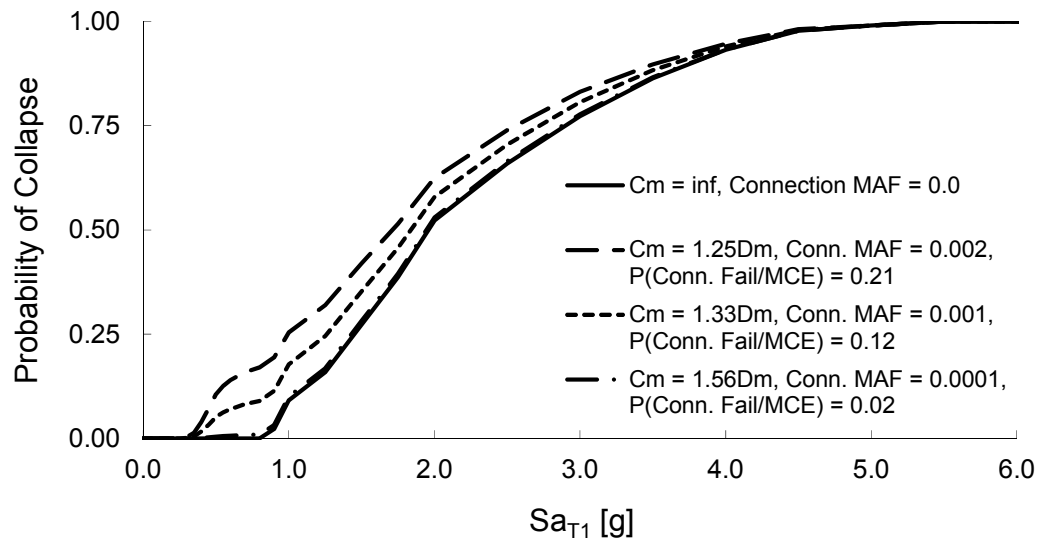
Figure A-6: Frame 1 collapse fragility curves with and without connection failures. 3 different median connection strengths are used for the simulation of connection failures.
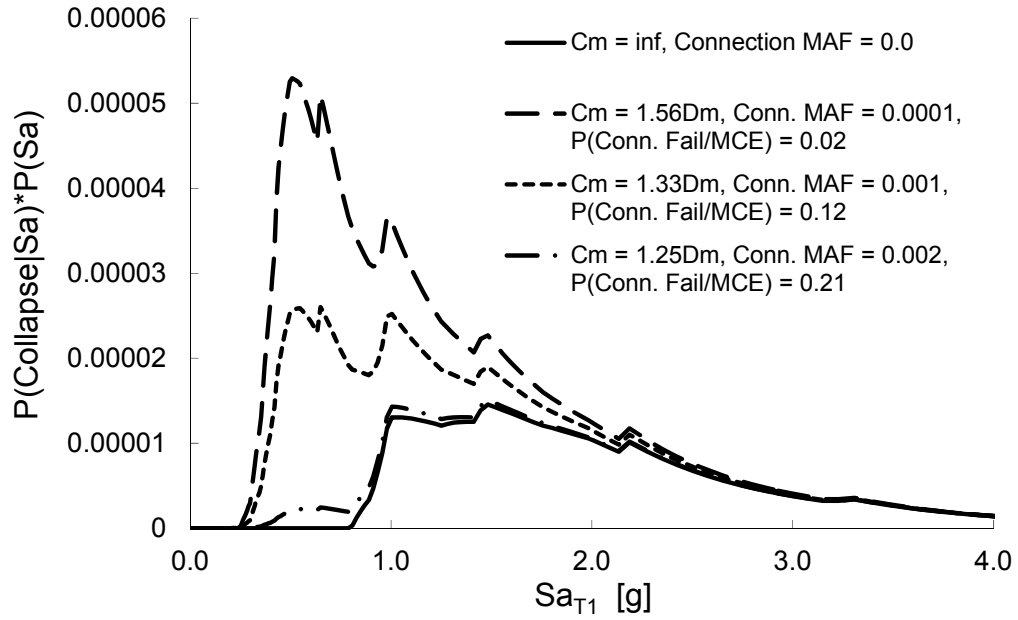
Figure A-7: Frame 1: Low *Sa* levels contribute significantly more to a frame MAF of collapse when connection failures are included.
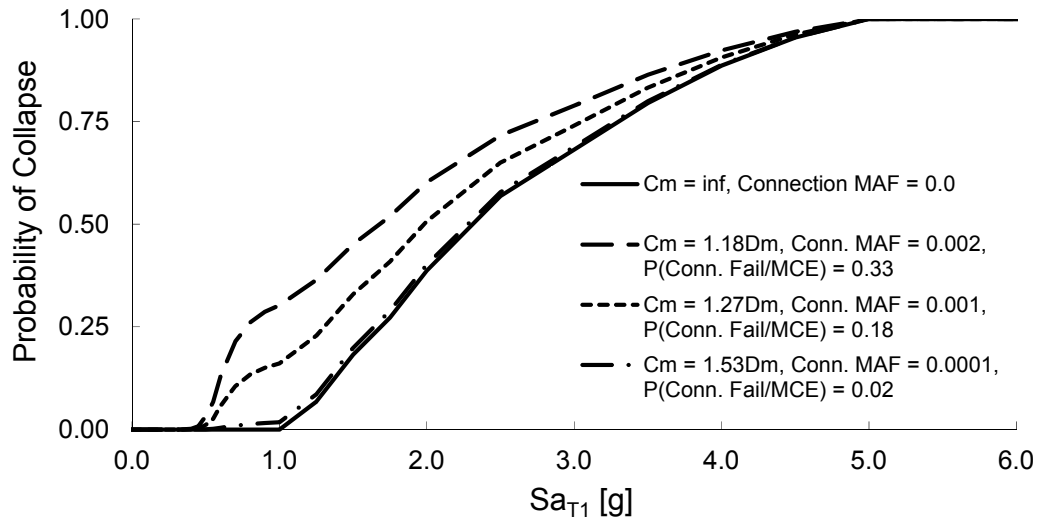
Figure A-8: Frame 2 collapse fragility curves with and without connection failures. 3 different median connection strengths are used for the simulation of connection failures
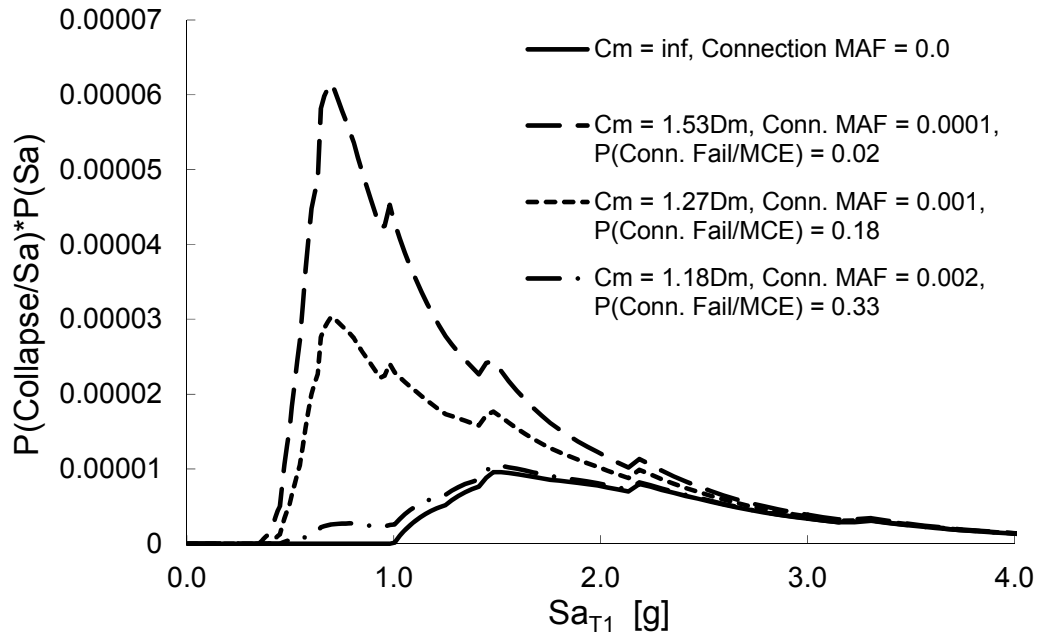
Figure A-9: Frame 2: Low *Sa* levels contribute significantly more to a frame MAF of collapse when connection failures are included.
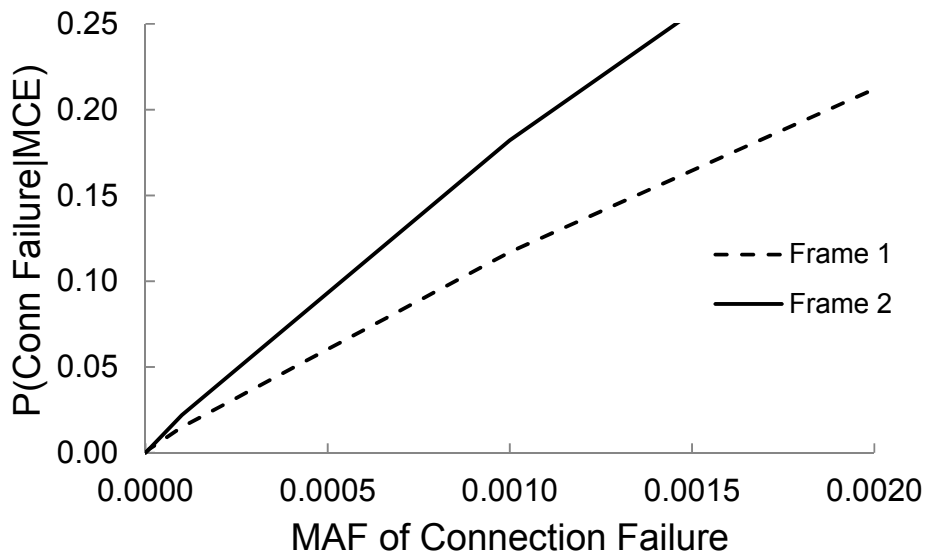
Figure A-10: If brace reliability calculations are conditioned at a fixed intensity level, e.g. the MCE spectral acceleration, the results will be inconsistent in terms of MAF of connection failures.
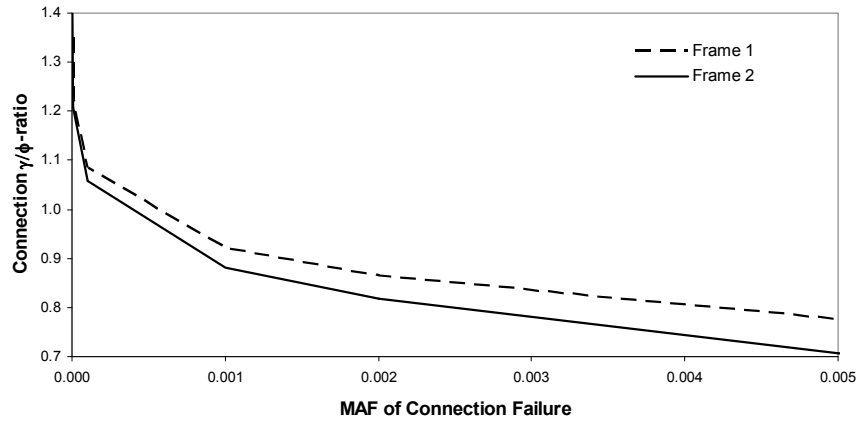
Figure A-11: The γ/φ – ratio can be determined based on the allowable MAF of connection failure.
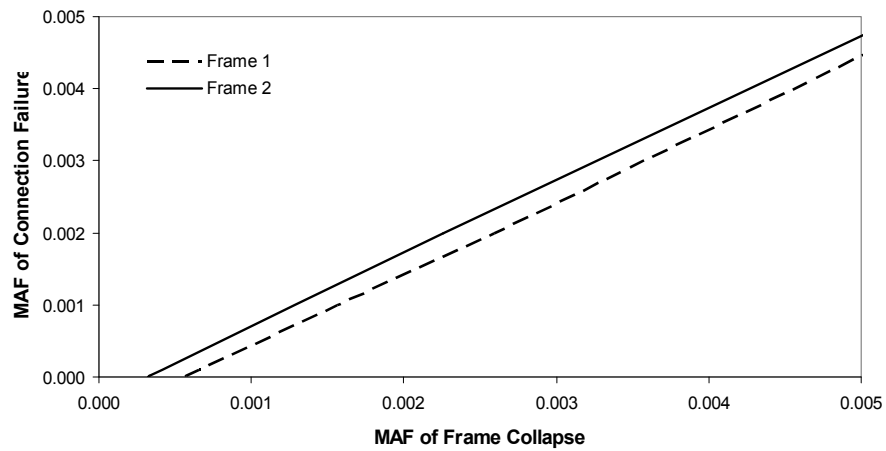
Figure A-12: Fixed MAF of frame collapse can justify higher MAF of connection failure for Frame 2 then for Frame 1.
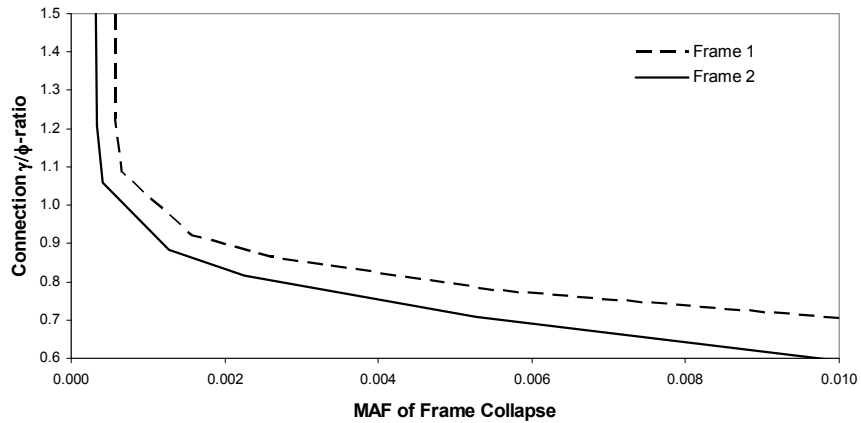
Figure A-13: Connection γ/φ – ratio can be based on MAF of frame collapse.

Appendix B

Conditional Spectrum Effects on Capacity-Designed Components

This appendix investigates the effects different ground motion selection methods have on the demand on capacity-designed components. The IDA SCBF analysis was performed using the ATC-63 ground motion set which is linearly scaled up for each increment in the analysis. Linearly scaling the ground motion set results in conservative estimates at extreme ground motions as it does not account for the unique spectral shape of extreme ground motions and their effect on behavior. The FEMA P695 methodology handles this issue by multiplying the median collapse point by a so-called spectral shape factor, SSF. The SSF is based on the buildings fundamental period, the period-based ductility and the applicable Seismic Design Category. For Frame 1 the spectral shape factor is 1.3 based on Table 7-1b from FEMA P695 *Quantification of Building Seismic Performance Factors* (FEMA, 2009), ductility index of 6 and fundamental period below 0.5s.

However, as the focus of this study was not to calculate the median collapse point, but rather to investigate the demand on capacity-designed components and the effect of their failure on the frame reliability, multiplying the median collapse point by a constant, does not tell us much. To analyze if the demand on capacity-designed components is sensitive to whether the spectral shape of extreme ground motions, a new set of ground motions were selected. These ground motions were chosen selected to match the target response spectrum mean and variance, i.e. the conditional spectrum or CS. The CS ground motions were selected using an algorithm created by Jayaram et al. (2010). Figures B-1 to B-4 provide comparison of the median earthquake response spectra of the CS ground motion sets and the ATC ground motion set for Sa_{TI} from 0.3g to 4.5g. Table B-1 lists the spectral accelerations associated with each "run" specified in Figures B-1 to

B-4. The figures show that as the spectral acceleration increases, the difference between the two ground motion sets increases as well.

The incremental dynamic analysis was re-run on Frame 1, now with the frame subjected to first the ATC-63 ground motion set and then the CS ground motion sets. The frame collapse fragility curves based on the two analyses are presented in Figure B-5. A lognormal distribution has been fitted to both results. Using the CS ground motions pushes the frame collapse fragility to the right, i.e. increases the frame collapse capacity, as expected. The ratio between the median collapse points, i.e. the spectral shape factors from the analysis is 1.39, which is reasonably close to the spectral shape factor of 1.3 suggested by FEMA P695.

Table B-2 and Figure B-6 present median and COV of the maximum braces forces at each spectral acceleration intensity for both analyses. The results indicate that the maximum braces forces are not sensitive to which ground motion set is used and that the spectral acceleration at which yielding is expected does not need to be multiplied by a spectral shape factor if linearly scaled ground motions are used. The results should not come as big surprise. In the elastic range, the response between the two ground motion sets should be very similar and therefore the demand on capacity-designed components as well. Also, the median earthquake response spectra are almost identical at low spectral accelerations, e.g. see Sa_{T1} = 0.31g and 0.41g in Figure B-1, the spectral accelerations where yielding is likely to begin. Past yielding, i.e. past $Sa_{y,exp}$ = 0.42g, the maximum brace forces saturate quickly to their maximum value and therefore the difference between the two analyzes is minimal at higher spectral accelerations, where the two response spectra differ considerably as for Sa_{T1} of 2.10g in Figure B-3 and higher spectral accelerations.

Table B-1: Sa_{TI} **associated with each "Run" in Figures B-1 to B-4**

Run #	Sa_{T1} [g]
1	0.31
2	0.41
3	0.51
4	0.56
5	0.71
6	0.78
7	0.96
8	1.25
9	1.70
10	2.10
11	2.50
12	3.00
13	3.75
14	4.50

Table B-2: Median and COV of normalized maximum brace forces, $P_{max}/P_{y,exp}$ from both analyses

Sa_{T1}	ATC Ground Motions		CS Ground Motions	
[g]	Median	COV	Median	COV
0.00	0.00	0.00	0.00	0.00
0.31	0.78	0.09	0.80	0.12
0.41	0.98	0.05	0.96	0.07
0.51	1.04	0.02	1.03	0.03
0.56	1.04	0.02	1.04	0.02
0.71	1.06	0.02	1.05	0.01
0.78	1.07	0.02	1.06	0.01
0.96	1.07	0.02	1.07	0.02
1.25	1.09	0.02	1.08	0.02
1.70	1.10	0.02	1.10	0.02
2.10	1.11	0.02	1.11	0.02
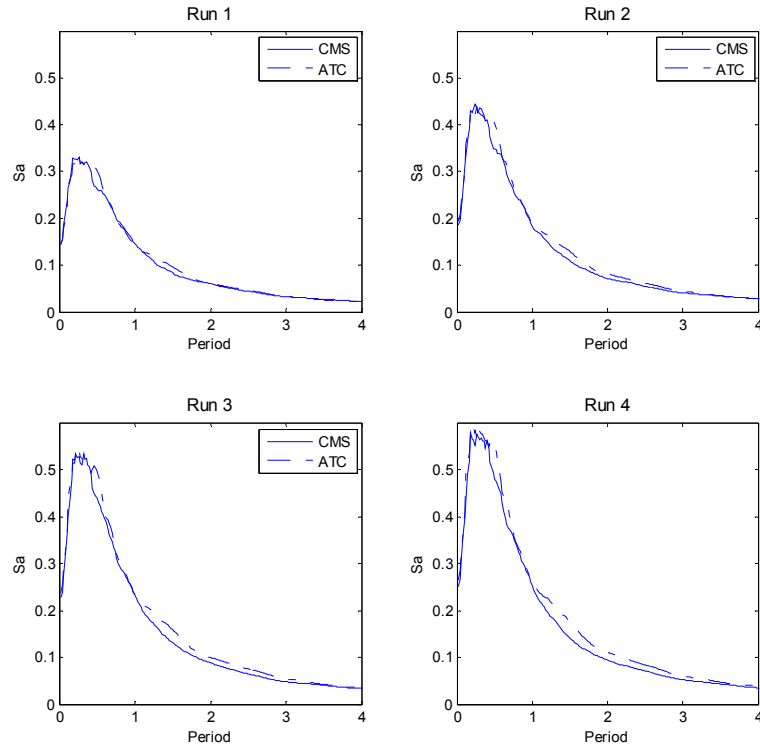
Figure B-1: Comparison between CS and ATC median earthquake response spectra for Sa_{T1} of 0.31g, 0.41g, 0.51g and 0.56g
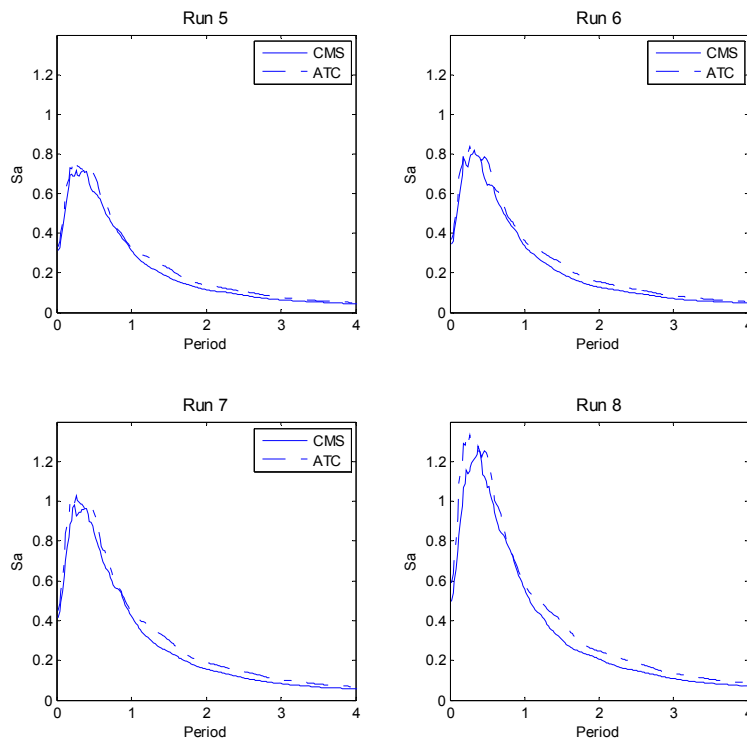
Figure B-2: Comparison between CS and ATC median earthquake response spectra for Sa_{T1} of 0.71g, 0.78g, 0.96g and 1.25g
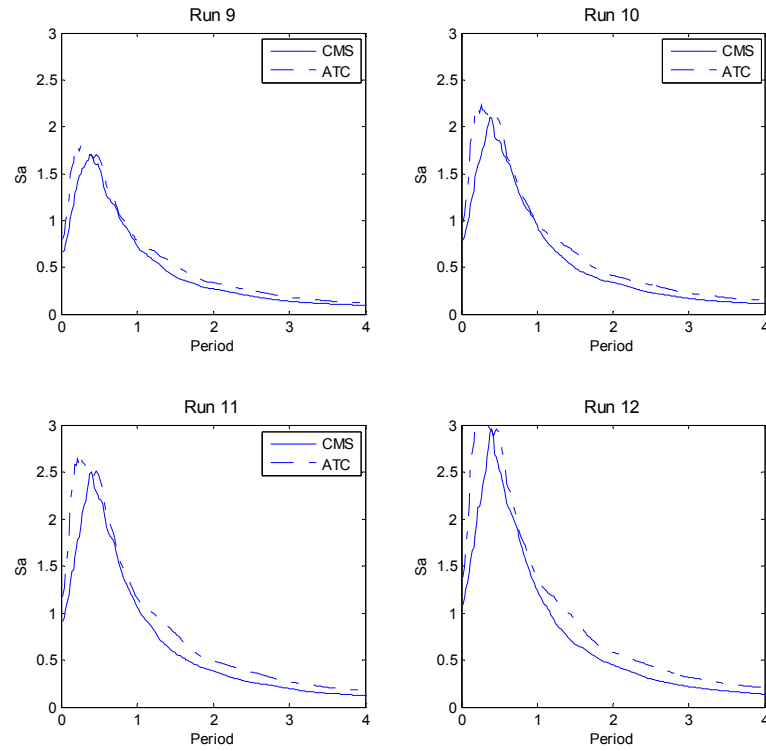
Figure B-3: Comparison between CS and ATC median earthquake response spectra for Sa_{T1} of 1.70g, 2.10g, 2.50g and 3.00g
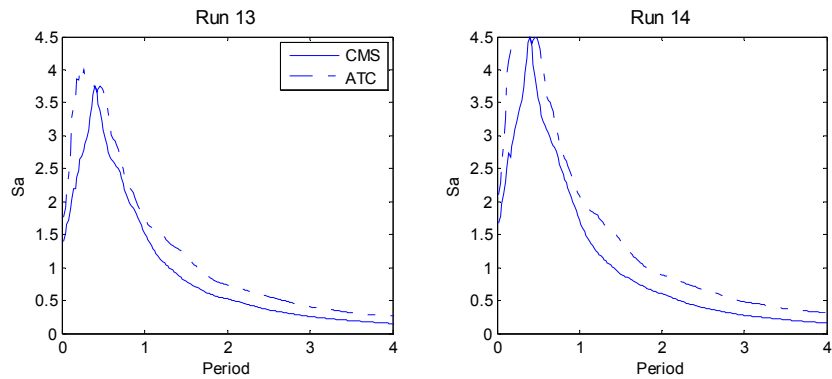
Figure B-4: Comparison between CS and ATC median earthquake response spectra for Sa_{T1} of 3.75g and 4.50g
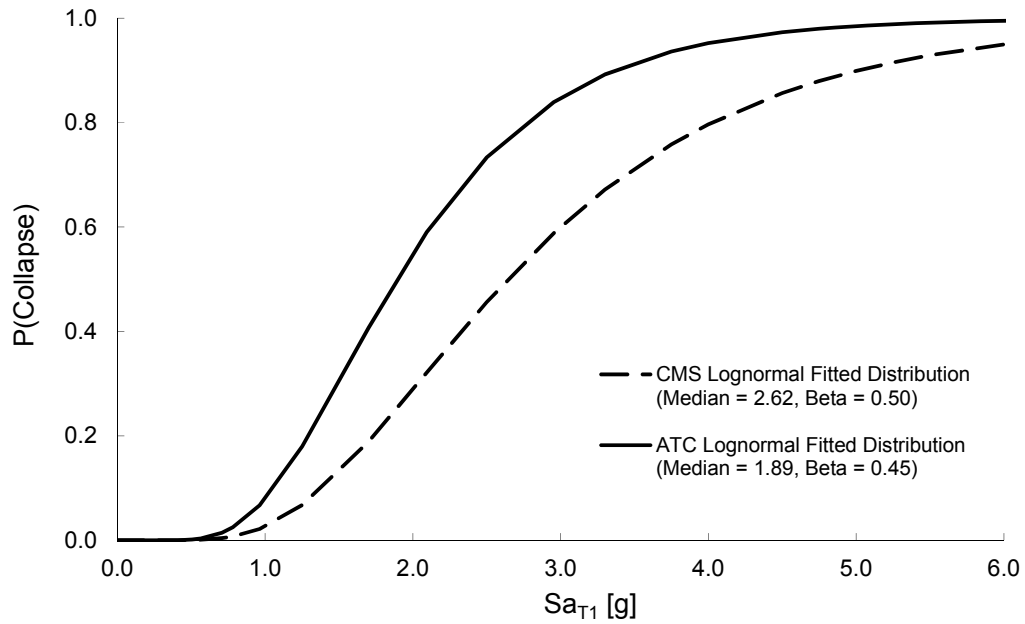
Figure B-5: Comparison of calculated collapse fragility curve based on CS ground motion set and the ATC-63 ground motion set.
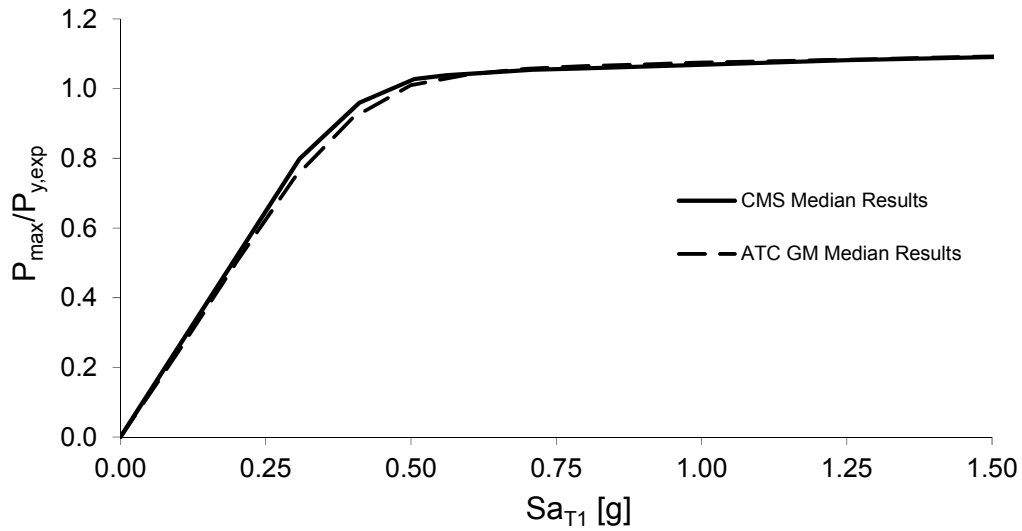
Figure B-6: Median of maximum brace forces from both analyses. Analyzing the frame with CS ground motions does not alter the demand on capacity-designed components.

Component Reliability Probability Formulas

This appendix provides a detailed derivation of the probability formulas from Chapter 2 used to perform reliability calculations for capacity-designed components conditioned at a specific deformation level or earthquake intensity level.

The design equation for capacity-designed components is generally of this form:

$$\phi C_n \geq \gamma D_n \tag{C-1}$$

where C_n and D_n are the nominal capacity and nominal demand, and ϕ and γ are the capacity and demand factors.

The limit state equation, which takes values less than zero when demand exceeds capacity, is written in the following format to facilitate an analytical solution below:

$$g = \frac{C}{D} - 1 \tag{C-2}$$

where C and D are the capacity and demand random variables.

At the boundary, equation C-1 can be written as:

$$\phi C_n = \gamma D_n \tag{C-3}$$

We can re-write equation C-3 as:

$$\phi C_n \frac{C}{C} = \gamma D_n \frac{D}{D} \tag{C-4}$$

$$\Rightarrow \frac{C}{D} = \frac{C/C_n}{D/D_n} \times \frac{\gamma}{\phi} \tag{C-5}$$

Substituting (C-5) into (C-2) gives:

$$g = \frac{C/C_n}{D/D_n} \times \frac{\gamma}{\phi} - 1 \qquad \text{(C-6)}$$

We have chosen to express capacities and demands in terms of ratios to nominal values, to facilitate standardized representation of uncertainties. We further decompose those capacity and demand ratios as follows:

$$C/C_n = (x_1 \times x_2 \times .... \times x_n) \qquad \text{(C-7)}$$

$$D/D_n = (x_{n+1} \times x_{n+2} \times .... \times x_{n+m}) \qquad \text{(C-8)}$$

The x_i's are the normalized random variables involved in each analysis, e.g. the material and fabrication variability or the model uncertainty etc. These x_i's will be defined as needed in the following examples. We are interested in calculating the probability that the demand exceeds the capacity, which can be evaluated using the limit state equation:

$$P_f = P(g \leq 0) = P(C/D \leq 1) \qquad \text{(C-9)}$$

Taking logarithms, this equation becomes:

$$P_f = P\big(\ln(C/D) \leq 0\big) \qquad \text{(C-10)}$$

Assuming lognormal distributions for C and D, it can be shown that the solution to (9-10) is the following simple formula, which depends only on the random variable medians and dispersions, V´s. (i.e. the first-order second-moment (FOSM) method reliability result is exact):

$$P_f = \Phi\left(-\frac{\ln\left(\hat{C}_m/\hat{D}_m\right)}{\sqrt{\sum_{i=1}^{n+m}\sum_{j=1}^{n+m} a_i a_j \rho_{i,j} V_{x_i} V_{x_j}}}\right) \qquad \text{(C-11)}$$

$$= \Phi\big(-\beta_{LRFD}\big) \qquad \text{(C-12)}$$

254

Where $\hat{C}_m$ and $\hat{D}_m$ are the median values of the capacities and demands, respectively, and their ratio is:

$$\hat{C}_m \Big/ \hat{D}_m = \frac{\hat{C}_m \Big/ C_n}{\hat{D}_m \Big/ D_n} \times \frac{\gamma}{\phi} \qquad \text{(C-13)}$$

Substituting from equations C-7 and C-8 we obtain

$$\hat{C}_m \Big/ \hat{D}_m = \frac{(\hat{X}_1 \times \hat{X}_2 \times ... \times \hat{X}_n)}{\left(\hat{X}_{n+1} \times \hat{X}_{n+2} \times ... \times \hat{X}_{n+m}\right)} \times \frac{\gamma}{\phi} \qquad \text{(C-14)}$$

The $\hat{X}$'s are the median values of the normalized random variables involved in each analysis and the V_x's their dispersions's. $\rho_{i,j}$ is the correlation coefficient between x_i and x_j and a_i is the gradient of the limit state function with respect to x_i. For the case of equations C-6 – C-8, a_i is +1 if x_i is a capacity random variable and -1 if x_i is a demand random variable.

Special Moment Frame Connections

This appendix assesses the reliability and the required design strength of bolted end plate moment connections in Special Moment Resisting Frames (SMRFs), using cyclic test data and the proposed Capacity Design Factor methodology. SMRFs are seismic load resisting systems where inelastic deformations are expected to mainly take place in beam plastic hinges (along with some column panel zone deformations). The beam plastic hinges are the energy dissipating components in a SMRF and are expected to provide ductility and hysteretic damping for the frame when subjected to severe seismic ground motions. Connections in SMRFs should be able to sustain a story drift angle of at least 0.04 radians when tested using a specific loading protocol. To ensure this desired behavior the AISC *Seismic Provisions* (2010a) have force-controlled components be designed to be stronger than the expected demands from beams when undergoing inelastic deformation. For example, connection strength should be larger than the beam hinge maximum probable moment (AISC, 2010b), column axial strength should exceed the nominal strength of all yielding members, including material overstrength and strain hardening, and the summation of column plastic moments should exceed the summation of beam plastic moments.

To illustrate the reliability framework for establishing the required design strength capacity-designed components in seismic resistant steel buildings, two failure modes for bolted moment-end plate connections are used. The selected failure modes are: 1) Tension bolt failure and 2) Shear bolt failure. The required design strength of bolted moment end-plate connections in SMRF has to be, according to the AISC *Prequalified Connections for Special and Intermediate Steel Moment Frames for Seismic Applications* (2010b) larger than the beam hinge maximum probable moment, $C_{pr}R_yF_yZ$. The current γ-factor is 1.15 (i.e. $C_{pr} = \gamma$) and the ϕ-factor is divided into two categories, $\phi_n = 0.90$ and

$\phi_d = 1.00$, where subscript n and d refer to non-ductile and ductile failure modes. Both of the selected failure modes are considered non-ductile according to the AISC *Prequalified Connection Requirements* (2010b).

$$\phi C_n \geq \gamma D_n = M_f \qquad \text{(D-1)}$$

where

$$M_f = M_{pe} + V_u S_h \qquad \text{(D-2)}$$

$$M_{pe} = C_{pr} R_y F_y Z_x \qquad \text{(D-3)}$$

$$V_u = \frac{2M_{pe}}{L'} + V_{gravity} \qquad \text{(D-4)}$$

The following are the results for the selected failure modes in bolted end-plate moment connections (Table D-3 and D-4). The results are represented as both the required capacity factor, ϕ, given a demand factor, γ, to achieve given probability of demand exceeding capacity in 50 years and wise versa. Only two possible failure modes are selected but the same method can easily be applied to other failure modes given statistical data has been collected or through expert judgment when data is not available. The results in tables D-3 through D-6 are based on the collected statistical data on demand and capacity presented in tables D-1 and D-2 and the reliability framework described in Chapter 3. For this example, a San Francisco site (Lat = 38.0, Long = -121.7) and a New Madrid site (Lat = 35.2, Long = -89.9) ground motion hazard curves at T = 0.2s are used and taken to represent the ground motion hazard in the Western US and the Central and Eastern US, respectively. Demands associated with the maximum forces developed in testing of end-plate moment connections subjected to cyclic loading protocols are considered to represent the demand on the connections up to the MCE ground motion demand and is used for the reliability calculations.

For $R_\mu = 4$, *P(Coll$_{D>C}$)* in 50 years of 0.1%, *P(Coll|D>C)* = 20% and a San Francisco site ground motion hazard curve, the range of recommended γ-factors is 1.15 – 1.43. The upper values represent a significant increase in the currently used γ-factor of 1.15 ($C_{pr} = \gamma$

= 1.15). Based on these results, the γ-factor needs to be increased or the tolerable *P(D>C)* = 0.50% in 50 years increased to justify the currently used γ- and ϕ-factors. Alternatively, the ϕ-factor could be adjusted to 0.72-0.93 while maintaining the γ-factor at 1.15, suggesting that the commonly used ϕ-factor of 0.75 for connections is more appropriate for the case of bolted moment-end plate connections.

Due to the shape of the hazard curves in the Central and Eastern US, the recommended γ-factors are lower. For $R_\mu = 4$, *P(Coll$_{D>C}$)* in 50 years of 0.1%, *P(Coll|D>C)* = 20% and a New Madrid site ground motion hazard curve, the range of γ-factors is between 1.02 and 1.29. Alternatively, the ϕ-factor could be adjusted to 0.80 - 1.01 and maintaining the γ-factor at 1.15.

Table D-1: Bolted Moment End-Plate Connection capacity[1] data used in reliability analysis

Failure Mode		Material	Fabrication	Connection Model	$X_{m,1}*X_{m,2}*X_{m,3}$
		X_1	X_2	X_3	ΣV_{xi}^2
Tension Bolt Failure	$X_{m,i}$	1.20	1.00	1.00	1.20
A325 Bolts	V_{xi}	0.07	0.05	0.00	0.09
Tension Bolt Failure	$X_{m,i}$	1.07	1.00	1.00	1.07
A490 Bolts	V_{xi}	0.02	0.05	0.00	0.05
Shear Bolt Failure	$X_{m,i}$	1.41	1.00	1.00	1.41
A325 Bolts	V_{xi}	0.07	0.05	0.05	0.10
Shear Bolt Failure	$X_{m,i}$	1.25	1.00	1.00	1.25
A490 Bolts	V_{xi}	0.02	0.05	0.05	0.08

Table D-2: Bolted Moment End-Plate Connection demand2 data used in reliability analysis

W-Shape Beams Gr. 50	Material	Fabrication	Load Model Parameter	Record-to-Record	$X_{m,4}*X_{m,5}*X_{m,6}*X_{m,7}$
	X_4	X_5	X_6	X_7	ΣV_{xi}^2
$X_{m,i}$	1.00	1.00	1.15	1.00	1.15
V_{xi}	0.05	0.05	0.11	0.03	0.14

1) Values are based on recommendations from Kulak, Fisher and Struik (1987)
2) Material values are based on data from Liu, J. (2003)
   Fabrication values are based on recommendations from Ravindra and Galambos (1978)
   Load model parameter values are based on cyclic test results on bolted moment end-plated connections reported in Sumner, Mays and Murray (2000)

Note: The current C_{pr} factor is set to 1.15 and from table D-2 it does well in representing the expected strain hardening of the beam as it undergoes cyclic loading. However, by definition, you can expect that the maximum demand will be exceed the predicted demand approximately 50% of the time.

Table D-3: Recommended ϕ-factors for selected failure modes in bolted moment end-plate connections in SMRF based on collected statistical data on demand and capacity, R$_\mu$ and *P(D>C)* in 50 years

Failure Modes	$\gamma = C_{pr} = 1.15$, Western US								
	R$_\mu$ = 1			R$_\mu$ = 2			R$_\mu$ = 4		
	P(Coll|D>C)			*P(Coll|D>C)*			*P(Coll|D>C)*		
	100%	20%	10%	100%	20%	10%	100%	20%	10%
Tension Bolt Failure (A325 Bolts)	0.85	0.96	1.02	0.77	0.85	0.89	0.72	0.78	0.81
Tension Bolt Failure (A490 Bolts)	0.78	0.87	0.92	0.71	0.78	0.81	0.67	0.72	0.75
Shear Bolt Failure (A325 Bolts)	0.98	1.11	1.19	0.88	0.97	1.02	0.82	0.90	0.94
Shear Bolt Failure (A490 Bolts)	0.89	1.00	1.07	0.81	0.89	0.93	0.76	0.83	0.86

Table D-4: Recommended γ-factors for selected failure modes in bolted moment end-plate connections in SMRF based on collected statistical data on demand and capacity, R$_\mu$ and *P(D>C)* in 50 years

Failure Modes	$\phi = 0.90$, Western US								
	R$_\mu$ = 1			R$_\mu$ = 2			R$_\mu$ = 4		
	P(Coll|D>C)			*P(Coll|D>C)*			*P(Coll|D>C)*		
	100%	20%	10%	100%	20%	10%	100%	20%	10%
Tension Bolt Failure (A325 Bolts)	1.22	1.08	1.01	1.34	1.22	1.17	1.44	1.32	1.27
Tension Bolt Failure (A490 Bolts)	1.33	1.19	1.12	1.45	1.33	1.28	1.54	1.43	1.38
Shear Bolt Failure (A325 Bolts)	1.06	0.93	0.87	1.17	1.06	1.01	1.26	1.15	1.11
Shear Bolt Failure (A490 Bolts)	1.16	1.03	0.97	1.27	1.16	1.11	1.36	1.25	1.21

Table D-5: Recommended ϕ-factors for selected failure modes in bolted moment end-plate connections in SMRF based on collected statistical data on demand and capacity, R_μ and $P(D>C)$ in 50 years

Failure Modes	$R_\mu = 1$ $P(Coll|D>C)$			$R_\mu = 2$ $P(Coll|D>C)$			$R_\mu = 4$ $P(Coll|D>C)$		
$\gamma = C_{pr} = 1.15$, Central & Eastern US	100%	20%	10%	100%	20%	10%	100%	20%	10%
Tension Bolt Failure (A325 Bolts)	0.86	0.97	1.04	0.82	0.91	0.97	0.79	0.87	0.92
Tension Bolt Failure (A490 Bolts)	0.79	0.88	0.94	0.76	0.83	0.88	0.73	0.80	0.84
Shear Bolt Failure (A325 Bolts)	0.99	1.13	1.22	0.94	1.06	1.12	0.91	1.01	1.07
Shear Bolt Failure (A490 Bolts)	0.90	1.02	1.09	0.86	0.96	1.02	0.84	0.92	0.97

Table D-6: Recommended γ-factors for selected failure modes in bolted moment end-plate connections in SMRF based on collected statistical data on demand and capacity, R_μ and $P(D>C)$ in 50 years

Failure Modes	$R_\mu = 1$ $P(Coll|D>C)$			$R_\mu = 2$ $P(Coll|D>C)$			$R_\mu = 4$ $P(Coll|D>C)$		
$\phi = 0.90$, Central & Eastern US	100%	20%	10%	100%	20%	10%	100%	20%	10%
Tension Bolt Failure (A325 Bolts)	1.21	1.07	0.99	1.26	1.13	1.07	1.31	1.18	1.12
Tension Bolt Failure (A490 Bolts)	1.31	1.17	1.10	1.37	1.24	1.18	1.41	1.29	1.23
Shear Bolt Failure (A325 Bolts)	1.04	0.92	0.85	1.10	0.98	0.92	1.14	1.02	0.97
Shear Bolt Failure (A490 Bolts)	1.14	1.02	0.95	1.20	1.08	1.02	1.24	1.12	1.07
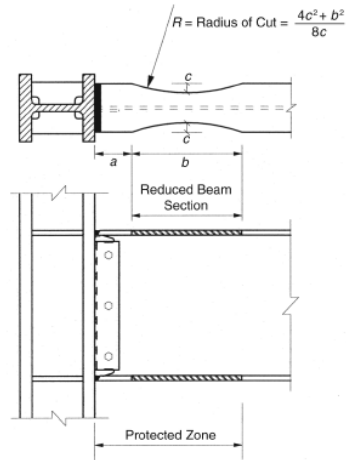
Figure D-1: Reduced beam section is commonly used in SMRFs to protect beam-column connections from excessive demands and ensure that plastic hinging forms in beams rather than columns. (Image from AISC, 2010b)

(a) Four-Bolt
Unstiffened, 4E

(b) Four-Bolt
Stiffened, 4ES

(c) Eight-Bolt
Stiffened, 8ES
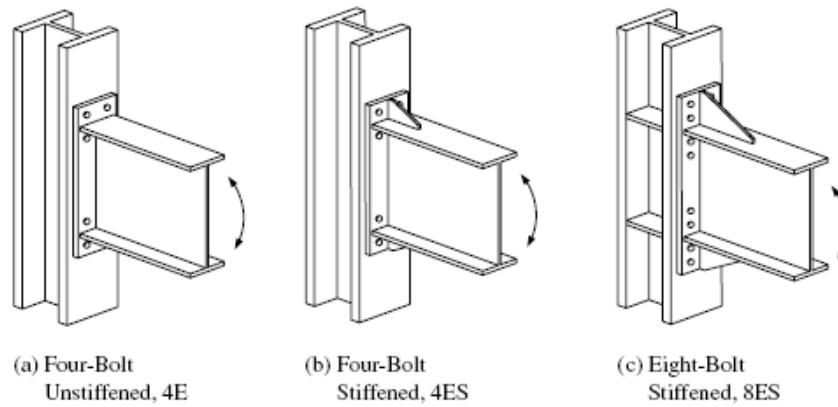
Figure D-2: Extended end-plate configurations (Image from AISC (2010))
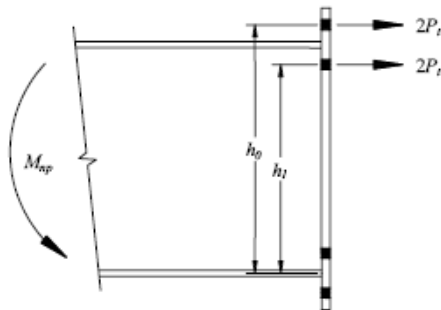
Figure D-3: Bolt force model for four-bolt connection (Image from AISC (2010))

Collected Statistical Data: Material Properties, Connection Capacity in SCBF and SMRF

This appendix provides a database of collected statistical data required for component reliability calculations. Tables E-1 to E-10 contain statistical data on material yield stress, F_y, tensile stress, F_u, and calculated correlation coefficient between F_y and F_u for different steel shapes and material specifications. Table E-11 provides data from brace cyclic tests. The normalized brace forces at 1% to 5% story drift ratios are reported. Table E-12 provides 13 tests results from 4 different experiments on net section failure. The force at which net section failure occurs is normalized by the expected force based on AISC (2010a) limit state equations. Similarly, Table E-13 provides 11 test results from 1 experiment on block shear failure, and Table E-14 the results from 133 tests from 8 experiments on block shear failure of bolted gusset plate. Table E-15 provides the data used for the component reliability calculations of brace connections in Chapter 6. Table E-16 provides data on the maximum moment developed at RBS sections versus story drift when subjected to cyclic loading. The data was collected from 37 cyclic tests on RBS sections from 4 different experiments.

Table E-1: Material properties of steel members - yield stress

Shape	Material Specification	Source	Type	$F_{y,nom}$	R_y	$\mu_{Fy}/F_{y,nom}$	COV	μ_{Fy}	$F_y/R_yF_{y,nom}$	No. of Samples
W-shape	A36	Liu, J. (2003)	Mill	36	1.5	1.57	0.05	56.5	1.047	56
	-	Lignos, D. (2008)	Flange coupon	-	-	1.25	0.12	45.0	0.833	101
	-	Lignos, D. (2008)	Web coupon	-	-	1.40	0.13	50.3	0.931	80
	A572 Gr. 50	Liu, J. (2003)	Mill	50	1.1	1.20	0.05	60.0	1.091	8
	-	Lignos, D. (2008)	Flange coupon	-	-	1.05	0.09	52.7	0.960	190
	-	Lignos, D. (2008)	Web coupon	-	-	1.10	0.11	54.8	1.004	190
	-	Jacques and Frank (1999)	Flange coupon	-	-	1.09	0.07	54.4	0.989	59
	-	Frank and Read (1993)	Flange coupon	-	-	1.10	0.09	54.9	0.998	13536
	A992	Liu, J. (2003)	Mill	50	1.1	1.10	0.05	55.0	1.000	112
	-	Lignos, D. (2008)	Flange coupon	-	-	1.10	0.10	55.1	1.002	33
	-	Lignos, D. (2008)	Web coupon	-	-	1.09	0.06	54.7	0.995	33
	-	Bartlett et al (2003)	Flange coupon	-	-	1.10	0.06	55.0	1.000	131
	-	Dexter et al (2000)	Flange coupon	-	-	1.12	0.06	55.8	1.015	20295
Angle	A36	Liu, J. (2003)	Mill	36	1.5	1.34	0.07	48.2	0.893	1668
	A572 Gr. 50	Liu, J. (2003)	Mill	50	1.1	1.29	0.07	64.5	1.173	232
	A588	Liu, J. (2003)	Mill	50	1.1	1.29	0.05	64.5	1.173	75
Channel	A36	Liu, J. (2003)	Mill	36	1.5	1.36	0.06	49.0	0.907	22
Plate, Bar	A36	Liu, J. (2003)	Mill	36	1.3	1.39	0.07	50.0	1.069	43
	A572 Gr. 50	Liu, J. (2003)	Mill	50	1.1	1.16	0.07	58.0	1.055	35
	A529 Gr. 50	Liu, J. (2003)	Mill	50	1.2	1.22	0.05	61.0	1.017	550
	A529 Gr. 55	Liu, J. (2003)	Mill	55	1.1	1.1	0.05	60.5	1.000	1328
	A572 Gr. 55	Liu, J. (2003)	Mill	55	1.1	1.13	0.08	62.2	1.027	1307
	A1011 SS Gr. 55	Liu, J. (2003)	Mill	55	1.1	1.12	0.06	61.6	1.018	102
	A1011 HSLAS Gr. 55	Liu, J. (2003)	Mill	55	1.1	1.15	0.08	63.3	1.045	301
HSS (round)	A500 Gr. B	Liu, J. (2003)	Mill	42	1.4	1.36	0.07	57.1	0.971	645
HSS	A500 Gr. B	Liu, J. (2003)	Mill	46	1.4	1.31	0.08	60.3	0.936	309
Pipe	A53 Gr. B	Liu, J. (2003)	Mill	35	1.6	1.59	0.11	55.7	0.994	228

Table E-2: Material properties of steel members - tensile stress

Shape	Material Specification	Source	Type	$F_{u,nom}$	R_t	$\mu_{Fu}/F_{u,nom}$	COV	μ_{Fu}	$F_u/R_tF_{u,nom}$	No. of Samples
W-shape	A36	Liu, J. (2003)	Mill	58	1.2	1.29	0.03	74.8	1.075	56
	-	Lignos, D. (2008)	Flange coupon	-	-	1.14	0.07	66.1	0.950	101
	-	Lignos, D. (2008)	Web coupon	-	-	1.18	0.07	68.3	0.981	80
	A572 Gr. 50	Liu, J. (2003)	Mill	65	1.1	1.2	0.04	78.0	1.091	8
	-	Lignos, D. (2008)	Flange coupon	-	-	1.1	0.07	71.4	0.999	190
	-	Lignos, D. (2008)	Web coupon	-	-	1.12	0.08	72.9	1.020	190
	-	Jacques and Frank (1999)	Flange coupon	-	-	1.11	0.04	72.3	1.011	61
	-	Frank and Read (1993)	Flange coupon	-	-	1.16	0.08	75.6	1.057	13536
	A992	Liu, J. (2003)	Mill	65	1.1	1.12	0.04	72.8	1.018	112
	-	Lignos, D. (2008)	Flange coupon	-	-	1.15	0.06	74.5	1.042	33
	-	Lignos, D. (2008)	Web coupon	-	-	1.15	0.06	74.9	1.048	33
	-	Bartlett et al (2003)	Flange coupon	-	-	1.1	0.05	71.6	1.001	131
	-	Dexter et al (2000)	Flange coupon	-	-	1.13	0.04	73.5	1.028	20295
Angle	A36	Liu, J. (2003)	Mill	58	1.2	1.22	0.04	70.8	1.017	1668
	A572 Gr. 50	Liu, J. (2003)	Mill	65	1.1	1.38	0.06	89.7	1.255	232
	A588	Liu, J. (2003)	Mill	70	1.1	1.27	0.05	88.9	1.155	75
Channel	A36	Liu, J. (2003)	Mill	58	1.2	1.18	0.04	68.4	0.983	22
Plate, Bar	A36	Liu, J. (2003)	Mill	58	1.2	1.23	0.04	71.3	1.025	43
	A572 Gr. 50	Liu, J. (2003)	Mill	65	1.2	1.26	0.07	81.9	1.050	35
	A529 Gr. 50	Liu, J. (2003)	Mill	70	1.2	1.22	0.05	85.4	1.017	550
	A529 Gr. 55	Liu, J. (2003)	Mill	70	1.2	1.22	0.01	85.4	1.017	1328
	A572 Gr. 55	Liu, J. (2003)	Mill	70	1.2	1.15	0.01	80.5	0.958	1307
	A1011 SS Gr. 55	Liu, J. (2003)	Mill	70	1.1	1.08	0.01	75.6	0.982	102
	A1011 HSLAS Gr. 55	Liu, J. (2003)	Mill	70	1.1	1.1	0.01	77.0	1.000	301
HSS (round)	A500 Gr. B	Liu, J. (2003)	Mill	58	1.3	1.24	0.04	71.9	0.954	645
HSS	A500 Gr. B	Liu, J. (2003)	Mill	58	1.3	1.27	0.04	73.7	0.977	309
Pipe	A53 Gr. B	Liu, J. (2003)	Mill	60	1.2	1.16	0.06	69.6	0.967	228

Table E-3: Combined mean and COV of F_y for steel members

Shape	Material Specification	$\mu_{Fy}/F_{y,nom}$	$F_y/R_yF_{y,nom}$	COV	No. of Samples
W-shape	A36	1.57	1.047	0.05	56
	A572 Gr. 50	1.2	1.091	0.05	8
	A992	1.1	1.000	0.05	112
Angle	A36	1.34	0.893	0.07	1668
	A572 Gr. 50	1.29	1.173	0.07	232
	A588	1.29	1.173	0.05	75
Channel	A36	1.36	0.907	0.06	22
Plate, Bar	A36	1.39	1.069	0.07	43
	A572 Gr. 50	1.16	1.055	0.07	35
	A529 Gr. 50	1.22	1.017	0.05	550
	A529 Gr. 55	1.10	1.000	0.05	1328
	A572 Gr. 55	1.13	1.027	0.08	1307
	A1011 SS Gr. 55	1.12	1.018	0.06	102
	A1011 HSLAS Gr. 55	1.15	1.045	0.08	301
HSS (round)	A500 Gr. B	1.36	0.971	0.07	645
HSS	A500 Gr. B	1.31	0.936	0.08	309
Pipe	A53 Gr. B	1.59	0.994	0.11	228

All specimens	μ_{X4}	1.24	0.99	Sum: 7021
	v_{X4}	0.12	0.10	
All excluding plates and bars	μ_{X4}	1.35	**0.95**	Sum: 3355
	v_{X4}	0.10	**0.11**	
Plates and bars only	μ_{X4}	1.14	1.02	Sum: 3666
	v_{X4}	0.08	0.07	

[*]Values are from report by Liu (2003) on R_y and R_t factors for steel members

Table E-4: Combined mean and COV of F_u for steel members

Shape	Material Specification	$\mu_{Fu}/F_{u,nom}$	$F_u/R_tF_{u,nom}$	COV	No. of Samples
W-shape	A36	1.29	1.08	0.03	56
	A572 Gr. 50	1.2	1.09	0.04	8
	A992	1.12	1.02	0.04	112
Angle	A36	1.22	1.02	0.04	1668
	A572 Gr. 50	1.38	1.25	0.06	232
	A588	1.27	1.15	0.05	75
Channel	A36	1.18	0.98	0.04	22
Plate, Bar	A36	1.23	1.03	0.04	43
	A572 Gr. 50	1.26	1.05	0.07	35
	A529 Gr. 50	1.22	1.02	0.05	550
	A529 Gr. 55	1.22	1.02	0.01	1328
	A572 Gr. 55	1.15	0.96	0.01	1307
	A1011 SS Gr. 55	1.08	0.98	0.01	102
	A1011 HSLAS Gr. 55	1.1	1.00	0.01	301
HSS (round)	A500 Gr. B	1.24	0.95	0.04	645
HSS	A500 Gr. B	1.27	0.98	0.04	309
Pipe	A53 Gr. B	1.16	0.97	0.06	228

All specimens	μ_{x1}	1.21	1.01	Sum: 7021
	v_{x1}	0.06	0.07	
All excluding plates and bars	μ_{x1}	1.23	**1.02**	Sum: 3355
	v_{x1}	0.06	**0.09**	
Plates and bars only	μ_{x1}	1.18	0.99	Sum: 3666
	v_{x1}	0.04	0.04	

[*]Values are from report by Liu (2003) on R_y and R_t factors for steel members

Table E-5: Combined mean and COV of F_y for W-shape A992 steel members

Yield Strength

Shape	Material Specification	Source	Type	$F_{y,nom}$	R_y	$\mu_{Fy}/F_{y,nom}$	COV	μ_{Fy}	$F_y/R_yF_{y,nom}$	No. of Samples
	A992	Liu, J. (2003)	Mill	50	1.1	1.10	0.05	55.0	1.000	112
	-	Lignos, D. (2008)	Flange coupon	-	-	1.10	0.10	55.1	1.002	33
W-shape	-	Lignos, D. (2008)	Web coupon	-	-	1.09	0.06	54.7	0.995	33
	-	Bartlett et al (2003)	Flange coupon	-	-	1.10	0.06	55.0	1.000	131
	-	Dexter et al (2000)	Flange coupon	-	-	1.12	0.06	55.8	1.015	20295

Table E-6: Correlation coefficient between F_y and F_u for W-sections (Lignos, D, 2008)

W-Sections		$\rho_{Fy,Fu}$	
Material Specification	Source	Flange Coupon	Flange Web
A36	Lignos, D (2008)	0.85	0.74
A572 Gr. 50	-	0.78	0.76
A991	-	0.78	0.9

Table E-7: Estimated correlation coefficient between F_y and F_u for steel members

Yield Strength

Shape	Material Specification	$F_{y,nom}$	R_y	$\mu_{Fy}/F_{y,nom}$	COV	μ_{Fy}	$F_y/R_yF_{y,nom}$	No. of Samples
	A36	36	1.5	1.57	0.05	56.5	1.047	56
W-shape	A572 Gr. 50	50	1.1	1.2	0.05	60.0	1.091	8
	A992	50	1.1	1.1	0.05	55.0	1.000	112
	A36	36	1.5	1.34	0.07	48.2	0.893	1668
Angle	A572 Gr. 50	50	1.1	1.29	0.07	64.5	1.173	232
	A588	50	1.1	1.29	0.05	64.5	1.173	75
Channel	A36	36	1.5	1.36	0.06	49.0	0.907	22
	A36	36	1.3	1.39	0.07	50.0	1.069	43
	A572 Gr. 50	50	1.1	1.16	0.07	58.0	1.055	35
	A529 Gr. 50	50	1.2	1.22	0.05	61.0	1.017	550
Plate, Bar	A529 Gr. 55	55	1.1	1.1	0.05	60.5	1.000	1328
	A572 Gr. 55	55	1.1	1.13	0.08	62.2	1.027	1307
	A1011 SS Gr. 55	55	1.1	1.12	0.06	61.6	1.018	102
	A1011 HSLAS Gr. 55	55	1.1	1.15	0.08	63.3	1.045	301
HSS (round)	A500 Gr. B	42	1.4	1.36	0.07	57.1	0.971	645
HSS	A500 Gr. B	46	1.4	1.31	0.08	60.3	0.936	309
Pipe	A53 Gr. B	35	1.6	1.59	0.11	55.7	0.994	228

Tensile Strength

Shape	Material Specification	$F_{u,nom}$	R_t	$\mu_{Fu}/F_{u,nom}$	COV	μ_{Fu}	$F_u/R_tF_{u,nom}$	No. of Samples
	A36	58	1.2	1.29	0.03	74.8	1.075	56
W-shape	A572 Gr. 50	65	1.1	1.2	0.04	78.0	1.091	8
	A992	65	1.1	1.12	0.04	72.8	1.018	112
	A36	58	1.2	1.22	0.04	70.8	1.017	1668
Angle	A572 Gr. 50	65	1.1	1.38	0.06	89.7	1.255	232
	A588	70	1.1	1.27	0.05	88.9	1.155	75
Channel	A36	58	1.2	1.18	0.04	68.4	0.983	22
	A36	58	1.2	1.23	0.04	71.3	1.025	43
	A572 Gr. 50	65	1.2	1.26	0.07	81.9	1.050	35
	A529 Gr. 50	70	1.2	1.22	0.05	85.4	1.017	550
Plate, Bar	A529 Gr. 55	70	1.2	1.22	0.01	85.4	1.017	1328
	A572 Gr. 55	70	1.2	1.15	0.01	80.5	0.958	1307
	A1011 SS Gr. 55	70	1.1	1.08	0.01	75.6	0.982	102
	A1011 HSLAS Gr. 55	70	1.1	1.1	0.01	77.0	1.000	301
HSS (round)	A500 Gr. B	58	1.3	1.24	0.04	71.9	0.954	645
HSS	A500 Gr. B	58	1.3	1.27	0.04	73.7	0.977	309
Pipe	A53 Gr. B	60	1.2	1.16	0.06	69.6	0.967	228

*Values are from report by Liu (2003) on R_y and R_t factors for steel members

Table E-8: Ratio between yield and tensile stress for steel members

Y/T - Ratio				Correlation Coefficients assuming:	
Shape	Material Specification	Mean Y/T	COV	Lognormal	Normal
W-shape	A36	0.76	0.04	0.58	0.58
W-shape	A572 Gr. 50	0.77	0.07	-0.19	-0.21
W-shape	A992	0.76	0.04	0.61	0.61
Angle	A36	0.68	0.05	0.72	0.72
Angle	A572 Gr. 50	0.72	0.04	0.82	0.82
Angle	A588	0.73	0.03	0.81	0.81
Channel	A36	0.72	0.03	0.89	0.89
Plate, Bar	A36	0.70	0.05	0.72	0.72
Plate, Bar	A572 Gr. 50	0.71	0.08	0.35	0.34
HSS (round)	A500 Gr. B	0.80	0.09	-0.35	-0.37
HSS	A500 Gr. B	0.82	0.05	0.84	0.85
Pipe	A53 Gr. B	0.80	0.09	0.57	0.57

*Values are from report by Liu (2003) on R_y and R_t factors for steel members

Table E-9: Combined correlation coefficient between F_y and F_u for steel members

Y/T - Ratio					
Shape	Material Specification	Mean Y/T	Mean T/Y	COV	No. of Samples
W-shape	A36	0.76	1.32	0.04	56
W-shape	A572 Gr. 50	0.77	1.30	0.07	8
W-shape	A992	0.76	1.32	0.04	112
Angle	A36	0.68	1.47	0.05	1668
Angle	A572 Gr. 50	0.72	1.39	0.04	232
Angle	A588	0.73	1.37	0.03	75
Channel	A36	0.72	1.39	0.03	22
Plate, Bar	A36	0.70	1.43	0.05	43
Plate, Bar	A572 Gr. 50	0.71	1.41	0.08	35
HSS (round)	A500 Gr. B	0.80	1.25	0.09	645
HSS	A500 Gr. B	0.82	1.22	0.05	309
Pipe	A53 Gr. B	0.80	1.25	0.09	228

All specimens	Mean	0.73	1.37
All specimens	COV	0.10	0.10
All excluding plates and bars	Mean	0.73	1.37
All excluding plates and bars	COV	0.10	0.10
Plates and bars only	Mean	0.70	1.42
Plates and bars only	COV	0.07	0.07

Correlation Coefficient	Lognormal
All specimens	0.60
Excluding plate and bars	0.62
Plate and bars only	0.77

*Values are from report by Liu (2003) on R_y and R_t factors for steel members

Table E-10: Brace test results used in reliability calculations
Brace Loading Paramter
x_6

| Authors | Shape | Story Drift |
		1	2	3	4	5
Fell et al (2007)	HSS4x4x1/4 FF	1.07	1.09	*1.09*	*1.09*	*1.09*
Fell et al (2007)	HSS4x4x1/4 NF -C	1.07	1.10	*1.10*	*1.10*	*1.10*
Fell et al (2007)	HSS4x4x1/4 FF (EQ)	1.11	1.13	*1.13*	*1.13*	*1.13*
Fell et al (2007)	HSS4x4x3/8 FF	0.94	1.01	*1.01*	*1.01*	*1.01*
Fell et al (2007)	HSS4x4x3/8 FF(EQ)	1.03	1.05	*1.05*	*1.05*	*1.05*
Fell et al (2007)	Pipe3STD FF	1.05	1.07	1.08	1.09	1.10
Fell et al (2007)	Pipe3STD# FF	1.01	1.06	1.06	1.08	1.08
Fell et al (2007)	Pipe5STD# FF	1.13	1.17	1.18	1.20	1.20
Fell et al (2007)	Pipe5STD FF	1.17	1.19	1.19	*1.19*	*1.19*
Fell et al (2007)	W12x16 NF-C	1.02	1.02	*1.02*	*1.02*	*1.02*
Fell et al (2007)	W12x16 FF	1.00	1.01	1.01	1.01	1.01
Yang and Mahin (2007)	HSS 6x6x3/8 NF-C	1.09	*1.09*	*1.09*	*1.09*	*1.09*
Yang and Mahin (2007)	HSS 6x6x3/8 FF	1.07	1.11	*1.11*	*1.11*	*1.11*
Yang and Mahin (2007)	HSS 6x6x3/8 FF	1.01	*1.01*	*1.01*	*1.01*	*1.01*
Yang and Mahin (2007)	HSS 6x6x3/8 NF-T	0.99	1.00	1.01	*1.01*	*1.01*
Shaback (2001)	HSS5x5x5/16	1.08	*1.08*	*1.08*	*1.08*	*1.08*
Shaback (2001)	HSS6x6x5/16	1.08	1.11	*1.11*	*1.11*	*1.11*
Shaback (2001)	HSS6x6x3/8	1.12	1.14	*1.14*	*1.14*	*1.14*
Shaback (2001)	HSS5x5x1/4	1.00	1.07	*1.07*	*1.07*	*1.07*
Shaback (2001)	HSS5x5x5/16	1.05	1.07	*1.07*	*1.07*	*1.07*
Shaback (2001)	HSS5x5x3/8	1.11	1.17	*1.17*	*1.17*	*1.17*
Shaback (2001)	HSS6x6x5/16	1.09	*1.09*	*1.09*	*1.09*	*1.09*
Shaback (2001)	HSS6x6x3/8	1.10	1.12	*1.12*	*1.12*	*1.12*
Lehman & Roeder (2008)	HSS 5x5x3/8	1.07	*1.07*	*1.07*	*1.07*	*1.07*
Lehman & Roeder (2008)	HSS 5x5x3/8	1.10	*1.10*	*1.10*	*1.10*	*1.10*
Lehman & Roeder (2008)	HSS 5x5x3/8	1.12	*1.12*	*1.12*	*1.12*	*1.12*
Lehman & Roeder (2008)	HSS 5x5x3/8	1.06	1.09	*1.09*	*1.09*	*1.09*
Lehman & Roeder (2008)	HSS 5x5x3/8	1.28	*1.28*	*1.28*	*1.28*	*1.28*
Han & Foutch (2007)	HSS4x4x1/8	*1.01*	*1.01*	*1.01*	*1.01*	*1.01*
Han & Foutch (2007)	HSS4x4x1/4	1.02	*1.02*	*1.02*	*1.02*	*1.02*
Han & Foutch (2007)	HSS4x4x1/4	1.03	1.05	*1.05*	*1.05*	*1.05*
Han & Foutch (2007)	HSS4x4x1/4	1.03	1.05	*1.05*	*1.05*	*1.05*
Black and Popov (1980)	W8x20	1.00	1.07	*1.07*	*1.07*	*1.07*
Black and Popov (1980)	W6x25	1.02	1.02	1.03	*1.03*	*1.03*
Black and Popov (1980)	W6x20	*1.02*	1.12	*1.12*	*1.12*	*1.12*
Black and Popov (1980)	W6x20	1.05	1.09	1.09	*1.09*	*1.09*
Black and Popov (1980)	W6x20	1.09	1.11	*1.11*	*1.11*	*1.11*
Black and Popov (1980)	W6x16	0.94	0.98	*0.98*	*0.98*	*0.98*
Black and Popov (1980)	W6x15.5	*0.99*	*0.99*	*0.99*	*0.99*	*0.99*
Black and Popov (1980)	W6x20	*1.04*	*1.04*	*1.04*	*1.04*	*1.04*
Black and Popov (1980)	W5x16	*1.00*	*1.00*	*1.00*	*1.00*	*1.00*
Black and Popov (1980)	Pipe 4 Std	0.99	1.04	*1.04*	*1.04*	*1.04*
Black and Popov (1980)	Pipe 4 Std	0.95	1.02	*1.02*	*1.02*	*1.02*
Black and Popov (1980)	Pipe 4 X-Strong	1.05	1.10	*1.10*	*1.10*	*1.10*
Black and Popov (1980)	Pipe 4 X-Strong	1.23	*1.23*	*1.23*	*1.23*	*1.23*
Black and Popov (1980)	Pipe 3-1/2 Std	0.99	*0.99*	*0.99*	*0.99*	*0.99*
Elchalakani et al (2003)	CHS 139.7x3.5 (HSS 5.563x0.134)	0.99	1.01	*1.01*	*1.01*	*1.01*
Elchalakani et al (2003)	CHS 139.7x3.5 (HSS 5.563x0.134)	0.95	0.97	*0.97*	*0.97*	*0.97*
	μ_{x6}:	1.05	1.07	*1.07*	1.08	1.08
	V_{x6}:	0.06	0.06	*0.06*	0.06	0.06

Italic values: If tensile force at a lower story drift is higher than at the higher story drift, the higher tensile force governs. Maximum value of failed braces is extrapolated passed its failure point until all braces have failed.

Table E-11: Experimental test results for net section failure

Net Section Failure

Experiment	Loading Protocol	Section		A_e	L_w	X_{hat}	U	F_u	P_{max}/A_eF_u
1	NF (T)	HSS 6x6x3/8* (in)	ASTM A500 Gr. B	6.23	15	2.25	0.85	65 (ksi)	1.200
1	FF	HSS 6x6x3/8* (in)	ASTM A500 Gr. B	6.23	15	2.25	0.85	65 (ksi)	1.326
2	NF (T)	Pipe3STD* (in)	A53 Gr. B	1.69	6.5	1.11	0.83	67 (ksi)	1.271
2	NF (T)	Pipe5STD* (in)	A53 Gr. B	3.45	12	1.77	0.85	61 (ksi)	1.327
1	NF (T)	Pipe 6 XS* (in)	A53 Gr. B	6.58	15	1.91	0.87	55 (ksi)	1.139
3	Monotonic	HSS 168x4.8* (mm)	Class C 350 MPa	1453	156	53.5	0.66	540 (MPa)	1.315
3	Monotonic	HSS 168x4.8* (mm)	Class C 350 MPa	1596	192	53.5	0.72	540 (MPa)	1.339
3	Monotonic	HSS 110x220x6.3* (mm)	S355J2H	1499	145	62.2	0.57	530 (MPa)	1.396
3	Monotonic	HSS 110x220x6.3* (mm)	S355J2H	1728	182	62.2	0.66	530 (MPa)	1.350
3	Monotonic	HSS 168x4.8* (mm)	Class C 350 MPa	1453	156	53.5	0.66	540 (MPa)	1.365
3	Monotonic	HSS 110x6.3x220* (mm)	S355J2H	2073	185	38.9	0.79	530 (MPa)	1.167
4	Monotonic	HSS 102x6.4* (mm)	Gr. 350W Class H	1451	170	32.5	0.81	449 (MPa)	1.274
4	Monotonic	HSS 220x8* (mm)	Gr. 350W Class H	3739	275	69.7	0.75	431 (MPa)	1.327

$\mu_y =$	1.292
$\sigma_y =$	0.079
COV =	0.061
$\sigma_{lny} =$	0.061
$\mu_{lny} =$	0.254
$Y_{0.5} =$	1.290

13 *number of tests in*
 4 *different experiments*

1: Yang and Mahin (2005)
2: Fell et al. (2006)
3: Willibald et al. (2006)
4: Cheng et al. (1998)
* No reinforcement at net section
FF = Far Field Loading Protocol. NF (T) = Near Field Tension Pulse. NF (C) = Near Field Compression Pulse

Table E-12: Experimental test results for block shear failure

Block Shear Failure

Experiment	Loading Protocol	Gusset Plate	L_w	b	A_{nt}	A_{nv}	F_y	F_u	P_{AISC}	P_{max}	P_{max}/P_{AISC}
1	Monotonic	500x750x4	50.0	60.3	241.2	200	309	402	171	216	1.26
1	Monotonic	500x750x4	95.3	57.5	230	381.2	309	402	234	314	1.34
1	Monotonic	500x750x4	98.3	77.5	310	393.2	309	402	270	347	1.29
1	Monotonic	500x750x4	150.3	78.6	314.4	601.2	309	402	349	430	1.23
1	Monotonic	500x750x4	49.3	98.8	395.2	197.2	309	402	232	295	1.27
1	Monotonic	500x750x4	96.0	97.8	391.2	384	309	402	300	395	1.32
1	Monotonic	500x750x4	150.0	99.9	399.6	600	309	402	383	475	1.24
1	Monotonic	500x750x4	47.3	148.8	595.2	189.2	309	402	309	386	1.25
1	Monotonic	500x750x4	96.0	148.2	592.8	384	309	402	381	467	1.23
1	Monotonic	500x750x4	101.3	56.4	225.6	405.2	309	402	241	306	1.27
1	Monotonic	500x750x4	149.3	98.2	392.8	597.2	309	402	379	433	1.14

$\mu_y =$	1.26
$\sigma_y =$	0.05
COV = V_y	0.04
$\sigma_{lny} =$	0.04
$\mu_{lny} =$	0.23
$Y_{0.5} =$	1.26

11 *number of tests in*
 1 *different experiments*

1: Topkaya (2006)

Table E-13: Experimental test results for block shear failure of bolted gusset plates

Block Shear of Bolted Gusset

Authors	Year	No. Of Tests	TEST/AISC$_{2005}$	COV
Hardash and Bjorhovde	1984	28	1.22	0.06
Rabinovitch and Cheng	1983	5	1.22	0.05
Udagawa and Yamada	1998	73	1.18	0.05
Nash et al.	1999	3	1.35	0.01
Aalberg and Larsen	1999	8	1.21	0.03
Swanson and Leon	2000	1	1.17	
Huns et al.	2002	10	1.13	0.16
Mullin	2005	5	1.15	0.04
Total		**133**	**1.19**	**0.07**

Table E-14: Experimental test results used for SCBF reliability analysis

Connection Capacity Model				
Failure Mode	**Source**	**Mean**	**COV**	**No. Samples**
Net Section Failure - Welded Connection	Yang and Mahin (2005)	1.22	0.08	3
-	Fell et al. (2006)	1.30	0.03	2
-	Willibald et al. (2006)	1.32	0.06	6
-	Cheng et al. (1998)	1.30	0.03	2
-	**Combined**	**1.29**	**0.06**	**13**
Block Shear of Welded Gusset	Topkaya (2006)	1.26	0.04	11
Block Shear of Bolted Gusset	Hardash and Bjorhovde (1984)	1.22	0.06	28
	Rabinovitch and Cheng (1983)	1.22	0.05	5
	Udagawa and Yamada (1998)	1.18	0.05	73
	Nash et al. (1999)	1.35	0.01	3
	Aalberg and Larsen (1999)	1.21	0.03	8
	Swanson and Leon (2000)	1.17	-	1
	Huns et al. (2002)	1.13	0.16	10
	Mullin (2005)	1.15	0.04	5
	Combined	**1.19**	**0.07**	**133**
Bolt Failure	Kulak, Fisher and Struik (1987)	1.35	0.05	-
Weld Failure (SMAW)	Ng et al (2004), Lesik & Kennedy (1990), Deng (2003)	1.17	0.16	86
Weld Failure (FCAW)	Ng et al (2004), Lesik & Kennedy (1990), Deng (2003)	1.17	0.17	54
Connection Fabrication				
Failure Mode	**Source**	**Mean**	**COV**	**No. Samples**
Net Section Failure - Welded Connection	Ravindra & Galambos (1978)	1.00	0.05	-
Block Shear of Welded Gusset	Ravindra & Galambos (1978)	1.00	0.05	-
Block Shear of Bolted Gusset	Ravindra & Galambos (1978)	1.22	0.06	-
Bolt Failure	Kulak, Fisher and Struik (1987)	1.00	0.05	-
Weld Failure (SMAW)	Ng et al (2004), Lesik & Kennedy (1990), Deng (2003)	1.00	0.10	86
Weld Failure (FCAW)	Ng et al (2004), Lesik & Kennedy (1990), Deng (2003)	1.00	0.10	54
Connection Material				
Failure Mode	**Source**	**Mean**	**COV**	**No. Samples**
Net Section Failure - Welded Connection	Liu, J. (2003)	1.02	0.09	3355
Block Shear of Welded Gusset	Liu, J. (2003)	1.14	0.08	3666
Block Shear of Bolted Gusset	Liu, J. (2003)	1.14	0.08	3666
Bolt Failure	Kulak, Fisher and Struik (1987)	1.00	0.05	-
Weld Failure (SMAW)	Ng et al (2004), Lesik & Kennedy (1990), Deng (2003)	1.40	0.14	86
Weld Failure (FCAW)	Ng et al (2004), Lesik & Kennedy (1990), Deng (2003)	1.66	0.14	54

Table E-15: Experimental test results on the maximum moment developed at RBS sections vs. story drift when subjected to cyclic loading

Story Drift	$M_{max,rbs}/M_{p,rbs,exp}$					
	All		No Concrete Slab		Concrete Slab	
	Mean	COV	Mean	COV	Mean	COV
0.001	0.12	0.26	0.11	0.26	0.13	0.27
0.002	0.22	0.20	0.20	0.20	0.23	0.25
0.003	0.31	0.18	0.28	0.18	0.34	0.24
0.004	0.41	0.18	0.37	0.18	0.45	0.24
0.005	0.50	0.18	0.46	0.18	0.55	0.23
0.006	0.60	0.18	0.54	0.18	0.66	0.23
0.007	0.69	0.18	0.63	0.18	0.75	0.22
0.008	0.77	0.17	0.71	0.17	0.84	0.21
0.009	0.85	0.17	0.78	0.17	0.92	0.21
0.010	0.90	0.18	0.84	0.18	0.96	0.20
0.015	1.05	0.17	0.98	0.17	1.11	0.20
0.020	1.11	0.16	1.05	0.16	1.17	0.20
0.030	1.15	0.14	1.08	0.14	1.23	0.19
0.040	1.16	0.15	1.09	0.15	1.23	0.18
0.050	1.18	0.13	1.10	0.13	1.25	0.17
0.060	1.18	0.13	1.10	0.13	1.26	0.16
0.070	1.18	0.13	1.10	0.13	1.27	0.15

*Values from cyclic test results reported in Engelhardt & Venti (2000), Gilton et al (2000), Ricles et al (2004) & Song et al (2000).
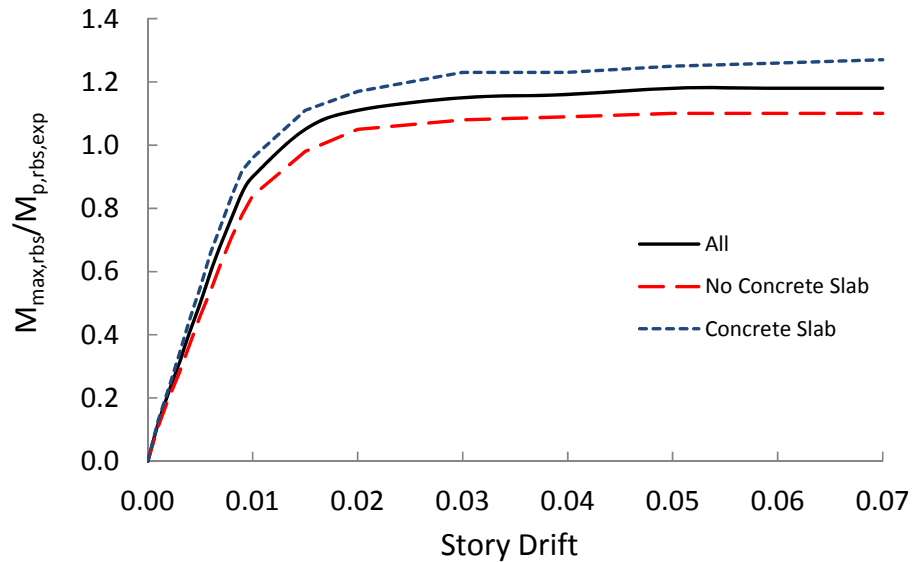

Figure E-1: Plot of the normalized mean maximum moments developed at RBS sections vs. story drift